UNIVERSITY OF LEICESTER

SYNERGISTIC USE OF AIRBORNE HYPERSPECTRAL AND LiDAR DATA FOR MAPPING MEDITERRANEAN FOREST IN PORTUGAL

Thesis submitted for the degree of
Doctor of Philosophy in Geography
at the University of Leicester

by

Prem Chandra Pandey MTech MSc

Department of Geography

University of Leicester

October 2015

Synergistic use of airborne hyperspectral and LiDAR data for mapping Mediterranean forest in Portugal

Prem Chandra Pandey

Abstract

Forests are the major source of biodiversity and provide natural sources of wood, fodder, gums, resins, and medicines. Forests encounter damage by nature and human factors, which needs to be monitored for all tree species, whether invasion or intentional damage. This study focuses on the classification of an open tall stand coastal surrounding site for the mapping and classification of tree species and ground features using airborne imagery. So, improving the classification and mapping accuracy of forest in surrounding coastal regions is essential for the restoration and management decisions. The first objective of this thesis is to use segmented Principal Component (PC) images to classify the ground features including different tree species and to improve the classification results. More specific goals include (a) Use of hyperspectral images to map and classify the forest region using a segmented PC image, (b) Investigating the gain in mapping accuracy with segmented PC image as opposed to hyperspectral imagery alone. The second objective is to assess and investigate the fusion of airborne hyperspectral imagery and LiDAR derived Canopy Height Model for classification and assessing the results. These objectives aim at investigating the gain in mapping accuracy with fusion image as opposed to hyperspectral imagery alone.

Thus, overall this study assesses the differences in classification outputs using a data fusion technique, segmented PC image and individual hyperspectral images, which differ in accuracy, in Mediterranean forest. MLC based supervised image classification method provided better accuracy (96.3%) with segmented PC images, (~92.9%) with the fusion of CHM and hyperspectral images than with hyperspectral image alone (89.6% with MLC and 67.5% with SAM). According to my results, CHM and HSI provide better classification and mapping results over extensive areas of forests.

The overall accuracy of the classified maps ranged from 67.5 to 96.3% and κ coefficient was found between 0.61 and 0.95. Segmented PC and PC fusion techniques provided a significant step to improve the distinction and classification results. Using the above methods, tree species and associated features could be classified and mapped, despite the problem of spectral mixing of different features. In future, more high spatial and spectral resolution images will provide a platform for the incorporation of enhanced characteristics for mapping and classification purposes.

Dedication

I dedicate this to my parents--

My mother who was a big source of inspiration throughout my academic career,

She passed away during the period of this doctoral programme in December 2013, a great setback for me at that time.

and,

my father, who encouraged me in this doctoral programme, over a number of years, with moral and emotional support throughout every situation of my life.

Acknowledgement

I would like to thank Dr. Nicholas J Tate and Prof Heiko Balzter, my supervisors who encouraged me and provided technical support, details and writing guidance throughout the entire period. Especially, I need to express my sincere gratitude and deep appreciation to him for providing me the depth of knowledge and support in terms of research ideas, proper guidance and remarks for writing up like organization of chapters, references which helped me throughout this research work. I would like to express my gratitude to both supervisors for providing me sufficient guidance and support to complete this research work. I am indebted to them for their valuable suggestions, support at every stage of this research, and took pain and time to comment, and help to edit this thesis.

I am thankful to Prof. Sue Page (former Head, Department of Geography-2014-2015) for her support throughout the study. My sincere thanks go to Dr. Kevin Tansey (Head of the Department), who helped me in providing feedbacks and support and paved the way to the University of Leicester, in 2011 with guidance and support. I express my gratitude to Late Prof. Pete Fisher (thesis chair, for his constructive comments and valuable suggestions that proved helpful in completing this thesis.

My sincere thanks also go to Dr. Virginia Nicolás-Perea for providing technical support and help during throughout the study. I am also indebted to persons especially, Prof. Lex Comber and Dr Jorg Kaduk for their support. I am also thankful to Dr Sue McLaren, Dr Claire Jarvis, Dr Jeniffer Dickie, Dr Kirsten Barret and departmental staff, Charlotte Langley, Clare Stanga, Allen Kerry, Vanessa Greasley, Ann Williams, Gary Hancox, Bill Hickin, Dr Sarah, Gemma and Adam Cox, for providing all support and help required during research work. I am thankful to all CLCR colleagues Ajoke Onojeghuo, Alex Cumming, Andrea Hurtado Mendoza-Rosales, Azad Rasul;, Bashir Adamu, Bernard Spies, Dr Beth Cole, Chloe Barnes, Mark Collins, David, Dimitris Stratoulias, Hao Wang, James Wheeler, Narissara, Gong Pan, Pedro Rodriguez-Veiga, Peshawa Najmaddin, Ramesh Ningthoujam, Sarah Cook, Velentin Louis, Yahaya Zayyana Ibrahim, and the list continues for their support and help. I am heartily thankful to Dr. Paul Arellano for his valuable suggestions during this research work.

I would like to extend my sincere gratitude to the Airborne Research and Survey Facility (ARSF, Gloucester, U.K.) and Natural Environment Research Council (NERC) for acquiring airborne data under EUFAR project EUFAR11/06 in 2011. I am also thankful to André Große-Stoltenberg (University of Münster, Germany) and Katurah Z. Smithson staff the University of Leicester for their help during field work. Thanks are also due to André Große-Stoltenberg and Prof. Tillmann Buttschardt (University of Münster, Germany) for providing the EUFAR11/06 datasets without which it was impossible to carry out this research work. I am thankful to Karl R. Sears, University of Leicester, for proofreading and improving the quality of my thesis according to the university's guidelines. I am grateful to Data basin and John Wiley and Sons (copyrights.com), for providing the permission to use figures in thesis.

I express my gratitude to Dr. Mark Warren and Emma Carolan, the research staff of PML- remote sensing group (Plymouth Marine Laboratory, Plymouth) for their help in hyperspectral data processing. I would like to thank Ministry of Human Resource and Development, Government of India (MHRD, GoI) for nominating and Commonwealth Scholarship Commission, UK (CSC) for providing research fellowship (INCS-155-2011) to pursue this doctoral programme at the University of Leicester.

I am very much thankful to my family members who always support me in a difficult time and provided a moral boost up. I am also grateful to my friend Ashu, who assisted and suggested with valuable support. Last but not the least, my special thanks go to my lovely wife Sneha, and Baby Adele for supporting me throughout the study period.

Table of contents

List of Tables

List of Figures

List of Abbreviations

AISA - Airborne Imaging Spectrometer for Applications

ANN- Artificial Neural Network

ARSF- Airborne Research and Survey Facility

ASD- Analytical Spectral Devices

ASPRS- American Society of Photogrammetry and Remote Sensing

AVIRIS- Air-Borne Visible Infra-Red Imaging Spectrometer

BIL- Band Interleaved by Line

BRDF -Bidirectional Reflectance Distribution Function

CHM- Canopy Height Model

DD-Degree Decimal

DEM- Digital Elevation Model

DGPS-Differential Global Positioning System

DMS- Degree Minute Second

DSM- Digital Surface model

EVI-Enhanced Vegetation Index

FLAASH- Fast Line-of-sight Atmospheric Analysis of Spectral Hypercube

FODIS - Fiber-Optic Down dwelling Irradiance Sensor

fPAR- Fraction of Photosynthetically Active Radiation

FWHM- Full Width Half Maximum

GIS- Geographical Information Science

GMT- Greenwich Mean Time

GPS-Global Positioning System

HDF -Hierarchical Data Format

HSI- Hyperspectral Imaging

IHS- Intensity Hue Saturation

INS -Inertial Navigation System

JM- Jeffries Matusita distance

LAI- Leaf Area Index

LDA- Linear Discriminate Analysis

LiDAR- Light Detection and Ranging

m- Metre

MDC- Mahalanobis Distance Classification

MLC- Maximum Likelihood Classification

MNF- Minimum Noise Fraction Transform

MOMS-01- Modular Optoelectronic Multispectral Scanner

NDVI- Normalized Difference vegetation Index

NERC- National Environment Research Council

OA- Overall Accuracy

PA- Producer’s accuracy

PCA- Principal Component Analysis

r-CHM- rescaled Canopy Height Model

RMSE- Root Mean Square Error

RS- Remote Sensing

SAM- Spectral Angle Mapper

SVM- Support Vector Machine

TD- transformed divergence

TM – Thematic Mapper

UA-User’s Accuracy

UFD- Uniform Feature Design

Chapter 1. Introduction

1.1 Introduction

Hyperspectral images can provide more information about the earth features than multispectral images using different classification techniques. However, as the number of spectral bands increases the dimensionality of the data also increases which results in an improved classification accuracy (Bellman, 1961, Hughes, 1968). This is also limited at certain points from where a further increase in spectral bands results in the decrease of the classification accuracy, which is known as the ‘Hughes Phenomenon’. High dimensional image requires more number of training samples for a classifier and need increases exponentially. Thus, in the classifier design, it leads to ambiguity in the classification, where the accuracy increases and declines after that points onwards with an increasing number of bands, while keeping the training samples constant (Hughes, 1968, Scott, 1992). There exist a relationship between the number of training samples, band numbers of the images and consequent classification accuracy of the classified image (Fukunaga and Hayes, 1989). This phenomenon cannot be prevented unless provided with sufficient number of samples. It means that by adding more spectral bands to a standard classifier, the classification result eventually becomes less accurate (Alonso et al., 2011, Hughes, 1968, Ma et al., 2013, Nishii et al., 1997, Scott, 1992). Too many input bands can thus lead to a degradation of the classified map, resulting in lower accuracy result for classified hyperspectral image. Thus, in this study segmented PCA was applied to reduce the 'Hughes Phenomenon' and enhance the classification accuracy.

There are several studies related to 'Hughes Phenomenon' for either reducing it or mitigating it (Shahshahani and Landgrebe, 1994). Band selection (selecting numerous bands out of all bands), PCA and MNF based feature transformations were some of the techniques evolved to reduce the 'Hughes Phenomenon' in hyperspectral image classification. There is also evidence of classification by SVM using feature selection for reducing data dimensionality (Pal and Foody, 2010). Initially, optimum band selection were used as one of the methods for classification of hyperspectral images (Ma and Zhang, 2011, Mausel et al., 1990). Band selection is a method of choosing few bands from several bands that may contain the unique information needed for classification (Chang et al., 1999, Mausel et al., 1990). Thus, band selection became the famous method of hyperspectral image classification, and sometime it lower the implementation of a classifier as some bands may have valuable information in discarded bands (Brunzell and Eriksson, 2000). Thus, choosing a better classification classifier may also produce lower accuracy results (due to data dimensionality). An attempt has been made to classify hyperspectral images using MLC while reducing the dimension of the image to generate the desired results.

This thesis aims to-

1) Classify forest tree species using hyperspectral images by reducing the 'Hughes Phenomenon' using segmentation of hyperspectral image.

2) Extract attributes from LiDAR and integrates with hyperspectral images to harness the robustness of image fusion and its classification.

3) To decide which techniques are suitable or whether additional attributes or properties included with the hyperspectral image can enhance its outcomes.

Researchers have shown the effectiveness of hyperspectral image and LiDAR contribution towards the classification purposes in forestry and related fields (discussed in detail in Chapter 2).

1.2 Background and Rationale

Earth observation is an emerging technology that has many applications in resource management, forestry, land use land cover classification and other research areas. Remote sensing has established its applicability in a wide range of research fields such as forestry, land cover, biomass estimation, mapping and classifications. Optical, hyperspectral and LiDAR remote sensing can assist in earth observation technology. Recently, researchers concentrated their work to map forest species, estimate biomass and measure biophysical parameters of forest using hyperspectral imagery (Treitz and Howarth, 1999). In the beginning of remote sensing era, satellite data has provided low spatial, spectral and temporal resolutions for research purposes, but nowadays satellite and airborne data provides high spatial, spectral resolution data to work and study different research fields. The advantage with enhanced remote sensing technology is the collection and acquisition of different images in terms of different spectral wavelengths (panchromatic, multispectral, hyperspectral) and low to high spatial resolution (Zhang et al., 2007).

Remote sensors provide information about Earth's features due to reflected/ emitted radiation (passive sensors) or returned pulses (Active sensors) (Schott, 2007). This information is captured remotely in the form of energy and stored in the image that allows researchers to determine their feature composition and their nature (Read and Torrado, 2009). Thus, the Earth observation sensor's capability to acquire surface radiance values have provided challenging research facilities. These capabilities were in terms of increasing spatial resolution, and spectral resolution with more periodic capture of earth surface features (Campbell, 2002). The surface features comprise of vegetation, soil and surrounding features that need to be identified using a remote sensing approach. The remote identification of features is quite difficult due to numerous persistent problems during data capturing. These problems are atmospheric interference, angle of view, spectral variance of proximity features and water contents during real-time measurements by sensors. Although researchers have made their best efforts to create spectral libraries of many unique vegetation species, these do not help when the same species were to be identified in different regions or places. Researchers have noticed that spectral signatures may not be unique (Cochrane, 2000), and thus they suggested that similar spectral characteristics may be shown by several species due to the variation in the spectral signature of surrounding species (Price, 1994).

The study site is located in the western coast of Portugal where diverse Mediterranean forest exists with forest fire susceptibility, invasion with exotic species and fragile environmental nature. The diverse and unique characteristics of the forest make this site ideal for the research purposes. Mediterranean forest is one of the most fragile environment ecosystems, which needs to be monitored with a species classification that faces frequent fires and destruction. These forest species were peculiar in their properties and functions. Forest species, accurate distribution and functions should be known to forest department so that preventive actions and rescue from disasters like fire, which is more, frequent in Mediterranean forests, can take place.

1.3 Hypothesis

The underlying hypothesis of the present study is that different tree species, with mixed group or spectrally similar features, ultimately affect the reflectance properties, which can be classified using hyperspectral images and more appropriate image processing/fusion techniques. It is quite difficult to identify forest tree species having similar spectral characteristics or mixed spectral characteristics using hyperspectral images. Sometimes two or more species were close enough in proximity to distinguish between them. That is why attributes such as elevation (height) and intensity information from LiDAR data were incorporated with hyperspectral images for forest mapping. The height information from LiDAR will be used to produce the above ground height difference of the forest region. LiDAR will contribute towards the generation of Digital Terrain Model (DTM) and Digital Surface Model (DSM) from return pulse. DTM represents the bare earth surface ground points without the influence of vegetation and other structures, whereas DSM represents 3D above ground structures along with visible ground (Ma, 2005, Miller, 2004). The DTM and DSM were utilised for the generation of Canopy Height Model (CHM) representing the height of the forest structure above the ground (Balzter et al., 2007, Popescu et al., 2003, Zimble et al., 2003). Integration of hyperspectral and LiDAR data for harnessing properties of hyperspectral and LiDAR data together (CHM integrated with PCA based techniques, selected regions will be taken). The importance of image integration in vegetation mapping is to improve image interpretation and enhance image classification.

The inclusion of height information derived from LiDAR data may be beneficial during image classification. Maybe we are using different integration algorithms for more good results when compared to current data integration techniques- PC integration technique. The next step will involve time series analysis of the forest species spread along the coastal forest region for further protection and coastal vegetation management. The use of temporal data set for forest extent and tree species wise forest extent mapping or change detection.

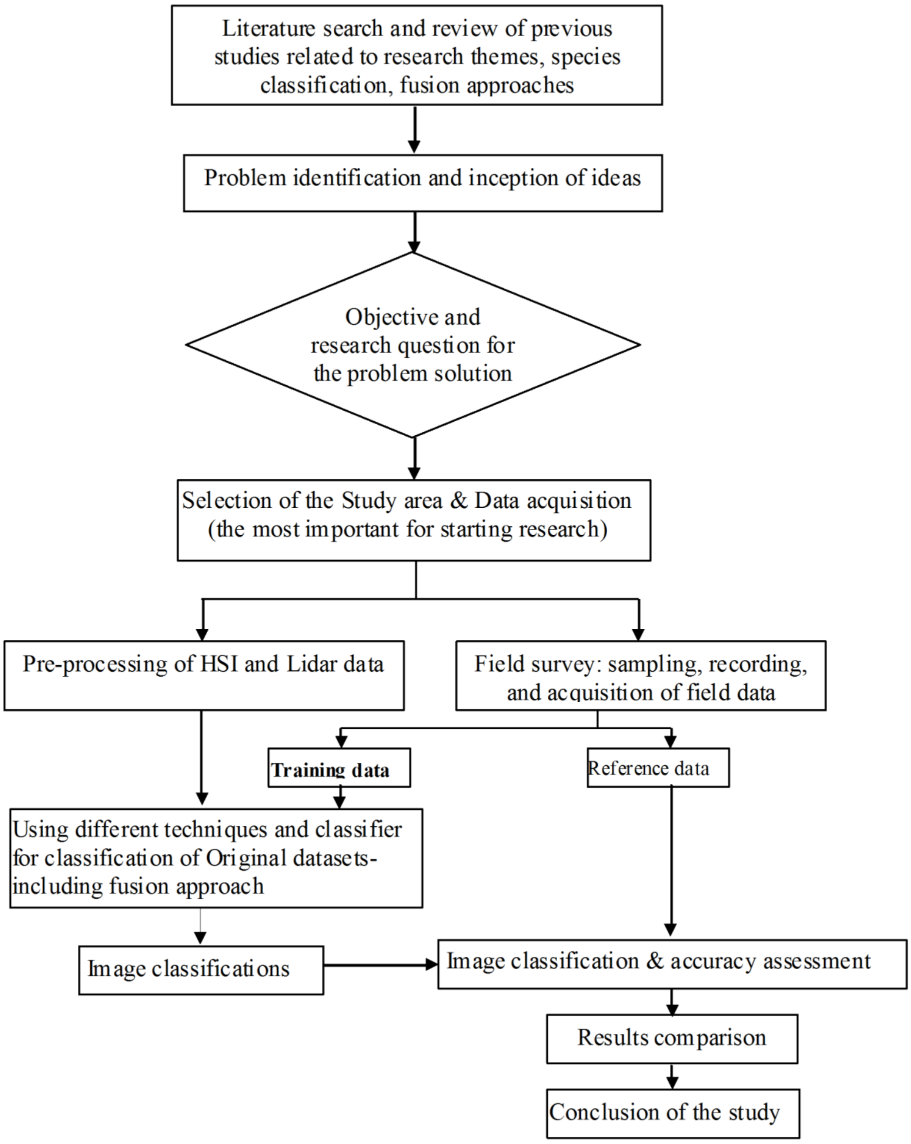

Figure 1.1 General research approach included in the study

1.4 Research Approach

The research approach used in the following study is an assemblage of different steps required for selecting the objectives. The general approach used in the research is shown in Figure 1.1.

1.5 Thesis Outline

This thesis comprises of six chapters. Chapter 2 provides a review of relevant literature, and provides a physiographical overview of Mediterranean forest, biological importance of the Mediterranean forest, introduction about hyperspectral and LiDAR data, data fusion concept and its applications. This chapter includes the description of Mediterranean forest, vegetation types, and its importance to forest mapping.

Chapter 3 gives a description of the study area, materials and the datasets utilised in this study. This chapter gives a description of the study site where this research is performed. This chapter gives emphasis to the concepts of airborne hyperspectral imaging, data specifications and pre-processing techniques applied to them. This chapter also includes the concept of airborne LiDAR dataset concepts, its specifications, pre-processing steps for further analysis and interpretations. Field work and ground samples collected during fieldwork are also discussed.

Chapter 4 explores the use and importance of segmented Principal Component Analysis (PCA) as a robust mapping technique, which reduces the 'Hughes Phenomenon' and give better results when compared to the original hyperspectral images. This part explains the process of SAM, MLC, the 'Hughes Phenomenon', and ways to reduce them using segmented PCA approach. This chapter exploits the airborne hyperspectral data for forest mapping using SAM and MLC techniques. The reference spectra used in the SAM technique is collected using a handheld radio-spectrometer. Thus, this chapter discussed the ability to exploit vegetation cover for the spectral discrimination and mapping of species using two different techniques with reference spectra. This chapter also demonstrates the SAM, MLC mapping results and accuracy assessment. Segmented PC image enhances the visual interpretation of different features of the images when compared to the hyperspectral image. Overall, this chapter describes the application of segmented PCA on hyperspectral imagery, as well as classification comparison of MLC of segmented PC images over SAM and MLC on hyperspectral images.

Chapter 5 encounters the fusion approach of hyperspectral images with LiDAR derived CHM. It also provides the integrated use of airborne hyperspectral and airborne LiDAR data for the classification and mapping of tree species. This chapter also presents algorithms for integrating airborne hyperspectral imagery and airborne LiDAR data to evaluate whether the classification or mapping can be simultaneously exploited to increase vegetation discrimination and enhance the mapping results. Increased discrimination of the vegetation (different tree species- *Pinus pinea*, *Pinus pinaster, Eucalyptus, Acacia longifolia*, shrubs etc) and non-vegetated areas (sandy area and ground feature class) is presented with a spectrum of fused images against a spectrum of hyperspectral image. Thus, Chapter 5 is concerned with the assessment of fusion approach for mapping and classification of different ground features using height attributes.

Chapter 6 moves on to discuss and examines the conclusion from the study. This chapter also includes recommendations and issues associated with the study. Finally, this chapter attempts to bring together, the summary, conclusion and limitations associated with it and future work recommendations.

This thesis represents a major advance on multi-data approach to explore species mapping, other feature identification and the efficacy of airborne hyperspectral data to classification and mapping aspects. Spectral segmented PC image analysis and PC image fusion techniques have been used to achieve the objectives using hyperspectral and LiDAR data. Moreover, this research work contributes towards segmented PCA techniques in reducing 'data dimensionality' as well as reducing the 'Hughes phenomenon' significantly, which contributed towards achieving better classification accuracy. This work presented the robustness of the multi-data integration technique (PC image fusion) for hyperspectral image and LiDAR data bringing them together to harness the attribute of both data sets.

Chapter 2. Literature Review

2.1 Introduction

This chapter provides a review of relevant literature. This chapter is divided into four main sections. The first section introduces hyperspectral imaging systems and its importance in research. The second section describes the characteristics of LiDAR data and literature review related to them. The third section looks at an application that describes the fusion of data, with reference to hyperspectral image and LiDAR data. Finally, the fourth section describes the present status, climatic condition and biological importance of Mediterranean forest.

This review of literature provides some concepts and knowledge about both hyperspectral images and LiDAR data. This chapter gives insight of the Mediterranean forest in relation to climatic conditions, which favours forest fire, different tree species and the importance of diversity aspects. This chapter puts forward the concepts of several studies and outlines why this work is important and provides a significant contribution towards the hyperspectral and LiDAR fusion community. The most important for carrying research is the requirements of data. Thus, the selection of the present study to perform research in Mediterranean forest relates to its diversity and the available remote sensing data to carry out the research.

Traditionally, the information on tree species types were gathered using repeated field surveys, periodic observations and interpretations of aerial photographs (Martin et al., 1998). Field activities were rigorous, expensive, time consuming and involve manpower to deliver information that may vary upon expertise or experience as well as data availability (Cho et al., 2009, Vohland et al., 2007). The use of remote sensing techniques can reduce above requirements and offer synoptic, timely and repeatable way of gathering information on forest species. Remote sensing techniques provide high spatial and spectral resolution with temporal datasets for the large areas that are being used in classification or broad utilisation in forestry (Dalponte et al., 2009b). The satellite data can be acquired repetitively from the same region therefore field investigations become easier and faster. Multi-temporal images (since 1972) provided by remote sensing (RS) techniques can be used for forest studies and monitoring changes in forests over large areas (Song et al., 2002).. With RS images, large areas can be covered in less time with relatively cheaper than repeated field surveys (Song et al., 2002). The spatial resolution/ properties of RS techniques provide information about the canopy structure that can be used to estimate tree size and tree cover. Since, the spatial patterns of a forest regions corresponding to remote sening images are also dependent on tree cover (Song and Woodcock, 2002). Thus, the variability in the spatial and spectral resolution has a pronounced effect on the tree species classification (Peña et al., 2013). Therefore, due to the combined spatial, spectral and temporal properties of remote sensing techniques, it can be feasible for forest research effectively as compared to field investigation (Song and Woodcock, 2002, Song et al., 2002).

This chapter will provide concepts on hyperspectral images and advantages over multispectral images to differentiate different features, their suitability for the vegetation or forest studies and classification. However, identification of different vegetation and tree species may be a difficult task due to almost similar spectral response pattern (Coleman et al., 1990, Niemann, 1995). Most often hyperspectral images alone do not result in good classification results (Coleman et al., 1990). The use of additional datasets such as CHM to hyperspectral imagery can enhance the accuracy of classified image (Franklin, 1994).

This chapter also discusses the LiDAR data and its importance in the vegetation research. The introduction of LiDAR data along with the hyperspectral imagery may prove beneficial to vegetation and tree species classification. For example, Franklin (1994) showed that classification results were improved by using topographic data, in addition, to multispectral remote sensing data. Franklin (1994) found the role of data fusion as an important technique to incorporate and bring the attribute of different dataset at a single place. Thus, this chapter presents the literature review related to hyperspectral images, LiDAR data and fusion approaches.

2.2 Hyperspectral Imaging

2.2.1 Introduction

The uses of airborne hyperspectral remote sensing data are in fashion nowadays because it overcomes the limitation of the poor spatial, spectral and temporal resolution of multispectral satellite data. Hyperspectral images have several contiguous bands comprising of visible, NIR, SWIR regions of relatively narrow bandwidths at wavelength ranges from 400nm -2500 nm (Nagendra and Rocchini, 2008, Thenkabail, 2012, Thenkabail and Huete, 2012, Thenkabail et al., 2011, Wang et al., 2010).Hyperspectral imaging is classified into two groups- space borne satellite imaging (Hyperion), and airborne hyperspectral imaging (AVIRIS, AISA).

Spaceborne hyperspectral images and airborne hyperspectral images include the Airborne Visible-Infrared Imaging Spectrometer (AVIRIS), HYPERION, Airborne Imaging Spectrometer for Applications (AISA), Compact Airborne Spectrographic Imager (CASI) and the Shortwave Infrared Full Spectrum Imager (SFSI). The airborne hyperspectral images include the Advanced Solid-State Array Spectro-radiometer (ASAS) (Irons et al., 1991, Ranson et al., 1994), Airborne Visible-Infrared Imaging Spectrometer (AVIRIS) (Porter and Enmark, 1987, Vane et al., 1993), Compact Airborne Spectrographic Imager (CASI) (Anger et al., 1990), Shortwave Infrared Full Spectrum Imager (SFSI) (Neville et al., 1995) and AISA (Makisara et al., 1993). Hyperion has 220 spectral bands at a spatial resolution of 30 m (Griffin et al., 2005). Hyperion also provides data over a large spatial scale that is accessible to the public for regional species mapping (Clark 2011). NASA's AVIRIS is a unique sensor delivering spectral radiance images in 224 channels at a spectral resolution of 10 nm and spatial resolution of 1.5 m (Green et al. 1998). These hyperspectral sensors have provided a high spectral resolution as well as high spatial resolution images, used for different purposes according to the user’s need and requirements.

2.2.2 History

The first optical multispectral images were acquired by Apollo 9 for use in mapping earth features (Rees and Rees, 2012). The spaceborne remote sensing applications were started in 1972- when NASA launched the first Earth Resources Technology Satellite (ERTS) known as LANDSAT-1 (Elachi and Van Zyl, 2006, Lauer et al., 1997). Thus, optical multispectral images were recorded from space for remote sensing applications and began an era of advanced remote sensing (Borengasser et al., 2010). This achievement marked a milestone in the history of remote sensing earth observations (Kirby, 1995). Hyperspectral imaging is one of the developments of remote sensing technology much like multispectral and digital aerial photos developed by NASA for earth monitoring and observation (Goetz, 2009).

Multispectral images (e.g. Landsat, SPOT, AVHRR, World View, LISS) measure the reflectance of the features at a broad wavelength range with 5 to 7 discrete bands (Lee et al., 2004, Ustin and Xiao, 2001). These 5-7 channels do not cover the full electromagnetic range and thus are incapable of providing the information in the wavelength region where no measurements are taken or captured. In contrast to this, hyperspectral sensors measure reflected radiation in a several narrow and contiguous wavelength bands (Shippert, 2004). The continuous spectral profile of the features provides the detailed information at each wavelength of the electromagnetic range. This began the application of remote sensing in various fields like agriculture, cartography, environmental monitoring, forestry, land use planning, coastal waterways (Bowles et al., 2005).

2.2.3 Uses of Hyperspectral Images

These hyperspectral images are voluminous in dimension and record information in highly compressed data with several bands (Stern et al., 2013). As hyperspectral images have several bands, imaged simultaneously, it creates n-dimensional hypercubes as shown in Figure 2.1 (hypercubes of the airborne data used in this study).Typically, hyperspectral cube is a digital array storing spatial information on the x and y axes, while containing the spectral wavelength (λ) information on the z-axis (Borengasser et al., 2010). The sides of hypercubes are pseudo-colour, ranging from black and purple (low response) to red and green (high response) (refer to Figure 2.1). Hyperspectral images consist of two spatial dimensions and one spectral dimension unique to each feature.

There is a significant variation in spectral signatures of vegetation in hyperspectral remote sensing data than the multispectral data. Due to its high spectral resolution, hyperspectral data can reveal subtle differences in spectral signatures of vegetation or features compared with multispectral data (Pearlman et al., 2003). Thus, hyperspectral image enables fine discrimination between different vegetation depending upon the amount of pigments, leaf structure or density, water content at different wavelength ranges when compared to multispectral images. HSI offers practical techniques to detect, classify and discriminate objects using the spectral signature of the targeted features (Landgrebe, 1999a, Landgrebe, 1999b). The narrow bandwidths of hyperspectral sensors are capable of detecting small variations in the reflectance as illustrated in Figure **2.2**. Consequently, hyperspectral images have the potential to identify and discriminate different vegetation types more accurately than multispectral data. Scientists have used hyperspectral imagery in vegetation studies, to identify different vegetation species (Cochrane, 2000), invasive species detection (Asner et al., 2008), precision mapping of agriculture (Cetin et al., 2005), environmental mapping (Cetin 2012) and to detect vegetation stress and disease (Kim et al., 2010). The high spectral resolution of hyperspectral images enables better identification of the features such as vegetation, crops and soils (Gong et al., 1992) as well as land use, and land covers (Jusoff, 2009, Petropoulos et al., 2012). Hyperspectral imaging has been used in many different applications from the last three decades (Eismann, 2012, Goward et al., 2009, Manolakis et al., 2003, Warner et al., 2009).

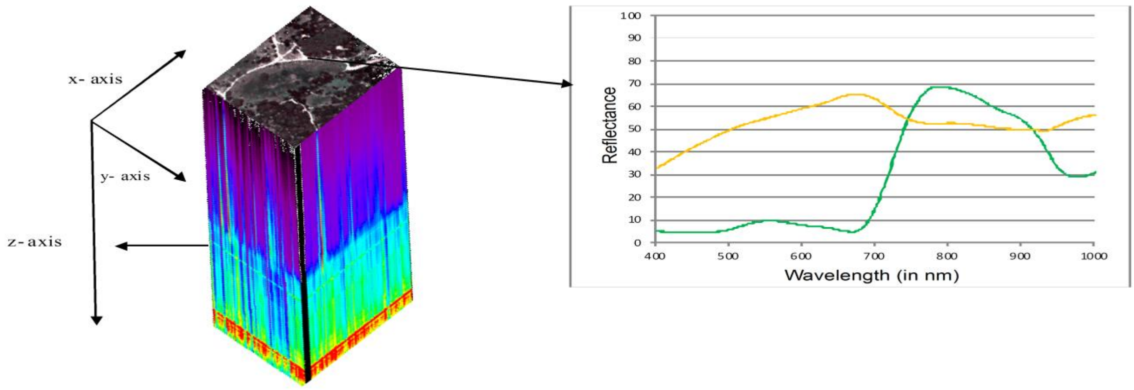

Figure 2.1 n-Dimensional hypercube representation of data (generated in ENVI 4.7), showing the spectral profile of vegetation (green colour) and sandy soil (red colour). X and Y-axis represent the spatial attributes while z-axis represents the spectral content of the data (bands).

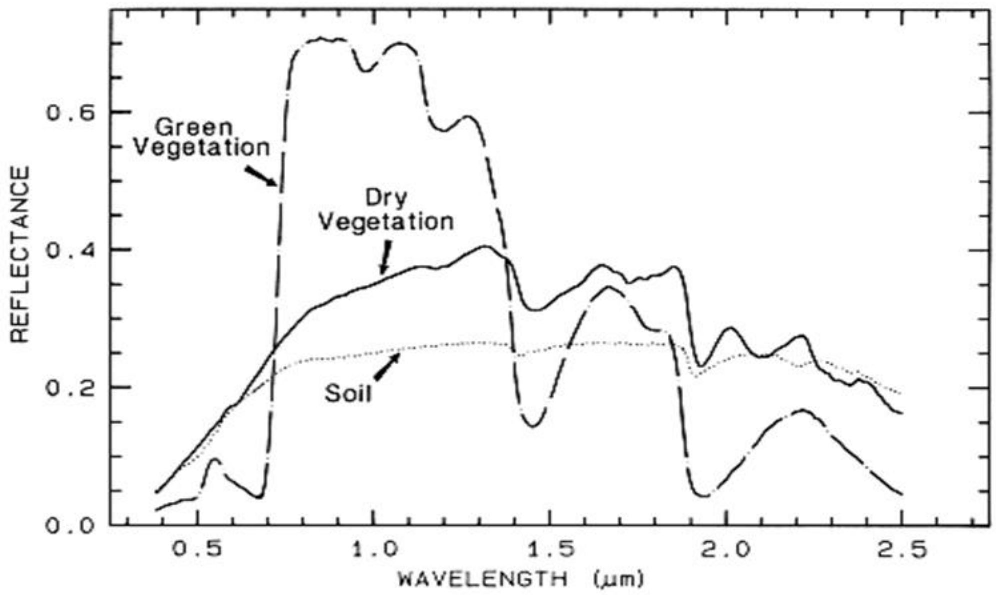

Figure 2.2 Typical spectral reflectance curves for green vegetation, dry vegetation, and soil (Source Clark 1999 Fig. 15, Adapted with the kind permission of Wiley and Sons inc.)

Figure 2.2 shows the reflectance curve of different features such as vegetation, soil and water, but hyperspectral imagers can also differentiate between the same features with different conditions like green vegetation and dry vegetation (Lillesand et al., 2004). Each feature has its own unique reflectance pattern that is characteristic to it (Lillesand et al., 2004). The shape of the reflectance spectrum can be used for the identification and discrimination of vegetation types and different features as shown in Figure 2.2 (Clark, 1999). The reflectance spectra can differentiate between different species (such as *Eucalyptus* and *Pinus pinea*) and the same species (such as *Pinus pinea and Pinus pinaster*) in various conditions. Sometimes the same species exhibit different spectral reflectance due to dry and green conditions: dry conditions have higher reflectance in the visible and NIR regions when compared to wet greener species as shown in Figure 2.2. In addition, the same vegetation type may express different reflectance spectrum profile depending on factors such as the leaf content, number of leaves and healthy tissues. The spectral characteristics of vegetation are unique and help in distinguishing different species. Spectral signature of vegetation/ tree species can be captured using radio-spectrometer, remote sensing images. These captured spectral properties enable to monitor vegetation conditions like growing or stressed stage, healthy or diseased. Monitoring of vegetation depends upon the studies of the spectral profile at different wavelengths providing the information about the pigments, water content and leaves structures. Hyperspectral imagery can distinguish the species type and thus assist in mapping different species of forest region due to narrow wavebands. Therefore, hyperspectral sensors provide high spectral resolution and have advantages when compared to multispectral images. All above properties make hyperspectral images more suitable and appropriate to discriminate various features and tree species. Thus, hyperspectral imagery can provide users a unique spectral profile of different trees by detecting differences that cannot be delivered through multispectral images.

Minor changes in mapping or classification differences with multispectral remote sensing are difficult to attain due to broad wavebands (Koch, 2010) which can be achieved with hyperspectral images. Hyperspectral data can reveal subtle differences in the spectral signatures of vegetation or ground features when compared to multispectral data (Jensen, 2000, Pearlman et al., 2003). Hyperspectral images enhance detailed forest species classifications and mapping with detailed spectral discrimination. The hyperspectral images aid the researcher by offering an accurate and detailed output of the species designation, land use classification, and height information. The robustness and usefulness of hyperspectral images can be assessed by the ability to perform a distinction between different features over the multispectral images. Thus, due to its ability to detect minor details of the ground features, hyperspectral image is selected to carry out the present research for species' classification and mapping.

The increased spatial resolution and spectral resolution of hyperspectral images has influenced various types of research like the mapping of reed weeds, coastal mapping (Chust et al., 2010, Schmidt et al., 2011), forest mapping and biomass estimation (Lefsky et al., 1999, Lim et al., 2003, Lu et al., 2012). Identifying small changes in mapping or classification differences with multispectral images can be difficult, while hyperspectral images can detect small variations due to its high spectral resolution (Koch, 2010). Contiguous spectral signatures allow the detailed analysis of the ground features using their biological and chemical properties (Govender et al., 2007). Therefore, HSI techniques provide better results for forest biomass classification and mapping with detailed species discrimination than multispectral images.

These properties of hyperspectral images discriminate different vegetation from non-vegetated features as compared to existing multispectral images (Cochrane, 2000, Ustin et al., 2004). Thus, hyperspectral has the capability to detect different features and species. Hyperspectral images were used to map and classify different forest regions, as well as discriminate species. Several studies were conducted to map tree species in tropical (Carlson et al., 2007, Clark et al., 2005), sub-tropical (Dennison and Roberts, 2003, Lucas et al., 2008, Yang et al., 2009) and temperate regions , (Boschetti et al., 2007, Goodwin et al., 2005, Martin et al., 1998, Plourde et al., 2007, Xiao et al., 2004) using hyperspectral images. Past studies have shown the use of hyperspectral data in different regions Mediterranean forest for invasive species detection (Varga and Asner, 2008, Carlson et al., 2007, Anderson et al., 2008), sand dune stabilization (Rascher et al., 2011a, Rascher et al., 2011b). Further research (Rodríguez-Echeverría et al., 2009, Marchante et al., 2003) has shown the detection of species (invasive species) among several species in coastal Mediterranean forest region using hyperspectral images.

Hyperspectral images can provide information about the different ground feature and tree species distinctively, and demarcate species and features very well. Researchers have demonstrated the future use of hyperspectral images for forest mapping and biomass estimation at precise levels when they integrate or fuse with other types of remote sensor data (Koch, 2010). Therefore, evident from the above argument, this study has included the hyperspectral images in the study of performing the identification and differentiation of different ground features including tree species. However, hyperspectral images are confronted with several constraints and limitations due to spectral mixing. In addition, boundaries between various vegetation/trees lack sharp edges and occur as smooth transitions. LiDAR can provide an overlap of structural boundaries to the hyperspectral images during the integration. Thus, LiDAR can provide support for the classification when HSI is not processed for the data redundancy. The present study also utilizes the LiDAR data for the estimation of the tree heights in conjunction with an extensive field measured data and hyperspectral analysis.

2.3 LiDAR data

2.3.1 Introduction

Light Detection and Ranging (LiDAR) is a remote sensing method that uses light pulse to measure ranges or height of the ground features on the Earth surfaces (NOAA, 2014). LiDAR is an active remote sensing technique that is used to acquire topographic data (ARSL, 2014, Hyyppä et al., 2004, Hyyppä et al., 2009, NOAA, 2014).

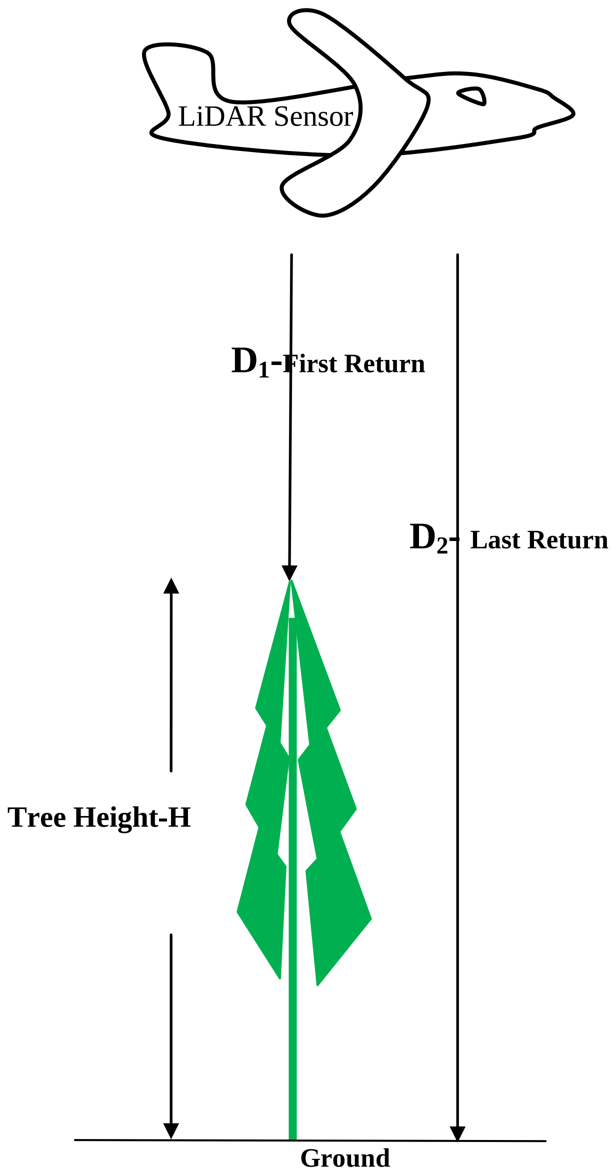

Figure 2.3 Basic of the LiDAR measurement of the tree heights, where D_1 represents a first return, and D_2 represents the last return.

Although, LiDAR system was introduced over 40 years ago as a fixed ground instrument for atmospheric particles and composition mapping (NOAA Coastal Services Center, 2012), but the first commercial airborne LiDAR system was introduced in 2001 (Flood, 2001). LiDAR technology is divided into two groups terrestrial LiDAR and airborne LiDAR. The airborne LiDAR instrument is a combination of different instruments like Laser, on board-sensor or scanner, GPS receiver, and platforms such as airplanes or helicopters. LiDAR is based on the simple concept of a laser pulse emission from the source towards the ground surface or target materials and back to the source along the orthogonal line to the flight direction (Flood and Gutelius, 1997, Chasmer et al., 2006). LiDAR techniques provide vertical and horizontal information at high spatial resolutions with high accuracies (Lim et al., 2003). Space-borne hyperspectral images may be disturbed by clouds, daylight and the night time, but LiDAR data can be acquired and operated continuously, and so has advantages over solar reflected instruments (Disney et al., 2009). LiDAR has emerged as the latest remote sensing technology with promising potential to map, monitor and assess forest information. Although expensive, LiDAR systems demonstrate the value of technology for measuring tree heights.

2.3.2 LiDAR- Types, Principle and Technique

There are two types of the LiDAR system- (a) Discrete or small footprint LiDAR and (b) Waveform LiDAR. Discrete return LiDAR records the reflected energy as points in time and space. Thus, recorded energy is quantised at amplitude intervals in discrete return LiDAR system. Discrete return LiDAR's footprint is usually small about 10 cm to 30 cm with a small divergence angle of 0.1 m-rad. (Lim et al., 2003, Zimble et al., 2003). Discrete LiDAR sensors record the times for the first return pulses (D_1) and last return pulses (D_2) that relate to hitting the top of the tree and potentially the ground respectively. As illustrated in Figure 2.3, both return pulses, i.e. first return D_1 and last return D_2, can calculate the tree height. LiDAR use in forestry is due to the ability of pulses that are reflected back from the top of the canopy to pass through it to reach the ground. Thus, the reflections of pulses from the top of the canopy, under storey vegetation, and base of the ground floor provide height information. Therefore, in the discrete return, LiDAR can estimate the ground surface as well as tree top surfaces. The generation of the ground terrain is processed from LiDAR's last return with local minima while the canopy surface requires local maxima.

Full waveform LiDAR data records the continuous signal from the energy reflected back to the sensor. LiDAR applications are based on the principle of laser ranging (Lefsky et al., 1999) and it is a means of measuring distance (height) and determining the range from a reflected laser pulse (Baltsavias, 1999, Lillesand et al., 2004). Thus, LiDAR instruments measure the total time taken by a laser pulse to travel between the sensor and target features (Dubayah and Drake, 2000, Lim et al., 2003). The precise time interval between the laser pulse emission and the backscattered pulse from the target surface is recorded (Baltsavias, 1999, Hyyppä et al., 2004). This is calculated as the product of the speed of light and the time required for an emitted laser pulse to travel. The basic equation used for calculating time using the speed of light is illustrated below (Boland et al., 2004, Baltsavias, 1999):

$$t=2\frac{R}{C} \qquad \text{Equation 2.1}$$

Where, c is the speed of light, 3 x10^8 m s^{-1}, t - Round-trip time intervals by light pulse and R - Distance between LiDAR sensor and the ground objects i.e. Range. This equation can be rearranged to calculate the range between the source and target object as follow given by (Baltsavias, 1999).This equation is modified to calculate the range and is illustrated below:

$$R=c\frac{t}{2} \qquad \text{Equation 2.2}$$

Where, c is the speed of light, 3 x10^8 m s^{-1}, t - Round-trip time intervals by light pulse and R - Distance between LiDAR sensor and the ground objects i.e. Range.

The laser pulse is converted into travel time (t) using Equation 2.2 to calculate the distance between the source and targeted objects i.e. Range (Wehr and Lohr, 1999). The aircraft position and orientation at the time of laser emission are determined using Differential Global Positioning System (DGPS) and Inertial Navigation System (INS), respectively. Thus, position and orientation information was combined with laser ranges and the corresponding scan.

Once laser pulses are emitted from the LiDAR systems, they return from the target features to LiDAR systems many times depending upon the number of features. The discrete LiDAR has a reasonably high chance of penetrating the vegetation canopy and hit the ground surface to provide ground samples. An energy pulse can be reflected from the top of the canopy, tree's trunk, branches and foliage and it can be reflected from the ground surface as illustrated in Figure 2.4. Figure 2.5 illustrates the hit on the surface by the LiDAR pulse. Tree height is measured correctly when LiDAR pulses intercept the top of the canopy (blue circle) and incorrectly, when other pulses hit the side of the tree canopy (black circle). The red circle represents the side hit of the tree by LiDAR pulses. Thus, LiDAR has power to provide accurate height of trees with its small footprint. However, there are limitation of the small footprint of LiDAR- first it may be completely absorbed by the tree top surface before it reaches the ground, and secondly it may miss the tree top surfaces as shown in the Figure 2.5 (Zimble et al., 2003). This results in an underestimation of tree heights or other ground features. Therefore, it is necessary to analyse the point spacing carefully while processing the LiDAR data for the DSM and DTM creation. This average post spacing of the points is an important part and to achieve the good results, post spacing must be at a density to support the level. It has been shown by Zimble et al. (2003) that an accurate estimate of tree height is possible with a small post spacing less than 2 m, whereas more than 2 m post spacing of the laser points will result in the less accurate estimate of tree height dispersion.

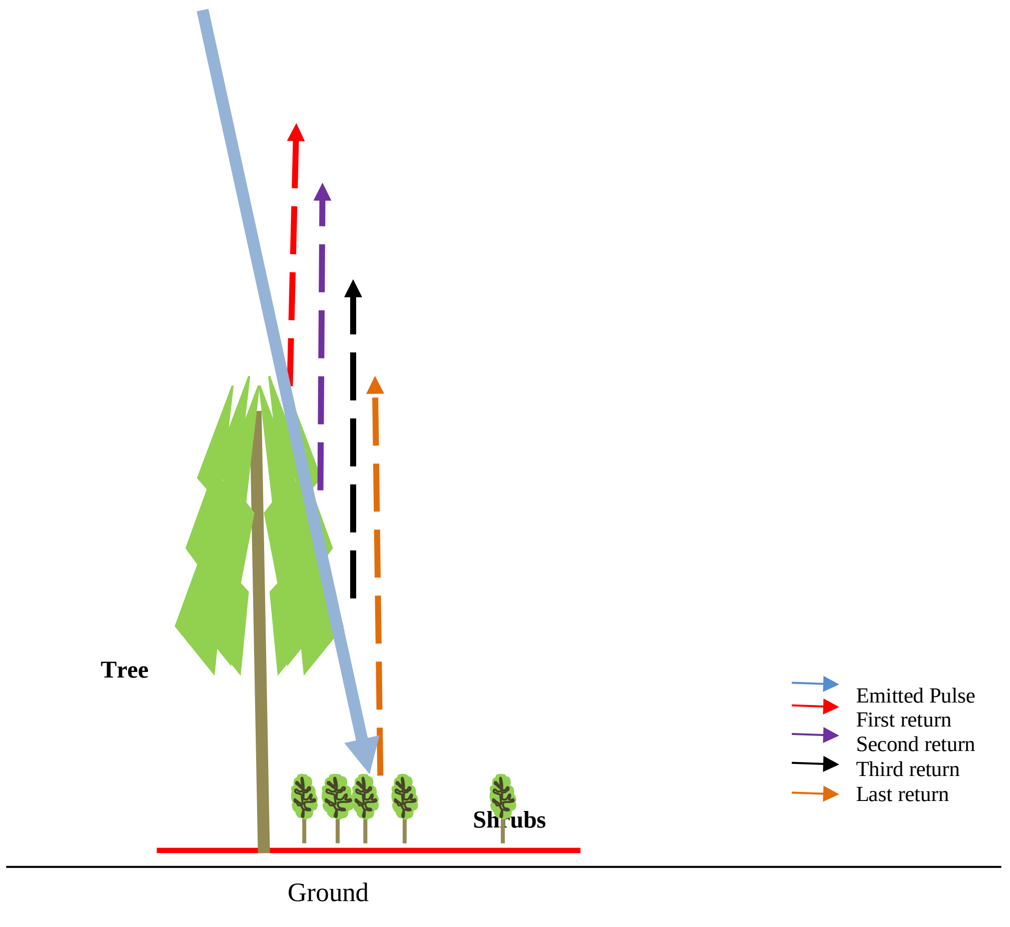

Figure 2.4 Number of pulse returns from the surface hitting the targets and the ground

Table 2.1 Details of forest structural parameters or characteristics and how they are derived from LiDAR data

Forest structural parameters or characteristics	**How it is derived from LiDAR**
Canopy Height	Direct retrieval from LiDAR
Crown cover	Direct retrieval from LiDAR
Forest crown canopy profile	Direct retrieval from LiDAR
3-dimensionalrepresentation	Direct retrieval from LiDAR
Canopy Density	Modelling and post processing of LiDAR
Canopy Cover - Above ground biomass	Modelling and post processing of LiDAR
Canopy Volume	Modelling and post processing of LiDAR
Mean stem Diameter	Modelling and post processing of LiDAR
Crown dimensions- Foliage cover	Modelling and post processing of LiDAR
Canopy Cover or Leaf Area Index (LAI)	In combination with other data
Life form Diversity	In combination with other data

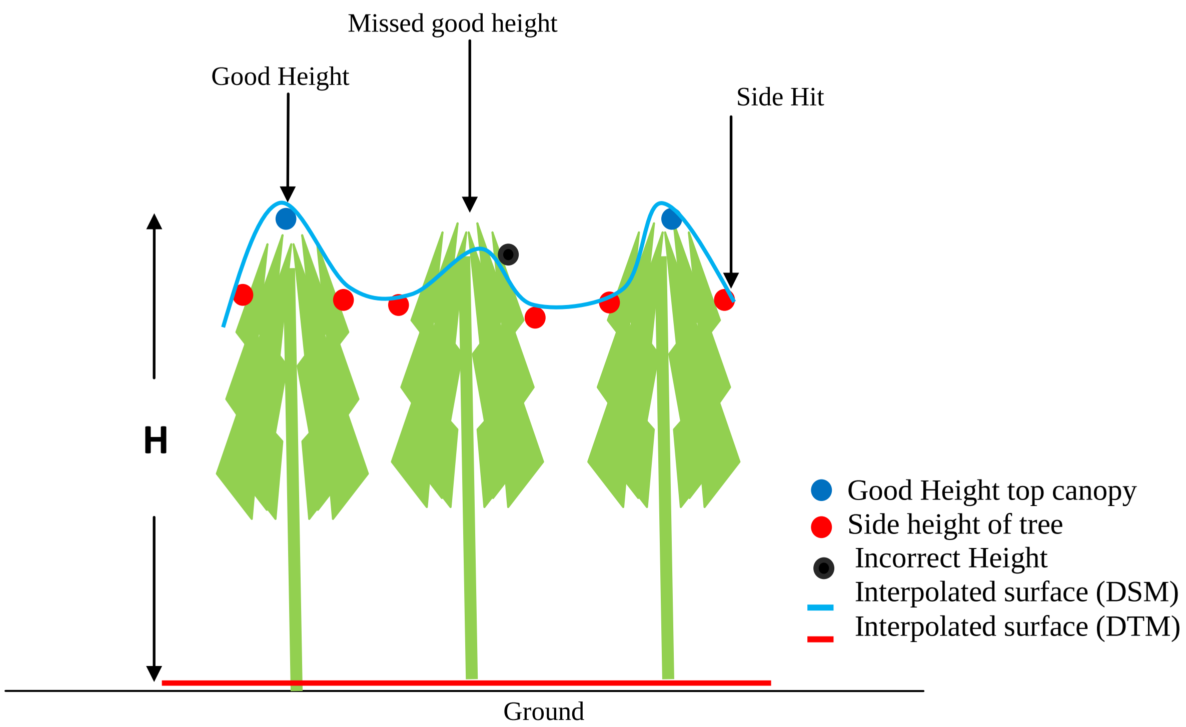

Figure 2.5 Illustration shows the discrete return LiDAR pulses sampling issues (Zimble et al., 2003)

2.3.3 Use of LiDAR and its Importance

The use of LiDAR technology in forestry research has been reported in the early 1980s (Lim et al., 2003, Van Leeuwen and Nieuwenhuis, 2010). From that time, LiDAR technology has achieved high importance in the field of remote sensing due to its accurate topographic data acquisition and promising resource for three-dimensional output (Meng et al., 2009). It is capable of providing horizontal and vertical information with accurate elevation data for both topographic surfaces and above-ground objects (Yunfei et al., 2008). Scientists used airborne LIDAR to generate more accurate and precise digital elevation models as well as terrain modelling (Flood and Gutelius, 1997, Hodgson and Bresnahan, 2004, Hodgson et al., 2005, Kraus and Pfeifer, 1998, Raber et al., 2002). However, LiDAR has found its place in several other research areas other than forestry.

The advantages of LiDAR data over other remote sensing applications (photogrammetric/stereo measurements) are that LiDAR provides relatively direct measurements of tree height (Zimble et al., 2003). However, other forms of measurements or assessment of physical properties can be inferred from vegetation amount or indices which are generated indirectly from the LiDAR data (See Table 2.1). As vegetation height acts as a function of species composition, thus vegetation height estimation forms the base of other biophysical measurements of vegetation being observed (Dubayah et al., 2000, Dubayah and Drake, 2000). Those measurements include the types of vegetation (tree, crop, shrubs) and biomass. Thus, the ability of LiDAR data to accurately measure tree heights is important because of the strong link between vegetation height and other biophysical characteristics (Dubayah and Drake, 2000). Many forests structural characteristics, which are not directly measured by LiDAR can be modelled based on these relationships.

Hence, the ability of LiDAR data to acquire accurate and high-resolution vertical structure or topographic data makes it more powerful and useful when compared to conventional topographic data acquisition methods such as photogrammetry (Baltsavias, 1999, Kraus and Pfeifer, 1998). LiDAR provides the researcher with an advantage as a replacement to *in situ* field surveying and photogrammetric mapping (Maune, 2001). The LiDAR data is used in various forestry measurements and applications. The applications of LiDAR in forestry were demonstrated in numerous studies for different purposes like terrain elevation determination, mean height and volume estimation, tree species classification, and growth (Brandtberg et al., 2003, Dalponte et al., 2014, Kraus and Pfeifer, 1998, Næsset, 1997a, Næsset, 1997b, Næsset et al., 2013a, Næsset et al., 2013b, Neigh et al., 2013, Ørka et al., 2007). Researchers have used ICESat (space borne LiDAR) for evaluating different forest structures such as forest structure and related biophysical parameters, direct measurement of the 3-dimensional canopies distribution, estimation of forest canopy height and aboveground biomass (Lefsky et al., 1998, Lefsky et al., 1999, Lefsky et al., 2002, Lefsky et al., 2005).

LiDAR use has become prominent and widespread within forestry research and the methods used to extract vegetation heights have improved over time. The ease of LiDAR data processing has been able to achieve more accurate results of forest structural parameters such as height (Hopkinson et al., 2004, Næsset, 2002). Thus, LiDAR data is utilised to derive several forest inventory measurements and information either directly or indirectly through modelling (See Table 2.1). Though LiDAR has an increasing number of forestry applications such LAI, *f*cover, biomass, *f*par, it is not possible to derive information at the species level or the ground feature level using LiDAR data alone.

However, there are limitations of LiDAR datasets over other RS data. LiDAR data is expensive to acquire due to a high flight cost, editing and processing can be time-consuming (Millette et al., 2010) and specific software is required for the processing. However, the advantage is that it canbe used in inaccessible terrains like mountains, hilly regions, and dense forests (McGlone, 2004) with accurate and timely acquisition. In a traditional field survey, measurement of the tree data is tedious and time-consuming while it is easier with LiDAR data, so LiDAR proves to be beneficial and significant in the research. LiDAR can acquire data more quickly and over an extensive area when compared to the field survey. In addition, it can deliver results for different forest characteristics like canopy height, canopy density, and canopy cover as illustrated in Table 2.1) from a single data when compared to the field survey measurements. In a field survey, when estimating the different forest characteristics, several parameters are required to record and measure the various data like stem width and height for getting the desired results. LiDAR data is used to derive or extract information at the tree level, but it is not very useful for information at the species' level of the study area. It can help to estimate the height of trees, but is not able to provide information regarding the species' classification. Thus, this study uses hyperspectral images along with LiDAR data to overcome the above problem at species level that can identify and discriminate the tree at a species' level and can identify different ground feature with subtle information.

2.4 Data Fusion

2.4.1 General Introduction and Concept

Data fusion is the process of integrating more than one image using different algorithms to generate a new composite image which delivers better-enhanced spatial and spectral information (Dong et al., 2009, Karathanassi et al., 2007, Pohl and van Genderen, 1998). Fusion process provides more information and achieves improved results for decision-making (Hall and McMullen, 2004). The objective of multi-image fusion is aimed to extract more information than can be derived from an individual or a single sensor data alone (Pohl and van Genderen, 1998). Fusion of multi-sensor data subject is still in its infancy stage, and there is much more to explore fusion steps (Lewis and Hancock, 2007). The individual images vary in properties that are spectral, spatial and temporal resolution and therefore provide a complete understanding of the target features through fused image. Data integration techniques have been applied to RS datasets for many reasons according to user need and requirements which include the sharpening of images, adding information, adding spectral characteristics and enhancing individual information to fused datasets. Thus, most common uses of fusion techniques are to enhance the image quality and to sharpen visualisation of the image. Therefore, image fusion improves the capabilities and performance of data and enhances the image interpretation and evaluation capability better than individual data alone. Thus, data integration is nowadays a popular geospatial technique to combine data from two different sources with different information.

With the advancement of RS technologies and the availability of large amounts of RS products such as multi-sensor images, multi-temporal datasets, and different types of data, there emerge many opportunities and methods which can quickly try to solve the purposes of different research areas in the remote sensing field. Researchers (Pohl and van Genderen, 1998, Shen, 1990) were interested in developing image integration techniques to harness the attributes of complicated multi-source, multi-sensor data to full information.The use of individual data is not preferred nowadays for more accurate and precise mapping or image interpretation of the study regions due to spectral mixing or due to underlying features. In such cases, data integration or data fusion seems to be a boon for mapping or feature interpretation with hyperspectral images and covering 3D structure from LiDAR datasets. Authors have worked on the data integration or fusion of either multispectral images with LiDAR data or hyperspectral images with LiDAR data (Goodenough et al., 2005, Frank et al., 2010, Lach et al., 2009, Rottensteiner et al., 2007, Sohn and Dowman, 2007).

Many studies have revealed that the best results were achieved with a fused or integrated dataset rather than a single data source (Banskota et al., 2009, Dalponte et al., 2008, Dees et al., 2006, Maltamo et al., 2006, Moghaddam et al., 2002, Pang et al., 2009, Straub et al., 2009, Treuhaft et al., 2003, Treuhaft et al., 2004). The best result is only due to the information contained in the types of data being used in the studies like spectral information from optical data, highly continuous spectral variations from hyperspectral and height/intensity information from LiDAR data. Data fusion provides an underlying platform for future research or studies with different techniques and applications. Synthetic aperture radar used along with hyperspectral images, multispectral with LiDAR data, and LiDAR data with hyperspectral images for various applications. The applications include forest biomass (Koch, 2010), forest species (Ke et al., 2010), woodland species and composition (Hill and Thomson, 2005), geomorphology of estuaries (Millette et al., 2010), coastal dune vegetation (Kempeneers et al., 2009), tree species in urban region (Sugumaran and Voss, 2007) and topographic signature of vegetation development (Bertoldi et al., 2011). Data integration of different spatial resolution has been used for various purposes, illustrating the benefit of data integration for future studies in any field.

2.4.1.1 Different levels or Methods of Data Fusion

Integrating different data is achieved at four different levels: the signal level, the pixel level, the feature level and the decision level (Pohl and van Genderen, 1998). These levels are according to the stage at which two datasets are integrated to each others (See Figure 2.6). This flowchart is shown with two data- HSI and LiDAR as an example here.

- Signal level- At this level, both the datasets are integrated during acquisition at signal level.
- Pixel level -The integration of different data sources required to be co-registered with each other and geocoded. This data integration is performed on raster data where both the datasets are integrated at pixel level merging their measured physical parameters.
- Feature level- As the name suggests, this type of fusion is performed on features extracted from both datasets. Features in the form of recognised objects were extracted from the data and fused together to perform analysis. Thus, both features correspond to the characteristics of the individual datasets.
- Decision level- At this level of fusion, the results were produced and analysis was performed individually. Then the results were analysed and interpreted at a common level to emphasize and elucidate added benefit of two different interpretations generated from two data sources. Finally, the decisions of the study were produced using the standard results of the two datasets.

Table 2.2 Fusion of various types of datasets

Data sources	**References**
Multispectral -Multispectral data	Millette et al., 2010
Multispectral-Hyperspectral data	Xu and Gong, 2007
Multispectral-LiDAR data	García et al., 2011, Tonolli et al., 2011
Multispectral-Radar data	Moghaddam et al., 2002
Hyperspectral- radar data	Koch, 2010, Treuhaft et al., 2003
LiDAR –Radar data	Bergen et al., 2009, Sun et al., 2011, Treuhaft et al., 2009, Tsui et al., 2013

Data fusion can follow different approaches, including multi-sensor data fusion and multi-temporal data fusion (Gilmore et al., 2008). Multi-sensor data fusion uses different datasets for image fusion (See Table 2.2). Data Fusion also includes the integration of different datasets differing in spatial, temporal, and spectral resolution. These four fusion levels can provide more enhanced results with a selection of appropriate fusion algorithms, when applied to various data sources. Therefore, it can be concluded that data integration furnishes better understanding of the results produced from two different data sources irrespective of the fusion at any level.

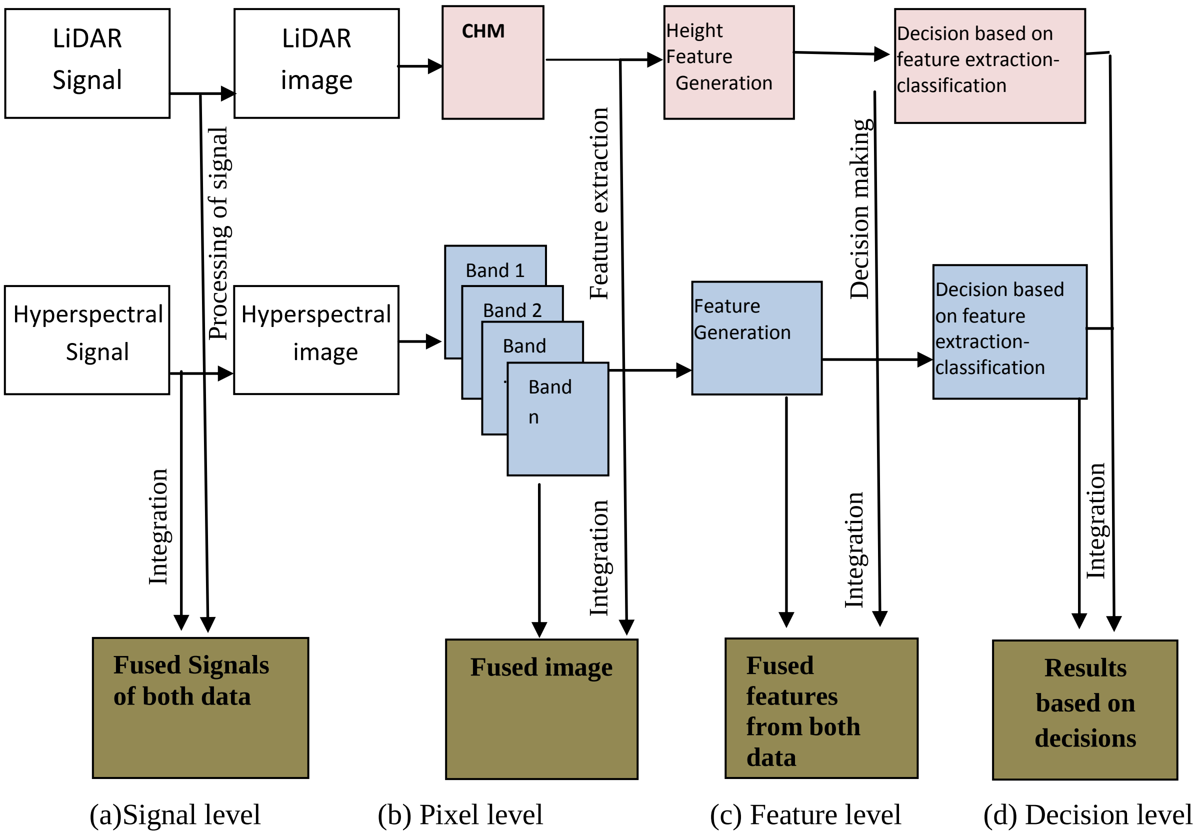

Figure 2.6 Different RS Data Integration Level Flowchart, showing different level of image fusion (a) Signal level, (b) Pixel level, (c) Feature level and (d) Decision level fusion

2.4.1.2 Initiation of Fusion Work

Initially, the researchers integrated the multispectral images and digital photographs with LiDAR for different research applications. The use of LiDAR with multispectral and digital photographs was manifested by different work like forest tree information extraction (Straub et al., 2009), wood volume estimations (Dees et al., 2006, Maltamo et al., 2006), leaf area indices and canopy cover (Dubayah and Drake, 2000, Mundf et al., 2006), Biomass and woodland species mapping and classification (Hill and Thomson, 2005, Ke et al., 2010, Swatantran et al., 2011), forest canopy fuel (Erdody and Moskal, 2010), and wetland vegetation (Elhadi et al., 2009). The fusion approach uses LiDAR data and photographs for forest inventory and monitoring purposes (Tickle et al., 2001). The uses of LiDAR and multispectral images have been used extensively in forestry for locating individual tree, mapping tree height, and species in the deciduous forests (Koukoulas and Blackburn, 2005). Pang et al. (2009) showed that results based on the integration of LiDAR and hyperspectral image data sources were superior when compared to individual data source.

2.4.1.3 Purposes and Importance of the Data Fusion

Various researchers have worked with different fusion techniques and algorithms for the purpose of enhancing the image quality and collecting more information. Example of this research includes Brovey Transformation, Wavelet Transformation, IHS, forward- reverse PC component transformation of two datasets. To achieve higher accuracy with the increasingly sophisticated satellite or airborne data, data fusion has been devised as a relatively new technique to exploit multisource data (Gamba and Chanussot, 2008).

The role of data fusion techniques has been demonstrated for different usage and functions. To accomplish a different design of research, certain forms of fusion techniques have been used to merge multi-source images. The purpose of data fusion includes sharpening of the images, enhance images, and improve classification results. The synergistic use of LiDAR and additional data sets (such as reflectance measurement of hyperspectral image) can achieve a good and most accurate results (Hese et al., 2005).

2.4.1.4 Limitations of Optical Data Integration

However, multispectral images have certain limitations in regards to spectral ranges that can be achieved only through the introduction of hyperspectral dataset. Therefore, there is the need to postulate the integration of hyperspectral data with LiDAR for various remote sensing purposes. The limitations of individual optical remote sensing or LiDAR data are overcome by the integration of a dataset with another type of data like LiDAR and hyperspectral images. Data integration will result in improvement in accuracy assessment and the spatial variation identification along with coastal sand dune vegetation mappings. As evident from the limitations and advantages of fusion approaches, this study aims to use hyperspectral and LiDAR data for fusion purposes.

2.4.2 Advances in Data Integration with Hyperspectral and LiDAR Data

As discussed earlier, fusion of multisource multispectral images proved beneficial for the classification assessment, and accurate results compared with individual image. Data fusion can provide better results with the introduction of hyperspectral images rather than multispectral images (as discussed in section 2.4). This discrimination is only due to the ability of hyperspectral images to detect small variations in the spectral reflectance in contrast to multispectral data. Targets were also put in place to achieve success in different terrestrial applications for which the LiDAR and hyperspectral data were fused together (Corp et al., 2009). Effort has been made to fuse multiple datasets for the creation of radiometrically accurate scenes for research purposes (Lach et al., 2009). The radiometrically accurate scene will help in enhancing the quality of research work and accuracy of the output. LiDAR and HSI data have been used to map tree species in the urban environment using fusion approach (Alonzo et al., 2014). In ecosystem studies, data integration techniques have played a pivotal role in ecological modelling (Patenaude et al., 2008), characterising forest environment (Niemann et al., 2007) for invasive species detection (Asner et al., 2008), spatial and structural patterns of species in forest (Anderson et al., 2011), temperate forest inventory (Anderson et al., 2008), canopy chlorophyll concentration estimation (Thomas et al., 2008), and spatial modelling for *f*PAR and photosynthesis of boreal mixed forest (Thomas et al., 2006, Thomas et al., 2009).

Researchers have used the fusion approach mentioned below, to quantify the forest structural parameters and its individual parameters at leaf levels like tree species mapping, classification, and stem diameter assessment. Data integration techniques were carried out in forestry or vegetation studies for various applications like LAI, Clumping Index (CI) and comparison between them (Lange and Solberg, 2008, Pang et al., 2009, Thomas et al., 2011), forest biomass mapping (Lucas et al., 2008, Swatantran et al., 2011), above ground biomass mapping (Clark et al., 2011), species distribution mapping (Jones et al., 2010), tree species classification (Liu et al., 2011, Puttonen et al., 2010), tree species identification in urban environment (Sugumaran and Voss, 2007), tree stem diameter estimation (Dalponte et al., 2009a), and species level assessment in savannah ecosystem (Sarrazin et al., 2010). LiDAR and HSI images were fused to achieve the profile of morphological attributes (Pedergnana et al., 2011). Even landscape level studies used fusion approach to perform landscape studies like forest classification, physical habitat classification and forest fuel mapping. This work involves complex forest classification (Dalponte et al., 2008), physical habitat quantification (Hall et al., 2009), fire fuel mapping (Varga and Asner, 2008) and the mapping of reedbed habitats (Onojeghuo and Blackburn, 2011). The fusion techniques were also applied in forest fire research with different fields like wildfire characteristic prediction (Koulas, 2009), fire fuels in volcanoes (Varga and Asner, 2008), forest information and vegetation management (Goodenough et al., 2008), and land cover management for fire management (Koetz et al., 2008). In forestry and vegetation, chlorophyll plays very significant role in productivity, data fusion technique have been used to estimate canopy chlorophyll content (Thomas et al., 2006), tree canopy structure (Miller, 2001), and how canopy structure affects the canopy reflectance (Niemann et al., 2005). It is confirmed that data integration has been used in different parts of forestry research such as LAI, biomass mapping, above ground biomass, canopy structure, tree species identification, species distribution mapping, stem diameter estimation, and forest structures. Therefore, fusion approach provides ample research opportunities in different fields of the forestry research; it can also be said that none of the research fields or their parts are untouched by the data fusion approaches.

2.4.3 Classification Results with Fused Hyperspectral and LiDAR Data

Various fusion studies have been carried out using airborne hyperspectral and LiDAR data for the classification of tree species. Object-oriented classification techniques with fused LiDAR and hyperspectral data were incorporated for tree species identification (Sugumaran and Voss, 2007). Puttonen et al. (2010) used the Support Vector Machine

(SVM) classifier for tree species classification using LiDAR and hyperspectral data. The research proves that the reflectance values range from 550- 580 nm and red-shift ranges are suitable for tree species study. Very small samples are taken from the region with mixed growth of deciduous and coniferous species. The selection of parameters depends on the shape and reflectance of the tree species in the study of the tree species classification. About 70% classification accuracy was achieved for individual tree species, with four combined-parameters such as shape single as well as paired and reflectance single and paired. Samples were taken from young trees, with small numbers, this affected result accuracy with mixed wavelengths. Thus, they stressed on the utilization of vegetation indices like NDVI, EVI that use reflectance (Myneni et al., 1995) in the studies. They have decided to include precise wavelength and spectral range with field information can be helpful in classifying tree species more accurately in future studies (Myneni et al., 1995).

One of the potential applications of hyperspectral and LiDAR data was demonstrated by Kaasalainen et al. (2010) for object classification. They used hyperspectral information with topographic attributes for automatic object classification. They proved this as a promising method for object classification. Frank et al. (2010) worked on a multi - sensor approach for vegetation management to utility corridors. The techniques SVM (Support Vector Machine) and SAM (Spectral Angle Mapper) were applied to discriminate vegetation species. They used LiDAR for extraction of power line, but no attempt has been taken to extract it from hyperspectral imagery. The comparison results were shown by calculating overall and kappa coefficient from the techniques mentioned above (SAM and SVM). Elaksher (2008) focused on coastal mapping using hyperspectral and LiDAR based digital elevation models. The geometric measurements were provided by LiDAR data and spectral information (discrimination between different features) from hyperspectral imagery during the study of the coastal mapping. Here LiDAR data and hyperspectral imagery were integrated to perform coastal monitoring. The result gave a 93% average detection rate of coastal line for the study, where positional accuracy is data dependent (Elaksher, 2008).

He et al. (2011) studied the importance of hyperspectral remote sensing to map and track the plant invasions. These researchers tried to achieve spatial, spectral and classification accuracies with time series analysis of an invasion (He et al., 2011). They discussed the future importance of hyperspectral data for promising research in invasive species mapping, spread and invasion risk analysis. It is possible only with the merging of hyperspectral and field sampling information. Ground information and hyperspectral profiling can provide reliable and accurate information for invasive species monitoring and mapping extent. Future work may include spectral profiling of invasive species using information integration from field sampling, chemical analysis, and laboratory spectrometry. Thus, it can be stated that all these parameters, when combined with LiDAR, can bring results that are more fruitful in coming days for different research fields.

One of the studies, where parcel based classification was performed using integrated hyperspectral and LiDAR fused data for complex woodland mapping (Hill and Thomson, 2005), focuses on the potential of data integration technique. In this study, field data has been incorporated with remote sensing data. The incorporated field data contained structures and composition of the species that were acquired for performing classification using remote sensing data, as well as the interpretation and validation. They used spectral information from HyMap imagery and canopy height details from LiDAR data for woodland mapping and classification. A segmentation algorithm was applied after performing PCA on the HyMap imagery for classification. PC1 and PC2 were used with LiDAR derived CHM data for the segmentation process that is further processed for unsupervised classification. Resultant classes were labelled with field-collected data for species-structure relationship. LiDAR and hyperspectral integration achieved better accuracy in tree species classification (Puttonen et al., 2010) and species distribution mapping (Jones et al., 2010) than when using individual data. For this reason, the advantages and benefit of the fusion methods can be observed at the stage, when one required accurate and reliable results.

This above argument is the reason for using HSI as well as LiDAR derived CHM in the present study of classification and mapping. The hypothesis behind the fusion of hyperspectral and LiDAR data is that both data contribute parameters together simultaneously. Hyperspectral images provide the spectral characteristics of the different tree species and ground features whereas LiDAR data provides the structural parameter i.e. tree heights to the fused image. The discussion, about reducing data redundancy, can be seen in Chapter 4 while contribution and feasibility of the data fusion can be seen in Chapter 5. Therefore, using the hyperspectral images and LiDAR data, this thesis aims to classify the reduced dimensionality hyperspectral images and incorporate canopy height with hyperspectral image to look after the improved classification accuracy.

2.5 Mediterranean Forest

2.5.1 General Overview

Forests are dynamic in nature and are constantly changing through a series of succession stages during which species composition changes within the forest (Binelli et al., 2000, Chaturvedi et al., 2011, Lau et al., 2003). Different parts of the world have different types of vegetation and forest (Olson et al., 2001). The Mediterranean regions are generally located along the west coasts of oceans, the Mediterranean Sea or running along the rugged hills (Bolle, 2003, O'Hara, 1994). Thus, the Mediterranean basin is characterised by plains, low elevated hills, large topographical variation in coastline, and typically represent the Mediterranean forests. The Mediterranean region constitutes a unique combination of terrestrial, freshwater and marine ecosystems, due to its distinct climatic conditions (Palahi et al., 2008).

Mediterranean forest zones lie in mid-latitudes at 30º-45º north or south of the equator as shown in Figure 2.7 (Hobbs et al., 1995, Scarascia-Mugnozza et al., 2000). Figure 2.7 represents the climatic potential for the existance of the Mediterranean region in the world, and these ecofloristic zones are based on the temperature regime and vegetation regime (FAO 2000). Similarly, Figure 2.8 represents the climatic potential for the Mediterranean climatic conditions in the European countries. Mediterranean forests represent natural, aesthetical resources and are sensitive to disturbances through natural and human pressures (Carter, 1988, Hanson and Lindh, 1993, Marchante et al., 2003, Swift, 1968). Mediterranean forests are quite fragile and are also very vulnerable to numerous problems (Allard et al., 2013) like forest fires (Alexandrian et al., 1999, Vélez, 1982, Vélez, 2002), invasive species, water depletion (Forrester et al., 2010), deforestation (Allard et al., 2013), degradation, soil erosion and over-exploitation (Carter, 1988, Hanson and Lindh, 1993, Palahi et al., 2008, Swift, 1968).

The Mediterranean basin is sensitive and vulnerable to an invasion of alien species (Gassó et al., 2009, Gritti et al., 2006, Gutierres et al., 2011, Marchante et al., 2003, Rascher et al., 2011a, Thuiller et al., 2005) particularly along the coastline (Chytrý et al., 2009, Marchante et al., 2003). Forest fire is also dominant in Mediterranean forest, causing much destruction (Laneve et al., 2006, Naveh, 1974). Pristine ecosystems are becoming rare due to these problems especially along the coastline in Portugal (Marchante et al., 2003). Thus, both plant invasion and forest fires interfere with the healthy ecosystem affecting its structure and functionality.

Table 2.3 Different forest characteristics in Mediterranean region and other continental regions of the World

Area	**Primary Forest (1000 ha)**	**Modified Natural (%)**	**Semi-natural (%)**	**Productive plantation (%)**	**Protective plantation (%)**
Africa	0.01	66.2	7.5	9.1	17.2
Asia	8.9	57.8	7.0	17.2	9.2
Europe	2.0	36.4	52.7	8.1	0.6
Total Mediterranean	2.8	42.4	41.7	9.5	3.5

(Source:Scarascia-Mugnozza and Matteucci 2012)

Table 2.4 Forest area in the some of the Mediterranean countries in 2010

Country	**Forest**		**Other wooded land**		Total land area (1000 ha)	% of total forest area in Mediterranean countries*
	Forest area (1000 ha)	% of the land in Forest cover	Other wooded land (1000 ha)	% of the land in wooded land		
Spain	18173	36	9574	19	49919	21
France	15954	29	1618	3	55010	19
Turkey*	11334	15	10368	13	76963	13
Italy	9149	31	1767	6	29411	11
Morocco*	5131	11	631	1	44630	6
Bulgaria	3927	36	0	0	10864	4.6
Greece	3903	30	2636	20	12890	4.6
Portugal	**3456**	**38**	**155**	**2**	**9068/9221**	**4**
Croatia	1920	34	554	10	5592	2.2
Slovenia	1253	62	21	1	2014	1.5
Albania	776	28	255	9	2740	0.9

(Source: Allard et al.2013, FAO 2010)

*Note: Mediterranean countries constitute the above European countries and other European countries like Bosnia and Herzegovina, Montenegro, Serbia, Asia -Cyprus, Israel, Lebanon, Syrian Arab Republic, Turkey, Africa-Algeria, Egypt, Libya, Morocco, Tunisia, and Jordon and others) Morocco and Turkey were included as they contribute 6 and 13 % of total forest area (to show consistency in the order).

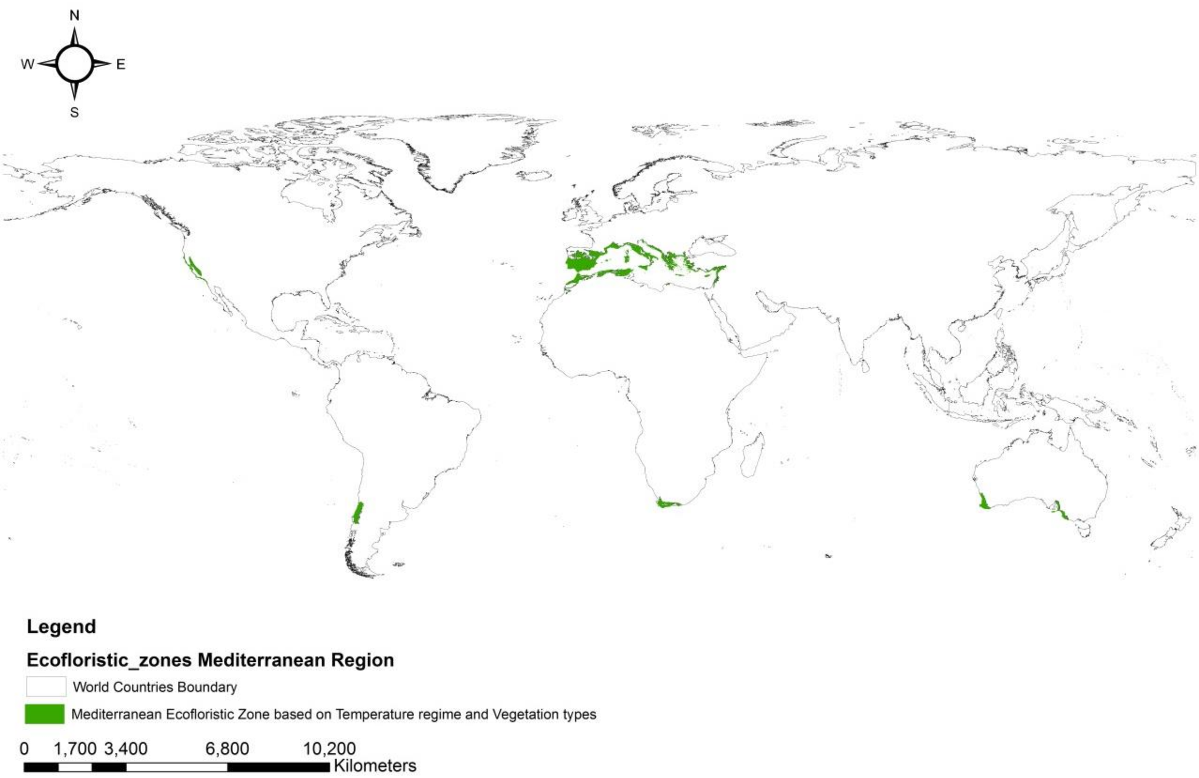

Figure 2.7 Extent of Mediterranean eco-floristic zones based on their temperature regimes and vegetation types (Source: FAO 2000 adapted from Ruesch, Aaron, and Holly K Gibbs 2008)

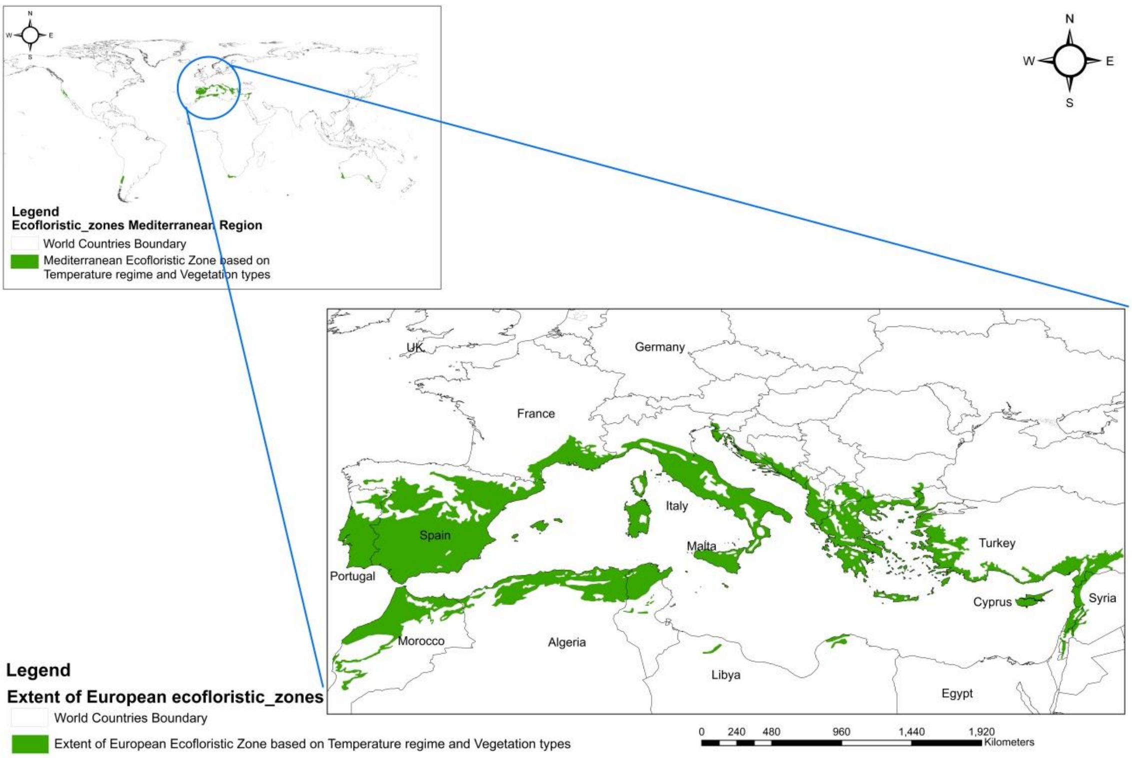

Figure 2.8 Extent of European Mediterranean eco-floristic zones based on their temperature regimes and vegetation types (Source: FAO 2000 adapted from Ruesch, Aaron, and Holly K Gibbs 2008)

2.5.2 Present Status of the Mediterranean forest

The Mediterranean region is termed as ‘the Cradle of Europe’ and has spread into parts of the Europe including Portugal (FAO, 2001, FAO, 2003). The Mediterranean region encompasses only 12 member states of the European Union namely Albania, Bosnia and Herzegovina, Croatia, Portugal, France, Spain, Italy, Slovenia, Greece, Malta, Cyprus, and Serbia as shown in Figure 2.8 (Data Basin, 2014, Lieutier and Ghaioule, 2005, Sundseth, 2009). Figure 2.7 represents the extent of Mediterranean forest in the world and Figure 2.8 represents the forest in the European Union, Africa and Asian countries.

Forest area

Mediterranean forests represent 2% of the world forest area as shown in Figure 2.8 (Fady-Welterlen, 2005), occupying merely 1.5% of the total wooded surface of the planet (M'Hirit, 1999). Table 2.4 displays the status of forestry and another land areas in 2010. It represents the forest area and its percentage, other wooded land, total land area, and the percentage of total forest area in Mediterranean countries (FAOStat, 2012). This represents 2% of the world’s forest area (4033 million ha) in 2010 (Allard et al., 2013) which is distributed unevenly over the Mediterranean basin covering different countries in Asia, Africa, and Europe as shown in Table 2.3 (FAO, 2010). Turkey, Spain and France covered more than 50% of the total forest area (as shown in Table 2.4 and Figure 2.7). Portugal has shared a contribution of almost 4% of Mediterranean forest. Table 2.3 illustrates the percentage and the contribution of different Mediterranean forests in world continents whereas Table 2.4 represent the share and contribution of European countries.

2.5.3 Climatic Conditions of the Mediterranean Region

The Mediterranean climate is mainly confined between 30° and 45° north or south mid-latitudes at the west coast of the continent in the European Mediterranean basin (Bolle, 2003, O'Hara, 1994, Scarascia-Mugnozza and Matteucci, 2012). The Mediterranean region is mostly confined to narrow coastal belts (Bolle, 2003) with frequently parallel rugged mountains that influence and modify climatic patterns in Mediterranean forest regions (O'Hara, 1994). The climate of the Mediterranean region is characterised by rainy winters and dry summer, with a high soil-water deficit condition especially in summer (Bolle, 2003, Gildemeister, 2004).

Mediterranean climate varies with the regions and is characterised by warm to hot dry summers and mild winters. It experiences high sun intensity due to clear and cloudless skies; low humidity also contributes to the high rate of evapotranspiration rates. The rain occurs in the late autumn, winter and early spring, but the rainfall patterns and amounts are variable, precipitation is higher in the Europe and lower in the Africa. Annual rainfall varies from 100 mm to 2500 mm and the average temperature ranges from 5-20 °C (O'Hara, 1994). The Mediterranean climate in winter has an average temperature below 15°C. There is a significant variation in total rainfall year-to-year and, occasionally, violent precipitation events may occur in combination with dry winds may favour the spread of forest fires (Vélez, 1982, Vélez, 2002). Precipitation is primarily from rainfall though sometimes coastal fog and light snowfall contribute to the precipitation of the Mediterranean region. At sea level, winter temperatures occasionally go below 0 °C (Scarascia-Mugnozza and Matteucci, 2012). Thus, the special characteristics shown by Mediterranean forests are hot-dry summers, mild, rainy winters followed by rainfall in winter as well as spring seasons. This region faces a violent precipitation and dry winds that favour the occurrence and spread of forest fires.

2.5.4 Mediterranean Plant Diversity

Mediterranean forests constitute a unique world natural heritage, as it has high genetic and biological diversity (Fady-Welterlen, 2005). Mediterranean forests has high species richnes and harbour about 25,000 species of vascular plants. Mediterranean forest has 201 endemic species out of 290 indigenous tree species and out of 25,000 vascular plants, almost 50% are endemic species (Scarascia-Mugnozza and Matteucci, 2012). Mediterranean forests have abundant plants and animals, represented by high genetic variability, species richness, and species diversity (Cowling et al., 1996, Fady-Welterlen, 2005). Mediterranean forest has habitat place of about 20% the Earth's plant diversity (Fady-Welterlen, 2005, Packham et al., 2004).

Mediterranean forests are composed of conifers, particularly *Pinus pinea*, *Pinus pinaster Juniperus* species and broad leaves, evergreen and deciduous such as *Quercus suber* and *Quercus ilex* (Scarascia-Mugnozza et al., 2000). Non-native species have been introduced in the forest lands, notably in the last century, such as *Eucalyptus globulus, Acacia longifolia* and various cypresses species (Costa et al., 2000). Mediterranean forests are an assemblage of different animal and plant species representing biodiversity with very high genetic variability inhabiting coniferous and broadleaf species. In the Mediterranean zones, along with Mediterranean forests, other vegetation types such as savannah, shrublands and grasslands show dominant presence. These Mediterranean regions are covered with forests, grassland, scrub, sand dunes and lagoons. Mediterranean forest is an open type forest structure that allow the growth of understory vegetation such as alien species (*Acacia longifolia*), herbs, shrubs and bushes (Rascher et al., 2011a).

Forests play a significant role in the lifestyle of inhabitant residing in and around the Mediterranean peoples. Their livelihood mostly depends on the products and services of the forests (Palahi et al., 2008). However, fragile status of the forests and several threats to them accelerates degradation and clearance. The main causes of forest deforestation and clearance are development pressure, population growth, unorganised land use policies. In turn, forest is losing its aesthetic values and risk to its existence in current form. To preserve and maintain these resources, World Wildlife Fund has classified the Mediterranean forests in the Global 200 categories (Olson and Dinerstein, 1998, Myers et al., 2000). The Global 200 have unique, valuable and endangered species of the world. These resources need to be preserved to maintain the heritage, aesthetics values and integrity of the biosphere.

2.5.5 Biological Importance of the Forest

Forests play a significant role in controlling global carbon and climatic cycle (Dixon et al., 1994, IPCC, 2007). Forests contain about 77% of the total global carbon reserve in the form of vegetation biomass (Dixon et al., 1994, IPCC, 2007). Mediterranean forests represent a diverse species richness representing high species diversity and genetic variability (Specht, 1988). Forests regulate the soil and water resources, which are likely to be affected by changes in global climatic conditions and atmospheric composition due to deforestation. Mediterranean forests provide several products and services to inhabitants (Blondel and Aronson, 1995, Scarascia-Mugnozza and Matteucci, 2012). Watershed protection, landscape quality, soil conservation, carbon sequestration and recreation resources are some of the services that are hardly recognised (Croitoru, 2007, Merlo and Rojas, 2000). Changes in forest system will have an impact on socio-economic status, and also influence above services (Winnett, 1998). Their conservation and appropriate management have crucial effects on the sustainability of water resources. Mediterranean forest in Portugal is confronted with forest fire (Américo and Mendes, 2005), deforestation and degradation (Palahi et al., 2008). Forest fires are mainly because of the monoculture of highly combustible species like Pine and Eucalyptus, the oil of which are highly flammable (Gomes, 2006, Vélez, 1982, Vélez, 2002). Harsh predictable climatic condition with severe socio-economic condition led to over-exploitation of Mediterranean forest (Thirgood, 1981). Forest fires alone destroy 1% of the forest per year than any other causes or threats (Pagliani, 2001). Thus, forest fire threat and chronic water shortages associated with ground water decline are acting as primary factors of destruction of the Mediterranean forest resources (Laneve et al., 2006). All these conditions will have an adverse effect on the forest tree species and their distributions of the Mediterranean forest.

Mediterranean forests are under tremendous pressure from humans, due to tourism and the need for forest products (Barbero et al., 1990, Davis and Richardson, 1995). These forest products include timber, oil, resins, gum, cork, fruits, medicinal plants, honey, wild flowers,aromatic plants, edible fungus,agroforestry and tourism planet (M'Hirit, 1999). In addition, this pressure is followed by problems such as soil erosion and the degradation of the valuable habitats (Isik et al., 1997). For this reason, an important step should be taken to collect information of forest species, their spatial extents and distribution in the region. Different species have different tolerant limits and some species help in promoting the forest fire with their supplement oil acting as fire fuels. The classification of different species is in need to take significant steps during the fire outbreak and approaching the species that act as a fire promoter to stop or prevent a fire from further spread. Therefore, due to the above situations, Mediterranean forest can be seen as a regional test area for global change study for many research purposes (Palahi et al., 2008, Scarascia-Mugnozza et al., 2000). Species and the ground feature information in forest research provide environmental parameters that may be significant and serves knowledge on climate change such as CO_2 level, biomass, and deforestation. This information is of particular importance in relation to land -use /land cover, changes in land use, and forest activities (Goodenough et al., 2001, Rosenqvist et al., 2000). Thus, regional operational forest species and ground features mapping and classification is a challenging research theme to enable an understanding and monitoring of forest and its environment.

Thus, the above review of the literature has concentrated mostly on the hyperspectral and LiDAR characteristic as well as the advantages of using them in the present research in Mediterranean forests. Some important concepts regarding spectral advantages of hyperspectral over multispectral and use of LiDAR for deriving height information were discussed, and the problems faced by the Mediterranean forest is also argued. Therefore, this chapter puts forward a basis for understanding the forest, its problems by knowing the exact status of the forest tree species and ground features. Finally, this chapter provided sufficient information on the Mediterranean forests, hyperspectral images and LiDAR data that form the base for the present study. The appropriate use of high spectral resolution hyperspectral image and LiDAR data for forest mapping in diverse coastal region, provide an opportunity to look at the classification results and their ability to discriminate the different features.

2.5.6 General Phenology of the Study Site-

This section describes the general phenology of the species present in the test site with emphasis on growth, leaf development, and adaptation to different ecological conditions such as counteractions of deleterious effects of the environment (Scarascia-Mugnozza et al. 2000). The forest tree species stand structure and their general phenology throughout the year is presented in this section.

The scenario of tall stand and structure of forest species are shown in Figure 2.9. *Eucalyptus* species occupy the highest place in the canopy among all other species with open canopy, long stand and are either in group (naturally grown) or fixed spacing (plantation). *Acacia* species occupy the underneath canopy position and can grow rapidly in the shade beneath other species without sunlight. *Eucalyptus* grows straight with a condensed canopy structure while *Acacia* species grow bilaterally with extending branches in all directions. Due to the mixed growth of *Acacia* and *Eucalyptus* species, there is a canopy startification occuring in all level, with *Acacia* spcies in the lower underneath and *Eucalyptus* in the upper highest canopy stratum. This canopy stratification also suggest that *Acacia* is substantially more shade tolerant than other species present in the test site. *Pinus species (pinaster and pinea)* are associated with two types of stand - one with a regular structure and one with an irregular structure (Barbeito et al. 2008). *Pinus pinea* species grow as a broad, flattened round canopy with spreading branches in all directions while *Pinus pinaster* species grow straight with elongated branches in a typical coniferous vegetation style. The crown shape of *Pinus pinea* resembles an umbrella shape with a single growth due to primary shoot growth and posterior axis differentiation as a result of secondary growth and down bending of the branches (Mutke et al. 2005).

Early development and quick growth of leaf region marks the phonological adaptation of species in Mediterranean forests. Various physiological responses that species are adapted to the environment (summer drought and wildfires) include tolerance to tissue dehydration, the ability to recover completely after a long summer drought period, photosynthetic balance and early spring photosynthesis growth of species (Scarascia-Mugnozza *et al.* 2000). To resist and avoid the disaster of fire, different species have different mechanisms: broadleaf species have a thick bark and a high sprouting nature whereas conifer species have early huge seed production and germination with ecological flexibility. In general, the tree species shed their leaves during November and start flowing with fresh leaves during spring starting in February and March. During fieldwork, all tree species were laden with mature leaves and spreading canopy.

Phenology of the tree species present at the test sites in the Mediterranean forests are described in the present paragraph. The test site is dominated by Eucalyptus species and overcrowded by invasive Acacia species, whereas other species make it mixed proportions. For the presentation of phenology, one has to observe them throughout the year for flowering, shoot elongation, leaf number and leaf shedding, branching, flowering, and fruiting. The pattern of active growth differs for different species regarding the shedding of leaves during new twig and leaf emergence. The timing of the main leaf flush and flowering of different species are determined solely by temperature, soil moisture or the photo-period of the Mediterranean study site. New leaves were produced intermittently during autumn and winter while the main leaf flush occurred in spring and summer. The cambium was intermittently active throughout the year with most trees growing in late autumn, winter and spring.

It has been demonstrated by Kramer *et al.* (2000), that water availability drives the phenology of the Mediterranean forest rather than the phonological timings, and controlling the development of leaf area. Drought has an impact on the phenology of the species, as it causes water stress that increases plant temperature and accelerates phonological development (Spano *et al.* 2013). Other factors that may affect phenology altering the time for shoot elongation, branching patterns and leaf survival are temperature, soil condition, genetical differences, age, herbivory, and below ground competitions (Oliveira *et al.* 1 994). Thus, at the test site, the phenology of *Pinus pinea* and *Pinus pinaster* was controlled by the water availability, resulting in the leaf area index of these two species. The *Pinus* species phenology passes through three different stages- such as formation of the needle, elongation of the needle shaped leaf, and ultimately the fall of the needle leaf. The rate of fall of the needle shaped leaf depends upon water deficit, wind speed and rain force that may remove a dead leaf from branches. Moreover, these species were natural as well as 'man-made' plantation regions have variable phenology depending upon several factors as discussed above.

The structure of the species can vary; the *Eucalyptus* species has tall stand with an elongated canopy whereas *Pinus pinea* has a scattered canopy. All species together makes the canopy layer uneven. The *Eucalyptus* species is natural as well as planted, so it has a both spaced canopy gap and a crowded canopy. It has been reported by (Rascher *et al.* 2011a, Rascher *et al.* 2011b) that *Acacia* species are almost taller than the native understorey shrubs reaching the height up to 3 m (See table 5.1 and 5.2 in Chapter 5). Moreover, it inhibits the growth pattern of the native species by affecting their seed germination and sprouting conditions.

Golden Sydney Wattle (*Acacia longifolia*) is mainly associated with a high growth rate in the Mediterranean forest (Marchante *et al.* 2003). These high growth rate is due to high-volume seed production, its longevity in the soil and high dispersal nature as compared to other plants' seed rare due to these problems especially along the coastline in Portugal (Cronk and Fuller 1995). Being a leguminous plant, it has the ability to fix nitrogen elements in the nutrient poor environment that enable it to cope the nutrient deficiency and invade the regions when compared to native species. Different shrub species, small grasses and invasive *Acacia* species form the major part of the understorey vegetation at the test site. Different shrubs are mixed with each other with no pattern of occupying majority regions. Thus, occupying mid-part of test site, these shrubs and herbs are small creepers with small flowering seasons. In summary, the test site has large patches of planted *Eucalyptus* species with patches of scattered conifers (*Pinus* species and *Acacia* species) and shrubs. The growth pattern of *Acacia* species is much higher when compared to other species in the test site.

Eucalyptus- tall stand (fixed distance)

Eucalyptus- closed growth and grouped canopy

Pinus pinea- flattened round canopy

Pinus pinaster –elongated tall stand

Acacia species- independent growth tall stand

Acacia species- underneath growth

Shrubs- woody & standing

Creeping herbs and shrubs

Figure 2.9 Different spcies structure and canopy presentation in the test site (Taken by the author during field survey in 2012).

2.5.7 Characteristics and Spectral Behaviour of Tree Species-

This section discusses the general spectral behaviour of the tree species in terms of their chlorophyll contents and intercellular spaces focusing mainly on the species such as *Pinus pinea*, *Pinus pinaster*, *Eucalyptus*. *Eucalyptus globulus* has chlorophyll peak in the green region of wavelength due to high amount of chlorophyll as compared to the *Pinus pinaster*. The red and red edge region of the electromagnetic wavelength, where vegetation shows a sharp increase in the reflectance due to leaf optical properties and act as a transition zone between visible and NIR region for chlorophyll activity and cellular structure of leaves. Reflectance in NIR region is dependent on the leaves and cellular structure; more the dense canopy or number of leaves, higher is the reflectance. Moreover, due to leaf structure and cellular structures, reflectance in NIR region is much higher than the blue, green and red regions. *Eucalyptus globulus* is shows a higher reflectance than *pinus pinaster*, so it is evident that *Eucalyotus* is having large number of leaves and dense canopy as compared to *Pinus pinaster*, that has needle shaped leave and thin canopy. Thus, reflectance of the feature provides their characteristics and can be distinguished from other features easily.

The spectral ranges can differentiate tree species and other ground features based on the chlorophyll content, leaf structure (broad leaf or needle shaped leaf). The physiological differences between tree species are apparent in the spectral region from 400 nm to 800 nm (Paap et al. 2008). This difference is within visible range and near red edge region of the reflectance spectra. Thus, the variation in this reflectance range can be used precisely to discriminate different species using hyperspectral datasets. The differentiating properties can be found with differences in green peak, sharp boundaries from red-edge to NIR, reflectance in NIR region and thermal regions.

Therefore, the differences can be observed in the visible range at the chlorophyll absorption region and also in the region starting from red edge to NIR ranges within the conifer needles of *Pinus* and broad leaves of *Eucalyptus*. In comparison, the *Pinus pinaster*'s needle like leaves appear bluish-light green in colour, that may be due to lower reflection in green areas of the visible spectrum as compared to *Eucalyptus* that appear dark green (high reflectance in green region). The region for choosing blue regions of spectrum stand on the base of light blue-green leaves colour of *Pinus pinaster* and *Pinus pinea* species.

2.6 Aims and Objectives

Based on the above literature review, there are several questions which can be considered 'very important' as they can lead us to a conclusion for performing the research.

1. How accurately can hyperspectral and LiDAR data distinguish tree Species in Mediterranean forest?
2. Whether segmented Principal Component Analysis (PCA) of hyperspectral data produces better classification accuracy than other approaches like standard Maximum Likelihood Classification (MLC) and Spectral Angle Mapper (SAM) of hyperspectral images?
3. Can data fusion approach of spectral characteristics of hyperspectral data and height characteristics of LiDAR data distinguish vegetation more accurately than using hyperspectral data alone? What is the added benefit of using hyperspectral and LiDAR data at same platform?
4. Does incorporating structural parameter distinguish the different features from fusion image, and how?
5. Do the selected classifier techniques prove to be superior among them or does fusion of HSI with canopy structure enhance or improve the classification results or not?

This study will examine the identification of tree species in the Mediterranean forest region (coastal vegetation) using airborne hyperspectral and LiDAR data. The biodiversity makes Mediterranean forest a good platform for forest research work. The forest research work can help in the conservation of forest, wild fire prevention and information regarding the species inhabiting the forests. Mediterranean forests are prone to wild fire that is generally human induced. The invasive nature of alien species at the coastal region has stimulated the study that is being carried out with spectral identification and data integration techniques. The data integration of RS will allow easy forest mapping when compared with individual data and help in the forest protection as well as coastal maintenance with ease.

The main aim of the present research is to identify species with the application of airborne hyperspectral and LiDAR data. It will include a generation of classification maps, with the primary focus on applying classification algorithms using PCA techniques. The two objectives to achieve the overall aim are:

1. The classification of hyperspectral images with different techniques, using segmentation of images and comparison of different classifiers performed over segmented PC images and hyperspectral image in Mediterranean Forest.

   -This will involve the use of MLC techniques for the classification of segmented hyperspectral images and the comparison of SAM and MLC of hyperspectral images of the coastal region.

2. The identification of tree species and surrounding ground features, incorporating attributes from both hyperspectral (spectral Information) and LiDAR data (Height)

   -This involves the fusion of hyperspectral image and LiDAR data with PCA techniques at the same platform for the mapping. This will enable the identification and classification of different features incorporating structural parameters while preventing spectral mixing (contributing height parameters to tree or shrubs and not to ground or sands or shrubs in fusion image).

Chapter 3. Study Site, Materials and Methods

3.1 Introduction

This chapter describes the principal datasets- airborne hyperspectral imagery and airborne LiDAR data along with the auxiliary field datasets used to assist processing, interpretation and validation of the generated map products. This chapter will outline the general pre-processing of airborne data used in the study, and the methodology adopted to achieve the objectives. The first section presents the study area and the presence of different tree species along with problems like forest fire and exotic invasive species like *acacia species* that has now become a part of the sand dune ecosystem. This section also took pains to discuss about the study area and reasons for selection of the site for performing the present research work. There is a section that describes the airborne data, software and equipment used throughout the study to achieve the outstanding results. RS data and their processing parts are discussed individually in detail. The field survey used during the study period was discussed regarding the collection of data. Recording and measuring different field data is also highlighted appropriately. Finally, the methodological approach used in the study has been discussed in the last section of the chapter. The general approach has been presented here and it forms the base of the study to carry out the present research. The detailed methodologies are mentioned and discussed in Chapter 4 and Chapter 5.

3.2 The Study Area- Site Location St. Andre, Portugal

3.2.1 General Overview

The present study area was chosen for the three principal reasons. The first among them is the availability of the datasets. Secondly, the study site has flat terrain that would assist an easy extraction of tree heights from the LiDAR data. The third reason is the diverse species composition with several species and the sandy areas provide a base to compare and contrast the outcomes. The unique and biodiverse forest, with susceptibility to forest fire, led to work for identification of species and the choosing of the study area. Data availability is also a constraint for choosing and selecting the region as study areas for the research work.The study area, Portugal is confined to the narrow coastline running parallel to hilly sand dunes. In order to provide an outline and knowledge to an understanding of the Mediterranean forests, current research has selected this study site. The site has a high biological diversity of tree species for which airborne RS data is available for carrying out the research work. The reason for choosing this area is also dependent upon the availability of the airborne RS data, which is the most important requirement of the research work. The focus of the present research is on a narrow coastal area located at Setúbal, Santiago Do Cacém in the south-western Portuguese coast as shown in Figure 3.1. Lagoas de Santo is natural reserves in Portugal, which was created in 2000. This site is protected by NATURA 2000 habitat protection directives (ICN, 2006). This region is of great biological importance, especially in ecological terms, ichthyological, botanical and ornithologica (Américo and Mendes, 2005).

A region of interest in the South of the flight area between 8°49'38.79"W and 8°51'2.14"W and 37°59'12.46"N and 37°59'35.02"N was chosen as the study area (refer to Figure 3.1. for the location of the study site). The study area is located between between Carvalhal and Sínes. This coastal area has a diverse topography with protected forests, freshwater lagoons, and dry sand dune vegetation. Mediterranean forests typically have broadleaved trees such as *Eucalyptus globulus* with the frequent presence of conifers like *Pinus pinea*, *Pinus pinaster* etc. Alien species like *Acacia longifolia* (also called Sydney Golden Wattle), which was introduced to stabilize the sand dunes, can become dominant due to its invasive nature (Rascher et al., 2011a, Rascher et al., 2011b). This coastal strip has a diverse topography with protected forests, freshwater lagoons, and dry sand dune vegetation. Thus, this area is dominated by chaemophytes, xerophytic scrubs; needle leaves tree species, and sand dunes. These forests are characteristic of the Mediterranean climate, and they represent high species richness and unique native species (Sundseth, 2009). Different tree species present in the study site area were presented in Table 3.1.

Table 3.1 List of important tree species in the study region of the Mediterranean forest, Portugal (Source: Costa et al. 2000)

	Tree species	**Family**
1.	*Pinus pinaster* (Maritime Pine)	*Pinaceae*
2.	*Pinus pinea* (Umbrella or stone pine)	*Pinaceae*
3.	*Eucalyptus globulus*- Exotic species	*Myrtaceae*
4.	*Acacia Longifolia* (Sydney Golden Wattle) Invasive species	*Fabacea*

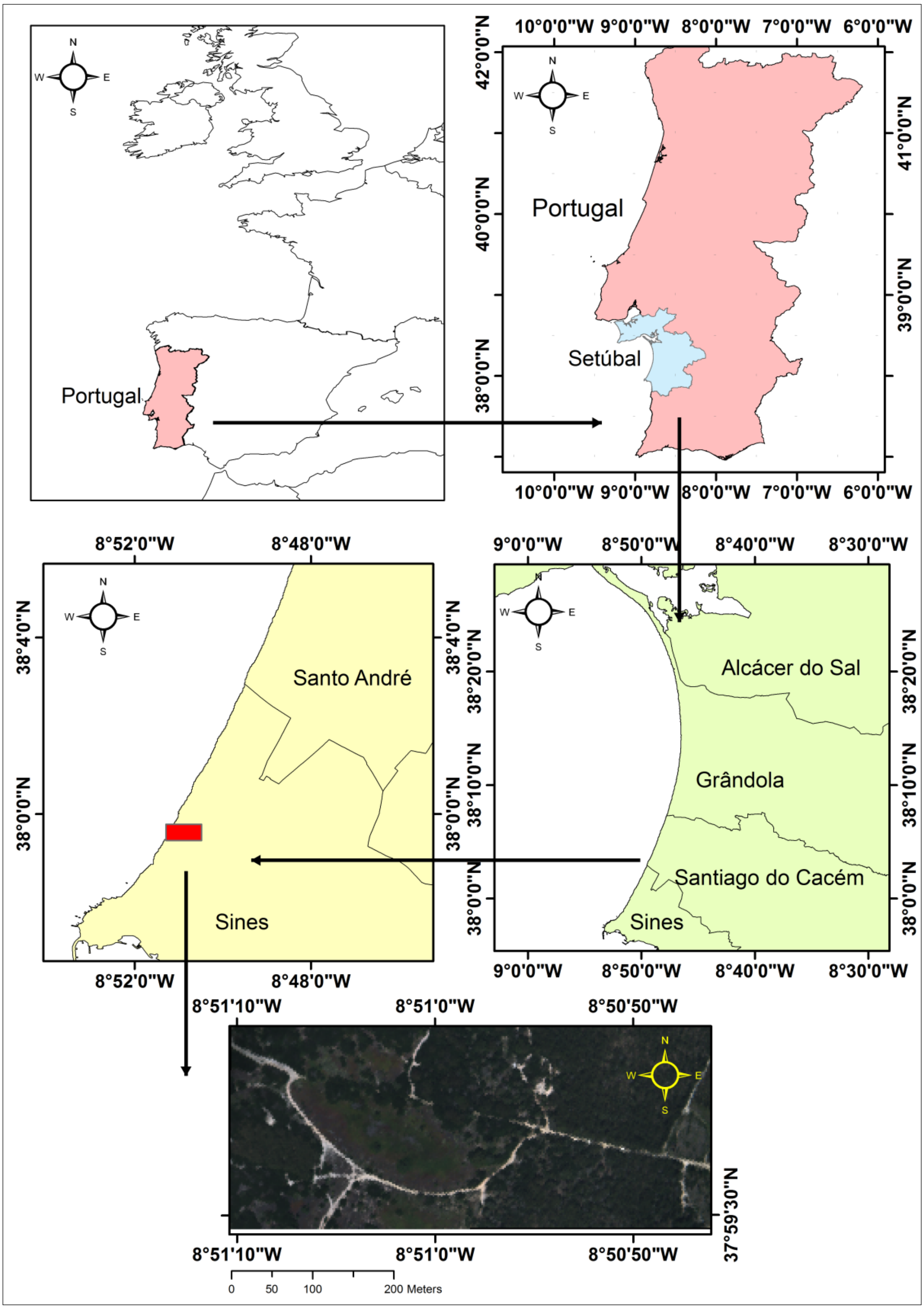

Figure 3.1 Location map of the study site showing Portugal, and its administrative boundaries generated in ArcGIS (Data basin 2014).

3.2.2 Physiographical Characteristics and Importance of the Study Site

Study site characterises the Mediterranean climate which have diverse species richness and unique native species (Sundseth, 2009). The study area chosen in the present research work is a part of Mediterranean forest located alongside a coastal zone. It is well known that, coastal ecosystems were very much susceptible to changes and disturbance and sensitivity to small changes or any biological invasions (Rascher et al., 2011a). Coastal vegetation is particularly important in respect of its biodiversity and natural structure at the study site.

Mediterranean forest may not be represented by dense forest (as shown in Figure 3.10 and 3.12) but they play a crucial role in the region. Although dense and vast expanses of forest, may not be a typical Mediterranean characteristics, but these forests play a significant ecological role in the region in the life of its inhabitants. Forest mapping plays a significant role in forest management and tree species protection: it helps to identify any changes due to deforestation and helps in tree afforestation and the management of the area.

The sand dunes in this region were not stabilised and thus management decided to introduce alien or exotic species for the stabilisation of the sand dunes (Marchante et al., 2003). The stability of a sand dune ecosystem depends on plant species diversity, roots of which hold soil particles and reduce soil erosion (Van der Putten and Peters, 1995). These introduced species were successful in stabilising the sand dunes but also distribution and dominated the region. *Acacia longifolia*, the alien species were introduced in these forest to stabilise the sand dune is one of the fastest growing species, and grows underneath the *Eucalyptus globulus* (as shown in Figure 3.2 a and b). This figure also illustrates that the *Eucalyptus globulus* are growing closer to each other and higher in density (Refer to Figure 3.2 a and b). Thus, these alien species have spread very rapidly and achieved substantial control over the region. With its fast spreading and dominating nature adjacent to the native (local) tree species inhibits their growth. Exotic alien species soon became invasive in the coastal region. Invasive species propagate across landscapes with or without facilitation by human or natural disturbance (Mooney and Hobbs, 2000). Thus, study site forests are susceptible to invasion by exotic species that grow much faster than the native species of the region (D'Antonio and Meyerson, 2002). Coastal areas of the study sites are susceptible because native flora species have evolutionary isolation effects, which means they cannot grow due to the inhibition effect of invasive species due to shadowing, chemical effects or any inhibiting properties expressed by them (Galil, 2000). Study has revealed that invasion by *Acacia* alter water and carbon balance in Mediterranean forest regions (Rascher et al., 2011b). The knowledge of tree species and other ground features are a necessary part to deal with the water crisis, plantation of more trees that are native and removal or clearance of unwanted alien species.

Therefore, this present research work is focused on tree species classification and mapping in the coastal region of Mediterranean forest. The availability of airborne RS data allows us to integrate hyperspectral and LiDAR data for forest mapping in the coastal region. This research uses different classifiers like the SAM and MLC based on supervised classification for segmented PC images for mapping more accurately than hyperspectral images. The research is also aimed to integrate hyperspectral images and a LiDAR derived Canopy Height Model for mapping using PCA fusion techniques.

(a) (b)

Figure 3.2 These photographs show the two specific characteristics of the study area (a) the growth of *Acacia longifolia* underneath the *Eucalyptus globulus* tree (b) sometimes Eucalyptus grow closely and some time with fixed distance (plantation), (Taken by the author during field survey in 2012).

3.3 Materials and Software Used

The purpose of this section is to provide an information of the materials and different software used during the study.

Table 3.2 Different data, lab software and equipment used in the study

Materials and software	**Descriptions**
Airborne Remote Sensing data	Airborne AISA- Eagle and Hawk data Airborne LiDAR Data Digital photographs
Software used	Arc GIS 10
	ENVI 4.5 (FLAASH)
	NERC-ARSF -*apl* software suite (apl trans, apl corr, apl map)
	pt_cloud filtering software
	Matlab
	Microsoft office
	View Spec Pro Version 6.0- for field radio-spectrometer
Field Equipment	Garmin GPS receiver, Abney Clinometer, Compass, Ordinary measuring tape, and ASD radio spectrometer

The NERC-ARSF *apl* software suite, Arc GIS® 10 from ESRI, Inc. and ENVI 4.5© image processing package (Research Systems Inc, 1999) were used as the major pre-processing and analysis tools in the present research. *Apl* software suite was used to pre-process the raw hyperspectral datasets to level 3b seamless images (ARSF, 2012). The ENVI spectral FLAASH function was used to perform atmospheric corrections on the hyperspectral image (Adler-Golden et al., 1999, Research Systems Inc, 2009). ENVI hyperspectral image analysis functions were used to mosaic, stack datasets and to perform PCA on hyperspectral images (Research Systems Inc, 1999). Whereas Arc GIS® 10 or higher versions were used to separate LiDAR first and last returns (Davis, 2012, ESRI White Paper, 2011, NOAA, 2012). Different extensions required for the processing of the LiDAR data in Arc GIS® were 3D analyst, and spatial analyst. Arc GIS applications were also used to generate DSM, DTM and CHM using the first and last returns of the LiDAR data (ESRI White Paper, 2011, Davis, 2012). The detailed pre processing steps are described in individual sections.

3.4. Airborne Hyperspectral Imagery- Eagle and Hawk Sensors

3.4.1 Introduction and Background

The Airborne Imaging Spectrometer for Applications (AISA) instrument is a dual passive hyperspectral scanner that measures electromagnetic radiation in the visible, near infra red to thermal wavelength region of the spectrum. AISA is dual sensor system mounted with Eagle and Hawk sensors. AISA was designed and built in 1992 by Spectral imaging company whereas the first test flight was performed in 1993 (Makisara et al., 1993). AISA has dual down dwelling radiation sensors called the Fiber-Optic Down dwelling Irradiance Sensor (FODIS). Eagle and Hawk are SPECIM’s high-performance airborne Visible Near-Infrared hyperspectral system. The AISA Eagle sensor is a push broom airborne hyperspectral system having a 1000 pixel swath width which records electromagnetic radiation in 253 wavelength spectral bands located in the visible near, short-wave infrared 400 nm-970 nm (Table 3.3) at 2 m spatial resolution (Specim, 2013). Eagle covers the visible spectrum as well as the near infra-red spectrum range of the electromagnetic radiation. The spectral resolution of the Eagle sensor is 2.9 nm of the wavelength.

The AISA Hawk sensor is also a push broom passive airborne sensor system having 320 spatial pixels that records at spectral range from 970 nm –2450 nm with 244 spectral pixels (Specim, 2012). The spectral resolution of the Hawk sensor is 8 nm of the wavelength. Thus, Hawk covers the short wave infrared wavelengths of the electromagnetic radiation (as shown in Table 3.4). It is suitable for the targets that are invisible to the human eye. Thus, it is the ideal sensor for data acquisition on spectral signatures characteristic of vegetation or minerals and studies related to them (Specim, 2012). The AISA Eagle and Hawk sensors are spectrally stable airborne hyperspectral sensors that provide high-speed data acquisition at high sensitivity (Specim, 2013). AISA Eagle is nowadays becoming very popular among researchers due to its high spectral resolution of 3.3 nm with 488 spectral bands that allow detection of the finest spectral characteristics of the features (Specim, 2012).

Table 3.3 Specification and characteristics of AISA Eagle hyperspectral images (Source: Specim, 2012)

AISA Eagle sensor	**Typical specifications**
Numerical Aperture	f/2.4
Maximum number of bands	244
Spatial pixels	Up to 1024, of which 70 - 80 FODIS pixels (optional)
Spectral resolution	3.3 nm
Spectral sampling/band	2.3 nm
Spectral range	400-970 nm
Frame rate	59 (frame /sec)
Outputs	12 bits

Table 3.4 Specification and characteristics of AISA Hawk hyperspectral images (Source: Specim, 2013)

AISA Hawk sensor	**Typical specifications**
Numerical Aperture	f/2.0
Maximum number of bands	254
Spatial pixels	320
Spectral resolution	12 nm
Spectral sampling/band	6.3 nm
Spectral range	970-2450 nm
Frame rate	59 (frame /sec)
Outputs	14 bits

3.4.2 Airborne Hyperspectral Data Acquisition

The Airborne hyperspectral imagery was acquired by the NERC-ARSF on 8 April 2011, concomitant with the airborne LiDAR data. EUFAR funded this project and data were provided by André and Prof. Tillmann Buttschardt, University of Münster, Germany. Hyperspectral data was captured using AISA on-board sensor having Eagle and Hawk sensors. These two sensor systems were enabled in such a way to capture simultaneously in 492 narrow spectral bands (Ortenberg, 2011). Twenty-six north-south trending flightlines of imagery with an overlap of around 50% between adjacent strips were acquired for the 35 km^2 area. For an average flying height of 411 m (around 1350 feet) above, each strip has a swath width of 3800 m and an average pixel size approximately 2 m. Four strips were found to contain data for the chosen coastal study site (as shown in Figure 3.4 d- representing the full scene). The strips of raw imagery were delivered as Level 1b *.bil* (Band Interleaved by Line) and ENVI header format (*hdr*) files. The *bil* format of the raster data “allows easy access to both spectral and spatial information” (Fanning, 2004). The navigation file information were also provided in *bil* format that helps in correcting the yaw, roll and pitch error. Radiometric calibration involved the conversion of the raw hyperspectral imagery data to at-sensor radiance units (μW cm^{-2}sr^{-1}nm^{-1}) (Grebby et al., 2012, Hill et al., 2010).

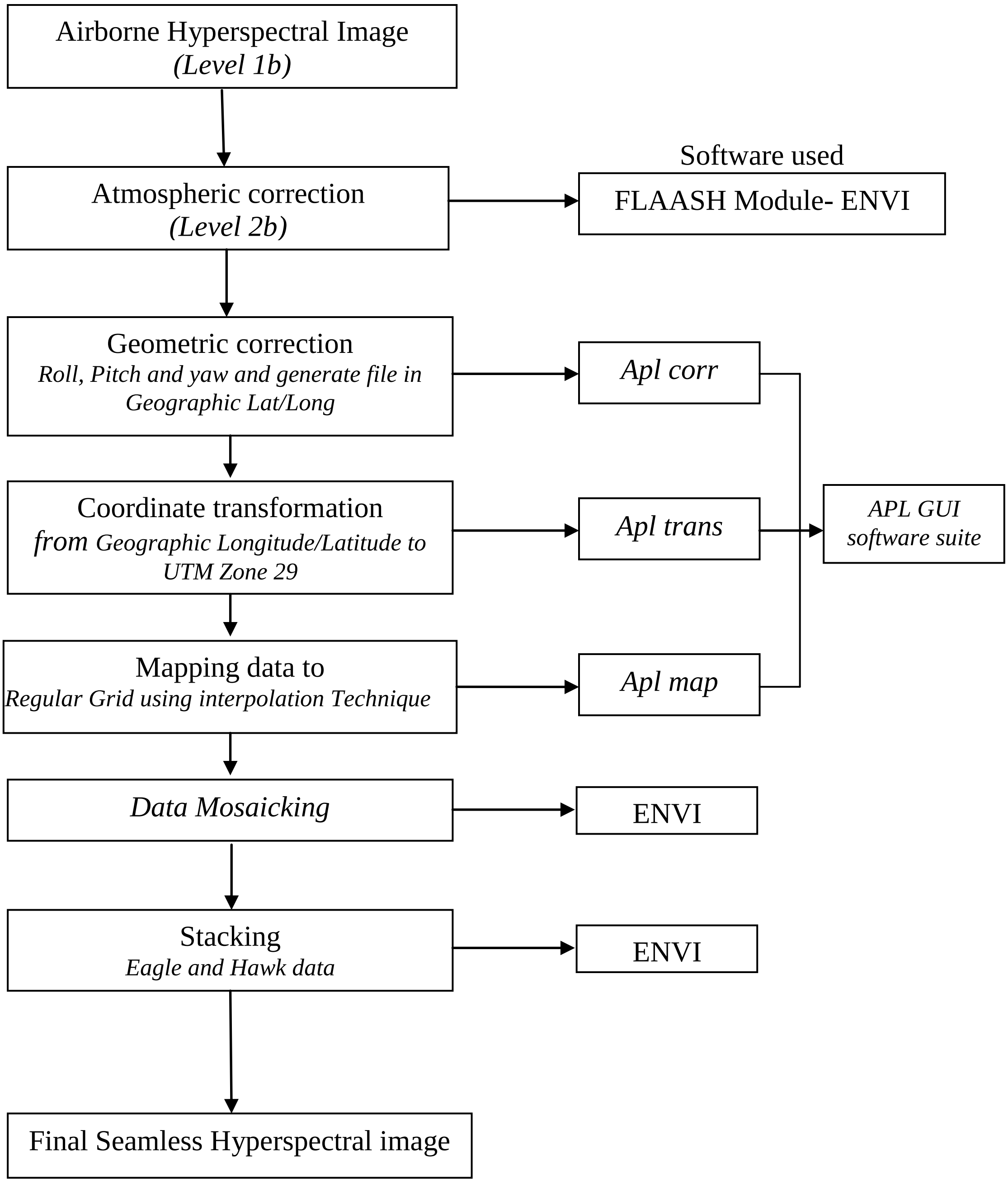

Figure 3.3 General Flowchart of the Hyperspectral image processing

3.4.3 Airborne Hyperspectral Data Pre-processing

The hyperspectral imagery was pre-processed using the *Apl* software suite and ENVI 4.5. This involved atmospheric correction, geometric corrections, transformation and mapping, mosaicking, and stacking of the Eagle and Hawk sensor data, which are described in the following subsections and illustrated in Figure 3.3 and Figure 3.4.

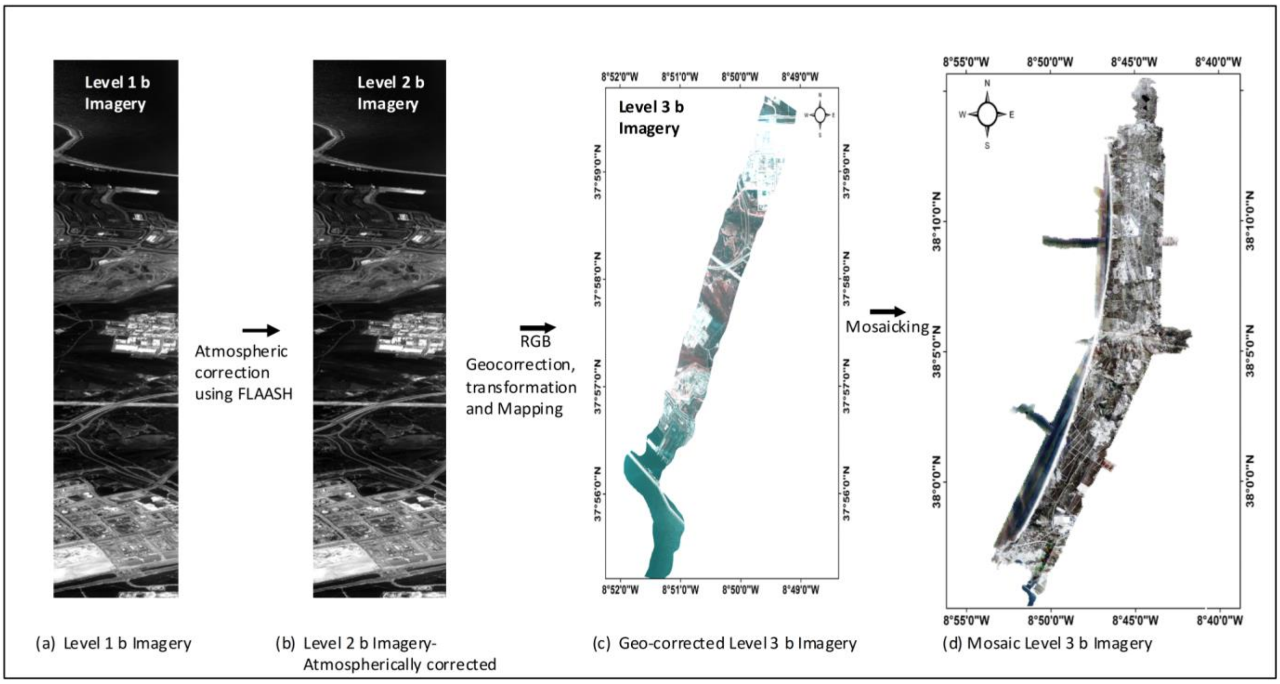

Figure 3.4 Systematic preprocessing of the hyperspectral images - Main pre-processing steps for the hyperspectral imagery (a) Level 1b image strips were (b) Atmospherically corrected image using FLAASH module, (c) Geo-corrected, mapped and then (d) Mosaicked and stacked together to generate a single seamless image of the study area

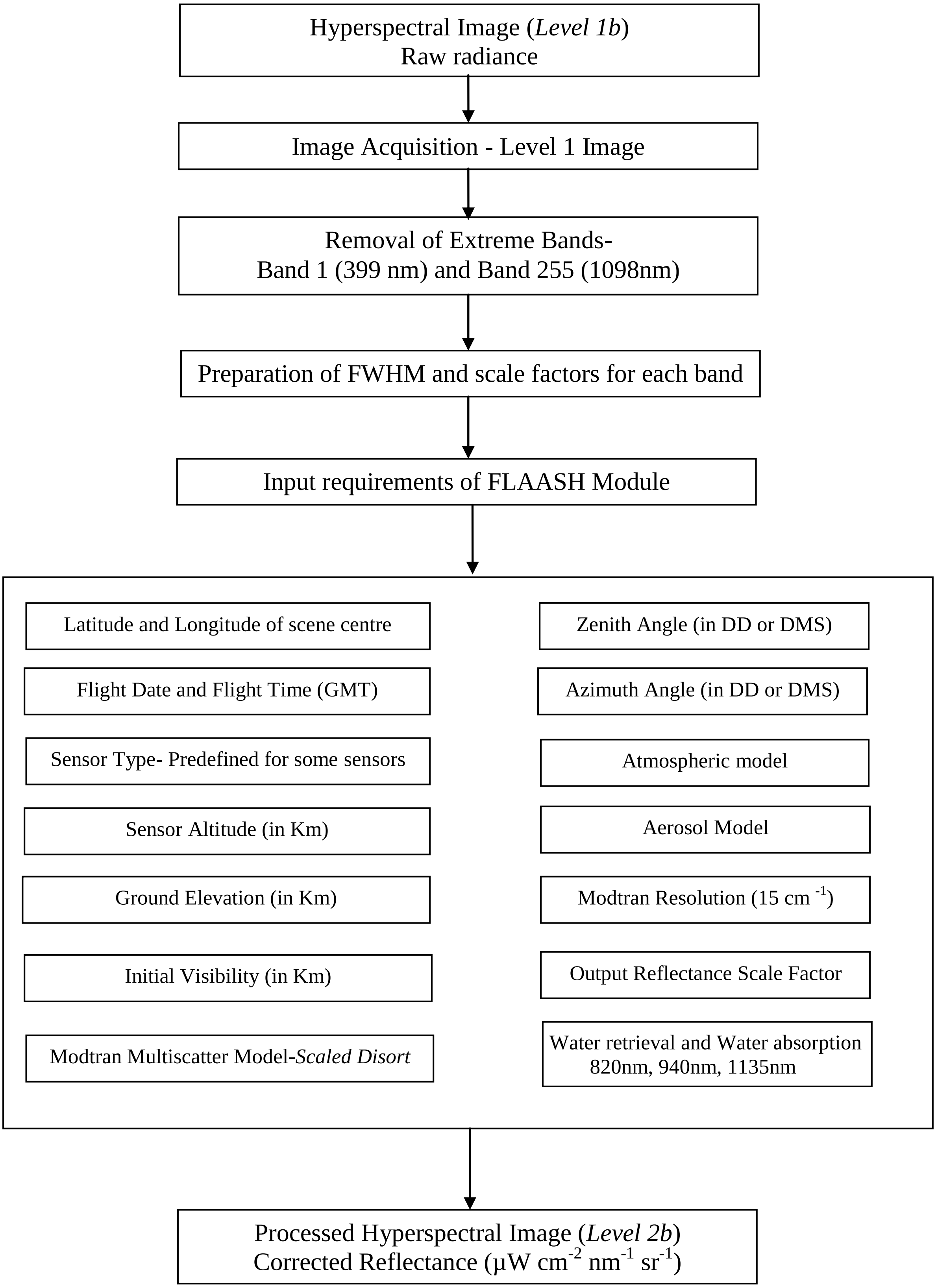

Figure 3.5 Flowchart showing input requirements for atmospheric correction of hyperspectral image (radiance image to reflectance image)

Table 3.5 Selected FLAASH parameters (ENVI software) for the atmospheric correction of the airborne hyperspectral image data.

Sensor Parameters	**Atmospheric parameters**
Scene centre location	Atmospheric model- Mid-Latitude summer
Flight Date- 8 April 2011	Aerosol Model- Maritime
Flight Time-	Water Retrieval-
Sensor type- AISA	Water absorption features-
Sensor Altitude (in Km)	Initial visibility- 40 Km
Ground Elevation (in Km)	Spectral polishing-yes
Pixel Size (in m)	Width (number of Bands)-9
	Wavelength recalibration- no
	Additional advanced FLAASH setting
	Zenith Angle- (in DD or DMS)
	Azimuth Angle- (in DD or DMS)
	Aerosol Scale height (km^2)
	CO2 mixing ratio (ppm)
	Use Square Slit function- No
	Use adjacency correction-Yes
	Reuse MODTRAN calculations- no
	Modtran Multiscatter Model- Scaled DISORT
	Number of DISORT streams -8
	Use tiled processing- yes- Tile size -200 Mb
	Output Reflectance Scale factor
	Output Diagnostic File

3.4.3.1 Atmospheric Corrections of Hyperspectral Data

The Level 1b Eagle imagery required geo-correction in order to rectify geometrically and geo-locate the imagery to the UTM projection (Zone 29 North) using the WGS-84 Earth ellipsoid model. The first (399 nm) and the last band (1098 nm) of the Eagle sensor needs to be removed before applying the atmospheric corrections to the hyperspectral data. The supplied level 1 Eagle imagery (Figure 3.4 a) has 255 bands with wavelength 399 nm to 1098 nm, but the first and last bands (399 nm/1098 nm) were removed during processing due to noise and ease in performing atmospheric correction techniques. These two bands of raw hyperspectral image (namely first 399 nm and Last 1098 nm) were severely affected by atmospheric scattering. Thus, the first band and the last band were removed from the raw dataset (Copley and Moore, 1993). Therefore, any subsequent pre-processing steps were only applied to Eagle bands 2-254 having wavelengths 400 nm to 998 nm. The Hawk image does not have any such first and last bad bands which hinder with atmospheric correction processes. Each strip of Eagle data was mosaicked pixel by pixel to generate a final seamless image composite as shown in Figure 3.4 d (Read and Torrado, 2009, Richards and Jia, 1999). Similarly, the Hawk data was processed to the same geometry and stacked with the Eagle imagery.

There are various algorithms for atmospheric corrections and retrieving surface reflectance from images such as the Fast Line-of-sight Atmospheric Analysis of Spectral Hypercubes (FLAASH) (Anderson et al., 2002, Cooley et al., 2002, Matthew et al., 2002), the QUAC model (Bernstein et al., 2005), the Atmospheric and Topographic Correction (ATCOR) (Richter, 1997, Richter, 1998, Richter and Schläpfer, 2002, Richter, 2004), the High-accuracy Atmospheric Correction for hyperspectral Data (HATCH) (Gao et al., 2009, Qu et al., 2001, Qu et al., 2003), the ATmosphere REMoval (ATREM) (Gao et al., 1996), and the Atmosphere CORrection (ACRON) (Miller, 2002). Kruse (2004) postulated, with a study using a comparison of ATREM, ACORN, and FLAASH with MODTRAN options that FLAASH is the most flexible and generated enhanced output with adjacency effects with essential enhanced corrections for hyperspectral images. Thus, the above discussion concludes that FLAASH module is reliable, fast and suitable for hyperspectral images having inbuilt AISA sensor specifications in ENVI software.

The level 1b images were processed using the FLAASH tool of ENVI 4.5 for atmospheric correction (as shown in the Figure 3.4 b and Figure 3.5). The FLAASH modele utilises different parameters for atmospheric correction including aerosol content, sensor altitude, ground elevation, pixel size, field of view, atmospheric model, water retrieval, wavelength calibration, zenith angle and azimuth angle (refer to Figure 3.5 and Table 3.5). FLAASH accurately compensates for atmospheric effects such as the amount of water vapour, aerosols, and visibility scene. As direct measurements of these atmospheric effects are rarely available, FLAASH infers them from their imprints on the hyperspectral radiance data. The demonstration of input for space borne hyperspectral sensor- Hyperion data (Felde et al., 2003) and CASI (Guanter et al., 2007) during atmospheric correction helped a lot in providing input for the airborne hyperspectral sensor. There is a slight variation in the input for airborne hyperspectral images as compared to spaceborne images; the input varies in term of ground elevation and sensor altitude. FLAASH uses these input properties to estimate correct surface reflectance correctly using highly accurate models of atmospheric radiation transfer (Adler-Golden et al., 1999). FLAASH uses different input that removes the effects of water vapour, aerosols, and atmospheric gases to convert at-sensor radiance values to ground-level reflectance. The input data for FLAASH requires its unit to be in µW cm^{-2} nm^{-1} sr^{-1} and generates the output in percentage (reflectance). The scale factor for this conversion is:

$$\frac{Integer\ radiance\ image}{Scale\ Factor} = I\ \ (\mu W\ cm^{-2}\ nm^{-1}\ sr^{-1})$$ Equation 3.1

Where, I= Floating point radiance image.

The scale factor was loaded in the form of *ascii* file, with FWHM information and scale factors. The scale factor should be constant for all bands. Other factors used as input for the atmospheric correction were latitude/longitude, sensor altitude, ground elevation, pixel size, flight date, flight time (GMT), aerosol model, water retrieval, atmospheric model (based on latitude and seasonal dependence) and initial visibility (refer to Table 3.5). The aerosol model used in this study was the maritime aerosol model and the atmospheric model was mid-latitude summer model. The corrected Reflectance image will provide a spectral profile of the different ground features and tree species that are unique to each feature. This will help in differentiating features using a spectral profile.

3.4.3.2 Hyperspectral Geo-correction

On delivery, the Level 1b *.bil* Eagle imagery required geo-correction in order to geometrically rectify and geo-locate the imagery to match the WGS 84 UTM zone 29-North coordinate system of the airborne LiDAR data (See Figure 3.3 a). To achieve this, all images of the flight line were individually geo-corrected using the Window-based APLGUI software, which was supplied with the data by the NERC-ARSF, Plymouth United Kingdom. Level 2 products (such as atmosphere corrected imagery) were created before geo-correction. These Level 1b (or Level 2) files were geo-corrected with the Airborne Processing Library (APL) software suite to produce Level 3 imagery. *apl* software suite contains *aplcorr*, *apltrans* and *aplmap* to generate level 3 images from provided data.

The Level 2 files were geo-corrected for roll, pitch and yaw with the *apl corr* software to produce Level 2b imagery in Geographic Longitude/Latitude (ARSF, 2012). Utilising the appended aircraft navigation information from a navigation file and a 4 m DSM generated from the LiDAR first returns, the apl trans APLGUI software (ARSF, 2012) was used to determine the geographic location of each pixel on ground and then interpolate these (using the default nearest-neighbour algorithm) to generate a 2 m raster image (.bil format) for each flight-line.

3.4.3.3 Hyperspectral Image Mosaicking and Stacking

Following the correction of atmospheric effects and geo-corrections, image strips were transformed, mapped and then mosaicked to generate a single seamless image (Figure 3.4 d). Geo-corrections and transformation were performed within AplGUI ARSF mapper (Graphical user based software provided by ARSF) and ENVI 4.5. Then each file was transformed from Geographic Longitude/Latitude to UTM North zone 29 using *apl trans*. Adjacent flight strips were co-registered through *apl* ARSF mapper using DSM, navigation file and nearest neighbourhood re-sampling within *aplmap*. Image stacking and mosaicking were performed in the ENVI software. During image mosaicking, colour balancing procedure was applied for the purpose of minimising the differences between adjacent strips. This method matches the spectral statistics among images, by calculating gains and offsets from a reference image. Thereafter, spectral matching uses these gains and offsets to adjust the values (DNs) of an overlapping image during mosaicking. These steps generate a seamless hyperspectral image for the further use or classification.

3.5 Airborne LiDAR data

3.5.1 Introduction and Data Acquisition

LiDAR can overcome problems associated with exhaustive field work such as time-consumption, lengthy procedures, and requirement of more man power . Though it is expensive, it can acquire data promptly over the all-region, which is processed to estimate the different forest characteristics. For the validation purposes of LiDAR derived results, the study still requires the field collected or measured data of the tree components. Thus, field survey is still valuable for the research purposes. It measures the tree height at specified spatial plot locations in the area and correlates the results with LiDAR derived canopy heights. In conclusion, LiDAR is offering an improvement to existing traditional inventory methods and procedure by providing reliable outcome in a quick and speedy manner. Both HSI and LiDAR can be acquired over a large area in less time when compared to the traditional field survey and measurements.

Table 3.6 Information content of Lieca LiDAR system

Properties	**Information details**
Time	It is the GPS time of week in seconds
Easting and Northing	Depends on the datum and projection of the data, but will usually be in metre
Elevation	In metre.
Intensity Values	between 0 and 255
Classification	It follows that of the ASPRS standard LiDAR point classes.
Return Number	It is between 1 and 4, where 4 is the last return.
Number of returns	For the given pulse it will be between 1 and 4.

Leica Geosystems was used to collect LiDAR data for the EUFAR project in April 2011. Airborne Leica LiDAR data were utilized in the present study was acquired on the 8th April, 2011 in the midday by the Natural Environment Research Council Airborne Research and Survey Facility (NERC-ARSF) (ARSF, 2012). Airborne Leica LiDAR data was collected from the Leica Geosystems-ALS-50 II instrument. The LiDAR survey was undertaken at an average flying altitude of 411m (around 1350 feet) above the sea level. The entire surveyed area comprises twenty-six north-south trending, overlapping strips covering approximately 35 km^2 and encompassing the chosen study area. Three of these strips of LiDAR contained data for the actual study area. The data was supplied as ASCII format and LAS 1.0 point cloud in ASPRS format (The American Society for Photogrammetry and Remote Sensing) as shown in Table

3.7. Before processing the data, it is checked for any anomalies like holes, spikes or any irregular minimum bounding shapes in the sampling datasets. The data in the point clouds are re-classified to highlight possible noisy points (7) and unclassified points (1) by ARSF Data Analysis Node. The processing consists of removal of noise, merging the files and then processing this together with the raw laser returns to generate a georeferenced point cloud. The processed filter LiDAR data is used to generate a DSM and DTM. The information contained by the LiDAR LAS file is illustrated in Table 3.6.

Table 3.7 The ASPRS Standard LIDAR classification (ASPRS, 2005, Graham, 2012).

Classification Value (bits 0:4)	**Meaning**
0	Created, never classified
1	Unclassified
2	Ground
3	Low Vegetation
4	Medium Vegetation
5	High Vegetation
6	Building
7	Low Point (noise)
8	Model Key-point (mass point)
9	Water
10	Reserved for ASPRS Definition
11	Reserved for ASPRS Definition
12	Overlap Points
13-31	Reserved for ASPRS Definition

The LAS format of LiDAR data is first processed by 3D Analyst's Toolbox in the Arc GIS platform using the point file information tool. It summarises the file contents of millions of points contained in the LiDAR datasets, and more than one data to single file. It also reports, statistical information about the raw LiDAR data, which is very important before LiDAR data, is handled for processing. This information includes minimum rectangle boundary, average point spacing, minimum/ maximum z-values and number of points. Out of this information, average point spacing is very important and should be uniform throughout the LiDAR data files because they are used for building geodatabase terrains and feature files in Arc GIS software. “The average point spacing is the product of the total number of points divided by the area of the LiDAR datasets” (ESRI White Paper, 2011) p.5.

Once acquired, the LiDAR data points can be processed to generate a DTM, by interpolating the x-y-z coordinates of the appropriate returns to a regularly spaced grid (also known as a raster). A DSM generated from the first returns is referred to as a Digital Surface Model, whereas a DTM generated from only ground returns is known as "a bare-earth" Digital Terrain Model. Although interpolation errors accompany rasterisation, LiDAR topographic data is more efficiently stored in the form of an Elevation model than in its raw vector point form (Chan et al., 2007). Moreover, there are many algorithms that easily enable qualitative and quantitative analysis of Elevation Models.

3.5.2 LiDAR Pre-processing

During data delivery, some of the noises were already classified and given values as per the American Society of Photogrammetry and Remote Sensing (ASPRS) standard LiDAR point classes and given classification value of 7 (ASPRS, 2005, Graham, 2012). These classified 7 value is removed using filtration script using point cloud filteration software (pt_cloud_filter.exe.) provided by ARSF while delivering data. A script has been used to run *pt_cloud filter.exe* in command prompt to remove the noise (classified as 7) provided in Appendix 1.

This processing produces the noise free (filtered ASCII files) LiDAR data which can be used for further processing, similarly, .LAS files can be filtered using LAS tools (Hug et al., 2004, Isenburg and Schewchuck, 2007). After this filtering, the LAS file is further processed in Arc GIS for generating DSM and DTM using the first and last return of the data. The LAS file is used to separate first and last return.

3.5.2.1 Processing of LAS File in Arc GIS Platform

The second step in LiDAR data processing involves the conversion of .LAS files to multipoint and to load them into the geodatabase using the 3D analyst toolset in Arc GIS platform. The LAS file was used to locate information associated with the *las* data like number of returns, ground spacing. Loading the several million points of LiDAR data into the geo-database feature type is known as multipoint. In this process, the LiDAR files were loaded in a geo-database that allows a seamless mosaic of the .LAS files at single or individual file for further analysis by Arc GIS tools. This generates a point density map of the LiDAR data . This conversion requires certain specifications for its completion like ground spacing (derived from point file information tool as discussed in step 1), coordinate system and the return number.

The average point spacing (for the processing of LiDAR) used in the current study is 0.43 to 0.61 meter and the point cloud field generated in the point returns is 108,203,294 records per row. These are part of storing, mosaicking, and separating data in multipoint feature class in a geo-database. Thereafter, raw elevation points of LiDAR data are converted into a geo-database terrain and an elevation raster file using a point to raster tool (Arc GIS conversion toolbox). The DSM and DTM were generated from the multipoint feature class (point to raster tool of ArcGIS) with z-heights of the features. For generating a DSM, a cell assignment is set to max values, pixel size is set to 2 meter and cell size is set to 4 times according to the average ground spacing of LiDAR points. In this case, average ground spacing of the LiDAR data is 0.54, so cell size is 2 m that corresponds to the spatial resolution of the hyperspectral images. Thus, DTM is derived from the LiDAR ground returns (last return of the LiDAR) using the same procedure where cell assignment type is set to minimum, and cell size is set to 2 m resolution corresponding to AISA hyperspectral images. For generating DSM, the Z-*max* option is used as window filtering whereas the Z-*min* window size filter was used for DTM generation.

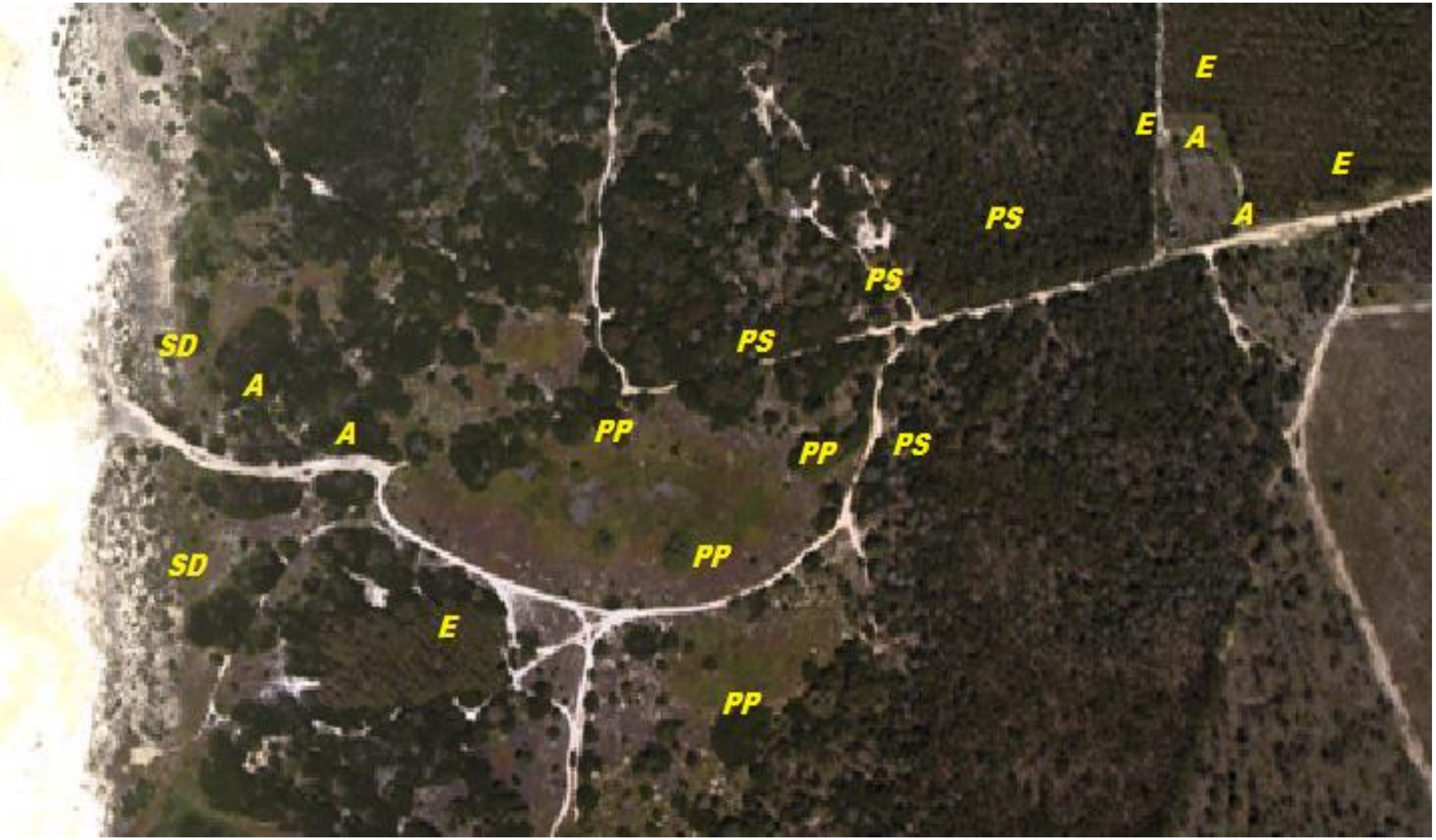

Figure 3.6 An aerial photographs showing the openness of the Mediterranean forest and sand dunes near a coastal region with some plots in study sites E- Eucalyptus species, PP- Pinus pinea, PS- Pinus pinaster, A- Acacia Species, S- Sandy region with few shrubs (Note- This is a priori knowledge based on field survey taken during September 2012 by the author).

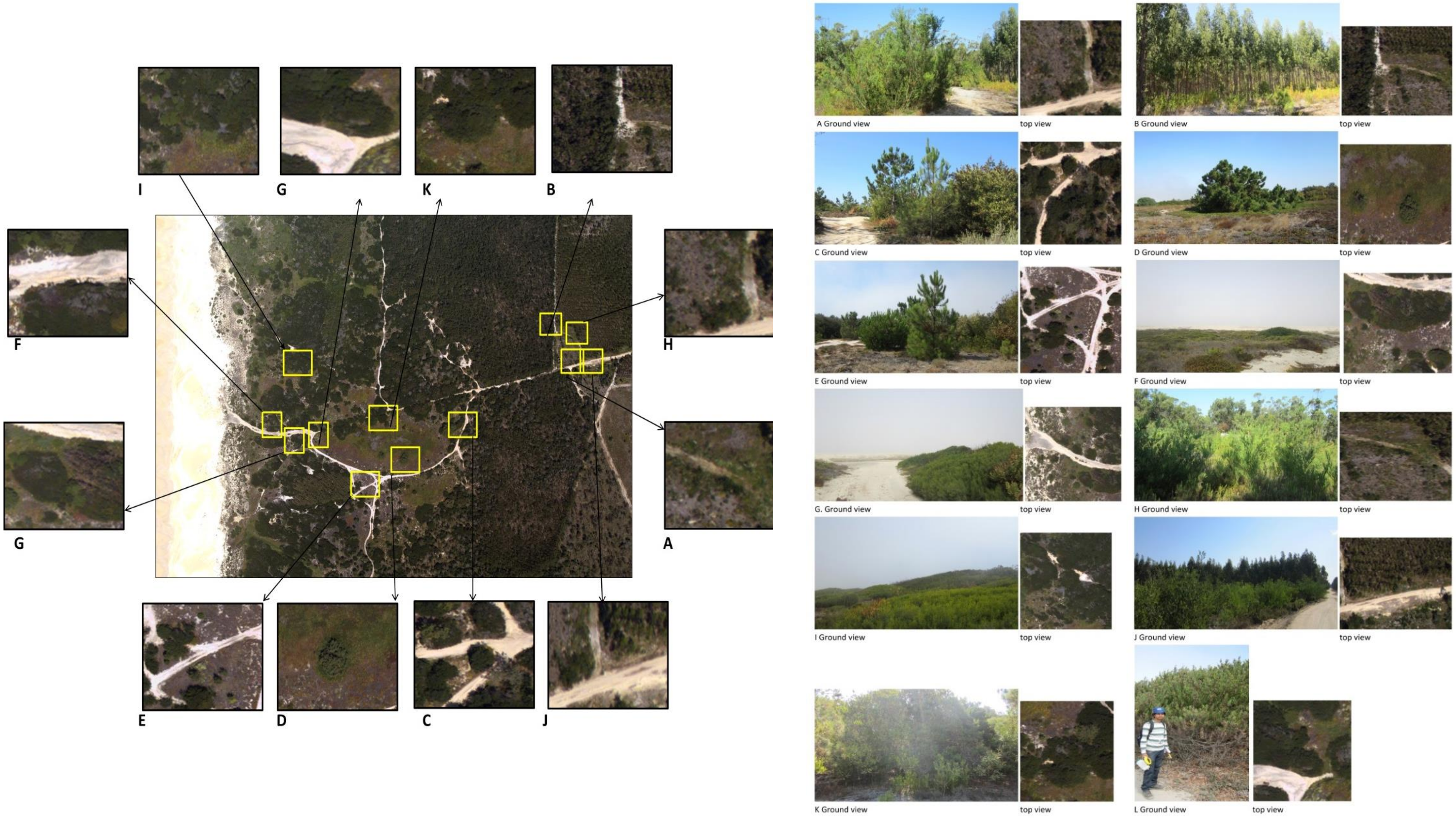

Figure 3.7 (A) Field plots showing different tree species, (B) Field photographs and aerial photographs showing upper canopy view and terrestrial view (a-L).

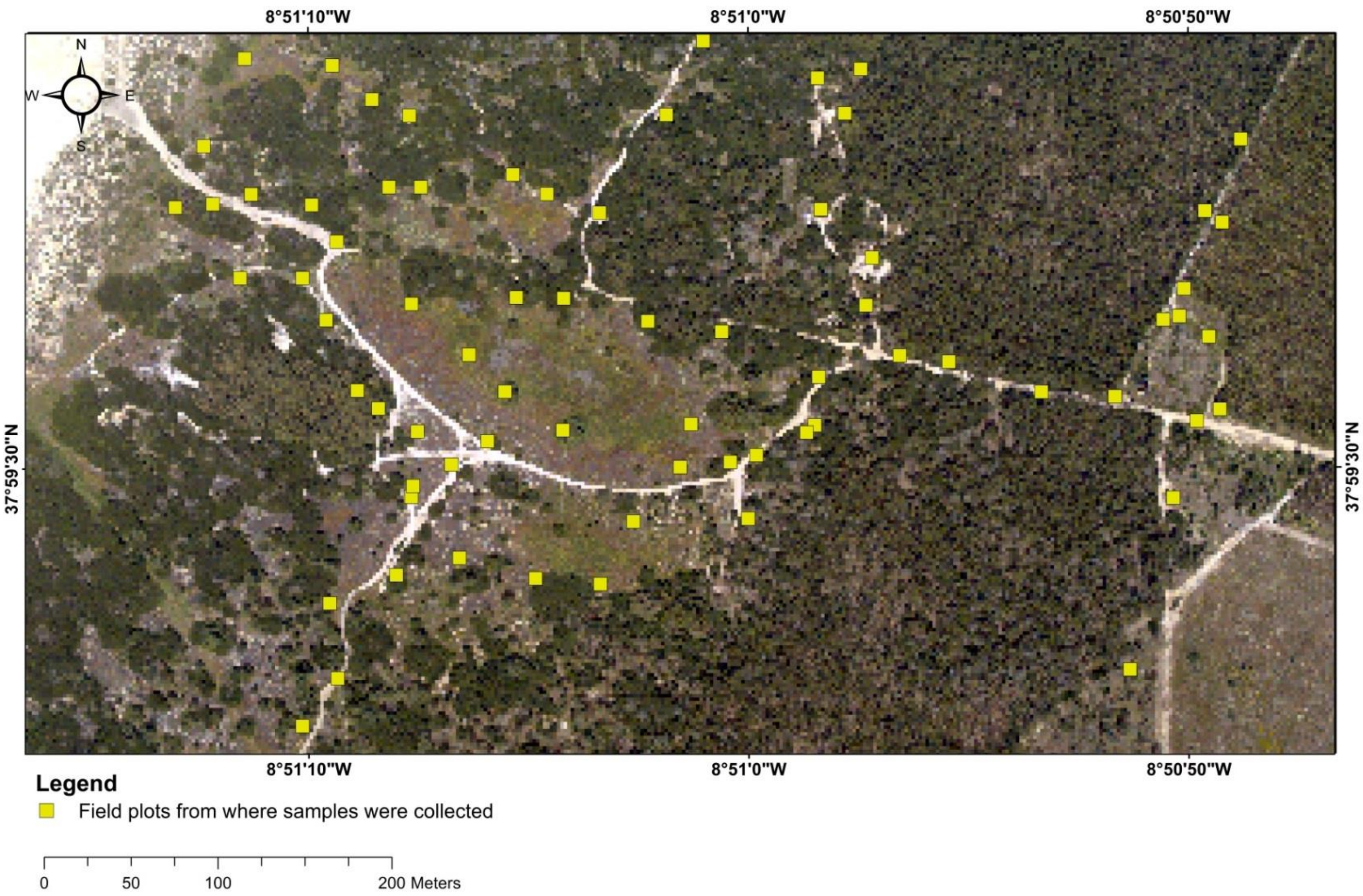

Figure 3.8 Location of field plot sites used for the training and classification of the images

3.5.3 Canopy Height Model Generation

CHM is generated using the subtraction method from DSM and DTM. The DSM and DTM need smoothing to remove the noise during processing but if the surface is not very noisy, over smoothing will create noise in the data (Tate et al., 2005). The raster DTM were smoothened using window size filter with z-max option and z-min in case of DSM smoothing, as some noises were removed during pre-processing of the .LAS files using point cloud filtering software (listed in Appendix 1. If the terrain is not relatively over flat, there comes the requirement of secondary thinning, otherwise not. This processing helps in getting the DSM and DTM, which were used to generate CHM using math tools in the Arc GIS platform. The CHM was generated from the difference of DSM and DTM generated from the first and last return separated from the LiDAR data (Balzter et al., 2007, Popescu et al., 2003, Zimble et al., 2003).

3.6. Fieldwork Methodology

Field methods were planned, and in the month of September 2012 and different materials such as digital aerial photographs, printed maps, reference materials and instruments (Abney Level, Handheld radio-spectrometer) were carried to the field for the collection of data (See Figure 3.6, 3.7, 3.8 and 3.9 for field information and instruments). The field data were collected in September 2012, by the author, and helped by colleagues from University of Leicester and (André Grobe Stoltenburg) University of Münster. The printed maps (from digital photographs taken during the data acquisition) were used during the field trip to locate and mark the sample points corresponding to the ground locations (See Figure 3.8). These shown points were collected in the field with GPS, marked on digital aerial photographs and maps. These were used as the training and validation points for this study test site. Aerial photographs were used to locate the point using the structure or shape of the field conditions. These field samples were collected on random sampling, where most of the points were selected according to their unique locations and landmark such as corner trees, single tree, isolated trees, and groups of two or three trees (triangle shape). The leaf samples from mid-canopy of species were collected for recording the spectral reflectance and for the low height species, reflectance was collected overhead. As the fieldwork was carried out in the month of September, the weather conditions were dry and hot with a clear sky. Moreover, the spectral reflectance was recorded at the same time for all species during the same time of the day to avoid any BRDF effect. Thus, precautions were taken to collect data in similar climatic conditions. Before the start of the fieldwork, the study site experienced rainfall in the previous month, but the conditions were favourable for the data capture and recording the spectral reflectance during fieldwork.

The data collected during fieldwork was point locations of the different native species, height of the trees, and photographs of the site simultaneously. The Abney level instrument was used to collect the height of the tree species in the field that was used to validate the LiDAR generated heights. Different tree species were sampled for spectral characteristics with a handheld radio spectrometer, including height of the tree using Abney level, and spatial location using Garmin Oregon GPS. It is known that “Garmin Oregon GPS has an accuracy of less than 36 feet (10 m) which is 95% typical accuracy” (Garmin, 2008) p.31. Numerous samples of tree species were collected in order to determine the representative spectral characteristics of each prior to use in guiding a conventional remote sensing approach to classification and mapping. The further spectral profile of the tree species was taken with a handheld radio spectrometer, with white reference and dark reference. About 70 samples of different tree species, particularly *Pinus pinaster, Pinus pinea, Eucalyptus and Acacia longifolia* were collected during field sampling. Latitude and longitude locations were recorded using Garmin Oregon GPS. Spatial locations of all sampling places were recorded using a Garmin Oregon GPS and marked on the digital photographs too.

Leica GPS was used to record the spatial location of each collected sample for the co-location of field data with the airborne datasets. The Leica GPS system provides real-time analysis, and was used to navigate in the forest area to log the position of the tree or sample with respect to the sampling points. The Leica GPS system was connected with the post processing software that exported the recorded points to the shape file (to be used in ArcGIS environment). The shape files were exported over the airborne hyperspectral image to locate them. The digital maps and photos were marked accordingly while in forest. These points were then, matched with the points marked on the digital photos during field work for its co-location. Spatial location of different tree species and ground features with forest information for a section of the study area was acquired during the field trip in September, 2012. The information gathered in the field visit were used to validate the classification results. This involved identifying tree species, recording heights and the spatial location of marked trees in the study area (in Figure 3.7 and Figure 3.8). A personal laptop (Arc GIS software) along with digital photographs was used to store the field information (e.g., any crossing or specific locations) to facilitate preliminary assessments of field samples collected using GPS. The marking and identification of places were performed using the digital photographs that were printed before the field trip with GIS to be readily accessed which helped in the interpretation of those sites while in the field.

In the field survey we sampled spectral profiles and recorded the height of different tree species like *Pinus pinaster, Pinus pinea, Eucalyptus species, and Acacia species.* During the field work, I sampled these vegetation types to identify them and evaluate their separability from each other. Field spectral profiles of native tree species were recorded using the Analytical Spectral Devices (ASD) FieldSpec-Pro handheld radio spectrometer (ASD, 2002) whereas tree height was measured with an instrument called an Abney level (Shapiro and Good, 2010). As discussed earlier, the tools used during field work includes a compass, measuring tape, GPS, Abney level and a Radio spectrometer.

The Field survey consists of identifying different tree species and ground features in the field site and marking them. These various ground features include sand regions, ground covered with grasses, shrubs and tree species like *Pinus pinea, Pinus Pinaster, Eucalyptus globulus, Acacia longifolia*. They were marked on digital photographs with markers like PP, PS, E, A, E, PP, PS and SD (refer to Figure 3.6). This information is based on the field survey undertaken in September 2012. The location of different ground features and tree species were marked on the digital photographs during the field survey (as shown in Figure 3.6 and Figure 3.7). Some of the field photographs taken during the field survey showing different places (spatial points) and marked with the letters A, B, C and so on (refer to Figure 3.6 and Figure 3.7). These photographs also show that Mediterranean forests are not dense, but open in nature. These studies help with image processing and classification purposes (refer Chapter 4 and 5).

3.6.1 Importance of Field Survey

A prior knowledge of the different vegetation types or ground features of the study area is essential and mandatory in considering the data validation and result assessment. For this reason, field research is required to record the tree height with spatial locations to match it with airborne images. Field survey data helps in relating the canopy height calculated from the LiDAR data using regression analysis of both datasets. However, conducting a field survey for recording or measuring tree heights is time-consuming and often difficult in dense forest due to a large area. Traditional field inventory methods are tedious and rigorous, based on the systematic sample plot measurements in forest stands. It is also obvious that the measurement using plot of each tree is quite impractical in nature. These traditional methods provide generalised results based on the measurements of sample plots for the whole forest stands. These generalised results may be inaccurate due to variability in the composition of the forest stand and sampling bias. In addition, the traditional field data collection is tedious, time-consuming, exhausting, lengthy, expensive, and it requires a number of people to cover the forest area. In conclusion, it requires both substantial financial and human resources for its completion.

3.6.2 ASD Radio Spectrometer

The handheld radio spectrometer was used to record the spectra measurements of different tree species. The instrument record spectral data over the range of 300 nm - 1000 nm (ASD Inc, 2008). First of all, measurements were taken by baseline using the dark current and white reference over a standard white board (provided with the Hand Held radio spectrometer). Thereafter, the spectrum were collected from the instrument for different tree species. The collected spectrum were pre-processed using HH2 sync and view spec pro software provided by ASD Inc™. HH2 sync was used to import the spectrum file from the instrument connected to it. Thereafter, the imported spectrum files were processed and export the binary files to text file for further analysis or comparison (ASD Inc, 2008). The export function available were jpg, bmp, .png, text files and export destinations were file, clipboard and printer (ASD Inc, 2008). The spectral profile of tree species were shown in Figure 3.9. These spectral profiles measured along with the spatial points considered for looking at hyperspectral images for locating features with similar profiles. Although some variation in ground based spectral profile and hyperspectral profile may be found due to difference in spatial resolution, distance of acquisition and canopy density.

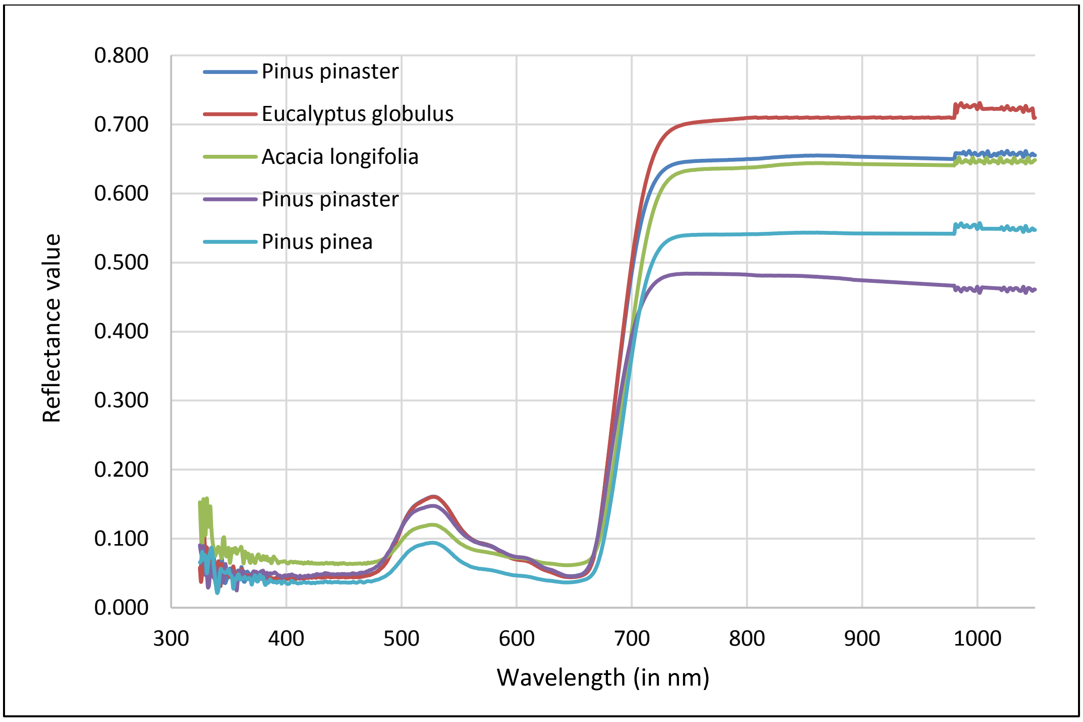

Figure 3.9 Field measured spectral profile using hand held radio spectrometer, where noises are present in initial and later part of the spectrum

There are some limitations associated with the airborne sensors that may affect the image quality.

-The forest or any land features may be observed by the satellite or airborne data from different viewing directions which depend upon the position of the sensors and position of the sun's angle. Thus, the viewing angle of the satellite with respect to the sun angle may affect the retrieval of surface reflectance. Thus, BRDF (Bidirectional reflectance distribution function) is one of the limitations of the satellite or airborne sensors when compared to the handheld spectrometer. In order to avoid BRDF and fulfill diffuse hemispherical condition, only direct solar radiation, and spectral data recorded in the field is primarily from a direct solar radiation under a clear sky (McCoy 2005) to measure the irradiance and radiance at all possible sensor positions and possible source positions.

-Aerosol particles or haze can affect the retrieval of the surface reflectance by the airborne sensors that may be avoided by the handheld spectrometer.

-Satellite or airborne sensor can view the features from above the canopy of the forest tree while a handheld spectrometer can be used to record the reflectance of ground leaf, upper canopy by destructive methods (leaves were plucked from the tree and clustered to record the reflectance). Thus, handheld spectrometer has advantage over the satellite or airborne data in terms of above-mentioned limitations.

3.6.3 Abney Level Instruments

An Abney level is a hand-held instrument used primarily in preliminary surveys to collect basic information about the height of the target objects (Keuffel, 1942). It is also used to measure degrees, percent of grade and topographic elevation (Keuffel, 1942). This tool was invented by Sir William de Wiveleslie Abney (Shapiro and Good, 2010). An Abney level is one of the most essential, useful and popular surveying instruments in forestry research field (Calkins and Yule, 1927). It provides the angle information helpful in calculating the inclination and height using trigonometry equations (Stanley, 1901). The popularity of this instrument can be assessed due to its stability, simplicity of design, its ease and speed of manipulation and relatively high precision results (Calkins and Yule, 1927).

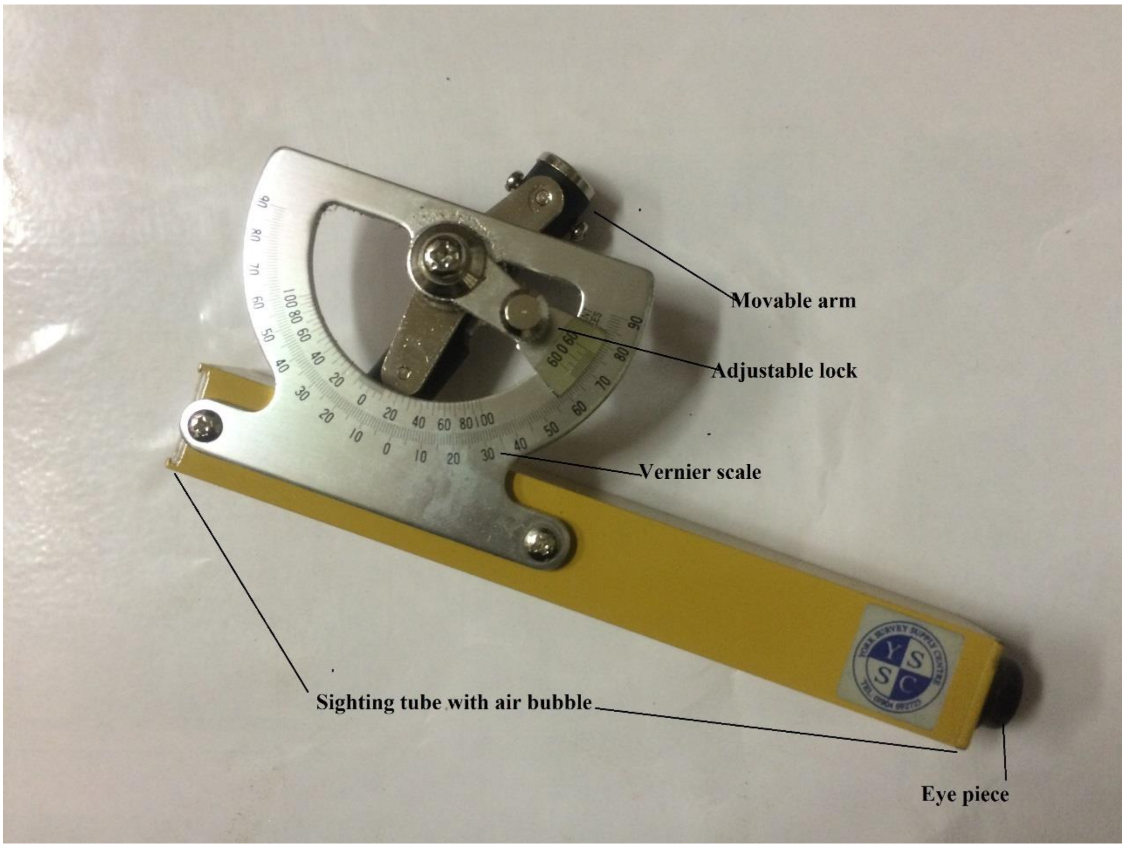

Figure 3.10. Abney Level used for collecting height information during field work (taken by the Author)

An Abney level (see Figure 3.10) consists of a sighting tube with a bubble level inside and the vernier scale with a movable pointing arm in (Erickson, 1914, wiseGEEK, 2014). The Abney level scale is "graduated to degrees, and read by vernier to 5 minutes" (wiseGEEK, 2014). The top of the target tree is looked through the eyepiece, and the protector is moved to fix when the air bubble is at the centre of the line of sight. The protector position is fixed with an adjustable lock so that exact position is maintained during handling and reading duration. This vernier scale provide the angle information required to calculate the height of the trees using trigonometry (Shapiro and Good, 2010). An Abney level is used to measure the height of a tree in fields using trigonometry methods (as shown in Figure 3.11, Equations 3.2 and Equation 3.3).

The measurement of tree height requires the calculation of the distance between observer and tree (H), the angle between the top of tree and an Abney level (i.e. Eye of observer), and height of observer Δh (See Figure 3.11). The Abney level was carefully pointed towards the top of the tree to view through the sight piece. In order to read the angle between top of tree and observer's eye the Abney level was held steadily. Ground horizontal distance (i.e. G) was measured using a measuring tape and the H_1 is calculated using the Equation 3.4. After that, the tree height is calculated by adding the Δh to the calculated H_1 using Equation 3.4 (See Figure 3.11). Providing equations and illustration to find the tree heights are easier to understand and apply (illustrated in the Equation 3.2, Equation 3.3 and Figure 3.11).

$$\mathrm{H}_1 = Ground\ Distance\ (G) \times Tan\ (a) \qquad \text{Equation 3.2}$$

Where, H_1= Vertical height (tree height - observer's Height), α= Angle between the top of the tree and observers' eye with Abney level, G= Horizontal distance between tree and observer.

The Equation can be modified if the laser distance-measuring instrument is used in place of an Abney level. The laser distance instrument measures the distance of the top of the tree from the observer (L).

$$\mathrm{H}_1 = Distance\ between\ top\ of\ tree\ and\ observer\ (L) \times Sin\ (a) \qquad \text{Equation 3.3}$$

$$\text{Tree Height } = \mathrm{H}_1 + \Delta h \qquad \text{Equation 3.4}$$

Where L= Distance between top of the tree and the observer, H_1= Vertical height (tree height at observer's Height), Δh= Height of the observer, α= Angle between the top of the tree and observers' eye with Abney level.

Tree heights of different species were recorded and measured using the above equations in the field site (relatively flat) and used later on to compare with the LiDAR derived tree heights (See chapter 5). An Abney level is a small, relatively inexpensive, easy to use and portable instrument.

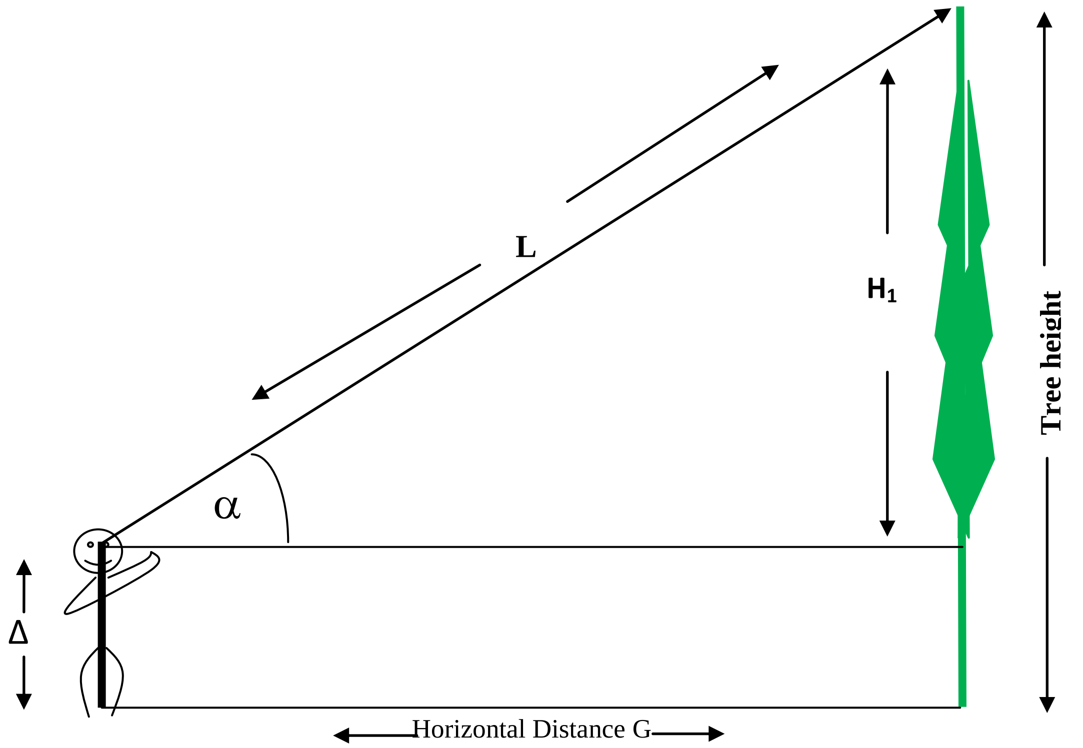

Figure 3.11 Illustration of trigonometric methods showing how to measure tree height using an Abney level

3.7 Methodology of the Remote Sensing Data

This section presents the general overview of the methodology adopted in the study as illustrated in the Figure 3.12. The broad methodology has been presented in this section while detailed methodology will be discussed in the respective sections (Chapter 4 and Chapter 5). The methodology is divided into two parts

1. The classification of the segmented PC images.
2. The synergistic use of the hyperspectral image and LiDAR derived Canopy Height Model i.e. fused image.

Overall, the study includes the acquisition of the airborne HSI and LiDAR data, recording and measurement of field samples (spatial locations, tree heights, spectral profile) and pre-processing of the raw data using different technique in various steps (as described in section pre-processing steps).

In the first methodology, supervised classifiers like SAM and MLC were used to classify hyperspectral images, and their accuracy is then assessed. The hyperspectral images were spectrally segmented based on the wavelength and histogram into five sections. Later on, the PCA technique was applied to the segmented hyperspectral image to reduce data dimensionality that is also known as the 'Hughes Phenomenon' that hinders the classification results (see Chapter 4). In the second methodology, PCA fusion technique was used to bring hyperspectral and LiDAR derived structural height at the same platform, and thus used for classification and mapping.

3.7.1 Methods for the Segmented PC Image and its Classification

This methodology presents a general idea about the process of segmentation of hyperspectral image, its classification using MLC and the comparison with classified original hyperspectral image using MLC and SAM classifier. The supervised classification technique of maximum likelihood algorithm is the most commonly and widely used method for classification purposes (Richards and Jia, 1999). The hyperspectral data is divided into five spectral data ranges based on their histogram statistics. The chosen ranges for segmentation are based on statistical properties, not on their wavelengths as radiances of a particular wavelength may overlap with neighbouring wavelengths (Pandey et al., 2014). Principal Component Analysis (PCA) is applied individually to each spectral range. The first three Principal Components (PC) of each range are chosen and are fused into a new data segment of reduced dimensionality. These PCs were used for classification using MLC. Spectral signatures were also analysed for the hyperspectral data and were validated with ground data collected in the field by a handheld spectro-radiometer. Different RGB combinations of PC bands of the segmented PC image were richly coloured and provide distinct feature identification. A comparison with other classification approaches (SAM and MLC of the original hyperspectral imagery) shows that the MLC of the segmented PCA achieves the highest accuracy, due to its ability to reduce the 'Hughes Phenomenon' (Pandey et al., 2014). The detailed methodology and its description will be discussed in Chapter 4.

3.7.2 Methods for Fusion of Hyperspectral image and LiDAR Derived CHM.

This methodology presents a clear idea about the process of integration of hyperspectral image and LiDAR derived CHM and its classification using MLC. The image fusion technique used in the present study is a PCA based fusion approach. This method employs the forward PC rotation application to the hyperspectral image and produces the PC image. Now, the PC1 band is removed from the PC image while integrating the CHM derived from LiDAR data. This CHM is numerically rescaled to the numerical values of the PC1 band and thus brings it to the same platform of the numerical strength of the PC1 band. The integration of the rescaled Canopy Height Model (r-CHM) in place of PC images is performed in accordance with the numerical strength of the PC1 band. Thereafter, this integrated PC image and r-CHM are set in the order of r-CHM, PC2, PC3, and so on. The inverse PC rotation technique was then applied to this integrated r-CHM and PC bands using the same statistical file generated during the forward PC application. Thus, the fused image is generated with this above methodology using PCA application. The applicability of the fusion techniques and results will be discussed in Chapter 5. Therefore, this chapter discusses about the study area, data acquisition and their processing and general methodology adopted in the study.

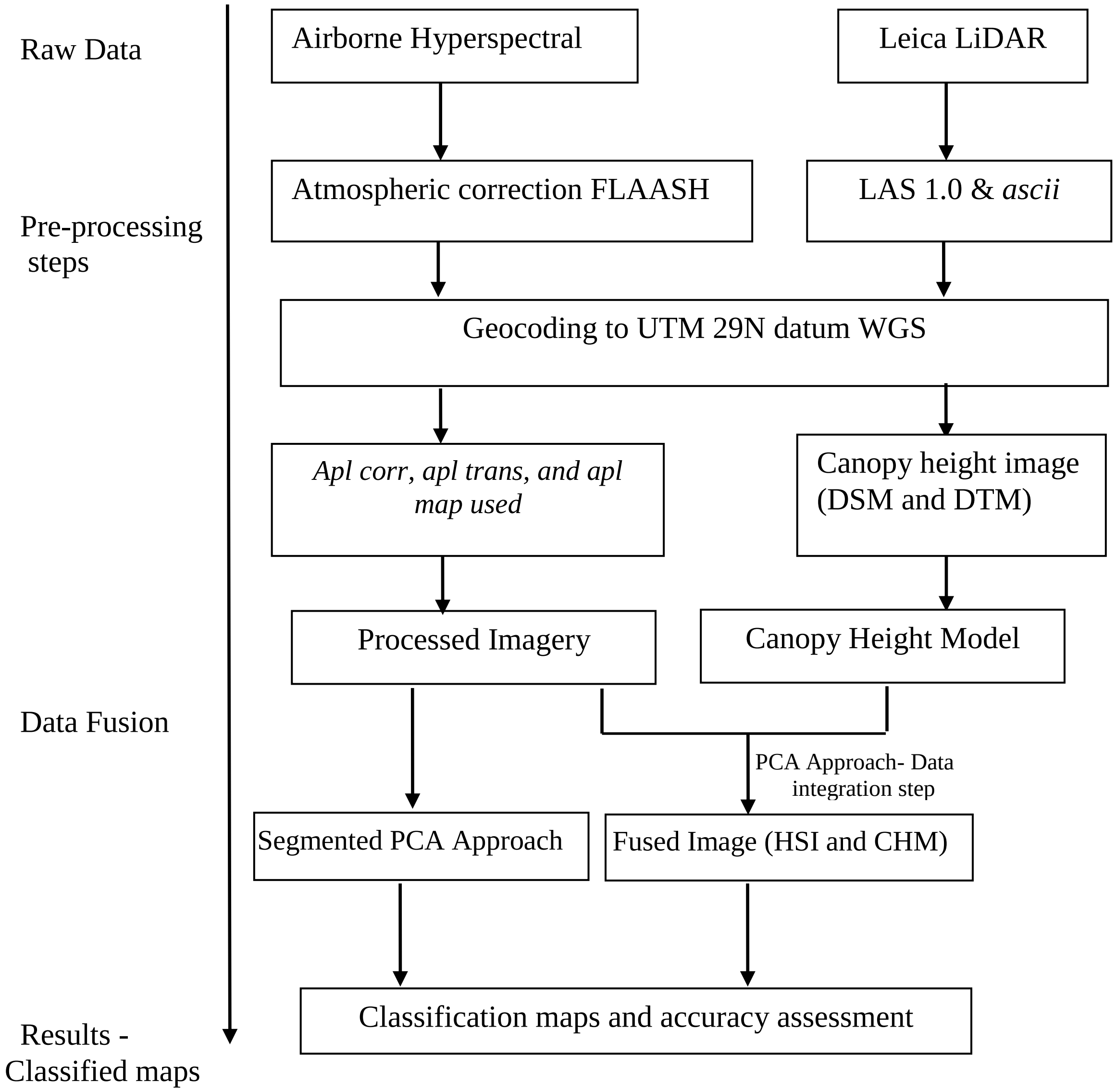

Figure 3.12. General methodology flowchart adopted in the study

Chapter 4. Segmented PCA Approach for Classification of HSI

4.1 Introduction

This chapter puts forward the concept of hyperspectral image segmentation and classification of hyperspectral images and segmented PC images. This chapter provides the segmentation analysis of the hyperspectral images using the PCA techniques that results in a new image called segmented PC image. The classification of hyperspectral and segmented PC image are performed using SAM and MLC classifiers. As discussed in chapter 2, classification or vegetation mapping is difficult with traditional or conventional methods. The field methods are time-consuming, difficult, expensive and require human or many manual works (Tueller, 1989). Due to these limitations, the field methods are not possible for a large region in a short time. Moreover in an inaccessible regions, it is quite difficult to acquire field data every time, there comes the role of airborne or satellite remote sensing as a valuable tool (Tueller, 1989).

Due to high dimensionality of hyperspectral images, it provide lower accuracy results (Thenkabail and Huete, 2012). Identification and classification of the tree species and ground features in the coastal Mediterranean forests are imperative for ensuring improved classification results and understanding the classification aspects using hyperspectral imaging sensors. It is now obvious that significant advances in the identification, classification, and mapping different tree species and ground features can be made using ground measurements and high-resolution hyperspectral images. However, a complete understanding of the HSI and its consistent applications is feasible only by adopting following conditions (Bellman, 1961, Hughes, 1968): (A.) performing hyperspectral data processing approaches (e.g., overcoming or reducing 'Hughes Phenomenon' or 'curse' of high data dimensionality), (B.) High correlation between the several the HSI band reduces and made uncorrelated to each other and (C.) Use of appropriate classification classifiers for identification and classification accuracy to facilitate accurate classification achieved for the processed HSI.

The use of segmentation of HSI and performing PCA applications on each segment of the HSI reduces the 'Hughes Phenomenon' as well as brings high data to low dimension. PCA application makes the high correlated bands of HSI to uncorrelated band assist the classification approach. In addition, PCA enhances the image and produces better visual display of the image than an original image (Jia and Richards, 1999) that helps in image interpretation and assists in image analysis along with ground measurements. Moreover, PCA generated images help in identification of various features easily, significantly differentiating vegetation from non-vegetated features (Castro-Esau et al., 2004).

Data redundancy, presence of noise, a significant variance among dataset makes a rigorous process and different application in hyperspectral images. Some authors have shown conventional parametric classification approaches i.e. maximum likelihood as limiting the ability to classify the high dimensionality data (Benediktsson et al., 1990, Jones et al., 2010). In the concern to these, segmented PCA approach is utilised with the incorporation of maximum likelihood classifier using the conventional methods for classification and mapping tree species. Due to a reduction in data dimensionality, conventional classification algorithm may provide good results. As the segmented PCA approach brings high dimensionality data to a reasonable dimension, which is handled with ease and hyperspectral imagery can be classified using maximum likelihood classification. This chapter discusses the 'Hughes Phenomenon', segmentation and PCA techniques and classification of resultant segmented PC image.

4.1.1 Hughes Phenomenon

Bellman (1961) investigated the relationship between the bands and the training samples for image classification. "The rapid increase with dimensionality in training sample size required for density estimation has been termed the 'curse of dimensionality' by Bellman" (Salehi et al., 2008) p.786. Thus, the dimensionality depends upon the number of bands, as the band number increases dimensionality of the image also increases (Bellman, 1961, Hughes, 1968). High dimensional image requires more number of training samples for a classifier and need increases exponentially. Thus, in the classifier design, it leads to ambiguity in the classification, where the accuracy increases and declines after that points onwards with an increasing number of bands, while keeping the training samples constant (Hughes, 1968, Scott, 1992). There exist a relationship between the number of training samples, band numbers of the images and consequent classification accuracy of the classified image (Fukunaga and Hayes, 1989). This phenomenon cannot be prevented unless provided with sufficient number of samples. It means that by adding more spectral bands to a standard classifier, the classification result eventually becomes less accurate (Alonso et al., 2011, Hughes, 1968, Ma et al., 2013, Nishii et al., 1997, Scott, 1992). Too many input bands can thus lead to a degradation of the classified map, resulting in lower accuracy result for classified hyperspectral image. Thus, segmented PCA was applied to reduce the 'Hughes Phenomenon' and enhance the classification accuracy.

There are several studies related to 'Hughes Phenomenon' for either reducing it or mitigating it (Shahshahani and Landgrebe, 1994). Band selection (selecting numerous bands out of all bands), PCA and MNF based feature transformations were some of the techniques evolved to reduce the 'Hughes Phenomenon' in hyperspectral image classification. There is also evidence of classification by SVM using feature selection for reducing data dimensionality (Pal and Foody, 2010). Initially, optimum band selection were used as one of the methods for classification of hyperspectral images (Ma and Zhang, 2011, Mausel et al., 1990). Band selection is a method of choosing few bands from several bands that may contain the unique information needed for classification (Chang et al., 1999, Mausel et al., 1990). Thus, band selection became the famous method of hyperspectral image classification, and sometime it lower the implementation of a classifier as some bands may have valuable information in discarded bands (Brunzell and Eriksson, 2000). Thus, choosing a better classification classifier may also produce lower accuracy results (due to data dimensionality). An attempt has been made to classify hyperspectral images using MLC while reducing the dimension of the image to generate the desired results.

Alternatively, other methods, mentioned below, were introduced which does not use selection of optimum bands but reduces the dimension of the data. These techniques or methods use all available images and transform them into a reduced number of dimensions without losing any information. Thus, various methods have evolved for classification of the hyperspectral images which neither discard any bands nor lose any little information. These approaches or techniques are feature based recognition (Miao et al., 2007, Mojaradi et al., 2009), K-L transform (Pu and Gong, 2000), segment K-L transform (Pu and Gong, 2000), CA transformation (Mallet et al., 1996), morphological transformations (Palmason et al., 2003, Pesaresi and Benediktsson, 2001, Plaza et al., 2002, Plaza et al., 2005), Wavelet transformation (Abibullaev and An, 2012, Bruce et al., 2002, Harvey and Porter, 2005, Kaewpijit et al., 2003, Mallet et al., 1997, Sarhan, 2013), vegetation index (Cho et al., 2008, Ma and Zhang, 2011, Pe'eri et al., 2008, Rosso et al., 2005, Smith et al., 2004, Zheng and Wang, 1992), and spectrum waveform characteristics in first order derivatives (Liu et al., 2011), second order differential, peaks, valleys (Chen et al., 1992, Demetriades-Shah et al., 1990, Li et al., 1993). These are the various methods to reduce the dimension of the hyperspectral images for different research and used according to objectives and aim of the research work.

4.1.2 PCA Approach

The PCA technique utilises conversion of inter-correlated bands into a new set of uncorrelated sets for spectral image. PCA technique reduces the dimensionality of the original image to lower dimension, converting 'n' to 2 or 3 new transformed principal component images, which contain majority of valuable information than rest of the bands (Chavez and Kwarteng, 1989). Thus, PCA is image transformation technique that mathematically transform original inter-correlated data into new uncorrelated bands known as components or axes (Chavez and Kwarteng, 1989). PCA technique is applied to the hyperspectral data which generates a set of uncorrelated bands such as PC1, PC2, PC3 from inter-correlated bands for spectral image (Chavez and Kwarteng, 1989, Karathanassi et al., 2007).

PCA technique helps in vegetation analysis with hyperspectral image particularly in two ways: it helps in data reduction by eliminating redundant bands and choosing top quality wavebands for modelling (Thenkabail and Huete, 2012). PCA condenses the original information of correlated bands into few uncorrelated variables with transformation of original data to new coordinate system. PCA acts as a step in reducing large number of wavebands to manageable wavebands without losing any valuable information. Thus, it does reduce the number of wavebands but retain most information of all wavebands. Other techniques that also reduces data but retain information were MNF, ANN, wavelet transformation, UFD (Uniform Feature design).

PCA is also considered as image enhancement method in remote sensing applications to distinguish between vegetated and non-vegetated features (Castro-Esau et al., 2004). It also assists in the classification of the vegetated areas especially over large spatial coverage. Thus, it also forms the basis of using this technique with segmentation part to identify and classification of the Mediterranean forest part.

PCA techniques reduce the data dimensionality and also produces better image visualization (Chavez and Kwarteng, 1989). Spectrum segmentation techniques was first used by Jia and Richards (1999) that took all the spectrum into account for generating each segment. Those results in fast clustering of spectral channels based on perceptions for visualization oriented segmentation. The colour representation of the selected PC component represents better visual colour than hyperspectral images (Du and Chang, 2003, Du et al., 2008, Tsagaris et al., 2005, Tyo et al., 2003). Du et al. (2008) in their recent research paper found that PCA based transformation produce better visualization of the hyperspectral images that are user based on combination of bands. In the present study, segmented PC image produced a better and enhanced visual image using different band combinations of segmented PC image.

4.1.3 Classification Approach

In this present study, SAM and MLC supervised based classification were used to analyze the occurrence or removal of 'Hughes Phenomenon' for hyperspectral image classification, in the region around St Andre, an important Mediterranean protected forest in the south-west of Portugal. The very first attempt to identify the tree species were based on the chemical composition of the leaves and performed by Wessman et al. (1988). The different remote sensors (optical and hyperspectral images) were introduced and used as a practical application to identify and classify the tree species of coniferous forest (Gong et al., 1997). Thereafter, to date several studies were carried out for mapping and classification of the tree species and ground features using airborne hyperspectral images (Clark et al., 2005, Dibley et al., 1997, Zhang et al., 2006). The different classifier techniques (like SAM, MLC, LDA, NNA) were used in the study, for discrimination of tree species and ground features. Identification of tree species were performed and distinguishability of tree species within the same genus were also reported for *Pinus* species by Van Aardt and Wynne (2007). Pu (2009) conducted studies using airborne hyperspectral imagery for discriminating tree species and mapping forest stands. The author achieved the classification accuracy above 80% using LDA and NNA methods.

Buddenbaum et al. (2005) performed the classification of coniferous tree species using a combination of spectral and textural characteristics in Germany. While using hyperspectral data only (spectral content), they used, namely SAM and MLC classifier techniques and reported an overall accuracy of 66% for that study. They found that MLC accuracy outcomes were generally higher than the results of the SAM (Buddenbaum et al., 2005). In one case, author reported the overall classification accuracy of 48.83% (SAM), 83.61% (ANN), 85.56% (MLC) and 50.67% (Decision tree) with random sampling using AISA hyperspectral images (Shafri et al., 2007). They demonstrated the performance of different classifier and illustrated that MLC outperforms the most advanced classifier techniques like SAM, ANN. The authors concluded that overall classification accuracy was higher for set of selected bands of hyperspectral images (85% and κappa= 0.77) than using the all spectral channels of hyperspectral images (77% and κappa= 0.65) (Möckel et al., 2014). This is also supported by Peña et al. (2013) that overall classification accuracy of SAM algorithm ranges from 60% to almost 80% depending upon the reflectance image, noise reduced reflectance images and resampling combinations of the pixel size (0.3 m, 0.6 m, 1.2 m, and 2.4 m pixel resolution). The pixel size of higher resolution i.e. 0.3-0.6 m has highest overall classification accuracy (almost 80%) as compared to the pixel size of 2.4 m that has an overall SAM classification accuracy of less than 60%. They found the lowest per class classification as low as 30% for the *Lythraea caustica* and *Acacia caven* (~50%) using SAM algorithms. This illustrates that spatial resolution also plays a prominent role in the classification results of the hyperspectral images instead of only spectral resolution. They concluded that spatial variation of hyperspectral has pronounced impact on the overall and per classification accuracy of the hyperspectral image associated with SAM algorithms. They also used Spectral Information Divergence (SID) algorithm and concluded the almost similar performance as SAM, but differ in that SID is more sensitive to decrease in the classification accuracy with the spectral degradation.

Le Cussan (1991) demonstrated that SAM classification of hyperspectral images (CASI-Compact Airborne Spectrographer Imager) resulted in 60.8% accuracy due to confusion between the sand dunes and *Bruguiera species* stands. Author argued about the relatively low accuracy with SAM is due to insensitivity to differences in relative brightness between pixels and the spectral library (Le Cussan, 1991). But the same area when mapped and classified using the MLC and data integration methods results in the higher accuracy (Held et al., 2003) as compared to the previous studies performed by Le Cussan (1991). Held et al. (2003) provided the better and improved results with the MLC algorithm and combined datasets for CASI and NASA AIRSAR images with higher accuracy as compared to SAM. Previously the Mahalanobis classifier based on supervised classification showed less classification accuracy (Ma et al., 2013). Moreover, some authors have shown conventional parametric classification approaches i.e. maximum likelihood as limiting in its ability to classify the high dimensionality data (Benediktsson et al., 1990, Jones et al., 2010). Although this statement makes MLC unsuitable but it can be used as useful classifier for classification after reducing the dimension of the hyperspectral imagery. Thus, the classifier techniques, wavelength and methods used to classify one species at one site may not give the desired results at another site due to change in data or environment (Clark, 2011).

In order to avoid the 'Hughes Phenomenon', the segmented PCA approach is utilised with the incorporation of maximum likelihood classifier for classification and mapping tree species. As the segmented PCA approach brings high dimensionality data to a lower dimension, which is handled with ease and classified using MLC. In order to increase the classification performance, the segmented PCA technique is a pre-processing for removing the redundant information substantially without losing significant information (Du and Chang, 2003, Jia and Richards, 1999). In this manner, MLC proved superior to another non-parametric classifier. MLC was chosen as a robust classifier in vegetation or forest mapping activities using either multispectral or hyperspectral imagery. Thus, MLC was chosen in the present study as a classifier after reducing the dimension of the hyperspectral using segmented PCA approach. Finally, the method or approach performed in the present study will be helpful for hyperspectral analysis by reducing the multidimensional data to a smaller dimension for processing while retaining most of the significant information. Therefore, SAM and MLC has been used in the study throughout for classification for maintaining consistency in the research.

4.2 Methods of Spectral Segmented PC Technique

The conceptual framework of the research followed the below mentioned main steps: geometric correction, atmospheric correction, image enhancement, image transformation [image conversion with PCA techniques (segmented PCA)], interpretation, classification, mapping and validation of the results. Most of these steps were already described in the pre-processing section of Chapter 3. The detailed methodology adopted in this present research are illustrated in Figure 4.1 and Figure 4.2. Figure 4.1 shows the flowchart of image segmentation and generation of segmented PC image (also represent the red block in Figure 4.2). Figure 4.2 illustrates the overall steps adopted in the study. Thus, the flowchart of the detailed methodology adopted in this study, the red rectangle shown in the flow chart is describing the details of segmentation and PC application for generation of segmented PC image illustrated in Figure 4.1.

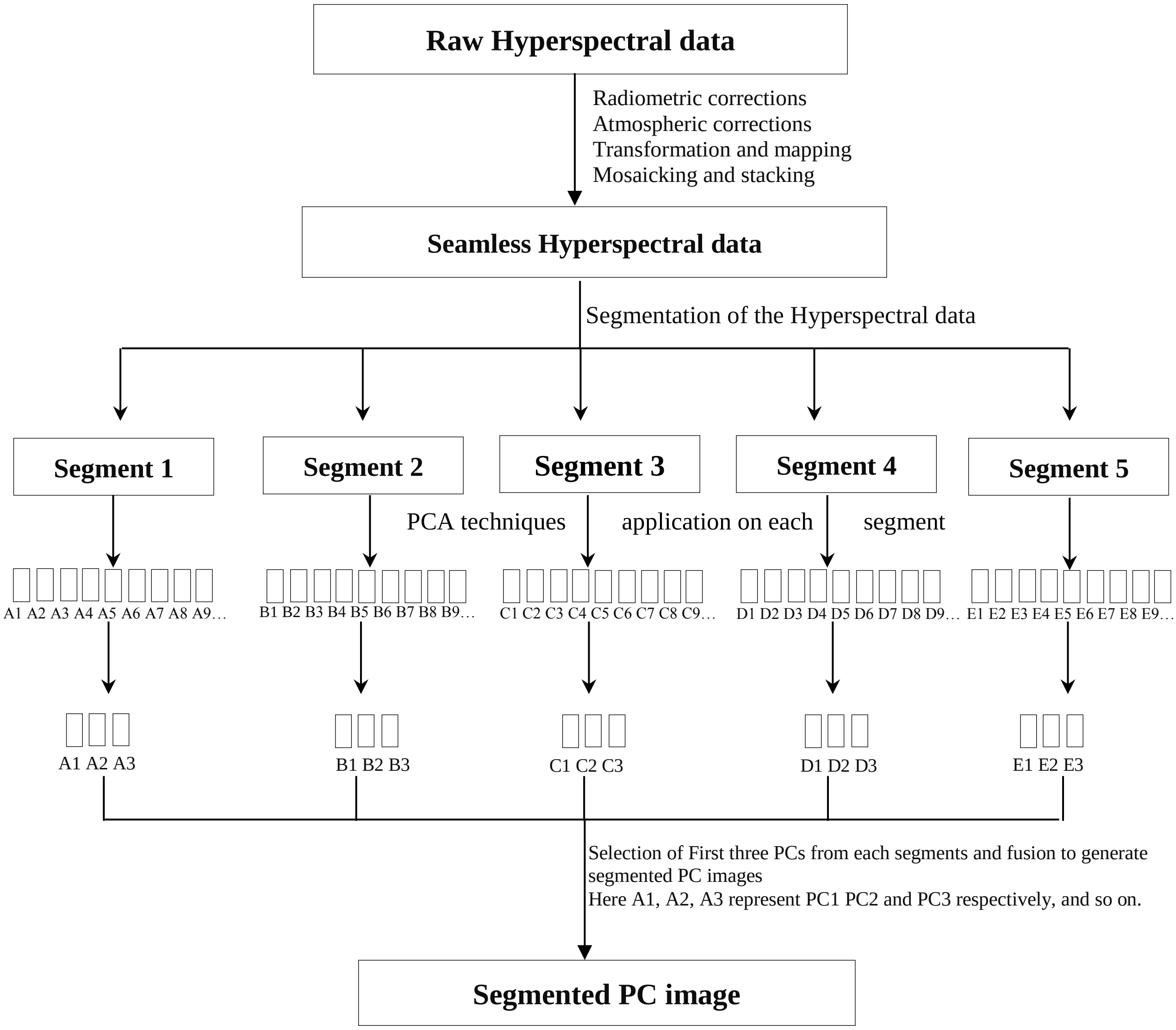

Figure 4.1 Flowchart illustration of segmented PC image generation for hyperspectral image

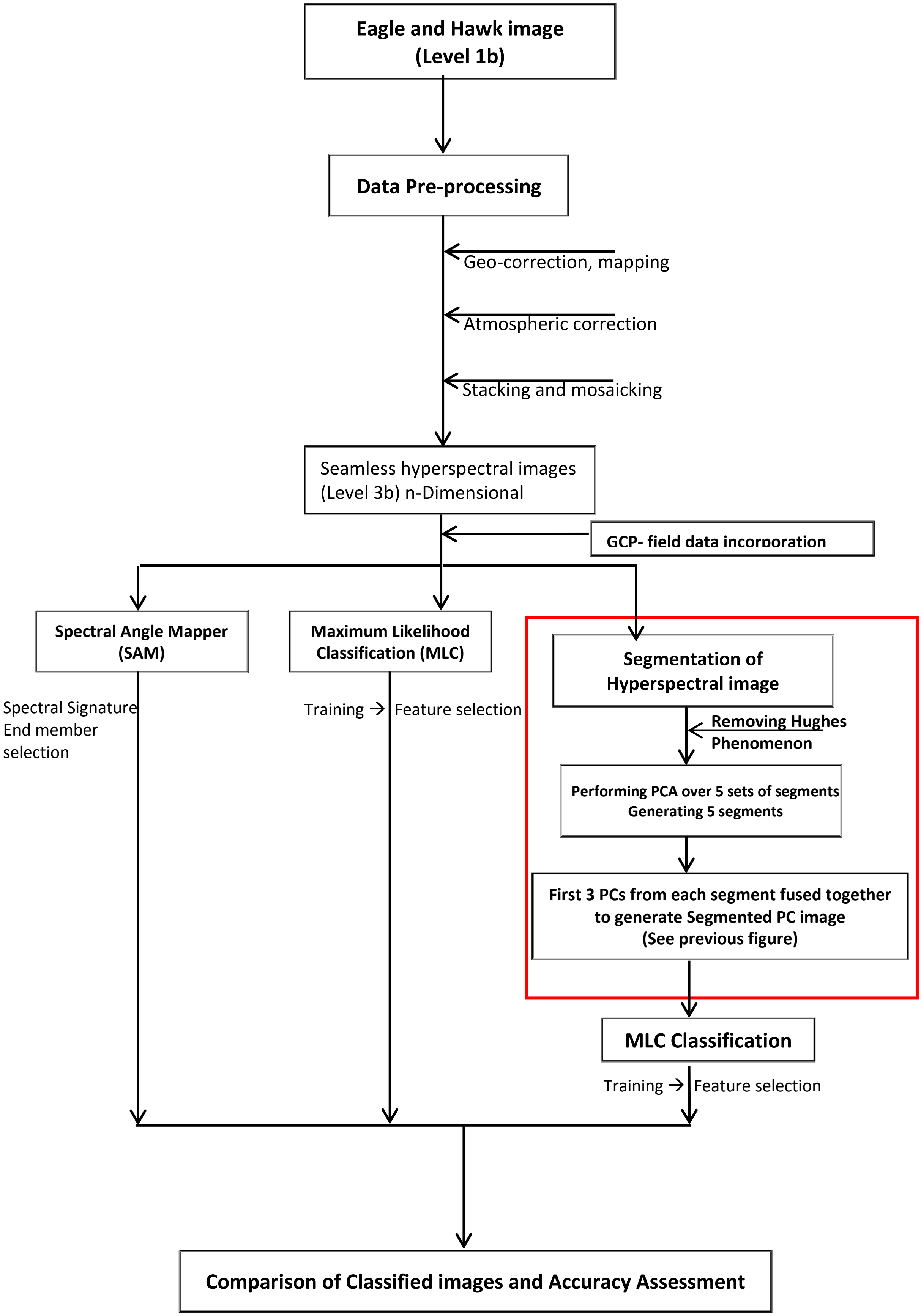

Figure 4.2 Methodology Adopted in the study of segmented PC image classification

4.2.1 Segmented PCA Approach

The segmentation mainly deals with the making segments at particular chosen ranges of the wavelength of electromagnetic radiation. Then, PCA techniques are applied to each segment of the image. Segmentation of the hyperspectral image is based on spectral and histogram information. Spectral criteria are chosen to keep the spectral range which are most important for discrimination of the vegetation and other ground features. So, blue, green, red, NIR and SWIR wavelength ranges are taken into consideration. Mostly, vegetation and other ground features are demarcated from each other in blue, green (demarcate different vegetation), red, NIR and thermal range. Thus, an optimal range is chosen such as it can distinguish several features. There is a difference between the traditional PCA and PCA application on segments of hyperspectral images. PCA applied in the segments of hyperspectral images compress the data thus reducing the data dimensionality whereas in Multispectral image PCA is able to find the spectral band with most of the variability. The PCA performed on 7 bands of multispectral images will results in the 7 PCs, out of which only first 3 or first 4 will contain the information (feature recognition ability from the image) and rest will contain noises. Therefore, only three PCs are available from multispectral PCA techniques. While for hyperspectral images, it can be made several segments (in my case 5), that generates corresponding PCs corresponding to the number of bands in the segment (segment is the part of hyperspectral with bands). Thus, each segment will contribute to PCs images, where first 3 PCs from each segment contain information against others. (Information here means- when they are displayed with ENVI software or other software, one can able to identify the features easily). So here these useful PCs were integrated to generate the segmented PC image which is not possible with the even high resolution multispectral image. This integration is the main difference which clearly states that it differs significantly as well as innovative difference between hyperspectral and multispectral image.

Earlier, Jia and Richards (1999) achieved the overall classification results of 98.6% and 97.0% for Jasper Ridge and Moffett Field images respectively, and confirmed the enhanced visual display of the segmented images than original AVIRIS images. They compared the segmentation technique with the traditional PC techniques for the classification and display enhancements. presented a segmentation method for Hyperion hyperspectral images for invasive species classification using 4 groups of data, and found the κappa coefficient ranging from 0.32 to 0.82 (0.32, 0.45, 0.44, 0.5, 0.52, 0.56, 0.57, 0.55, 0.61, 0.81, 0.64, 0.69) and overall accuracy varies from as low as 42% and up to 86% for the classification. These four group consists of visible, NIR, SWIR 1 and SWIR 2 for the above research. This present work differs from the above in the adoption of five segments and comparison of segmentation techniques with airborne AISA hyperspectral images, where blue, green, and red wavelength ranges were considered. As these three ranges plays a significant role in tree distinguishing capability. Reflectance pattern in different amount in green, and blue region leads to different colour of the tree leaves, such as dark green (*Eucalyptus globulus*), light green (*Acacia longifolia*), bluish green (*Pinus pinea*).

This is argued by Cheriyadat and Bruce (2003) that sometimes PCA fails to extract the useful information for separating different targets, and this may be possible that higher order PCs do not always retain information to distinguish target features. Thus, using PC on the full range of wavelengths, particular small spectral segment ranges were taken into consideration while making the segmentation of hyperspectral images. The segments were selected based on the spectral response, reflectance behaviour and patterns shown by tree species and histogram data distribution of the image (See section 4.3.2, Figure 4.4, Figure 4.5 and Table 4.2).

Histogram statistics of the image provide information regarding the distribution of the image values. Each band of hyperspectral image has values that define ranges and their distribution that differ for each single band. This information is used to look at the distribution of image value for each single band and generate the histogram statistics. The bin values are created to include all ranges (min-max). The frequency is plotted using the image value of the each band against the bin values (See Figure 4.4). The x-axis of the figure represents the image values (tonal variations) and the y-axis represents the number of pixels (frequency). This information is only used to segment the hyperspectral images in the study (Figure 4.5 shows the some bands of hyperspectral image).

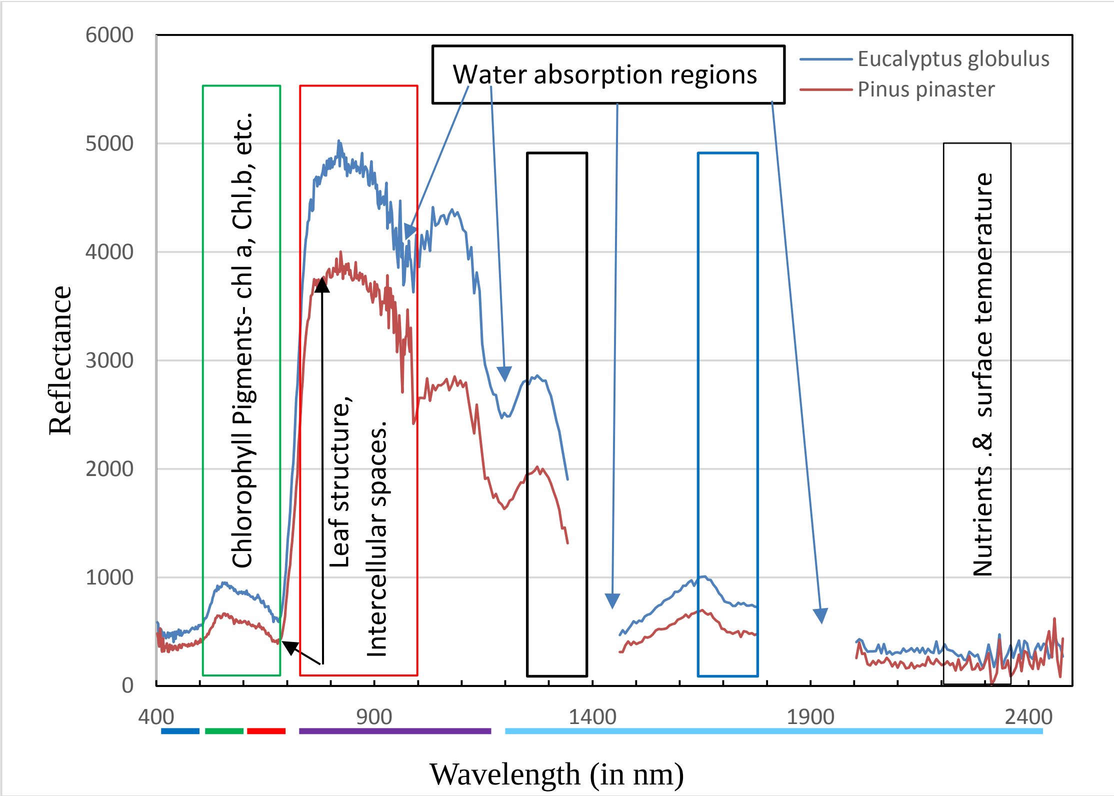

Figure 4.3 Reflectance comparison of two tree species, *Eucalyptus globulus* and *Pinus pinaster*, for their unique signature

Figure 4.3 shows the spectral profile of *Eucalyptus globulus* and *Pinus pinaster* for comparison of signature unique to them. The tree species are mainly distinguished from each other at blue, green, red wavelength region due to absorption by different pigments such as chlorophyll, a, b carotenoids, xanthophyll (Blackburn, 2007, Devlin and Baker, 1971, Zarco-Tejada et al., 2001), red-red edge region due to sharp increase in reflectance, and NIR regions as multiple internal reflection takes place in leaves internal structures (Tucker and Garratt, 1977). Sometimes at the thermal region absorption are caused by water contents as shown by arrows in the Figure 4.3 (Gupta et al., 2001, Jacquemoud and Baret, 1990). The thermal region of the wavelength are often used to measure the nutrients, surface temperature as well as water stress condition of the tree than comparing and differentiating species. Thus, Figure 4.3 illustrates the electromagnetic regions related to leaves photosynthetic pigments, structural parameters, water content and nutrients present in the different tree species.

The green box shows that *Eucalyptus globulus* has chlorophyll peak in the green region of wavelength due to high amount of chlorophyll as compared to the *Pinus pinaster*.

The black arrows show the red and red edge region of the electromagnetic wavelength, where vegetation shows a sharp increase in the reflectance due to leaf optical properties and act as a transition zone between visible and NIR region for chlorophyll activity and cellular structure of leaves.

Reflectance in NIR region is dependent on the leaves and cellular structure; more the dense canopy or number of leaves, higher is the reflectance. Moreover, due to leaf structure and cellular structures, reflectance in NIR region is much higher than the blue, green and red regions. *Eucalyptus globulus* is showing a higher reflectance than *pinus pinaster*, so it is evident that *Eucalyotus* is having large number of leaves and dense canopy as compared to *Pinus pinaster*, that has needle shaped leave and thin canopy. Thus, reflectance of the feature provides their characteristics and can be distinguished from other features easily.

Now, in accordance with Figure 4.3, the spectral ranges that can differentiate tree species and other ground features can be seen with marked arrows and rectangular box. The physiological differences between tree species are apparent in the spectral region from 400 nm to 800 nm (Paap et al., 2008). This difference is within visible range and near red edge region of the reflectance spectra. However, in the present scenario, this range is 500 nm to 850 nm in Eagle-Hawk sensor of hyperspectral data (Figure 4.3). Thus, the variation in this reflectance range can be used precisely to discriminate different species using hyperspectral datasets. The differentiating properties can be found with differences in green peak, sharp boundaries from red-edge to NIR, reflectance in NIR region and thermal regions.

Therefore, the differences can be observed in the visible range at the chlorophyll absorption region (506.15 nm -623.48 nm- segment 1) and also in the region starting from red edge to NIR ranges (728.31 nm -988.37 nm- segment 4) within the conifer needles of *Pinus* and broad leaves of *Eucalyptus*. In comparison, the *Pinus pinaster*'s needle like leaves appear bluish-light green in colour, that may be due to lower reflection in green areas of the visible spectrum as compared to *Eucalyptus* that appear dark green (high reflectance in green region). The region for choosing blue regions of spectrum (400 nm to 506.15 nm-segment 2) stand on the base of light blue green leaves colour of *Pinus pinaster* and *Pinus pinea* species. Red region (623.48-728.31 nm) is left between above three selected ranges, and it is selected as selected as third segment.

Furthermore, the water absorptions at 1400 nm, 1900 nm and 2400 nm (1002.3–2238.71 nm) and water content differ in depth and shape among different tree species types. This whole spectrum range is selected as segment 5 to complete the segmentation technique (unless study focuses on the water stress or diseased conditions of the vegetation). Thus, several factors such as chlorophyll, leaves structure, water content and absorption influence reflectance spectra of vegetation at different spectrum of wavelength giving unique signature for different tree species. The typical reflectance shown by tree species evidently shows the difference at five discussed wavelength regions.

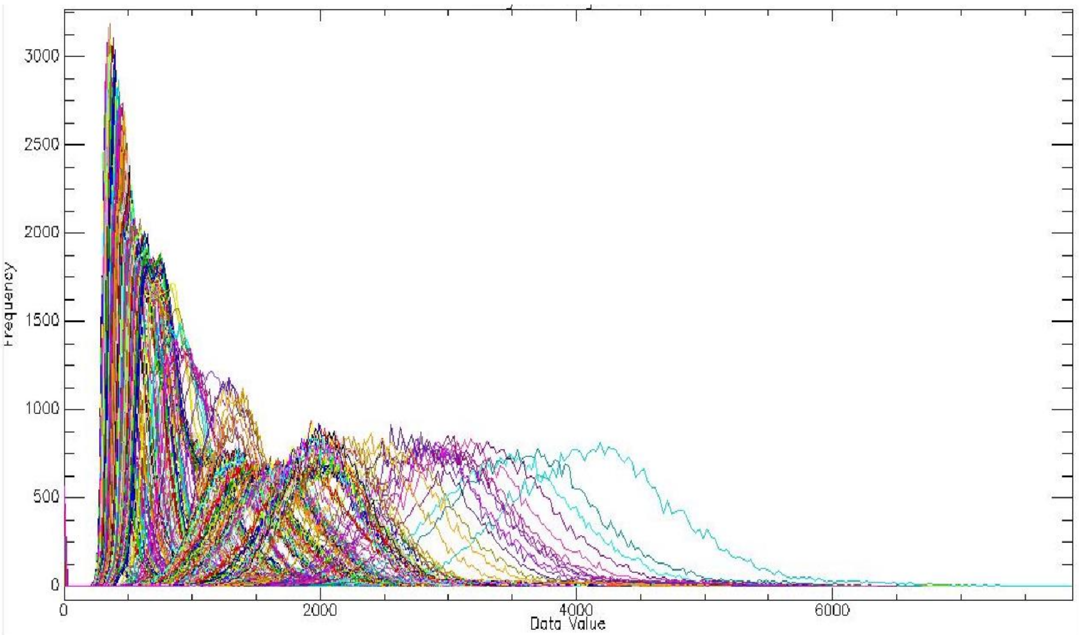

Figure 4.4 Frequency distribution of the hyperspectral image

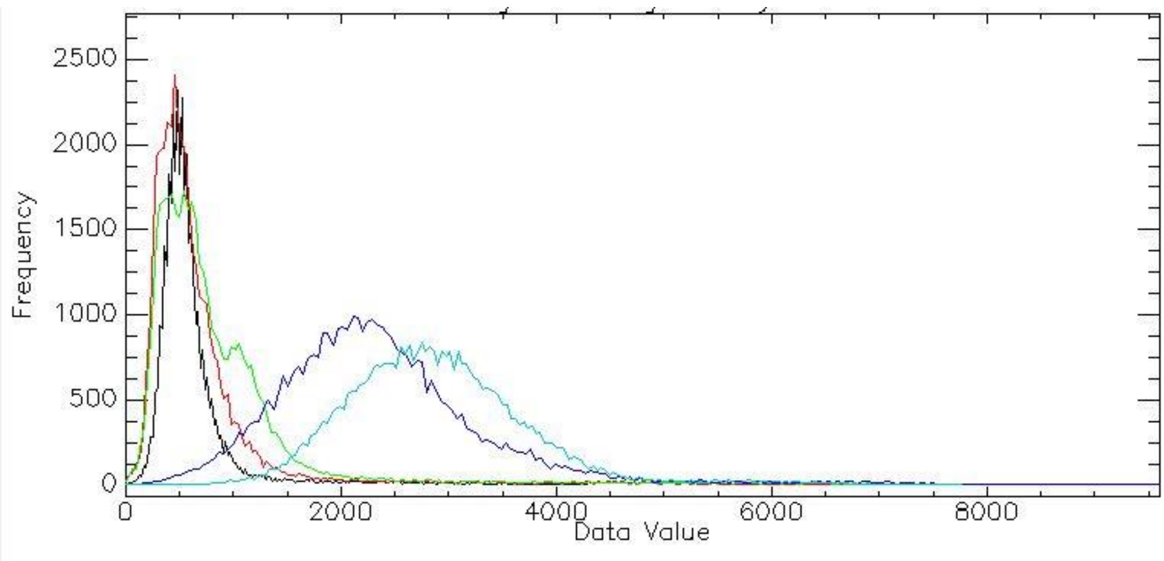

Figure 4.5 Histogram of band 1 (red), band 49 (black), Band 99 (green), band 142 (blue) and last band 20 (sky blue) (hawk image) in sequence.

Table 4.1 Segmentation approach and retention of information in comparison with data dimensionality

Segmentation of HSI	**Number of PCs from each segment**	**Number of Integrated PCs**	**Conclusions**
4 Segments	3PCs	12	Less dimension with lesser information
5 Segments	3PCs	15	Less dimension and most of the information
6 Segments	3PCs	18	Higher dimension and more information

Table 4.1 shows that if four segments were considered it has total 12 bands, for five segments it has 15 bands, and for six segments it will result into 18 segments (when first 3 PCs were chosen to generate the segmented PC image). According to it, five segments is suited better as it has less number of bands as well as more information of the data (see Table 4.1). It is assumed on dimensionality basis, to have as much as lower dimension and have more and more information. The reason, for choosing the five segments, is in fact it covers the spectrum in different range and providing the blue, green, red, NIR and thermal range of the spectrum regions as well. This range is not possible with the four segments and six segments as they may overlap with one or two ranges of the spectrum regions as well as distributing the image values overall (see the

proximity of the histograms – initial bands are very close to each other as against the later bands in Figure 4.4 and Figure 4.5). Thus, it is assumed that generating the segments of HSI brings down dimensionality and provide more information too. Thus, the five segments of the HSI are one of the most feasible ways to maintain the most of the information while reducing the data dimensionality. It will generate 15 integrated PCs from 5 segments of HSI. Thus, it has most of the information as well as reduced dimension. Let us consider six segments, it will have 18 integrated PCs with the most information, but again, it will have higher dimension than the 15 integrated PCs. While considering 12 Integrated PCs – It is assumed that is will be generated from 4 segments, which have lower dimension but less information than above cases (See Table 4.1).

Moreover, it has been shown that higher amount of variance is shown in the short wavelength region by hyperspectral images, where visible and NIR ranges dominate the PCA techniques (Tsai et al 2006). Therefore, segmentation techniques for PC application are extracted from visible and NIR regions. Segmentation of hyperspectral images suggests the step to make several small segments of a single image into many parts. Five segments of the hyperspectral imagery were generated using the important spectral ranges and variation in overall histogram statistics. Thus, segmentation of the hyperspectral images is based on the spectral properties as well as histogram properties. Segmentation is performed to bring down the high data dimensionality to lower dimensions, as well as to maintain the most of the information of the HSI.

Figure 4.6 (a) represents the covariance matrix generated from the statistic of PCA analysis, which provide the information regarding uncorrelated variables and correlated variables. In the case of completely unrelated variables in the data, the matrix would be uniformly grey except along its diagonal whereas, in case of correlated variables, the matrix would not be uniformly grey, where black, grey and white represent to negative, none and positive covariance respectively. In the case of a correlation matrix, a black portion maps to low correlation whereas white parts map to the high correlation between the data dimensions. The graph in Figure 4.6 (b) showing the white part represent the diagonal elements of the matrix are variance of each band and the other non-diagonal elements are the covariance of the corresponding band in row and column. Clearly, this is evident from the both Figure 4.6 (a) and (b) about the correlation between variables. Matrix of the hyperspectral data set was representing the correlations between the bands hyperspectral image, where black represent no correlation and white to the highest correlation (White= ±1 and Black= 0). The diagonal represents the highest correlation value 1 illustrated in white, whereas, the darker tones, i.e. grey and black represent the lower absolute value of the correlation.

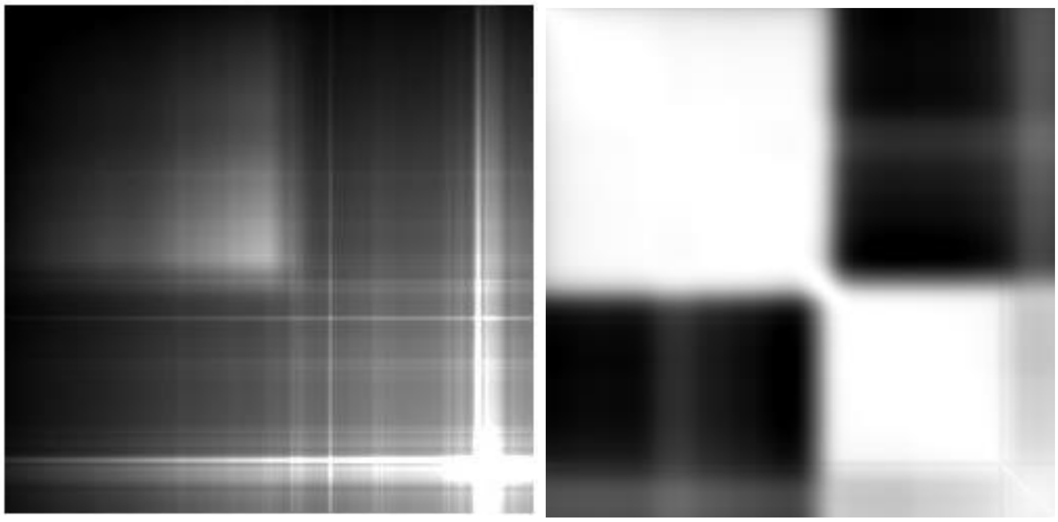

Figure 4.6 (a) Covariance matrix and (b) Correlation matrix generated from a hyperspectral image .

Principal component analysis was performed on the each segment of the hyperspectral images to get five segmented PC images. Each of the segmented PC image have the same number of PC bands as the number of inputs bands (see Table 4.1). Out of those PC bands, first 3 PCs were chosen from each segmented PC image and fused together to make an integrated segmented PC image. Thus, 3 PCs from 5 segmented PC images will constitute 15 integrated segmented PC images (See Table 4.1). PCA produces PC images that generate uncorrelated bands having different features at different corners that are not possible in original hyperspectral images. In hyperspectral image, different features are found to be on the same diagonal line, means they are highly correlated with each other.

The importance of performing PCA analysis in the present research, is illustrated in Figure 4.7 and Figure 4.8. Figure 4.6 shows that all bands are highly correlated with each other. Thus, Band 1 and Band 2 of the hyperspectral images provide an idea that both are highly correlated due to location of feature class on the straight diagonal line passing through the origin. The different class features lie on a straight line passing through the origin of the two bands. The scatter plot shows that the various features were highly correlated in Figure 4.7. The scatter plot generated from the PC1 and PC2 shows that the various features were highly uncorrelated in nature, and they are located at the extreme corners of the scatter plot (as shown in Figure 4.8). The location points of different tree species, sandy regions and other features were related to their reflectance properties.

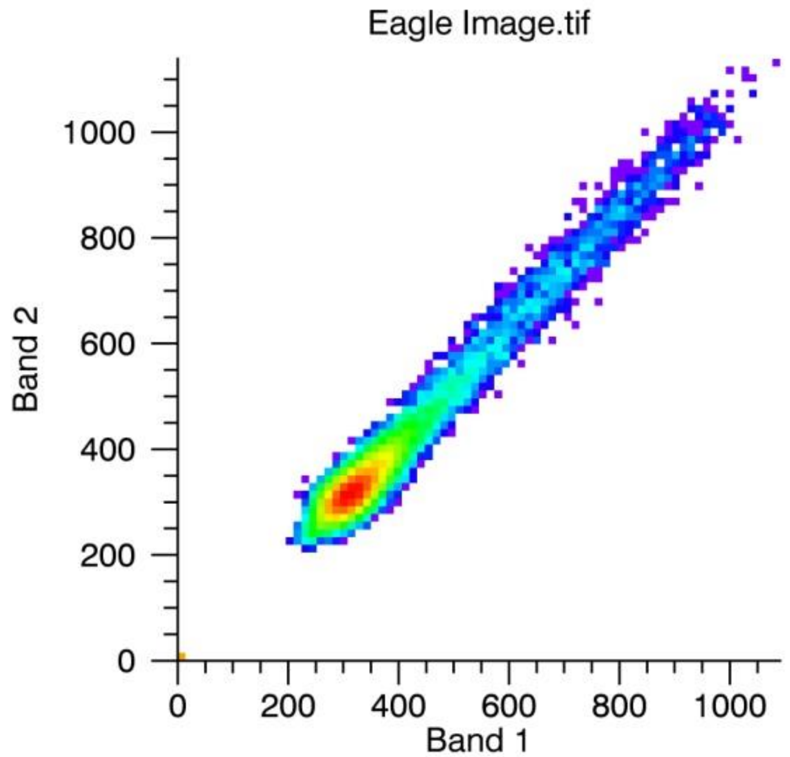

Figure 4.7 Scatter plot between Band 1 and Band 2 of hyperspectral image showing high correlation between different bands

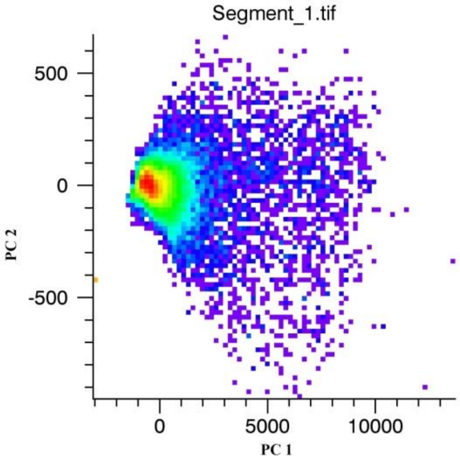

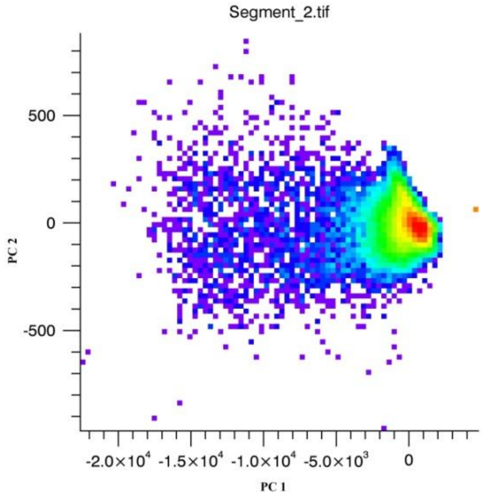

(a) Segment 1 (b) Segment 2

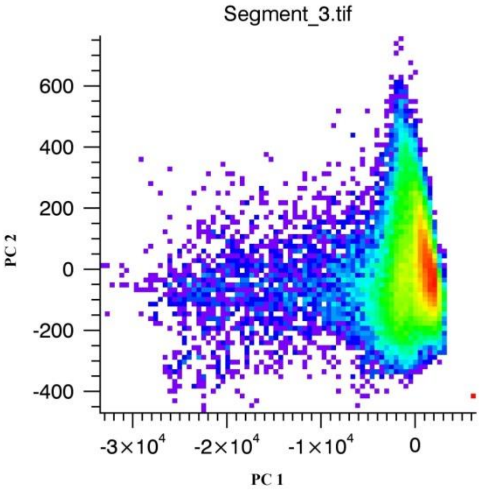

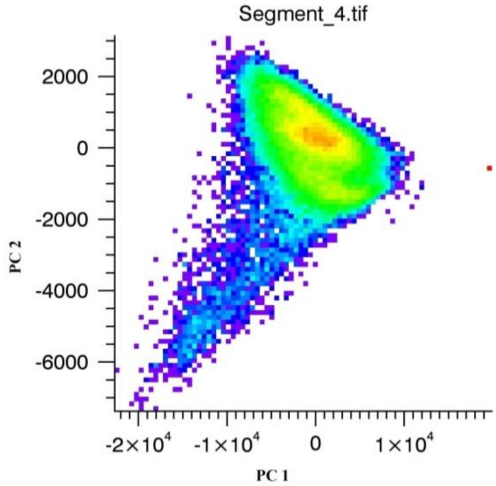

(c) Segment 3 (d) Segment 4

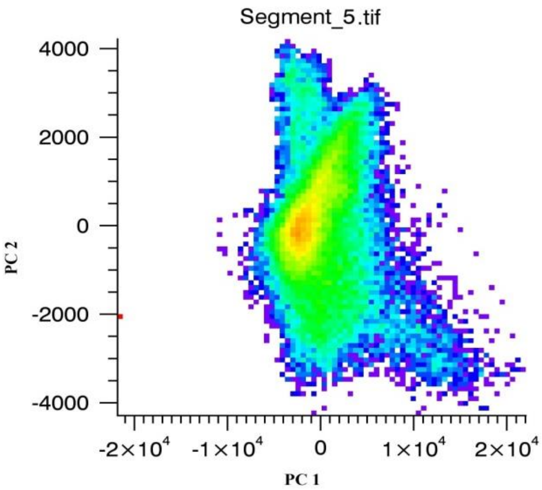

(d) Segment 5

Figure 4.8 Scatterplot between PC1 and PC2 of PCA images showing uncorrelated bands of five segments of hyperspectral images (a-e)

These PCA transformation techniques provide uncorrelated output bands (as shown in Figure 4.8) from the highly correlated input bands (as shown in Figure 4.7). Thus, PCA is needed to generate uncorrelated bands from highly correlated bands where data ranges differ significantly between original bands. This technique generates a new set of transformed orthogonal axes having an origin at the data mean. To maximize the variance among the data, orthogonal axes is rotated along the origin. Figure 4.7 shows the correlation between the band 1 and band 2 of original data whereas Figure 4.8 shows the relationship between PC1 and PC2 of the PCA outputs of five segments (PC images of five segments).

4.2.1.1 Savitzky-Golay FIR spectral smoothing filter

“Savitzky-Golay smoothing filters (also called digital smoothing polynomial filters or least-squares smoothing filters) are typically used to "smooth out" a noisy signal whose frequency span (without noise) is large” (MathWorks, 1994). In this filtering, a significant amount of noise with high-frequency content from the signals were removed as compared to other standard averaging filters (Luo et al., 2005b, Luo et al., 2005a, Orfanidis, 1996). For the purposes of removing the noise and smoothing the raw spectral reflectance data, Savitzky-Golay least squares filter was used in the present study. This filter smoothened the spectra profile while maintaining the position, shape and depth of the spectral features that means it does not affect the spectral profile but removes the noises. Thus, it has minimal effect on spectral profile curve’s position and shape. Therefore, Savitzky-Golay was selected for smoothening spectral profile with minimal consequence shape and depth of spectral curves (Press et al., 1996). The Savitzky-Golay filter is applied to the spectral profile collected from atmospherically corrected hyperspectral data. This filter is mainly applied in the spectra to reduce the high and low frequency in the spectral profile of tree species. The relative widths and heights of noisy spectral curves are reduced to a visible level by this filter, thus providing smoothing without loss of resolution in spectral data. The spectral reflectance obtained after applying Savitzky-Golay filter is shown in the result section 4.3.1.

4.2.2 Use of Classifier Techniques.

In the present study, two different classifiers SAM and MLC were selected for classification of hyperspectral data and their comparison. The selection of two classifiers depends upon the previous performance of the classifiers presented in the previous studies as well as user-friendly environment of the classifiers. This study utilises the two classifiers for classification of HSI and segmented PC image.

4.2.2.1 Spectral Angle Mapper

SAM algorithm is a physically-based spectral classification (Kruse et al., 1993) which calculates the spectral similarity between a pixel spectrum and a reference spectrum as "the angle between their vectors in a space with dimensionality equal to the number of bands" (Kruse et al., 1993). SAM uses the calibrated reflectance data for classification and thus relatively insensitive to illumination and albedo effects. End-member reference spectra used in SAM were collected from hyperspectral imagery. SAM compares the angle between reference spectrum and each pixel of an image in n-D space (Boardman, 1992). SAM classification uses reflectance data for classification, not the radiance data. However, use of radiance data does not produce significant error because the origin is still near zero (Boardman, 1992, Boardman and Kruse, 1994, Boardman, 1995, Boardman et al., 2006, Kruse et al., 1993). This 'spectral angle' (α) is calculated as:

$$\propto = \cos^{-1}\left(\frac{t.r}{\|t\|\,\|r\|}\right) \qquad \text{Equation 4.1}$$

Where, α = Angle formed between reference spectrum and image spectrum, and t = Image spectrum, and r = Reference spectrum.

This equation can be written in other formulation as shown below and given by Boardman in 1992 (Boardman, 1992):

$$\propto = \mathbf{cos}^{-1}\left(\frac{\sum_{i=1}^{nb} t_i r_i}{\left(\sum_{i=1}^{nb} t_i{}^{2}\right)^{1/2}\left(\sum_{i=1}^{nb} r_i{}^{1/2}\right)^{1/2}}\right) \qquad \text{Equation 4.2}$$

The SAM value is expressed in radians, where minor angle α, represents the major similarity among the curves. The angle α, determined by $\cos^{-1}$, presents a variation anywhere between 0^o and 90^o (Equation 4.1 and 4.2). The above equation can also be presented as Cos α. In these conditions, the best estimate acquires values close to 1. Thus, SAM uses an n-Dimensional angle to match the pixels to reference spectra. SAM assumes reflectance data for the classification. However, if radiance data were used, the error was not significant because the origin is still near zero. Hyperspectral image was classified using SAM and output was compared with the result of MLC classification.

4.2.2.2 Maximum Likelihood Classification

MLC technique was used to classify both the original hyperspectral images as well as segmented PC image. The concept of MLC was understood before proceeding to the techniques. According to Richards and Jia, MLC techniques are described as:

> "Maximum likelihood classification assumes that the statistics for each class in each band are normally distributed and calculates the probability that a given pixel belongs to a particular class. Unless a probability threshold is selected, all pixels are classified. Each pixel is assigned to the class that has the highest probability (that is, the maximum likelihood). If the highest probability is smaller than a specified threshold value, the pixel remains unclassified" (Richard and Jia,1999, p.240).

MLC is calculated for the discriminant functions for each pixel in hyperspectral image by ENVI software and represented in mathematical form mentioned below (Richards and Jia, 1999):

$$\boldsymbol{g_i(x)} - \ \mathbf{ln}\, \boldsymbol{p}\ (\boldsymbol{\omega_i}) - {}^{\mathbf{1}}\!/_{\mathbf{2}}\, \mathbf{ln} \,|\textstyle\sum_{\boldsymbol{i}}| - {}^{\mathbf{1}}\!/_{\mathbf{2}}\, (\boldsymbol{x} - \boldsymbol{m_i})^{\boldsymbol{t}} \textstyle\sum_{\boldsymbol{i}} \mathbf{-1}\, (\boldsymbol{x} - \boldsymbol{m_i})_{\boldsymbol{i}} \qquad \text{Equation 4.3}$$

Where, i = class, x = n-dimensional data (where n is the number of bands)

$p(\omega_i)$ = probability that class ω_i occurs in the image and is assumed the same for all classes, $|\Sigma_i|$ = determinant of the covariance matrix of the data in class $w_{i,}$

Σ_i^{-1} = its inverse matrix , m_i = mean vector.

Some authors have shown conventional parametric classification approaches i.e. maximum likelihood as limiting in its performance to classify hyperspectral image (Benediktsson et al., 1990, Jones et al., 2010). As segmented PCA approach brings high dimensionality data to a reasonable dimension, which is handled with ease and classified using maximum likelihood classification. In order to increase the classification performance, segmented PCA technique is a pre-processing for removing the redundant information substantially without losing significant information. After that MLC method was used for classification purposes.

4.2.2.3 Accuracy Assessment

For the assessment of the classified image, different accuracies were used such as overall accuracy, producer accuracy, user accuracy and kappa coefficient. The error matrix was calculated using the reference data used for generating error matrix of each feature in classified images (Congalton et al., 1983, Stehman et al., 2009). The error matrix generated different accuracy parameters like user's accuracy, producer's accuracy, mapping accuracy and overall accuracy for comparison purposes of different classified images (Congalton, 1991, Congalton and Green, 2008). In addition to these accuracies, κappa statistics was also calculated for each classified images to test the significance of the difference in accuracy of classified images. The equations to calculate overall, user, producer accuracy and κappa coefficient are given below:

$$\text{Overall Accuracy} = \sum_{i=1}^{k} \frac{n_{ii}}{n} \qquad \text{Equation 4.4}$$

$$\text{User Accuracy} = \frac{n_{ii}}{n_{i+}} \qquad \text{Equation 4.5}$$

$$\text{Producer Accuracy} = \frac{n_{ii}}{n_{+i}} \qquad \text{Equation 4.6}$$

$$\kappa = \frac{N \sum_{i=1}^{r} xii - \sum_{i=1}^{r} (x_{i} . x_{+i})}{N^2 - \sum_{i=1}^{r} (x_{i+} . x_{+i})} \qquad \text{Equation 4.7}$$

Where, r= is the number of rows in the matrix, x_{i+}= are the marginal totals of row *i*, x_{+i}= are the marginal totals of column *i*, x_{ii}= is the number of observations in row i and column *i*, N= is the total number of observations.

Generally the κappa values (coefficient of agreement) ranges from 0-1, with a positive correlation between the classification and reference data for remote sensing images (sometime they may range from -1 to 1). Usually, values greater than 0.80 represent a strong relationship between the reference data and remote sensing images. Values between 0.4-0.8 represent moderate agreement between the two data. Lastly, a κappa value that is below 0.4 represent a poor agrrement or relationship between the remote senisng images and reference data whereas a perfect classification of image would produce a κappa value of one. (Congalton et al., 1983, Congalton, 1991, Congalton and Green, 2008, Story and Congalton, 1986). Therefore, it has been considered that κappa is one of the better tool for comparing different methods of classified images, because overall accuracy does not compensate for the chance agreement whereas κappa does it better than all (Skidmore, 2002). A κappa of 1 illustrates perfect agreement, while a κappa of 0 value indicates agreement that is close to chance (Carletta, 1996). Therefore, studies performed over different features or several observations include κappa statistics, which sometimes agree or disagree simply by chance (Viera and Garrett 2005). Therefore, the use of κappa statistics is better than other statistics such as overall accuracy. Thus, these statistics provide a better platform, which is directly comparable with each other classification results.

4.3 Results

This section of the chapter discusses the outcomes from classification of HSI and segmented PC images. This section also presents the spectral profile of raw hyperspectral image, atmospherically corrected hyperspectral image and use of the smoothing filter in the spectral profile of the features generated from the original atmospherically corrected hyperspectral image. This section mainly deals with the results discussion in relation to the classified images (SAM and MLC classification of hyperspectral image and Segmented PC image). After that, it presents the accuracy assessment of all three classified images generated in the study.

4.3.1 Spectral Profile of Hyperspectral Image

The surface reflectance of the tree species and surrounding areas is the foremost requirement of hyperspectral image classification using classifier techniques. An atmospherically corrected hyperspectral image is required to perform the qualitative analysis of the surface reflectance. Surface reflectance is achieved by removing the atmospheric effects such as water absorption, scene visibility from the raw hyperspectral image, discussed in Chapter 3. Radiance values from the raw hyperspectral image (level 1b) and reflectance values extracted from the atmospherically corrected HSI (level 2b) of the study scene were presented in Figure 4.9.

The result and outcome achieved with airborne hyperspectral imagery were shown and discussed in this section. The spectral profile of raw hyperspectral image and atmospherically corrected image is shown in Figure 4.9. The raw hyperspectral image showed the calibrated radiance (X axis- Band Number and Y axis- DN values) whereas atmospherically corrected hyperspectral image showed the surface reflectance (X axis- Wavelength and Y-axis- Reflectance values). After application of FLAASH on the radiance image, the resultant reflectance image shows an apparent decrease of high frequency or noise and actual surface reflectance of the vegetation as shown in Figure 4.10 b.

The classification map was generated through the classification of the atmospherically processed hyperspectral imagery (Eagle sensors) according to vegetation reference spectra in the form of the collected reflectance spectra from hyperspectral imagery using ground data and aerial photographs. Thus, endmember spectra used in SAM for classification was generated from ROI average spectra from hyperspectral imagery. Spectral classification was performed using the SAM: spectral matching algorithms that are popular for vegetation mapping applications and commonly included in remote sensing software packages (such as ENVI 4.4 ©). Before going for SAM classification, the spectral profile of the different species was recorded from hyperspectral Eagle stacked imagery using z-spectral profile application tool of ENVI. The reflectance spectra were mixed with different high and low frequency and also associated with atmospheric signals (Figure 4.10 a). To remove these high-frequency noises and atmospheric signals, Savitzky-Golay smoothening filters were applied to the atmospheric processed hyperspectral imagery (See Figure 4.10 b).

The data in the spectral range of 989.69 nm - 1002.32 nm, 1191.55 nm- 1197.85 nm, 1349.3 nm to 1462 nm and 1790.8 nm to 1999.0 nm were severely affected by atmospheric oxygen and water absorption as illustrated in Figure 4.10 (a). When both the reflectance spectra as shown in Figure 4.10 were compared, the filtered reflectance showed less noise. Those noise were present prominently at the wavelength range 989.69 nm - 1002.32 nm, 1191.55 nm- 1197.85 nm, 1349.3 nm to 1462 nm and 1790.8 nm to 1999.0 nm.

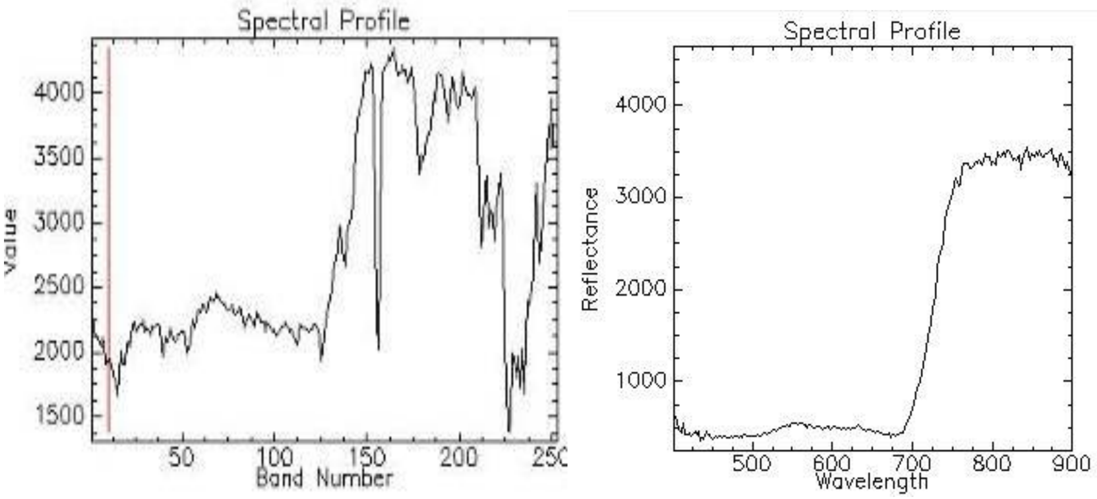

Figure 4.9 Spectral profile of vegetation pixel in a hyperspectral image (a) calibrated radiance of the original image (X axis- Band Number and Y axis- DN values) (b) surface reflectance of hyperspectral image after atmospheric correction with FLAASH (X axis- Wavelength and Y-axis- Reflectance values).

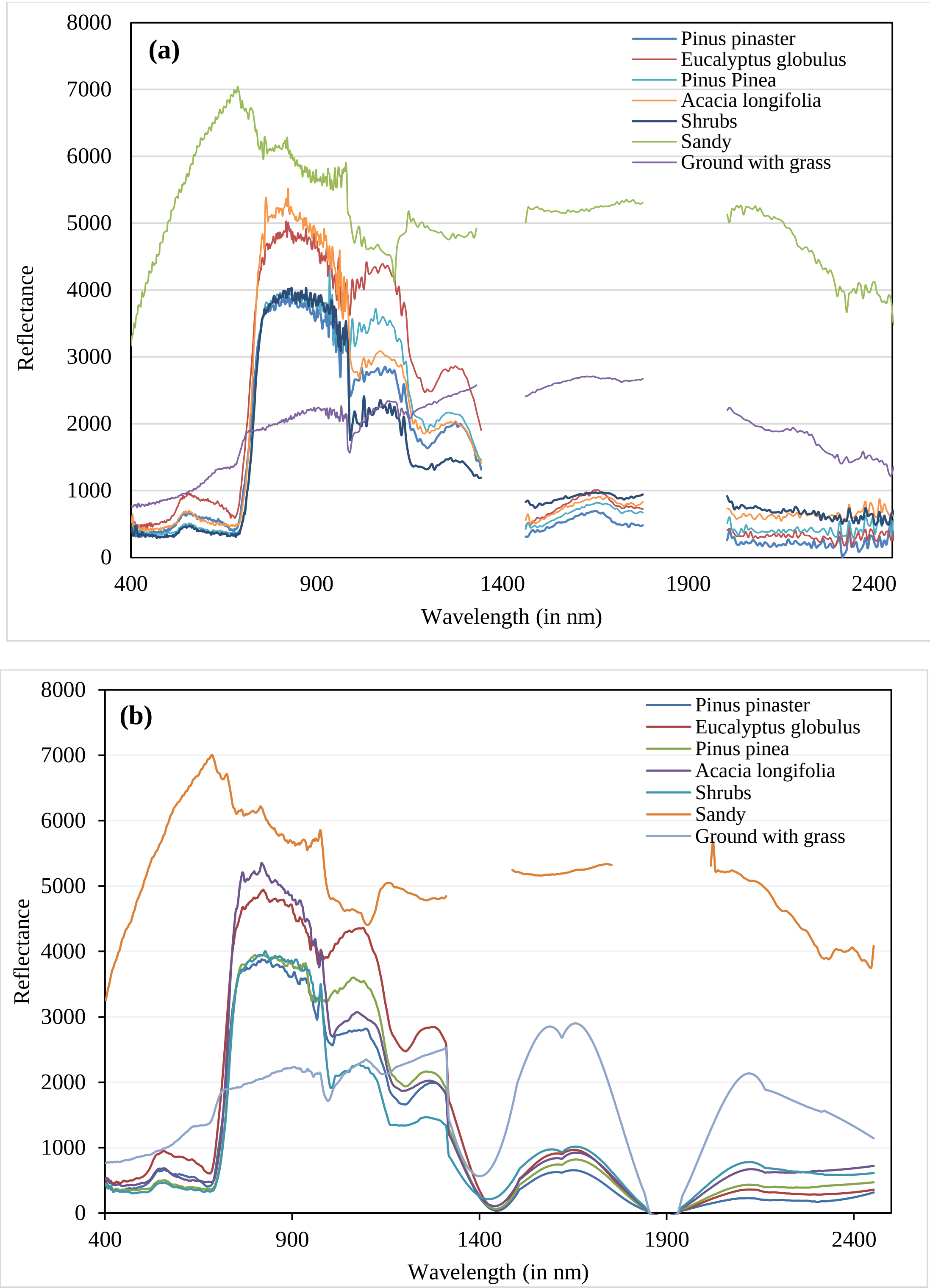

Figure 4.10 Typical reflectance spectra of tree species and sand from hyperspectral data (a) FLAASH corrected reflectance and (b) reflectance after Savitzky-Golay smoothing filter application

All noises and high frequency are at the water absorption region of the electromagnetic radiation. Out of these four high frequency points, first range (989.69 nm- 1002.32 nm) is an overlap between the Eagle and Hawk images, which is an advantage because it provide an average of smoothening for that region. Thus, the filtered reflectance has a distinct spectral profile and shows an apparent decrease of high frequency or noise from FLAASH corrected reflectance. Figure 4.10 (a) (b) and shows the reflectance value of tree species (*Eucalyptus species*, *Pinus pinea*, *Pinus pinaster* and *Acacia* species) at wavelength range 400 nm to 2450 nm using eagle and hawk sensor. Reflectance was collected using 3 x 3 z-profile average moving window sizes in ENVI from hyperspectral image. Focusing on different wavelengths of hyperspectral image, distinctions between species were exhibited at different wavelength ranges, at visible range, with the maximum spectral difference occurring in NIR and short wave infrared.

4.3.2 Segmentation and PCA Approach

The segmentation of the hyperspectral image was performed using the spectral range of the wavelength and histograms of the image. In this, selection of different wavelength ranges were performed using spectral characteristics, and histogram image data distribution. Previously, some studies demonstrated the segmentation techniques using the wavelength range and different number of segments that produced varying results with different classifiers. During the segmented PC techniques, selection of different combination of band in different channels was attempted in order to obtain the enhanced display of the image of the study. The enhanced PC image helps in the interpretation and image classification. The result of PCA techniques is the generation of the same number of PC bands where first PC component (PC1) contains the highest percentage of the data variance, second PC component (PC2) contains the second largest data variance, and this feature of data variance continues. The data variance and useful information contained by PC bands were determined by the Eigenvalues where at a certain point PC bands contain only the noise. Thus, the point where Eigenvalues fall to less than 1, PC bands do not provide useful information due to the noise or very less information. It is due to some reason, either they have very little variance or due to noise in the original spectral bands.

One of the useful applications of PCA is that PC bands combination can produce more colourful composite images in comparison to the original spectral bands (see Figure 4.12). It is due to uncorrelated data of the PC bands as compared to original images. Moreover, Figure 4.11 shows the Eigenvalues of the PC bands which represent the significant useful bands. This graph shows the percent of the total variance contained in the different principal component bands. The Eigenvalues 0-1 those whose values are less than 1 is neglected and it happens at the forum where eigenvalues become constant is known as Elbow Point. The Elbow point is found to be near PC band three after which Eigenvalues falls to 0. The Eigenvalues indicate the amount of variance described by each of the new coordinate axes. Eigen values are are used to reduce the dimension of large data sets by a significant amount and to find new variables that are uncorrelated. Thus, hyperspectral image is optimised to prepare it for achieving higher classification accuracy using image interpretation with the help of ROI and field samples.

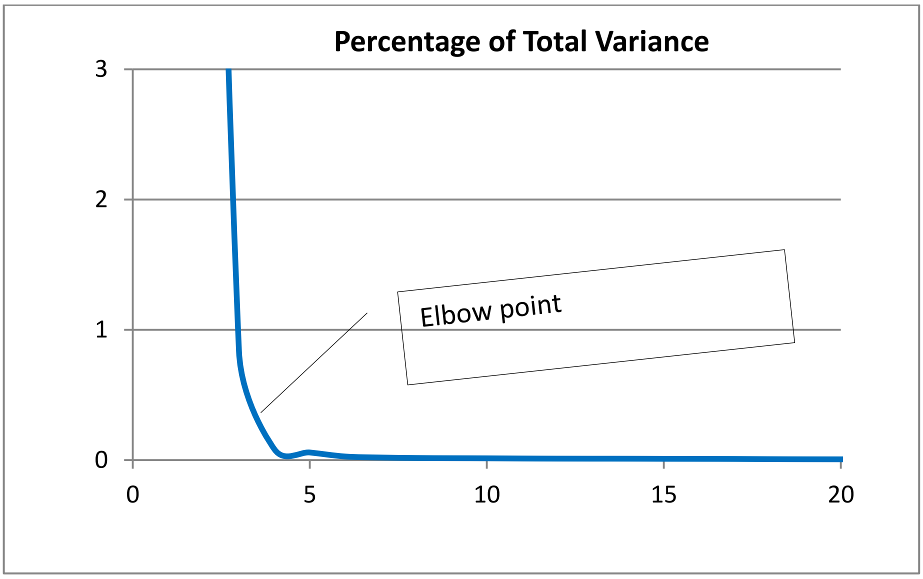

Figure 4.11 (a) Plot of Eigen values against the PC bands showing the elbow points from where the Eigenvalues falls below 1

Table 4.2 Segmentation of hyperspectral data applying PCA on the five spectral data segments

Hyperspectral segment	**Band range based on spectral and histogram statistics**	**Wavelength range**	**Total no of PCs**	**First Three PCs of segments (named as)**	**Cumulative Percent of Eigenvalues**	**No of selected PCs**
Segment 1	1-48	400.-506.15 nm	48	A1-A2-A3	99.8811	3
Segment 2	49-98	506.15-623.48 nm	50	B1-B2-B3	99.9805	3
Segment 3	99-142	623.48-728.31 nm	44	C1-C2-C3	99.9585	3
Segment 4	142-249	728.31-988.37 nm	107	D1-D2-D3	98.4053	3
Segment 5	16-252 (Hawk range)	1002.3–2238.71 nm	196	E1-E2-E3	99.4480	3
Average Cumulative Percent of 15 PCs of 5 Segments together					99.5347	-
Total PCs selected to generate a segmented PC image-					--	15

The segments of the hyperspectral image were assumed on the basis of differentiating behaviour of the different features described in section spectral profiles of hyperspectral image and histogram distribution. In segment five there are some bands from Hawk image were removed as they are either having similar range as to Eagle image or affected in the absorption region of the spectrum. The affected bands are present at the 1900 nm and 2100 nm range of the spectrum. As seen in the Table 4.2, segment 5 is having 16-252 band, the reason for removal of the band 1-15 is overlap with Eagle image (overlap of wavelengths at the last bands of Eagle and starting bands of the Hawk). Thus, some bands are removed from the Hawk data to avoid overlap of wavelengths. Segment 1 is lying near the blue wavelength range, segment 2 covering the green region, and segment 3 near the red wavelength region of the electromagnetic spectrum range. While segment 4 covers and segment 5 cover NIR and SWIR spectrum region of the electromagnetic wavelength respectively.

Table 4.3 Eigen values for the first three PCs derived from the segmented PCA of the hyperspectral image and Eigen values of PCA performed on entire hyperspectral image.

	Total no of PCs	**First Three PCs**	**Variance**	**Cumulative Percent of Eigenvalues**
Hyperspectral image	492	PC1	85.140	85.40
		PC2	13.22	98.62
		PC3	0.80	99.42
Segment 1	48	PC1	99.3637	99.3637
		PC2	0.4657	99.8294
		PC3	0.0517	99.8811
Segment 2	50	PC1	99.7738	99.7738
		PC2	0.1871	99.9209
		PC3	0.0596	99.9805
Segment 3	44	PC1	97.3580	97.3580
		PC2	2.5132	99.8712
		PC3	0.0873	99.9585
Segment 4	107	PC1	94.6019	94.6019
		PC2	3.3843	97.9863
		PC3	0.4190	98.4053
Segment 5	196	PC1	79.1370	79.1370
		PC2	19.0847	98.2216
		PC3	1.2274	99.4480

As seen from the Table 4.2, the cumulative percent of the variance differ in each segment of hyperspectral image. Cumulative variance percentage is maximum in the first three segments showing the importance of selected range for the study. Moreover, segment 4 and segment 5 too contains the higher information than the individual hyperspectral image. The average of cumulative variance of all three PCs from each segment is found to be 99.53 % which is greater than the cumulative variance percentage of three PCs of hyperspectral image (see Table 4.2 and Table 4.3).

Therefore, spectrum based segmented images were created and PCA techniques were performed to produce 15 PC based imagery for better visualization and interpretation of imagery. PCA performed on each segment caused the transformation of the bands. This maximized the variance of bands of each segment of hyperspectral image. Thus, PCA on spectrum segments can produce visualization-oriented spectrum segmentation which results in multi-colour image with better interpretation (as shown in Figure 4.12.). Moreover, false colour composite is usually used in remote sensing to distinguish the different features. Thus, FCC with red, green and blue channels was used as a tool for representing multispectral or hyperspectral data after processing. Thus, here several FCC was made using different combinations of PCs of segmented PC image (as shown in Figure 4.12). Thus, several colour maps were generated with different RGB composition of the 15 PCs of segmented PC image, which also help in collecting training data for classification. Therefore, it is also considered as initial process in an effort to distinguish different features from the imagery. It is assessed that fusion of the structural component of Lidar data can also result in better visualization and differentiation of some feature promptly than hyperspectral images alone (to be discussed in Chapter 5).

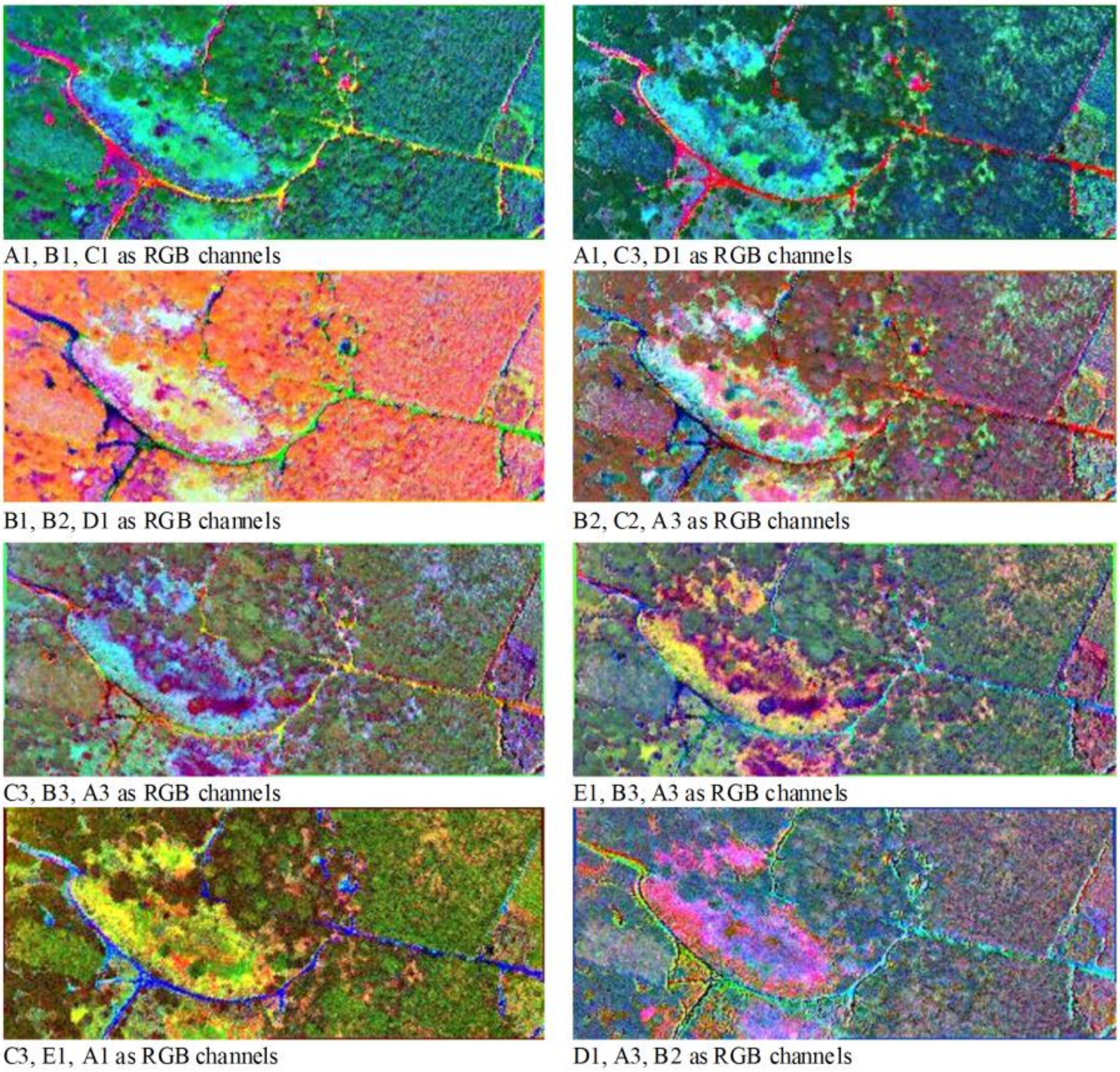

Figure 4.12 R, G, B channel Colour composite image produced using different PC bands of 15 integrated PC images (for A1, A2, A3, B1, B2, B3 etc. refer Table 4.2)

4.3.3 Classification Results

The classification results for the hyperspectral dataset and segmented PC image are shown in Figure 4.13, Figure 4.14, and Figure 4.15. The statistical accuracy analysis results of the classifications are given in Table 4.5, Table 4.6 and Table 4.7. The overall accuracy of the MLC of the segmented PC images is significantly higher than the SAM and MLC approaches applied to the hyperspectral data (See Table 4.4). The SAM classification is reliant on spectral image characteristics which can be influenced by the 'Hughes phenomenon' for high-dimensional data. The MLC performed on the segmented PCA bands reduces the 'Hughes phenomenon'. The MLC and SAM classification accuracies for hyperspectral datasets are presented in Table 4.5 and Table 4.6. User's and producer's accuracy for different tree species and feature classes were presented in Table 4.5, Table 4.6, and Table 4.7. The accuracy of the MLC based on the segmented PCA is 96.38%, which is much higher than for the MLC classification of the original hyperspectral data (89.67%) and SAM (67.5%). The κ coefficient confirms the superior performance of the MLC on the segmented PC image over the SAM and MLC classifications of the hyperspectral data. The κ coefficient for the three classification approaches gives the same order of classification performance of the three classifier techniques (Table 4.4). The results of the 3 different classification techniques are shown in Figure 4.13, Figure 4.14 and Figure 4.15.

Table 4.4 Overall accuracy and Kappa coefficient for MLC, SAM and MLC on Segmented PCA classification

	Classifier techniques	**Overall Accuracy (%)**	**κ- Coefficient statistics**
1	SAM on Hyperspectral data	67.5	0.60
2	MLC on Hyperspectral data	89.67	0.87
3	MLC on Segmented PCA	96.38	0.95

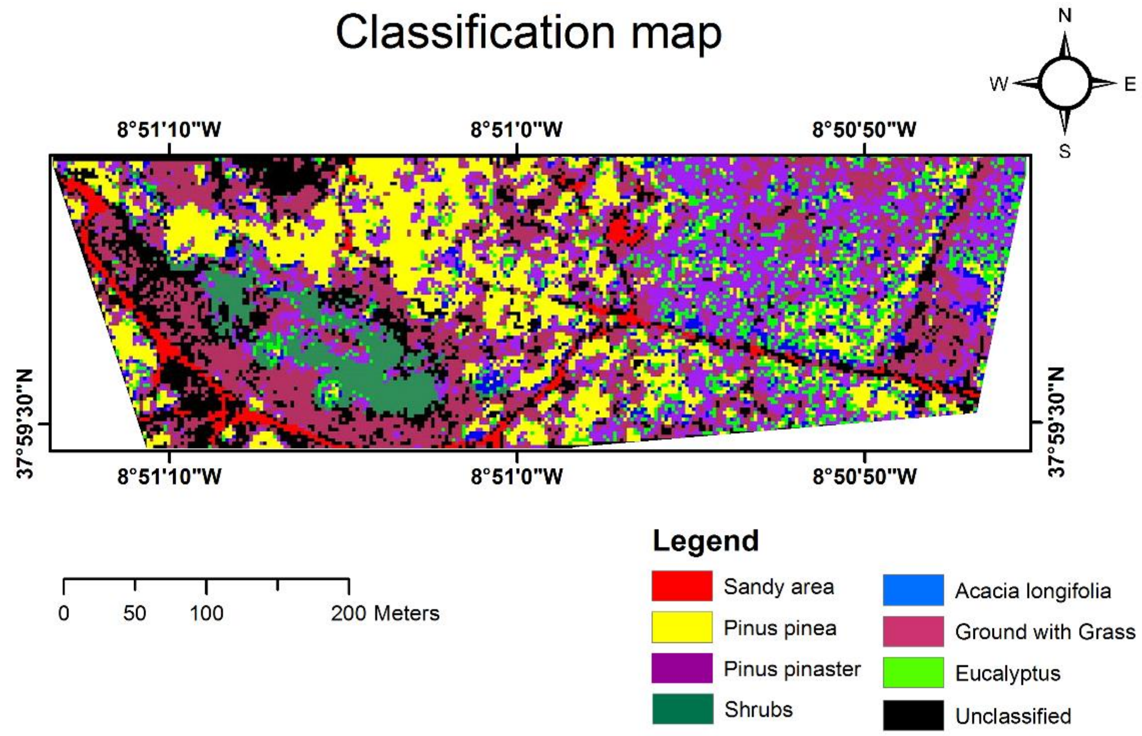

Figure 4.13 SAM Classified map of hyperspectral image

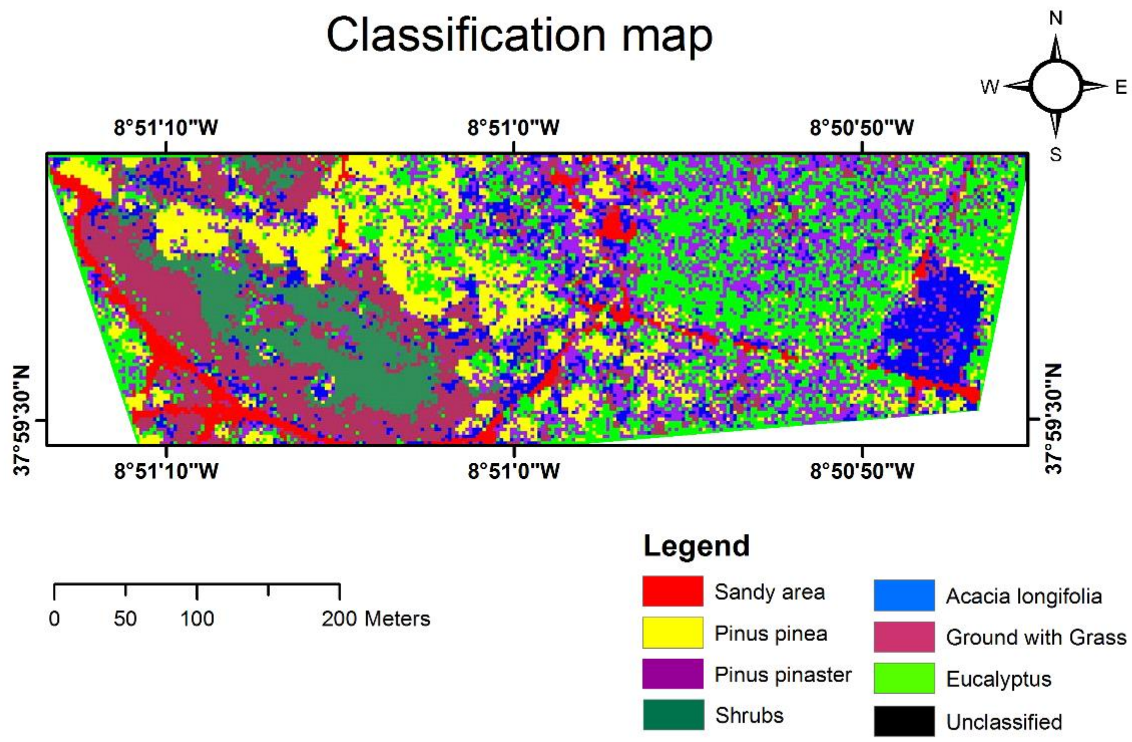

Figure 4.14 MLC classified map of hyperspectral image

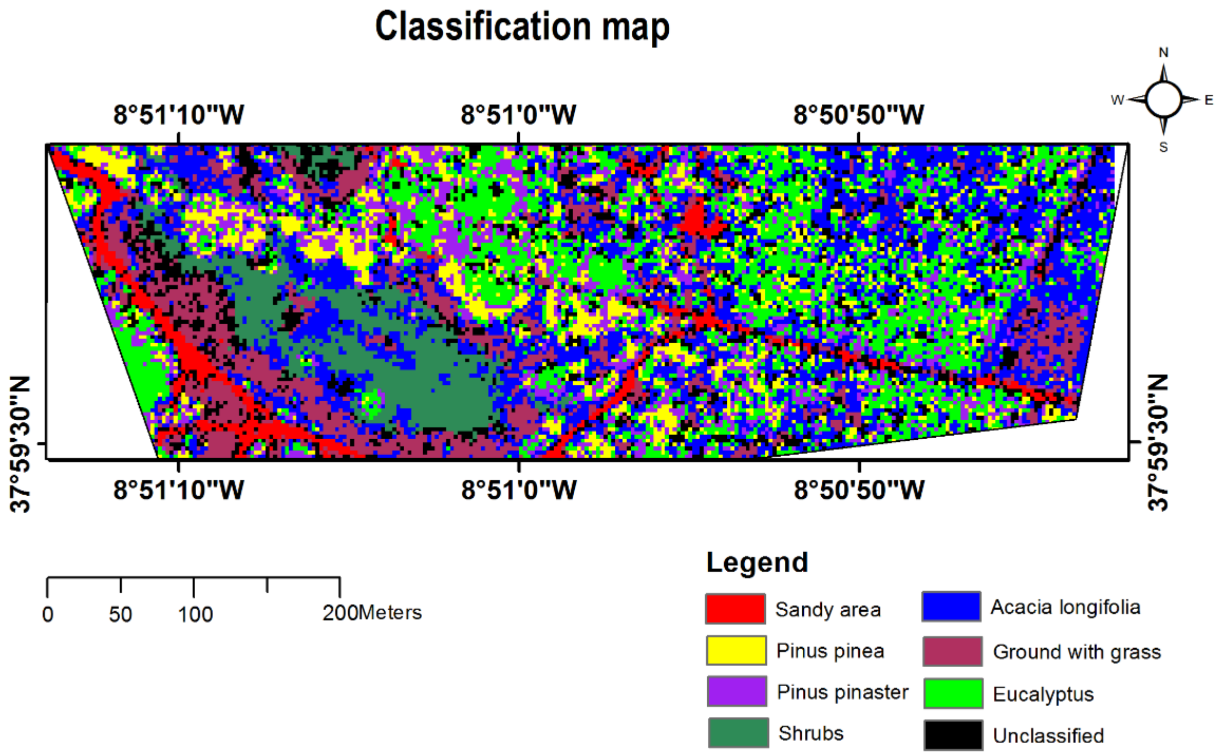

Figure 4.15 Classified map of the segmented PC image

4.3.3.1 Classification of Hyperspectral Image

The classification map generated using the SAM classifier is shown in Figure 4.13. End member spectra used in SAM techniques come from ASCII files collected and saved from hyperspectral imagery (as ROI average spectra) collected during field sampling as training data. Training data and aerial photographs (See Figure 3.7) were used to locate the various features on imagery to know the locations, during field survey it was marked for the features using GPS and Known locations.

Different tree species and ground features classified in the SAM were *Pinus pinaster*, *Pinus pinea*, *Eucalyptus* species, *Acacia longifolia*, Sandy area, shrubs and ground covered with grasses (See Figure 4.13). The black portion illustrated in the SAM classified map are unclassified pixels contributed by ground surfaces, sandy area, or may be gap between the canopy. These features were kept unclassified in the map; it was tried to reduce this pixel as much as possible by significantly collecting vegetation spectra from the hyperspectral imagery.

Similarly, hyperspectral image was classified using the MLC techniques for the same study site area using the training and reference sites. The classification map generated using the MLC techniques was shown in Figure 4.14. MLC was performed to check the robustness of two classifier techniques in the same study site for the same image.

4.3.3.2 Classification of Segmented PC Image

The resulting 15 PCs contain approx 99.53 % of the information content when combined together as gainst the 99.42% of the information content of the original hyperspectral image (See Table 4.2 and Table 4.3). These PCs were used to generated the segmented PC image that is classified using maximum likelihood classification Figure 4.15. Thus, the 15 PCs of the segmented PC image were uncorrelated containing more than 99% of the information of the original hyperspectral image. Different PC combinations of the segmented PC image were used for visual display using three bands displayed as the red, green and blue channels (RGB channels in Figure 4.12). The various RGB combinations of the segmented PC images provide visual distinctions between land cover and forest types and other features. This process enhances the colour contrast by providing visual clarity for image interpretation, thus helping in selecting the training samples used during classification. These distinctive features in the RGB images were not visible in different band combinations of the original hyperspectral images. A comparison of segmented PC image classification with SAM and MLC of the original hyperspectral image classification shows that the MLC of the segmented PCA achieves the highest accuracy, due to its ability to reduce the 'Hughes Phenomenon' (Pandey et al., 2014).

The SAM classification is reliant on the spectral image characteristics which can be influenced by the 'Hughes Phenomenon' for high-dimensional data. Thus, spectral mixing as well as 'Hughes Phenomenon' may result in lesser accuracy of the classified features. The MLC performed on the segmented PCA bands reduces the 'Hughes Phenomenon' and thus helpful in getting better accuracy than the SAM classification. segmented PC image provides better and higher accuracy than the SAM and MLC of hyperspectral image classification. This is attributed to the reduced dimensionality in segmented PC image due to segmented PC approaches.

After classification steps, the classified maps were assessed for accuracy for the three techniques (SAM and MLC of hyperspectral image and Segmented PC image). The accuracy assessments results were shown in Table 4.5 for SAM, Table 4.6 for MLC maps and table 4.7 for segmented PC image as error matrix. These accuracy assessment were generated using the error matrix (also known as confusion matrix). The overall accuracy of the MLC map was 89.67% that is higher than the accuracy of SAM classified result of 67.5%. κappa coefficient was 0.87 for the MLC classification as compared to κappa coefficient of SAM classification (0.60). A discrete multivariate technique known as κappa coefficient was used to analyse the accuracy assessment (Congalton and Mead, 1983).

4.3.3.3 Classification Accuracy Assessment

The error matrix generated during the above SAM; MLC classification of hyperspectral images and segmented PC image were shown in Table 4.5, Table 4.6 and Table 4.7. The error matrix was calculated using the reference data used for generating error matrix of each feature in classified images The error matrix generated different accuracy parameters like user's accuracy, producer's accuracy, mapping accuracy and overall accuracy for comparison purposes of different classified images. The error matrix produce overall accuracies and κappa statistics to test the significance of the difference in accuracy of classified images.

The classification of hyperspectral image using SAM classifier produced an overall accuracy of 67.5 % that showed that the method is not able to well discriminate different species and surrounding features. The classification of hyperspectral image with MLC gave a better overall accuracy of 89.67% that showed better results than SAM, but it has some limitations in respect of discriminating some species and features. However, MLC of segmented PC image showed that the differentiation becomes better and overall accuracy is increased up to 96.38 % that was about 7% more than MLC on original hyperspectral image.

Table 4.5 Error matrix for the SAM classification

	Reference data							
Classified data	Sandy	Eucalyptus	Ground with grass	Pinus pinea	Pinus pinaster	Acacia longifolia	Shrubs	Row Total
Unclassified	6	0	6	3	12	2	0	29
Sandy	216	0	0	0	0	0	0	216
Eucalyptus	0	354	60	12	150	36	0	612
Ground with grass	24	12	294	0	100	0	0	430
Pinus pinea	0	30	0	338	0	0	18	386
Pinus pinaster	0	114	50	6	282	32	0	484
Acacia longifolia	0	42	18	49	68	155	6	338
Shrubs	0	0	10	18	0	0	198	226
Column Total	246	552	438	426	612	225	222	2721
PA	87.80	64.13	67.12	79.34	46.08	68.89	89.19	
UA	100.00	57.84	67.43	87.56	58.26	45.86	87.61	
Average PA	71.79							
Average UA	72.22							

Table 4.6 Error matrix for the MLC classification

	Reference data							
Classified data	Sand	Eucalyptus	Ground with grass	Pinus pinea	Pinus pinaster	Acacia longifolia	Shrubs	Row Total
Unclassified	0	2	1	0	5	2	4	14
Sand	234	0	0	0	0	0	1	235
Eucalyptus	0	502	6	17	2	3	0	530
Ground with grass	12	7	407	0	27	0	0	453
Pinus pinea	0	6	18	360	26	22	19	451
Pinus pinaster	0	35	0	45	547	0	6	633
Acacia longifolia	0	0	0	4	5	198	0	207
Shrubs	0	0	6	0	0	0	192	198
Column Total	246	552	438	426	612	225	222	2721
PA	95.12	90.94	92.92	84.51	89.38	88.00	86.49	
UA	99.57	94.72	89.85	79.82	86.41	95.65	96.97	
Average PA	89.62							
Average UA	91.86							

Table 4.7 Error matrix for Segmented PC image classification

	Reference data							
Classified data	Sand	Eucalyptus	Ground with grass	Pinus pinea	Pinus pinaster	Acacia longifolia	Shrubs	Row Total
Unclassified	0	1	1	0	1	1	0	4
Sand	234	0	0	0	0	0	0	235
Eucalyptus	0	521	0	0	15	11	6	553
Ground with grass	11	0	431	0	0	0	0	442
Pinus pinea	0	17	0	420	0	0	0	437
Pinus pinaster	0	13	0	0	587	0	0	600
Acacia longifolia	0	0	0	6	9	213	0	228
Shrubs	0	0	6	0	0	0	216	222
Column Total	246	552	438	426	612	72	222	2721
PA	95.53	94.38	98.40	98.59	95.92	94.67	97.30	
UA	100.00	94.21	97.29	96.11	97.83	93.42	97.30	
Average PA	96.40							
Average UA	96.63							

Table 4.8 Improvement in terms of increase or decrease in the accuracy of Three classifications – SAM, MLC and MLC of segmented PC image

	Producer statistics			Changes (improvement or decline)			User statistics			Changes (improvement or decline)		
Species	SAM	MLC Hyperspectral image	MLC Segmented PC image	Changes from SAM to MLC	Changes from SAM to MLC segmented PC image	Changes from MLC to MLC segmented PC image`	SAM	MLC Hyperspectral image	MLC Segmented PC image	Changes from SAM to MLC	Changes from SAM to MLC segmented PC image	Changes from MLC to MLC segmented PC image`
Sand	87.8	95.12	95.53	-7.32	-7.73	-0.41	100	99.57	100	0.43	0	-0.43
Eucalyptus	64.13	90.94	94.38	-26.81	-30.25	-3.44	57.84	94.72	94.21	-36.88	-36.37	0.51
Ground with grass	67.12	92.92	98.4	-25.8	-31.28	-5.48	67.43	89.85	97.29	-22.42	-29.86	-7.44
Pinus pinea	79.34	84.51	98.59	-5.17	-19.25	-14.08	87.56	79.82	96.11	7.74	-8.55	-16.29
Pinus pinaster	46.08	89.38	95.92	-43.3	-49.84	-6.54	58.26	86.41	97.83	-28.15	-39.57	-11.42
Acacia Longifolia	68.89	88	94.67	-19.11	-25.78	-6.67	45.86	95.65	93.42	-49.79	-47.56	2.23
Shrubs	89.19	86.49	97.3	2.7	-8.11	-10.81	87.61	96.97	97.3	-9.36	-9.69	-0.33

Average PA and average UA for SAM is 71.79% and 72.22%, whereas average PA and UA is 89.62% and 91.86% for MLC of hyperspectral image. The average PA and UA for the segmented PC image is 96.40 % and 96.63%. The overall accuracy for the SAM, MLC and segmented PC classified image were compared to each other to assess the performance of each classifier. To better understand the user accuracy and producer's accuracy, an example has been taken from one the classified feature classes. MLC classifier algorithm correctly classified 89.38 % *Pinus pinaster* pixels (in reference data) as the *Pinus pinaster* whereas for user needs about 86.41 % of the pixels classified as *Pinus pinaster* pixels are indeed *Pinus* species by MLC classifier (see Table 4.6). This is based on the individual producer and user's accuracy of the error matrix. Table 4.8 demonstrate the assessment of the user and producers statistics for improvement or decline from one classification steps to another, such as SAM to MLC hyperspectral, SAM to MLC segmented PC image, and MLC hyperspectral to MLC segmented PC image. There is little change in the sandy region and shrubs in the producer statistics and large improvement in *Eucalyptus*, ground with grasses and *Acacia* species, and small increase in shrubs. While, there is no significant improvement in the sandy region using the user statistics. The improvements are found in the *Pinus pinea*, *Acacia longifolia,* shrubs, and *Eucalyptus* species.

The overall accuracy of the SAM classification is 67.5% and κappa coefficient is 0.60 whereas the overall accuracy of the MLC map is 89.67% and κappa coefficient was found to be 0.87. The results achieved by segmented PC classified image is higher than the other classified results. Overall accuracy for the segmented PC image is 96.38% and κappa coefficient is 0.95 (See Table 4.5, Table 4.6 and Table 4.7). Moreover from these results it is found that segmented PC image have higher κappa value than other classified results. Thus, higher κappa value of segmented PC classified results among all shows the advantage of segmentation techniques and use of appropriate classifier in enhancing the accuracy rate of classified image. The segmented PC image also provide better enhanced visualization as compared to the hyperspectral image, as it provide more information in 3 PCs (Refer to Figure 4.12) . The user's accuracy and producer's accuracy of *Pinus pinea, Pinus pinaster, Acacia longifolia, Eucalyptus and shrubs* for all three classified images were shown in Table 4.5, Table 4.6 and Table 4.7.

Thus, it was demonstrated, through classified and accuracy results that the segmented PC image achieved higher accuracy for overall as well as some of the individual features. These results give a good overlook on the performance of the classifiers and the segmented PC approach being used in this Chapter. As segmented PC classification has provided high overall accuracy when compared to the individual image classification. The following chapter will present the overview regarding the integration of hyperspectral Eagle images and LiDAR derived CHM and classification of the resultant image. It was consequently shown, both qualitatively and quantitatively that the abundant tree species and surrounding ground features can be classified and distinguished.

4.4 Conclusion

The present study reveals that the Segmented PCA approach is a useful technique for hyperspectral image classification while reducing 'Hughes Phenomenon'. 'Hughes Phenomenon' is mostly described as a curse to hyperspectral classification. The classification accuracy increases with Segmented PC image as compared to when entire hyperspectral images are used. Before Segmented PC image classification, we separated hyperspectral data into five segments, and PCA- based transformations are applied to each segment. Among all the obtained PCA bands in each segmented hyperspectral image, the first three PCs bands contain maximum information contained in the each segmented hyperspectral image. After the first 3 PC bands, virtually all remaining PCs bands contain only noises. PC application performed on the hyperspectral segments results into respective PCs of each segments. The first three PCs contain most of the information about the feature sharpness, delineation and identifiable from the images. The number of PC selection such as three PC comes from the cumulative percentage of Eigenvalue associated with them (refer to Table 4.1, Table 4.2 and 4.3). After application of PC analysis on each segments, the cumulative percentage of Eigenvalues were calculated (shown in Table 4.2 and 4.3). Results indicate that first PCs together retained more than 99 percent of the information of the image for the identification of different features (See Figure 4.12). The first segment provides information about the chlorophyll contents of the tree and grasses while other segment provides information for the intercellular space, and water content of the tree species. 3 PCs from each segment were brought at the same platform and integrated to form Segmented PC image containing 15 best PCs from five different segments of hyperspectral images. Thus, the use of the Segmented PCA approach reduces the 'Hughes Phenomenon' for hyperspectral image classification; and proved beneficial and productive. It considerably decreases the amount of data to be handled and achieves practically acceptable and accurate classification results with a maximum likelihood classifier. This result is comparable with those obtained using the hyperspectral image data using SAM and standard MLC. The accuracy of the classification of the hyperspectral image and segmented PC images is assessed using the error matrix analysis with reference data and classified data. The classification from two datasets i.e. hyperspectral image and segmented PC image are compared to estimate whether the additional segmentation of the hyperspectral images contributed significantly to the classification accuracy or not.

Tree species classification from hyperspectral imagery is of limited accuracy if the data dimensionality is not reduced, because the 'Hughes phenomenon' leads to a loss of accuracy if too many bands are added. This study explores the classification accuracy achievable from hyperspectral data using the segmented PCA approach. It compares this approach to the SAM and MLC methods of the original hyperspectral data. The classification accuracy and κ coefficient are much higher for the segmented PCA (>96%; κ=0.95) than for the other methods when validated with ground control points. The conclusions from this study are:

- Segmented PCA based on data normalization using histogram attributes reduces the dimensionality of the hyperspectral imagery while increasing the classification accuracy.
- The MLC of the segmented PCA produces much more accurate tree species maps than the MLC and SAM classifiers.
- 15 bands of the first 3 PCs of the 5 segments from the full hyperspectral dataset contained >99% of the original spectral variance.
- Compression techniques like segmented PCA to reduce the hyperspectral image dimensionality lead to much improved information content by reducing redundancy of very similar spectral bands.

Some authors have shown conventional parametric classification approaches as good classifier. Le Cussan (1991) demonstrated that SAM classification of CASI resulted in 60.8% accuracy due to confusion between the sand dunes and *Bruguiera species* stands.

Author argued about the relatively low accuracy with SAM is due to insensitivity to differences in relative brightness between pixels and the spectral library. But the same area when mapped and classified using the MLC and data integration methods results in the higher accuracy (Held et al., 2003) as compared to the previous studies (Le Cussan, 1991). Held et al. (2003) provided the better and improved results with the MLC algorithm and combined datasets for CASI and NASA AIRSAR images with higher accuracy as compared to SAM.

It has been previously demonstrated that MLC as being limited in their ability to classify high dimensionality data (Benediktsson et al., 1990, Jones et al., 2010). Although this makes MLC unsuitable for raw hyperspectral data, this study shows that MLC can be used after reducing the dimensions of the hyperspectral imagery. Moreover, MLC proves to be superior to SAM single endmember as it generates higher overall accuracy results than using SAM with multiple endmember (Yang et al. 2012).

The segmented PCA method enhances the contrast of the imagery and provides better visual clarity for image interpretation, thus helping in selecting the training samples used during MLC. Thus, it provides better training samples and better accuracy (Baatuuwie and Van Leeuwen, 2011, Hunter and Power, 2002, Shafri et al., 2007). MLC was chosen in the present study as a classifier after reducing the dimensionality of the hyperspectral data using the segmented PCA approach as seen from Table 4.2 and Table 4.3.

Finally, the segmented PCA approach used in the present study will be helpful for hyperspectral analysis by reducing the multidimensional data to smaller dimensionality for image processing while retaining most of the information. This image compression technique can be used with other classification algorithms to achieve accurate tree species identification results by reducing data dimensionality and data volume. This classification approach can be used for other applications like urban mapping, land cover mapping, plant stress detection due to its visual enhancement, fire scar mapping etc.

This is also demonstrated by Cho et al. (2010) that conventional SAM produces lower accuracy results as compared to the multiple endmember use for SAM approaches, which increases the producer's and user's accuracies. The range of classification accuracy varies from 44.5% to 64.1% (using all spectral bands), 39.9%-62.3% (known chemical and physical spectral features) and 47.5%-65.1% (selected band of the hyperspectral image). The authors obtained high producer's accuracy and user's accuracy with SAM classifier using multiple end members approach generated higher overall accuracy classification outcomes (54.5%± 3.2 CI) as compared to mean spectra training sets with SAM classifier (20.5% ± 0.94 CI). The outcomes inferred that best band selection method also results in an overall accuracy of 64.1% (mean overall accuracy= 54.5%) for the multiple endmember SAM classifier approach. Thus, they showed that the SAM classification accuracy results varies from 44.5%-65.1%, depending upon the end member selection and band selection approaches.

The two classifier techniques, i.e. SAM and MLC were used in the present study for classification of HSI, segmented PC image and PC fusion image (refer to Chapter 5). The original reflectance image produced slightly better classification results in case of MLC technique. It has produced an overall accuracy result of 89.67 % as compared to SAM classifier (67.5%). The use of appropriate method like a segmented PC technique has increased the classification accuracy of the images up to 96.38 % as compared to original reflectance images. Thus, MLC outperforms the SAM when it has been used with segmented PC images than original reflectance image and reported better accuracy with segmented PC approaches used in the study. The results of this study, therefore, reiterate the fact that the segmentation PC approach and use of appropriate classifier for mapping and classification will be more suitable and can be effectively used in other research areas such as urban tree mapping, plant stress detection due to its enhanced visual capability and higher accuracy results.

4.5 Summary of Chapter

This chapter described the classification of segmented PC images and hyperspectral images using two different classifier methods namely SAM and MLC based on supervised classification. The overall accuracy, producer's accuracy and user's accuracy of these two methods were assessed using reference data and classified datasets. The classification of the segmented PC image using MLC classifier performed significantly better (>96%; κ=0.95) than the SAM and MLC methods used for performing classification on hyperspectral image (>67%; κ=0.60 and >89%; κ=0.87 respectively). Tree species classification from hyperspectral imagery is of limited accuracy if the data dimensionality is not reduced because the 'Hughes Phenomenon' leads to a loss of accuracy if too many bands are added. This study explores the classification accuracy achievable with hyperspectral data using the segmented PCA approach. It compares this approach to the SAM and MLC methods. The classification accuracy and κ coefficient are much higher for the segmented PCA than for the other methods (>96%; κ=0. 95) when validated with the ground control points.

The next chapter 5 describes the process of image fusion of hyperspectral images and Canopy height derived from LiDAR data from the same study area. It represents the comparison of the field recorded height and LiDAR derived height using a scatter plot for different tree species. The fused image is classified using Maximum Likelihood Classifier based on supervised classification. Finally, the accuracy of the classified fused image is compared with the classification results performed in this section.

Chapter 5. Fusion of HSI and LiDAR Data

5.1 Introduction

This chapter mainly addresses the second important objective about image fusion. This chapter focuses on the integration of the Eagle hyperspectral image and LiDAR derived CHM using PCA techniques. The hyperspectral and LiDAR fused image is classified, and its importance in term of integration is discussed in the research. This chapter also provides a comparison of predicted canopy height (CHM) with the measured canopy height (field). Thereafter, this chapter provides a detailed step of integration methods of hyperspectral and CHM using PCA forward -inverse techniques. The accuracy of the classified fused image is assessed using the error matrix analysis with reference data and classified data using the same methods as in Chapter 4. The fused image is assessed and analysed for its spectrum whether it can delineate different tree species, shrubs, and grasses with non-vegetated regions or not. The spectrum of the fused image is compared with each different tree species and its associated habitat features namely sandy area, ground covered with grasses. It is analysed whether the incorporation of height attributes from LiDAR data contribute significantly to the accuracy of the classification than hyperspectral image. Thus, this chapter mainly illustrates the robustness of the image fusion approach.

5.1.1 Problems and Solutions

Recognition of different surface features from hyperspectral data can pose problems because of the high data dimensionality (Liu et al., 2011). Reflectance from vegetation depends on the absorption that is related to wavelength-specific biophysical properties like chlorophyll content, leaf water content and cellular spaces (Blackburn, 2007). Hyperspectral imaging systems have been used for successful discrimination of surface features and vegetation types. These properties demonstrate their usefulness in forestry, hydrology, and geology (Richards and Jia, 1999). Despite the richness of spectral information available in HSI datasets, interpretation of these data are still very challenging. Sometimes it can be difficult to identify ground features using single data acquisitions with fine spectral and spatial resolution (Price, 1994). These problems are caused by high correlation and the high data dimensionality, also known as the 'Hughes phenomenon' (Hughes, 1968). The classification of tree species and other features should have a unique spectral signature that is an assumption made by researchers

(Ghiyamat et al., 2013, Jensen, 2000, Lillesand et al., 2004). Ghiyamat et al. (2013) found a problem associated with this assumption, that there are certain conditions when species show spectral disparity within-species that is sometimes variable may lead to failure of a unique spectral identifier per species. To come out of these problems, data redundancy and hyperspectral indices are used further to perform the classification. Several studies have shown the use of hyperspectral indices for vegetation feature identification and species classification (Cho et al., 2008). These previous studies highlight the fact that spectral mixing creates difficulties for analyzing hyperspectral images for species discrimination in mixed-species sites such as inland coastal habitats.

Although the high data quality of hyperspectral images can provide information on the spectral absorption features of vegetation, it is often not possible to classify individual tree species using HSI remote sensing techniques alone (Price, 1994). This is caused by several species having similar reflectance spectra, which cannot be distinguished using only hyperspectral images (Liu et al., 2011). A single sensor type alone is often incapable of providing reliable image classifications (Fauvel et al., 2008). Moreover, the integration of additional details like structural information or biochemical properties can enhance species level mapping and classification (Ustin and Gamon, 2010). Despite several advantages of hyperspectral imaging, classification of the full spectral channels provides a lower accuracy for tree species classification and mapping using SAM and other algorithms (Buddenbaum et al., 2005, Möckel et al., 2014, Peña et al., 2013, Pandey et al., 2014, Shafri et al., 2007). Only when combined with additional structural information such as canopy height or canopy volume, HSI can enhance the quality of mapping and classification accuracy (Dalponte et al., 2008, Erdody and Moskal, 2010, Sarrazin et al., 2010, Tonolli et al., 2011). Although it was proved earlier, that LiDAR derived tree height information influences the tree species classification (Ghosh et al., 2014).

The term ‘data fusion’ describes the integration of diverse datasets, here hyperspectral and LiDAR data, into a new enhanced dataset (see Chapter 2). In the early phase of data fusion research, optical multispectral data were fused together with resolution merging techniques. In these previous studies, low-resolution multispectral images were merged with high-resolution panchromatic images to enhance the spatial resolution of the coarse-scale bands while maintaining the high spectral resolution. Several techniques have been used for the fusion of spectral and structural parameters. together: at the sensor level, pixel level, feature level and decision level as discussed in Chapter 2 (Pohl and van Genderen, 1998). These different techniques were applied in many studies to achieve better results than individual datasets would allow. HSI and LiDAR data are currently emerging as the most promising remote sensing technologies for data fusion for forestry applications. This study aimed to evaluate the synergistic use of HSI and Lidar data using a data fusion approach for the classification of a Mediterranean forest site and assessment of any improvements in comparison with a classification of only the hyperspectral imagery.These data fusion methods are characterized by the stage at which both datasets are integrated to each other for analysis.

Data fusion can follow different approaches, including multi-sensor data fusion and multi-temporal data fusion either at pixel level or feature level (Gamba and Chanussot, 2008, Gilmore et al., 2008). Several recent studies have integrated different datasets to improve the classification accuracy. Studies on HSI and LiDAR data fusion have used combined supervised and unsupervised classification approaches and these techniques enhance the classification accuracy (Debes et al., 2014). A fusion of HSI and a LiDAR-derived DSM and classification were performed using openness and physical properties of the features by Yokova et al (Yokoya et al., 2014). Data fusion techniques have been applied to enhance spectral imagery, to increase its spectral resolution, to fill in missing values, etc. The detailed use depends on the user needs, type of data and purpose of the study. Previous studies have shown the usefulness of adding LiDAR-derived CHM data to spectral reflectance channels (Dalponte et al., 2008, Puttonen et al., 2010).

Asner *et al.* (2008) worked on airborne imaging spectroscopy and LiDAR for invasive species detection in Hawaiian rainforests. They reported that hyperspectral signatures are uniques for trees but mapping based on spectral reflectance properties alone is confounded by several issues such as canopy senescence, mortality, intra and inter canopy gaps, shadowing and terrain variability. Asner *et al.* (2008) used a combination of the carnegie airborne observatory (CAO) and small footprints LiDAR system with AVIRIS data to map structural properties of invasaive species. The present study differs from the above in term of the use of airborne hyperspecetral Eagle and Hawk data, the use of spectral segmented techqniques and the incorporation of CHM with spectral properties in the Mediterranean forest. Moreover, they have used in flight data integration while pixel based integration is performed in the present study. The selected study site was Hawaiian rainforest but this study was performed in the Mediterranean forest, Portugal.

5.1.2 Need of Additional Information

The segmented PC approach and classification techniques described in chapter 4 involve the use of AISA hyperspectral image only. This chapter will mainly deal with image fusion of hyperspectral image and LiDAR derived CHM conveying more reliable classification results. As seen from the discussion in Chapter 2, hyperspectral imaging and LiDAR are the two promising and essential remote sensing technology for species mapping and classification. However, hyperspectral images are limited to horizontal plane and perform its analysis in 2-dimensional ways. This limitation of HSI provides limited insight pertaining to the structural parameters of the forests (tree heights). The incorporation of CHM using fusion techniques can enhance and remove this limitation, adding some advantages to classification results.

Ghosh et al. (2014) demonstrated the use of four essential elements required for classification of the tree species, they are spatial resolution, spectral resolution, input predictors, classifiers and forest characteristics. Out of these, the AISA hyperspectral images are very high in spectral and spatial resolution with more than 243 spectral bands and 2 m spatial resolution. A high spatial and spectral resolution of AISA hyperspectral images provide a better platform for carrying out the research. Considering the use of Input predictors, PCA method is included that allow the reduction of inputs bands from the original number to best PCs during the processing. The use of this type of input predictor helps in reducing data redundancy as well as strong correlation between bands. The classifier techniques chosen are SAM and MLC that are considered good for classification, when data redundancy is reduced to eliminate its effect on classification results. However, forest structural parameters are crucial and still found its place in the classification of tree species. LiDAR derived tree height information influences the tree species classification (Ghosh et al., 2014), that it helps an understanding to use structural parameters for classification using fusion approach performed in this study.

Many studies have revealed better results to achieve with fused or integrated data sets rather than single data source (Pang et al., 2009, Moghaddam et al., 2002, Treuhaft et al., 2003 & 2004, Banskota et al., 2009, Straub et al., 2009, Dees et al., 2006, Maltamo et al., 2006). These better results are only due to the information content on the types of the data being used in the work. Due to this high potential, data integration techniques are useful and successfully taken into many applications like forestry, coastal region, oceanology, geological exploration, lithological mapping, forest fire, volcanoes, estuaries, civil engineering, ecosystem monitoring etc. The fused data contains detailed information from both individual data set acquired with different spatial and spectral resolutions.

Data redundancy, presence of noises, a large variance among dataset makes a rigorous process and different application in hyperspectral images. Using the spectral properties only, it is quite difficult to obtain good results with hyperspectral images for classification or distinguishing different features. Thus, classification is enhanced with the addition of structural height with spectral properties using LiDAR data. This would depend on the attribute of both the data sets like spectral attributes of hyperspectral image and height attribute from LiDAR data sets. The data used in the present study are AISA Eagle image and the airborne LiDAR discrete returns systems.

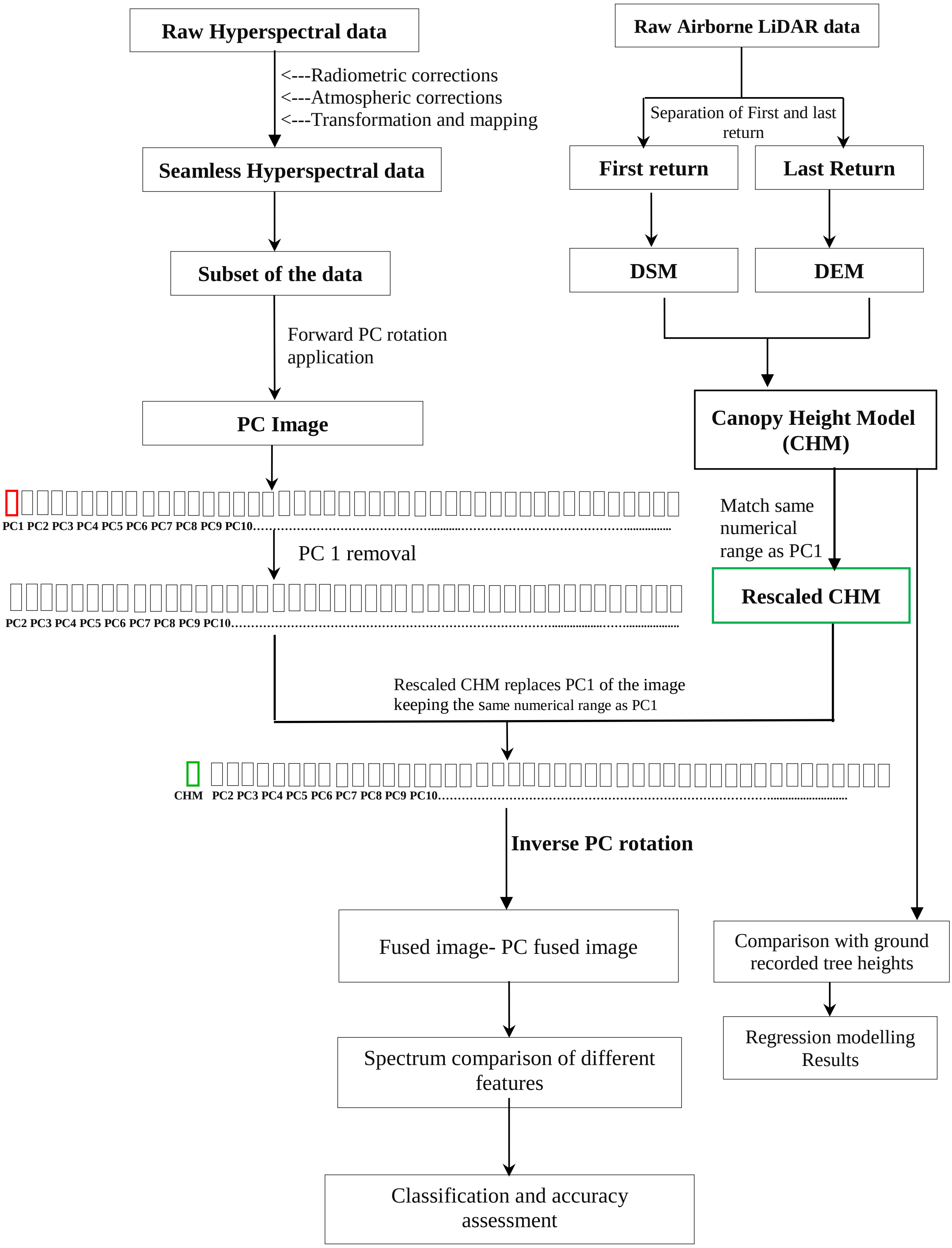

Figure 5.1 Detailed method of the image fusion technique and classification

5.2 Materials and Methodology of Remote Sensing Used in the Study

The data used in the study includes airborne Eagle hyperspectral image and airborne LiDAR data (discussed in Chapter 3). The conceptual framework of the research followed main steps: geometric correction, atmospheric correction, image transformation (PCA image fusion) and classification. LiDAR processing includes the generation of the CHM. The fused image is classified and interpretation of the result is discussed. The methodology adopted in this chapter is illustrated in the flowchart as represented in Figure 5.1. First of all, it includes the processing of the raw hyperspectral data to generate the seamless hyperspectral data ready for further processing and application of different techniques (already discussed in Chapter 3, hyperspectral section) to achieve the objectives of the study. Secondly, the LiDAR data was processed to generate the CHM used during the integration with hyperspectral images (for data pre processing-refer Chapter 3- LiDAR section).

5.2.1 Hyperspectral Image- Eagle Data processing

In brief, as discussed in chapter 3, various applications and extensions of different software were used to process the data. The NERC-ARSF *apl* software suite, Arc GIS and ENVI © image processing package were used as the major pre-processing and analysis tools in the present research. *Apl* software suite were used to pre-process the raw hyperspectral data sets to level 3b seamless images. ENVI spectral FLAASH function was used to perform atmospheric corrections on the hyperspectral images ENVI hyperspectral image analysis functions were used to mosaic, stack data sets and to perform PCA on hyperspectral images.

5.2.2 LiDAR Derived CHM

Arc GIS® 10.2 version were used to separate LiDAR first and last returns. ArcGIS applications were used to generate DSM from the first return and DTM from the last return (see chapter 3). CHM was generated using the math tool of ArcGIS by subtracting DTM from DSM as shown in Figure 5.2 (ESRI White Paper, 2011). Different extensions required for the processing of the LiDAR data in Arc GIS® were 3D analyst and spatial analyst.

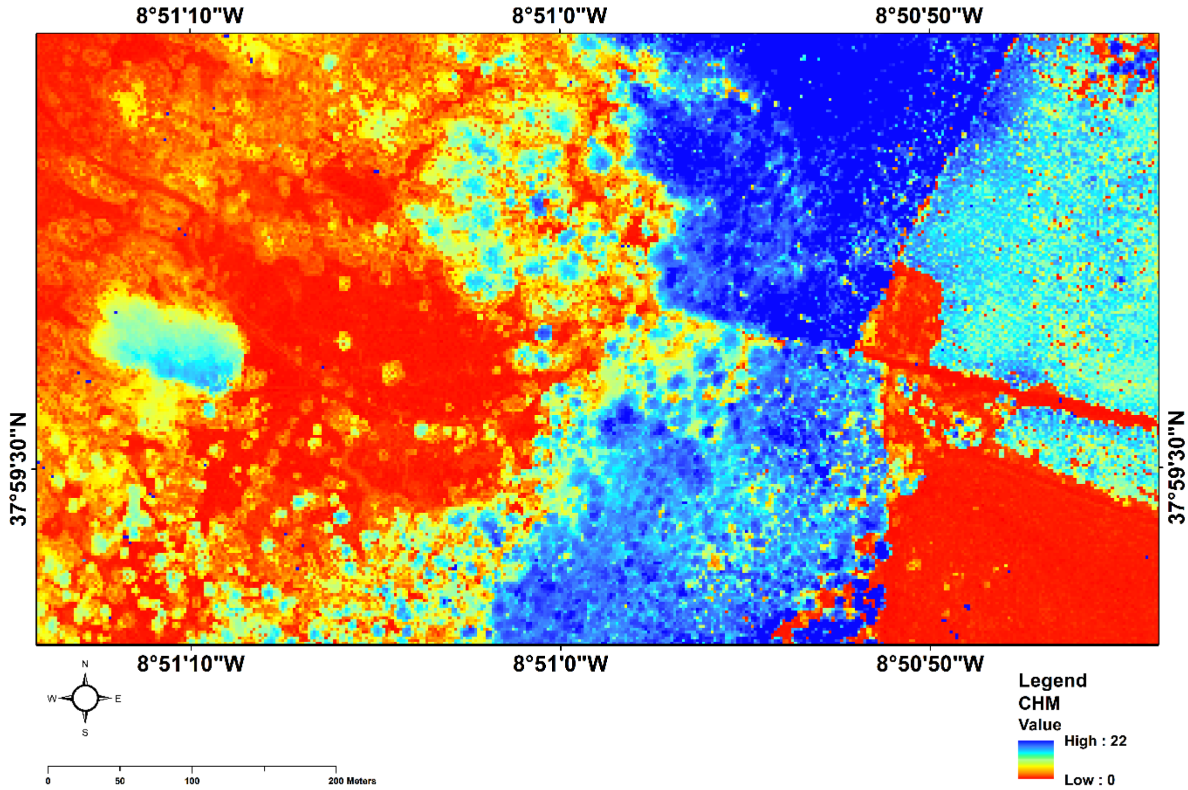

Figure 5.2 CHM generated from the decomposition of DSM and DTM (using the minus tool of ArcGIS)

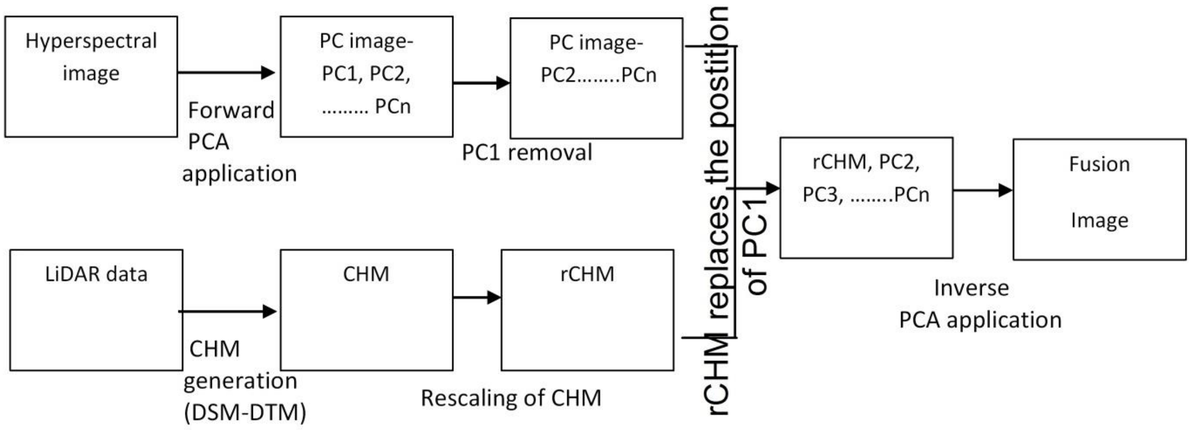

Figure 5.3. Flowchart showing PCA data integration technique outline generating PC fusion image, where PC1 is replaced with rCHM (refer to Equation 5.1 and Figure 5.1).

5.2.3 PC Image Fusion Technique Method

The aim of the objective is to merge the spectral information of HSI with the height information of the LiDAR derived CHM. Thus, this PC fusion technique is employed to retain the spectral information and generates the final PC fused image with the addition of the height information from the LiDAR derived CHM. Data integration may either be through the integration of raster formats or vector formats. The raster formats fusion were performed over PCA at a pixel level (or MNF based functions) whereas vector based integration involve overlay operations in ArcGIS environment. The PCA image fusion technique is a raster based methods to integrate the spectral content with the height information. The ENVI software is used to perform the fusion step during the study. Detailed description of PC fusion technique can be understood with the flowchart provided in Figure 5.3.

PCA techniques were discussed in Chapter 4, as PCA fusion approach utilises PCA method it is mentioned here. The major assumption behind using this technique is the properties related to scene luminance of the hyperspectral data (Welch and Ehlers, 1987). The primary aim of the fusion method is to retain the spectral information of all bands of the hyperspectral data. Therefore this assumption is considered: First of all, PC-1 contains only overall scene luminance of the data and all inter-band variation is contained in rest of the PCs, and secondly scene luminance in the SWIR regions are identical to Visible band scene luminance. The assumption that PC1 contains only scene luminance and whereas all information is stored in other PCs, is used to integrate HSI with CHM. Moreover, scene luminance matches with the SWIR scene luminance, so PC1 is replaced by rescaled CHM during integration. Thereafter, reverse PCA is performed to obtain fused image with both data quality. These all steps are considered while performing the fusion so that the mathematics of the reverse PC (Inverse PC transform) do not distort the thematic information of the image.

The equation used to re-scale the CHM to PC1 is based on a minimum and maximum values of the PC1 and matching the value of CHM to PC1 using the statistics of PC1. The rescaling equation is performed using the Band math tool ENVI is given below:

$$Rescaling \; = \frac{CHM - CHM_{Min}}{CHM_{max} - CHM_{min}} * (PC1_{max} + PC1_{min}) - PC1_{Min} \qquad \text{Equation 5.1}$$

Whereas, CHM = Canopy Height Model, CHM_{min} = the minimum value of the CHM,

CHM_{max}= the maximum value of the CHM, $PC1_{max}$ = the maximum value of the PC1, and $PC1_{min}$ = the minimum value of the PC1.

After processing of hyperspectral image and LiDAR data, PC image fusion step was applied. The corresponding subset of the study area for Eagle hyperspectral image and the corresponding subset of the CHM were generated, and fusion process of PCA is employed on hyperspectral image. The PC images produced were incorporated with CHM replacing the PC1 and again inverse PC technique was applied using the statistic files of the hyperspectral images. The inverse PC technique generated an image containing the same number of original the hyperspectral images. This integrated image contains the attributes of the CHM along with the spectral information of the image. This integrated image is capable of providing the spectral profile of the ground features and tree species.

With the above hypothesis, the PC techniques have been used on the hyperspectral data, forward PC transformation yields PCs bands, and statistic files were generated too. The numerical range of the PC1 was determined from the statistics file. The numerical range considered is min and max of the histogram of the PC1. Thereafter, CHM was rescaled to match the same numerical range as of PC1 and rescaled CHM was generated (see Equation 5.1). PC1 was removed from the PC images, and the order of PC images was like PC2, PC3, PC4 and so on (PCn). Now this rescaled CHM was integrated into the PC images replacing the position of PC1 from the PC images and arranged in the same order as PC images were before replacing PC1 like CHM, PC2, PC3, PC4 and so on. Now, these organized PC image was applied with reverse PC rotation using the same statistics generated during forward PC rotation technique. This overall process using hyperspectral image and CHM using forward and inverse PC rotation generate fusion image containing both spectral and structural properties of hyperspectral image and LiDAR data at the same platform. In parallel to this CHM derived tree heights were compared with the field recorded tree heights using regression model. The tree heights were compared for each species and their coefficient of determination was calculated and results were presented.

5.3 Results and Discussion

The result part discusses the comparison of the field-recorded tree and LiDAR derived canopy heights. Thereafter, this section focuses on the fused image, how it is important for different ground features and classification results. A significant difference in the accuracies of the classification of species and different ground features are due to mixed behaviour of the spectrum (acquired from grasses, vegetation, non-vegetated ground and height attribute) preventing spectral difference from surroundings.

5.3.1 Height Comparison- LiDAR derived and Field Recorded

As discussed in Chapter 3, DSM and DTM were generated from the airborne LiDAR data. These DSM and DTM outputs were used to produce the desired CHM for the study purpose (see Figure 5.2). Thereafter, height of the different tree species were extracted using the point extract feature tool of ArcGIS 10. Then, the extracted height values were compared with the tree height recorded in the field using Abney level. Both the measured and predicted tree heights were used in regression modelling, and they were used to get some information regarding canopy occupancy among all tree species.

From CHM, it is quite easy to derive the heights of different tree species. The data illustrated in Table 5.1 and Table 5.2 represent the mean canopy heights of different tree species, the difference in average canopy heights per-species of maximum and minimum ranges. According to LiDAR derived canopy height, the height range occupied by Pine species were distinct and overlapping with the same group of genus (*pinaster and pinea*) ranging from 5.96 m to 12.88 m (± ≤ 1.90 m) for *Pinus pinaster* and 4.09 m to 12.17 m (± ≤ 2.08 m) for *Pinus pinea*. Eucalyptus species show canopy height range of 10.24 m to 19.15 m (± ≤ 3.25 m), occupying a relatively unique height range in the study area. Within all species, *Eucalyptus* species had an average canopy height of 14.17 m occupying the highest strata among all species in the region (See Figure 5.4). Average canopy height for all other species like *Acacia* exhibit overlap and ranged from 2.23 m to 3.43 m (*Acacia* species SD ± ≤ 0.39m).

While field recoded height of the *Pinus pinaster* ranged from 6.5 m to 13.5 m (± ≤ 1.95 m) and ranged from 3.5 m to 10.25 m (± ≤ 2.07 m) for *Pinus pinea*. *Pinus pinea* has similar SD in both cases. Eucalyptus globulus has an average field height of 14.97 m while it ranges from 10 m to 21m (± ≤ 4.03 m). A slight variation in the height may be attributed by temporal data collection (Chapter 3), as LiDAR data was collected in 2011 and field survey was done in September 2012.

A regression model was used to compare the field measured tree heights (estimated heights) and LiDAR derived CHM (predicted tree heights) (coefficient of determination R^2= 0.9616, r =0.9806) as shown in Figure 5.4. Figure 5.4 illustrates a scatter plot of the LiDAR derived tree heights values versus field-measured tree heights values. In situ recorded tree height with the LiDAR derived tree heights were compared directly to each field point location. As seen from Figure 5.4, this comparison resulted in a correlation coefficient of r =0.9806. Figure 5.5 represent the plot of residual versus fitted values where residuals are distributed equally around their median value. Although, there is a temporal difference in both the data acquisition and collection, but it shows a strong correlation which is significant at 99% confidence as it is greater than 0.8 values (Davis, 1986). The values of R^2 is 0.9616 that means 95% of total variation of LiDAR derived tree heights can be explained by a linear relationship between *in-situ* field measurement and LiDAR derived heights. Figure 5.4 represents the residuals of the LiDAR derived tree heights after subtracting the Abney level derived tree height for each plot. In Figure 5.4, the dotted line represents a 1: 1 correspondence while the solid line is a best-fit linear regression to the data. It has been calculated that there is an average difference of 0.21 m between field measured height and LiDAR derived tree heights that account for 2.51% of average height of all tree species. The comparison of field height and CHM derived height of different tree species was performed using quartiles methods as shown in Figure 5.6. A box-and-whisker plot displays the mean, quartiles, minimum and maximum height observations for a LiDAR heights and field heights. The horizontal line in the box interior represents the median height, and marker represents the average canopy height of tree species, in both the LiDAR and field measured values.

It has been demonstrated by the research in that temporal difference causes some variation in the measurement of LiDAR and Field survey data (Streutker and Glenn, 2006). Authors assessed on the difference of height found while performing research on the LiDAR derived heights and field measure height and inferred that there is some difference in height if samples were collected over time. In most of the cases, CHM height was found to be lower than field recorded measurements. Seeing the above results, it can be assumed that the temporal difference of the data acquisition (both LiDAR and Field data) may have a certain extent of influence. It might be either due to some growth in the regions, specially *Acacia* species grows very fast and spread rapidly. This may be the one possible reason that contributes to the results of the comparison in case, but it would have caused a minor impact in the present study.

Table 5.1 The tree height statistics generated from CHM

	Pinus pinaster	***Pinus pinea***	***Acacia longifolia***	***Eucalyptus globulus***
Mean average height	11.30	7.43	2.69	14.17
SD	1.90	2.081	0.39	3.25
Max Value	12.88	12.17	3.43	19.15
Min Value	5.96	4.09	2.23	10.24
Range	6.92	8.08	1.2	8.91
n	15	17	13	15

Table 5.2 The tree heights statistics recorded in field survey

	Pinus pinaster	***Pinus pinea***	***Acacia longifolia***	***Eucalyptus globulus***
Mean Average height	11.37	7.28	3.21	14.97
SD	1.95	2.07	1.06	4.03
Max Value	13.5	10.25	5.5	21
Min Value	6.5	3.5	2.25	10
Range	7	6.75	3.25	11
n	15	17	13	15

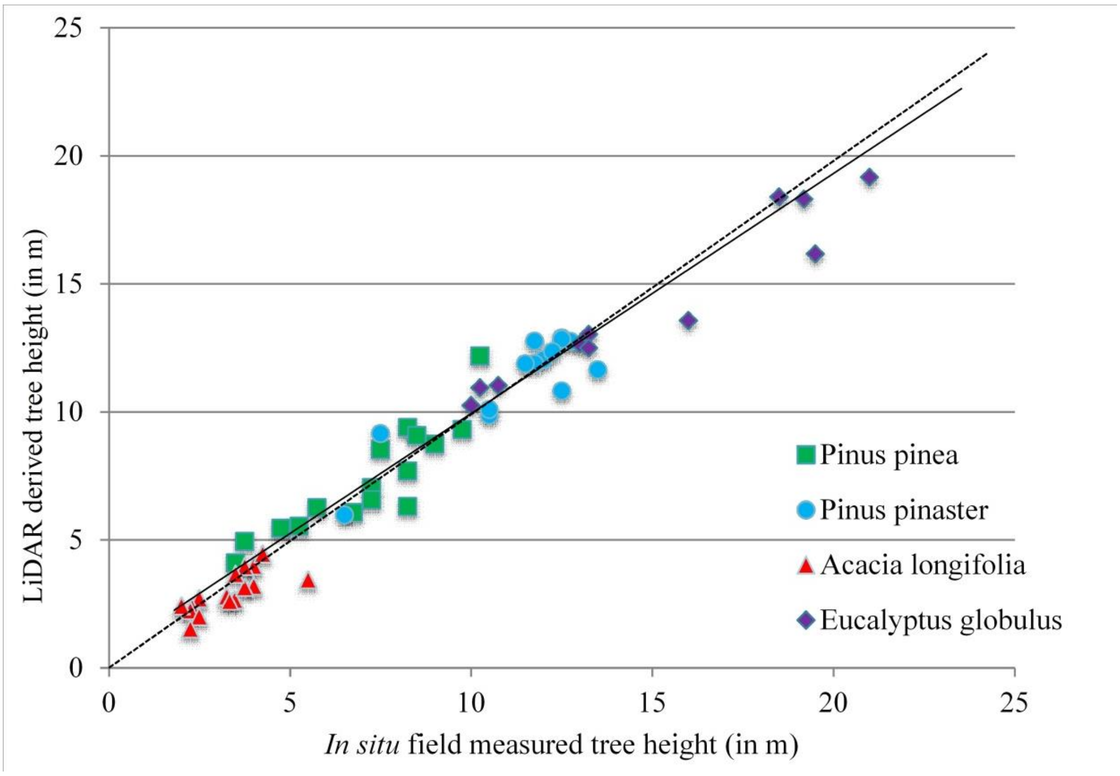

Figure 5.4 The correlation coefficient between LiDAR derived tree heights and field measured tree heights where, the solid line is intercept line and represents a best-fit linear regression to field and LiDAR derived heights, while the dotted line represents a 1:1 correspondence.

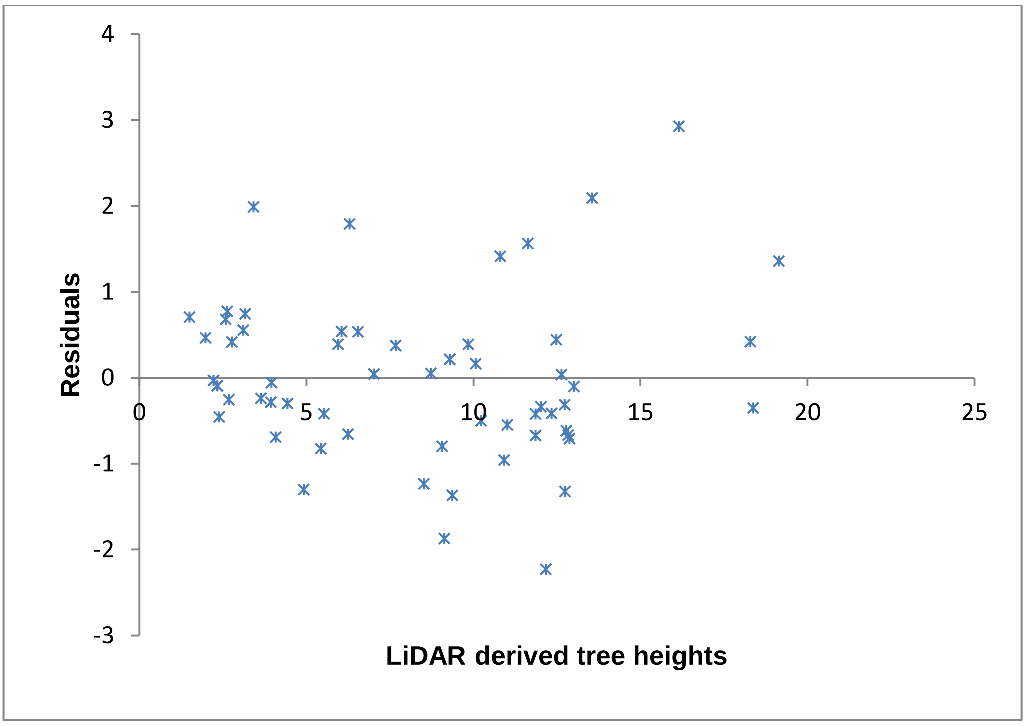

Figure 5.5 Residual plot of the LiDAR derived CHM over the field plot locations after subtraction of the field measurements of tree height with an Abney level. Residual plot the LiDAR derived tree heights against field measurement height values

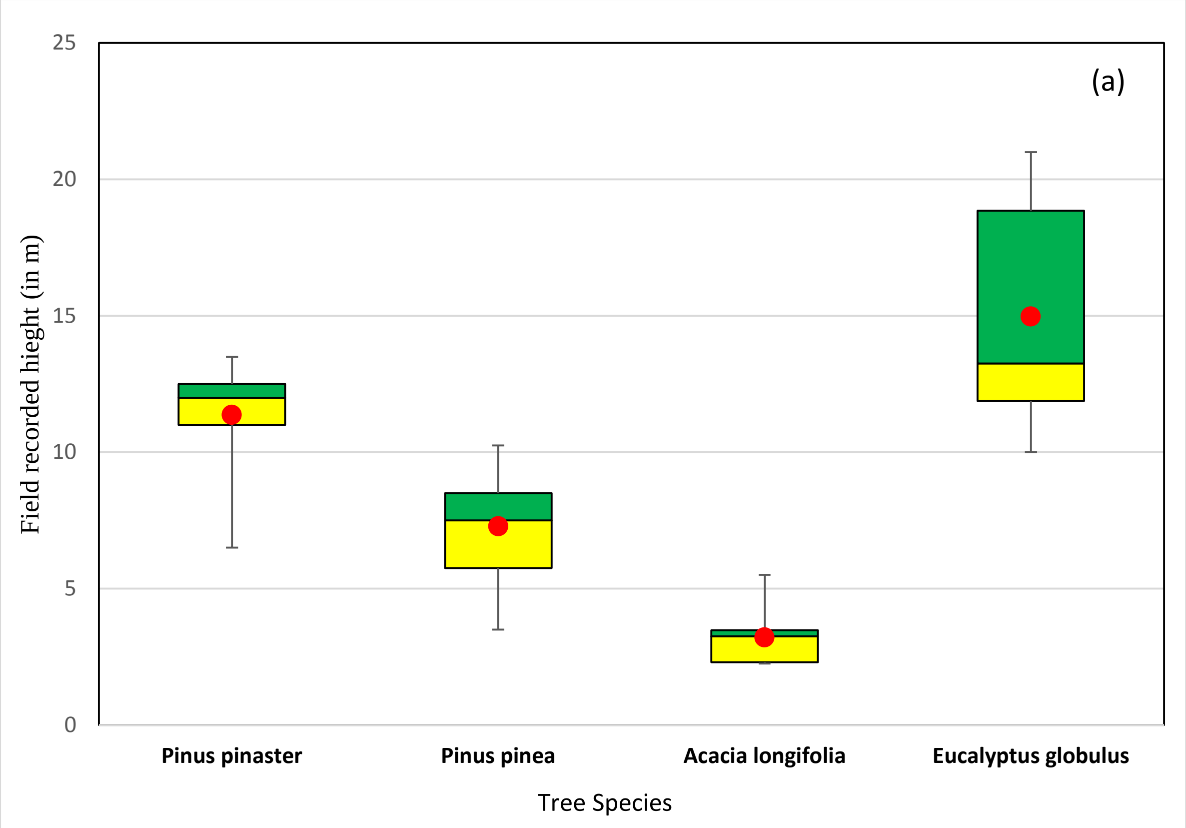

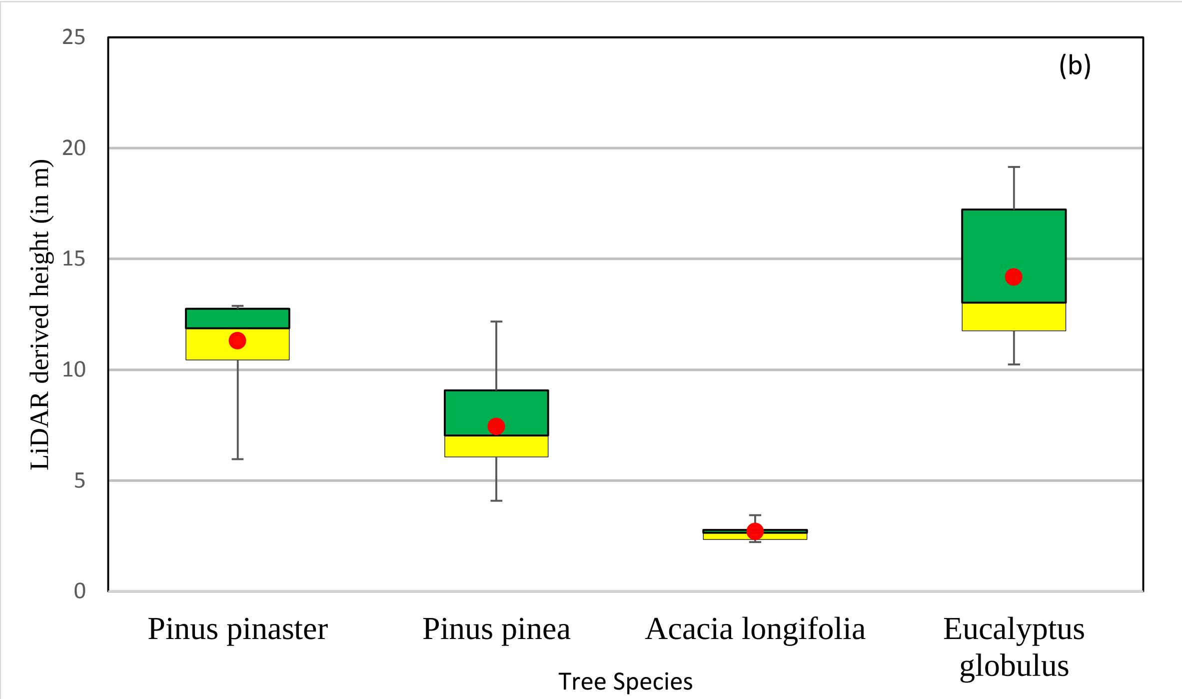

Figure 5.6 Comparison of (a) Field height and (b) CHM LiDAR derived Height of different tree species using Whisker box plot graph with maximum and minimum heights, Boxes encompasses the 25% quartile and 75% quartiles, and the solid middle line represents the median of all the field height and LiDAR derived heights. The red markers represent the average height of the tree species.

Taking data, field recorded tree heights and LiDAR derived tree heights, a regression model is performed. The linear regression model demonstrates that LiDAR derived heights are found to be approximately less than the field recorded tree heights (see Figure 5.6). Tree height estimates from the field recorded Abney level instrument correlated well with LIDAR-derived height estimates (CHM). The airborne AISA Eagle/Hawk hyperspectral data and Leica LIDAR were acquired simultaneously in April 2011. The field measurements were collected in September 2012 almost one year after airborne LiDAR data which were collected in the year 2011. This temporal difference accounted for the slightly poorer prediction of tree heights from LiDAR data. Despite this temporal difference, both predicted tree heights and estimated tree heights were successful in estimating a good correlation between both of the measurements.
During the study, it was realized that this method produces predicted values of canopy height that is compared with the absolute estimated values of tree height recorded in the field. As tree height recording differs and subjective to temporal difference and depend upon the time of sampling, the result can be little different due to time variation in data acquisition and field sampling. Figure 5.4 shows the correlation between LiDAR predicted tree heights with ground expected tree height result. Altogether 60 measurements were used to calculate the Pearson correlation coefficient of tree heights that showed a satisfactory result (R^2=0.9616).

5.3.2 Fusion of HSI and CHM

This section provides a comparison between the spectral profile generated from the fusion image and compared with the spectral profile of the tree species and ground features generated from atmospherically corrected hyperspectral image. The second part of this section deals with the classification of the fusion image and its accuracy assessment.

5.3.2.1 Spectrum Comparison of Hyperspectral Images and Fused Image

The resulting spectrum generated from the fused dataset is shown in Figure 5.8. It shows that the distinction between different features is clearer from the fused image bands than from the hyperspectral image bands. The spectral signatures of different tree species are detectable from the high information content of the hyperspectral imagery, but the fused image has the added advantage that it distinguishes very clearly between vegetated and non-vegetated areas.

Figure 5.7 shows that ground covered with grasses is not clearly visible in the original hyperspectral image but stands out in the fused dataset. This class confusion in the original hyperspectral data means that any classification with SAM or MLC is likely to lead to poor classification accuracies. Spectral reflectance profiles were extracted from the original hyperspectral and fused data, using z-profiles with an average window size of 3*3 as it was found to be optimal for maintaining the spectral purity.

The Savitzky-Golay smoothing filter was applied to the mean spectral reflectance values of hyperspectral and fused data respectively, for removing noise and peaks of the reflectance curves (Luo et al., 2005b, Luo et al., 2005a). This filtering notably reduces any high noise in the curves but does not affect the originality of their shape. This filtering notably reduces the high noise in the curves with minimal effect of the position, shape and depth of the spectral features (Press et al., 1996).The spectral profiles of the original datasets and the fused data are illustrated in Figure 5.7 and Figure 5.8.

The mean reflectance profiles of different tree species and ground covered with grasses as well as sandy areas are shown in Figure 5.7 and Figure 5.8. The spectrum of the fused data bands shows that the mean spectrum of different tree species, ground covered with grasses and sandy regions typically is clearly distinguishable. The spectral profile of the fused bands for ground covered with grasses shows a clear improvement in the separability in comparison to the original spectral profiles. Feature extraction is much more difficult from the original hyperspectral images alone, where other spectral profiles resemble that of sandy soil (Figure 5.8). Thus, the data fusion approach improves the accuracy of classification based on HSI and LiDAR data for vegetation and non-vegetation discrimination.

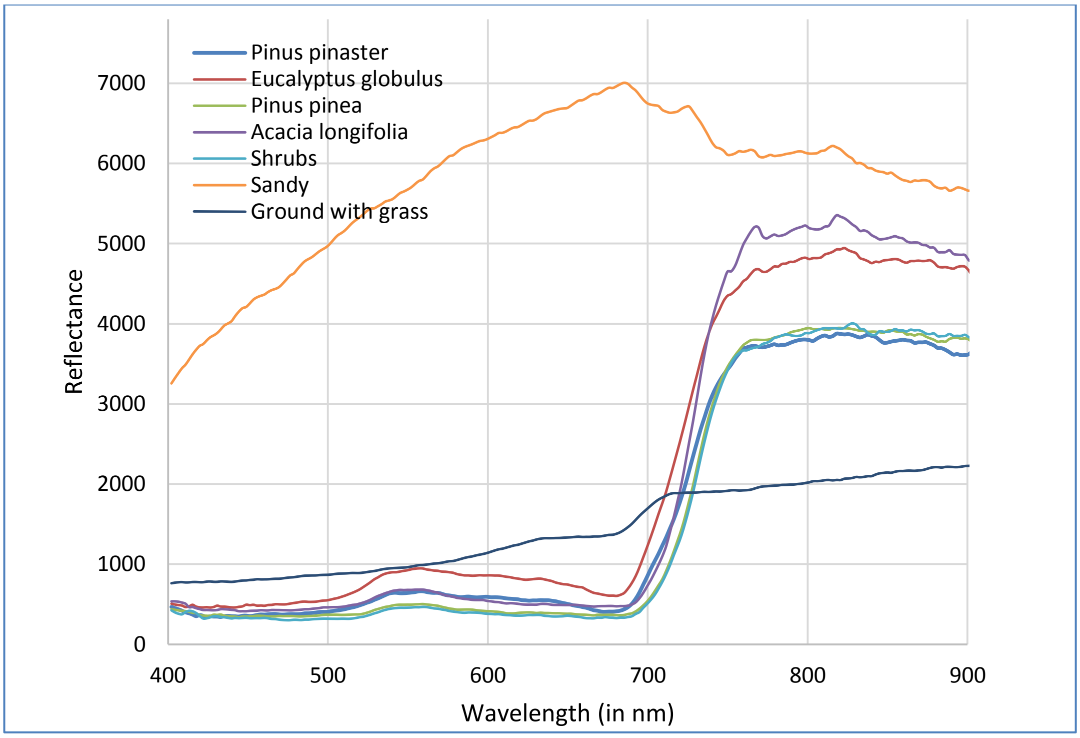

Figure 5.7 Spectral profiles of different features generated from atmospherically corrected hyperspectral images (S-Golay filtered) over a subset of the study area.

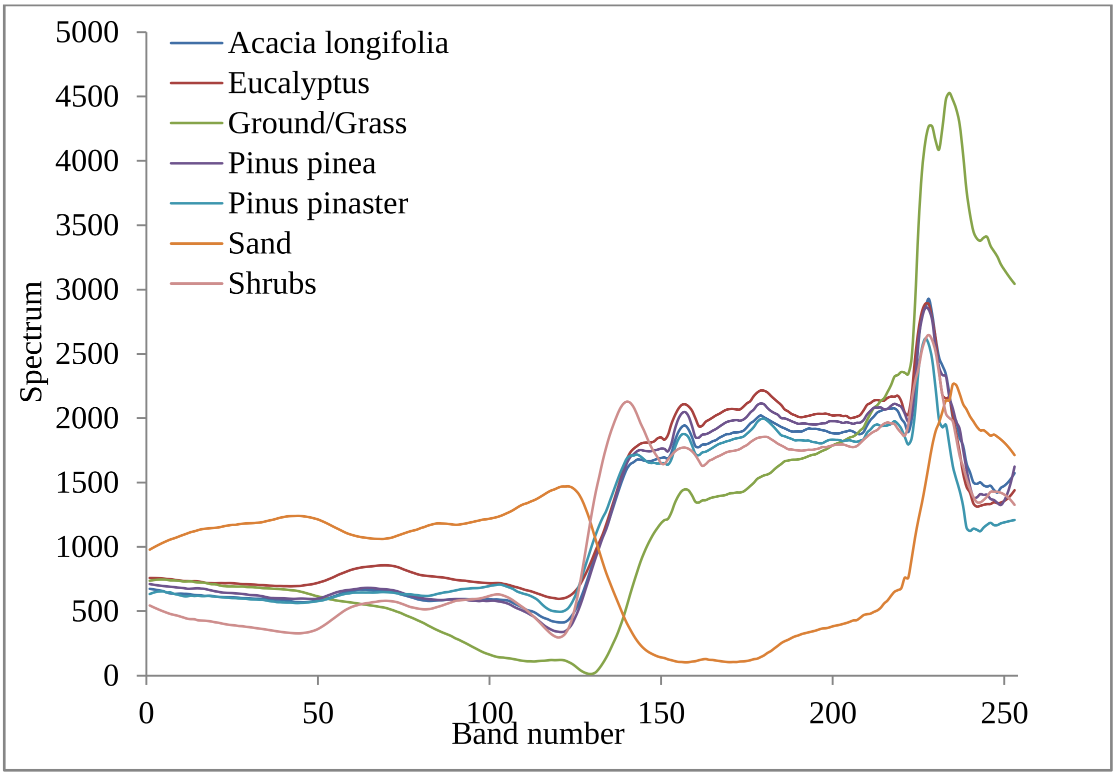

Figure 5.8 Spectral comparison of different features from the fused bands derived by inverted PCA axis rotation with the CHM replacing overall scene luminance (PC1) in the HSI data, showing signatures of tree species and non-vegetated features. Shrubs or grasses can be discriminated from other features much better than from the HSI spectral bands alone shown in Fig. 5.7.

5.3.2.2 Classification Results

MLC of fused data set of hyperspectral with canopy height showed that the differentiation becomes better and overall accuracy is increased up to 92.91% that was about 3 % more than MLC on original hyperspectral image. Therefore, a qualitative, as well as a quantitative assessment of classified maps, demonstrates that the result of fused image is much better than the original counterpart datasets. Table 5.3 illustrates the result of quantitative evaluation of different classified images. (OA< PA and κappa coefficient). The classified fusion image is shown in Figure 5.9.

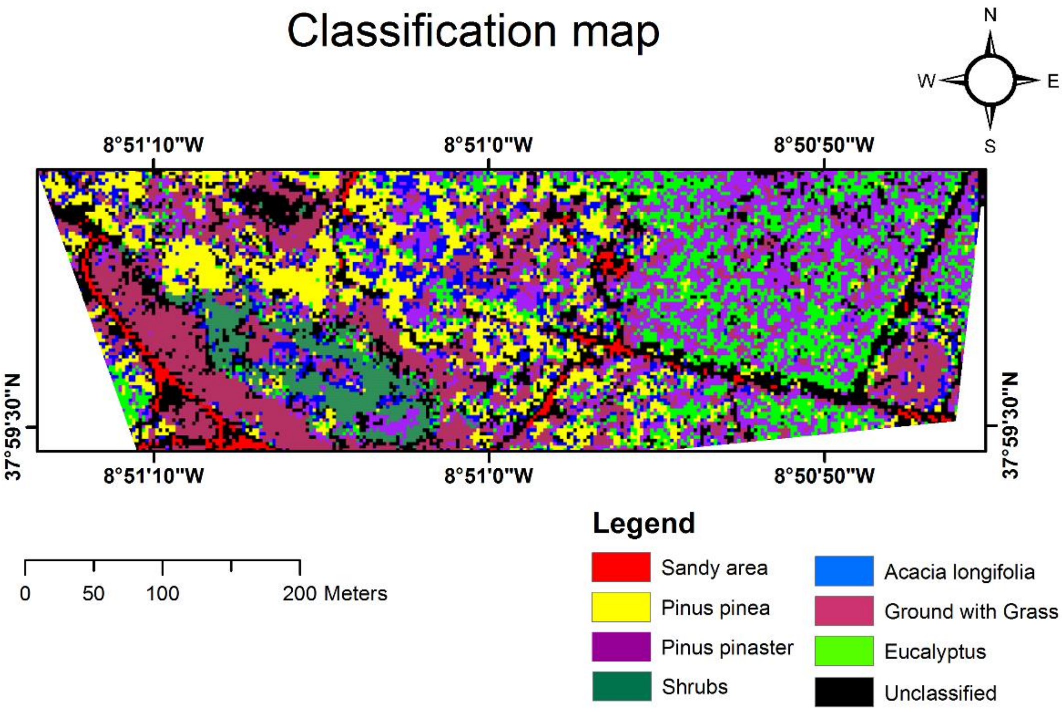

Figure 5.9 Classification map of PC fusion image

The overall accuracy as well as κappa coefficient was found to be much higher in case of fused HSI-canopy height image. The overall accuracy of original HSI was 89% and κappa coefficient 0.87 whereas it was 92.9% and 0.91 in case of fused HSI-canopy height image. As the main objective of the results was discrimination of different species, the feature accuracy was also calculated for each species and other features of study area. Therefore, the qualitative as well as a quantitative assessment of classified maps demonstrates that the result of fused image is much better than its original counterpart datasets. Table 5.4 illustrates the result of quantitative evaluation of different classified features (OA, PA of feature classes). Moreover, higher kappa (0.91) shows the advantage of fusion technique to discriminate and separate different features easily and effectively than individual image (0.6 and 0.87) as shown in Chapter 4.

Table 5.3 Overall accuracy and Kappa coefficient for PC fusion image classification

Classifier techniques	**Overall Accuracy (%)**	**κ- Coefficient statistics**
MLC on Fused image	92.91	0.91

Table 5.4 Error matrix for fused image classification

	Reference data							
Classified data	Sand	Eucalyptus	Pinus pinea	Ground with grass	Pinus pinaster	Acacia longifolia	Shrubs	Row Total
Unclassified	0	2	0	2	2	0	1	7
Sand	242	0	0	0	0	0	0	242
Eucalyptus	0	473	6	6	23	14	5	527
Ground with grass	4	0	420	0	1	0	0	425
Pinus pinea	0	29	0	401	16	0	0	446
Pinus pinaster	0	30	8	1	570	5	0	614
Acacia longifolia	0	18	4	6	0	206	0	234
Shrubs	0	0	0	10	0	0	216	226
Column Total	246	552	438	426	612	225	222	2721
PA	98.37	85.69	95.89	94.13	93.14	91.56	97.30	
UA	100.00	89.75	98.82	89.91	92.83	88.03	95.58	
Average PA	93.72							
Average UA	92.56							

5.3.2.3 Classification Accuracy Assessment

The error matrix generated during the classification of PC fused image was shown in Table 5.4. The error matrix was calculated using the reference data used for generating error matrix of each feature in classified images (Congalton et al., 1983, Stehman et al., 2009). The error matrix generated different accuracy parameters like user's accuracy, producer's accuracy, mapping accuracy and overall accuracy for comparison purposes of different classified images (Congalton, 1991, Congalton and Green, 2008). In addition to these accuracies, κappa statistic was also calculated for each classified images to test the significance of the difference in accuracy of classified images. It has been considered that κappa is one of the better tools for comparing different methods of classified images (Skidmore, 2002). Thus, these statistics provide a better platform, which is directly comparable with each other classification results.

The classification of hyperspectral image using SAM classifier produced an overall accuracy of 67.7 % which showed that the method is not able to well discriminate different species (see chapter 4). The change map is generated for the Figure 5.9 with classified image from hyperspectral image (See Figure 5.10). This map demonstrate three classes illustrating the changes, No change in class, unclassified, and changes from one class to other class. Unclassified refers to pixels, which are not classified in both images, and change refers to classed which are different in both classified images. The average producer accuracy and user accuracy for the features were 93.72% and 92.56% respectively as shown in Table 5.4. The classification of hyperspectral image with MLC gave a better overall accuracy of 89.67%, which showed better results than SAM, but it has some limitations in respect of discriminating some species and feature. However, MLC of fused data set of hyperspectral with canopy height showed that the differentiation becomes better and overall accuracy is increased up to 92.91 % which was about 3.24 % more than MLC on original hyperspectral image. Though it is able to classify different feature but its overall accuracy (92.91 <96.38), overall producer accuracy (93.72 <96.40) and overall user's accuracy (92.56 < 96.63) remains below the segmented PC classification results. One of the probable cause of these differences may be attributed to non-removal of data dimensionality (as fusion image has same number of bands as the original hyperspectral Eagle image).

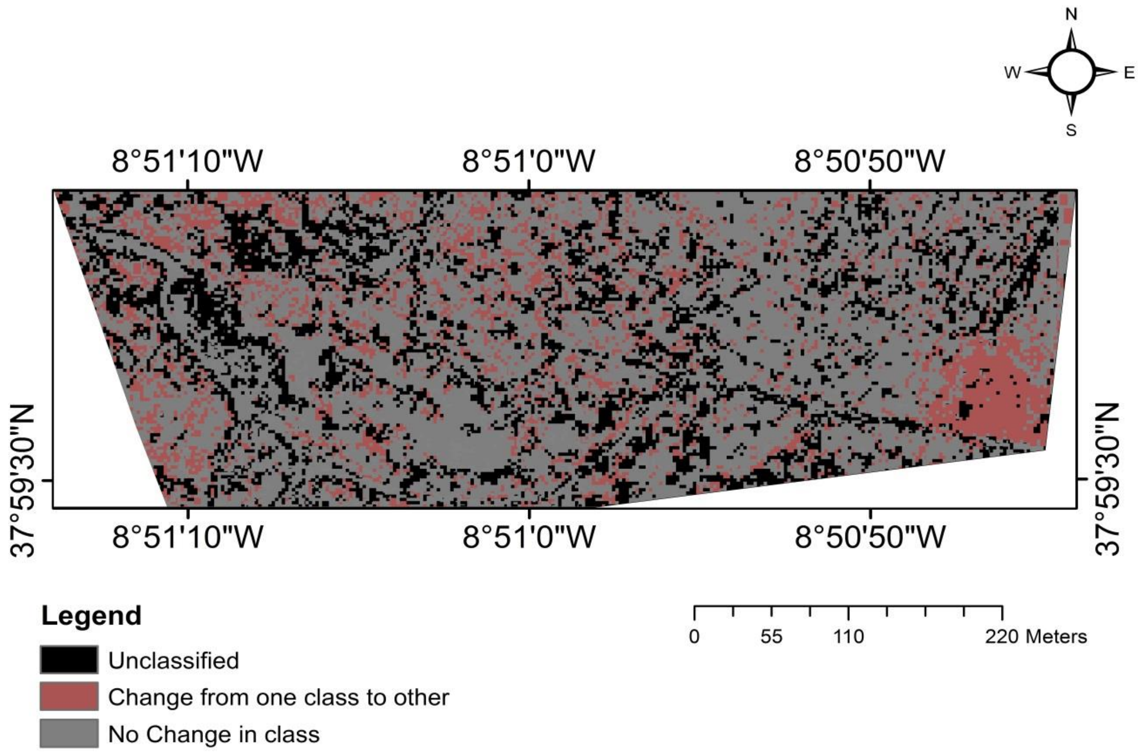

Figure 5.10 Change map for figure 5.9 with the previous image in classified image from hyperspectral image.

5.4 Conclusion

As seen from the above results, it can be concluded that LiDAR data have provided the significant results when compared to field data. While LiDAR data was shown helpful in the forest eco-system, it can be used in terrain regions for deriving the height features. The fusion image showed better results than individual hyperspectral image in overall accuracy. Fusion image was able to differentiate some ground features, which were not significantly observable in the hyperspectral images. Thus, incorporation of the spectral with structural attribute may provide better results than individual data assessment.

Moreover, in *Eucalyptus globulus* dominated area, the mean LiDAR derived canopy height was found to be 14.17 m and it ranges from 10.24 m to as high as 19.15 m. The average *Eucalyptus* tree height recorded in the field was 14.97 m, while some of eucalyptus tree height ranged as high as 21 m (minimum height recorded as 10m). This illustrates that *Eucalyptus globulus* occupy the privilege of the upper canopy in the study region. Similarly, *Acacia longifolia* LiDAR derived height was found to be in the range 2.23m to 3.43 m, while the individual average height of the species ranged to as high as 2.69 m. The field-measured height of *Acacia longifolia* was found to be 2.25 to 5.5 m and mean height was 3.21 m. This gives a light on the fast growing nature of the invasive species in the region that are spreading understorey *Eucalyptus globulus* tree. This height measurement was found to be a valuable information regarding the tree height variation in the study region of the Mediterranean forest and better distinguished tree species level. Moreover, the fusion of HSI and LiDAR derived CHM has shown the applicability of the technique to distinguish the shrubs, ground with grass as against other features and tree species.

Streutker and Glenn, (2006) tried to classify the sagebrush vegetation using the LiDAR data and validated with ground measurements. They put forward a question, 'whether LiDAR can effectively identify or distinguish grasses from open bare ground surfaces or not?' (Streutker and Glenn, 2006). The present study, thus, provides a platform for distinguishing the grasses/shrubs from bare sandy ground and other tree species using a fusion image of HSI and LiDAR derived CHM. A solution to this can be seen in this chapter using the PC image fusion techniques.

Kempeneers (2009) tried to merge airborne digital photo with LiDAR data to map coastal vegetation with the help of ground reference points. They measured tree heights in the field and compared them with that predicted height from the LiDAR data in the laboratory for its accuracy. They found good correlation (R^2 = 0.99, RMSE=0. 34) between measured and predicted heights in the research work. That was high results with LiDAR and field recorded data. In the present study, temporal variation in data may have some impact on lower accuracy rate, but this has not affected the fusion classification result.

While hyperspectral images have been used widely in forestry research, this present study shows that additional information along with hyperspectral image can be significant for use in forestry and another research area with height differences. Possible future use includes assessing and finding disturbance in croplands or forestry, rangelands or other low canopy areas. The applicability of proposed fusion method can be applied in rugged terrain with several features and its necessity can be addressed in future. The success of fusion method lies in the distinction of different species and feature with good user and producer accuracy results, and it indicates the robustness of the proposed methodology. The results of this study have shown that data fusion of

LiDAR and HSI can improve the classification accuracy of tree species and other features.

1) Fusion of spectral information content and vegetation structural parameters enhances the capability to distinguish features. This causes improved classification outcomes from the fused data, which are superior to the original individual images.
2) Data fusion enables the distinguishing capability of vegetation from non-vegetation much more accurately than hyperspectral images alone, as it has been confirmed that PCA helps in the discrimination of vegetated from non-vegetated features. Grounds partially covered with grasses were easily demarcated from shrub areas and other features. Thus, the PCA data fusion approach improves the accuracy achievable with HSI and LiDAR data for vegetation mapping.
3) Data fusion results in better classification accuracy than the individual HSI dataset.

The identification of various features was straightforward for some tree species and ground feature classes, but the distinction between some specific features was enhanced by data fusion with the CHM derived from LiDAR data. This type of fused data is beneficial for regions with a larger number of features like water, mixed vegetation, ground, shrubs, etc. This technique differentiates features from each other based on their canopy or surface height as well as spectral absorption properties. The importance of the present study lies in its quantitative assessment of the achievable accuracy improvements from data fusion of LiDAR and HSI. Given the highly accurate feature discrimination between shrubs, grasses and trees, the data fusion approach can be extended to other mapping applications such as burned area mapping and others. In future studies, different fusion processes should be compared to diverse research areas in order to test the spatial transferability of the methods. In future studies, different fusion processes should be compared for diverse study areas in order to test the spatial transferability of the methods.

5.5 Summary of Chapter

This chapter presented the PC fusion techniques for hyperspectral image and LiDAR derived CHM. Thus, it brought the two different attribute of dataset together and enhanced the capability of image classification. The classification of the PC fusion image using MLC classifier performed significantly better (>92.91 %; κ=0.91) than original hyperspectral image. The lower accuracy of PC fusion classified image than segmented PC results may be the presence of the data dimensionality as we have performed inverse PCA technique for generation of fusion image. This study explores the classification accuracy achievable with synergistic use of the two datasets: airborne hyperspectral and LiDAR data. The classification accuracy and κ coefficient increased above the hyperspectral images as expected from the assumption, CHM contributed towards an increase in the results. Thus, PC image fusion may be able to provide increased classification results than hyperspectral image alone. This confirms that additional attributes from other data source if incorporated in another increase the results as compared to individual image result.

The next chapter discusses the contribution of the present research, limitations were faced, and recommendations and future works. Finally, the chapter concludes the research with the outcomes, and some future assumptions or techniques to include in coming time.

Chapter 6. Conclusion

6.1 Introduction

This thesis explores the two main novel objectives- spectral segmented PC image classification and fusion techniques incorporating LiDAR generated CHM and spectral characteristics of hyperspectral image for the mapping and classification of Mediterranean forest in Portugal. Overall it has been demonstrated that both airborne hyperspectral imagery and airborne LiDAR data can be synergistically utilised to overcome data redundancy and spectral mixing which is unidentified by multispectral imagery that critically limit the conventional use of multispectral remote sensing to essentially identify different species precisely. To summarise, the main contribution, some limitations faced during the study period, recommendations, possible techniques and future scope are presented in this chapter. Thus, this chapter presents an overview of the present research conducted in the Mediterranean forest.

As discussed earlier, there are four elements, which are essential, and a foremost requirement, for the classification of tree species and surrounding ground features. The present study utilises 2 m high spatial resolution, very high spectral resolution, additional input of height attributes and appropriate classifiers. The segmented PC and PCA fusion methods adopted in the study have incorporated all the required parameters necessary for the classification of the tree species and surrounding regions. As seen from the present research, species can be identified and mapped through spectral profiling with their unique and distinct characteristics, but the inclusion of additional properties of the feature (such as height attributes from LiDAR) can improve the results. The results can be improved by reducing the data dimension of the images as well. Techniques like PCA demonstrated in the present study, are capable of identifying tree species and ground features for mapping with more detail and accuracy, with the help of *priori* knowledge and collected data from the study site. A possible alternative to PCA approach is the MNF transformation that has not been used and examined in this study, but it can be used later on.

In future studies, airborne hyperspectral imagery and airborne LiDAR data can be used to map detailed and accurate species trees and forest attributes that are consistent with field-based data. Overall, the innovative application of airborne hyperspectral imagery and airborne LiDAR data have the significant potential to aid information regarding integration and helps in more accurate mapping campaigns over large forest areas, agricultural and non-vegetated regions.

6.2 Importance of the Present Research

This thesis presented a method of segmented image generation and classification based on standard maximum likelihood classifier. It also used the integration of hyperspectral and LIDAR derived CHM to classify and assess the accuracy of the resultant image.
The aims of the present study were

1) To classify hyperspectral images with different techniques, using segmentation of images and comparison of different classifiers performed over segmented PC images and hyperspectral images in Mediterranean forest.
2) To identify tree species, incorporating attributes from both hyperspectral (spectral information) and LiDAR data (height).

The aim of the thesis is achieved with good accuracy results, with segmented PC techniques and PC image integration method as discussed earlier in chapter 4 and chapter 5. The importance of the research stands with the improved results while providing processing methods of airborne Eagle and hawk data. The objective of the thesis mainly focuses on the classification results generated using the segmented PC image techniques which is particularly novel in itself. This technique is novel as it has used segmentation of the hyperspectral image, and application of PCA on those segments resulting in same corresponding PC image as segments bands. Finally those informative PC images from segments were integrated together to generate a segmented PC image. Thus, this segmented PC image is a new in itself and the study is performed in the Mediterranean region, which suggests the first use of this presented techniques. Similary, PC image integration techniques presented in the present work is novel and incorporated first time using airborne hyperspectral image and LiDAR data for the forest mapping in the Mediterranean test site. Moreover, both the techniques are applied for the Mediterranean forest, is one of the first to use the above methods. The main strength of the thesis is that the present methods can delineate the species and structure corresponding to open tall stand in simple heterogeneous conditions as compared to the close dense forest species such as Amazon rain forests.

Different classes were considered for classification of the hyperspectral and segmented PC image- *Pinus pinea, Pinus pinaster, Eucalyptus, Acacia longifolia*, grasses covering ground, shrubs, and sandy region. These different classes form the coastal habitat and its surrounding regions. Two different classifier techniques were analysed for their potential use in classification as well as comparison among them. These two different classifier techniques: SAM and MLC based on supervised classification were incorporated for classification of different images. Different images like original reflectance hyperspectral image, segmented PC image and fused image were classified accordingly using these two classifier techniques. Three different classification results were compared with each other for better classification, namely SAM classification of hyperspectral image, MLC of hyperspectral image and segmented PC image.

As expected, the classification outcome from fusion data was found to be better than the classification of the original dataset. These have produced better results in term of the user's accuracy, the producer's accuracy, overall accuracy and κappa statistics. Efficacy of fusion of HSI and LIDAR can be shown with significantly better results in terms of overall accuracy and class mapping accuracy of different species and feature classes. A very obvious benefit of the fusion of HSI and LiDAR derived CHM is temporal consistency of both data, as both images are acquired at the same time.

It is obvious from the study that the high resolution of HSI and the addition of some structural components to the fused image is the main reason for higher accuracy compared with the original HSI image. Spectral mixing of two tree species and feature classes can be avoided by adding some additional parameters like structural properties, as the height will be providing the other response than the low height feature classes that help in distinguishing the different feature classes and tree species.

This can be evident from the results that shrubs, different tree species, ground with grasses were prominently distinguished in segmented PC image and fusion image as compared to other classified results. It may be the probable reason that structural variation in the fusion images has created its distinguishing capabilities. Thus, it may be able to produce better results due to variation in the different classes enhanced by adding structural parameters, ultimately producing better classification results and separation capabilities. The distinguishing capabilities of fusion image are due to avoiding the spectral mixing of two classes due to structural components which might have created more variation between species and different feature classes, and producing anticipated results.

This study presented a method of image fusion for hyperspectral images and LiDAR canopy height based on Principal Component Analysis. These techniques also helped to differentiate the tree species from a non-vegetation region very accurately. It also looked at the segmentation of hyperspectral images and applying PCA to segments of hyperspectral images to get the corresponding PCs, and integration of the first 3 PCs from each segment results in segmented PC images. Based on this method, segmented PC image was classified by the standard maximum likelihood classifier and compared with classification results of SAM and MLC of hyperspectral images. This also presented a method of classification and comparison between different classifier techniques for hyperspectral images and segmented PC image. Based on the image fusion, it is also investigating how tree species can be differentiated from each other and associated habitat features like sandy region, shrubs and ground covered with grasses.

6.3 Contribution of Present Research

The major contribution of this research was the tree species and surrounding features identification using image fusion technique and image classification technique for segmented PC image. This study suggests the robustness of image fusion for the classification and differentiation of tree species to each other and from non-vegetated features. PCA image fusion could have the potential for better discrimination and classification results than using hyperspectral image individually, and it has not yet been used or presented in earlier published studies. The range of classification results obtained for the hyperspectral image (also CHM inclusion in fusion) varies from 67% to 96% depending upon the classifier used and techniques applied on the image. Classification performed on hyperspectral images (SAM, MLC) and classification results of segmented PC and fusion images provide different results in the study. Here, the study aims at the synergistic use of the hyperspectral image and LiDAR derived CHM as well as segmented PC, so more stress is aimed at them.

As anticipated, the research questions of the present study were explained with reasonable results and justification. They are concluded in summary here:

1. Hyperspectral images have capabilities to distinguish tree species and other features provided that they are processed with some more reliable and better techniques. The MLC classification of HSI and segmented PC images provided >89 % and > 96% overall accuracy respectively. CHM generated from LiDAR is compared with field recorded height, which produced coefficient r^2= 0.9616; an indication of good correlation. Thus, it can be assessed that hyperspectral images and LiDAR data have the ability to distinguish different tree species and other features in parallel with other techniques.
2. Segmented PCA of hyperspectral data uses better classification accuracy than other approaches like standard MLC and SAM of original images. It has given about >96% overall accuracy and κ-0.95, which is clearly indicating better classification results (see Chapter 4 results).
3. The fusion of HSI and CHM, generated images with both spectral contents as well as structural parameters which help in distinguishing the feature more effectively than using original images. As concluded from the results, grounds with grasses were easily and effectively separated from other features. Particularly, this feature has been the most distinguishing results in MLC classification of fusion image (producer accuracy and user's accuracy is higher than other classification results, see Chapter 5 results).
4. The results are indicating that structural parameters incorporation help in distinguishing different features more effectively than MLC classification and segmented classification of HSI. It does this work with different features with the ability to provide spectral as well as structural parameters, which is not in the case of individual hyperspectral image.
5. SAM, MLC and fusion approaches were able to present some different results in all cases, but they have different advantages over classifying different features. As expected, they proved to be able to classify the tree species and other ground features effectively as expected.
6. As discussed earlier, MLC classifier is an effective algorithm and additional techniques like segmentation and fusion approaches enhance the images and thus improve the classification results.

This thesis aims to provide a base for the use of data dimensionality reduction as well as integration techniques to harness most of the information content of the datasets. One can use the spectral range to determine the noise or bad band using the PCA techniques. Moreover, MNF method can work as an alternative to data dimensionality reduction depending upon the type of data- satellite borne or airborne data. Above discussion conclude that the aims were achieved with desired results.

6.4 Limitations

As expected, the aim and objective of the research was provided with reasonable justification and outputs. However, time limitations should be taken into consideration as data was acquired in April 2011 and the field survey was performed during September 2012. Further, some more work could have been included in the present study, but the high cost of data resulted in failure to acquire temporal data for the study area.

Though more than enough points have been collected for training data and accuracy assessment, a second field survey could have added some more ground data to study, which might have provided more reliable results. The outcomes of the research could have been more effective, if there was a second fieldwork with more collected ground points and samples.

The other limitations or hurdles faced during the research includes-

1. Gaps in the data collection or acquisition: it may be one of the reasons for accuracy disparity (airborne data in 2011 and field data in 2012).
2. Data processing with apl-suite software, due to a bug issue during geometric correction and mapping that required a very large amount of cache memory and disk space (due to large file size during processing). This is a big hurdle while working with the massive size data such as airborne hyperspectral and LiDAR data.
3. Non-availability of temporal airborne datasets. Due to high cost and expenditure, it was not possible to check the vitality of the techniques for two time periods.
4. In technical aspects, PCA performed in ENVI software is unable to generate correlation and covariance reports for the hyperspectral data due to a large number of variables. This is processed and read in Matlab software. Matlab has a problem in that it cannot displays summaries of the variables with more than

524288 elements (in case of image values for generation of histograms) and therefore they were analysed separately.

5. During transportation while returning from the field work, the radio spectrometer broke down. Most of the spectra recorded were not recovered with reference line, but some of them were recovered successfully. If all those spectra would have been recovered it that may have added a comparable spectra from hyperspectral imagery. The field-recorded spectral files are good in quality and differ substantially from different tree species and corresponds to image spectra.
6. No further technical problems or limitations were observed in the study.

6.5 Recommendations and Future Works

In particular, the method proposed in this research work will be helpful for image classification that reduces hyperspectral data dimensionality. This will also contribute towards data fusion aspect where both hyperspectral and LiDAR data contribute their image properties that aid in the image and generate distinct features spectrum. Considering results, it may be possible to resample the AISA images at a higher spatial resolution, like 1 m for future studies. Thus, it will provide much higher spectral as well as spatial enhancement with additional properties of the LiDAR data. This will try to counter the possibilities of spacing between two trees and can assess much more information on canopy gap feature identification. In the study site, the trees are planted with a spacing by the forest conservation management and they clear *Acacia longifolia* from the region frequently. The current scenario of the study site is illustrated in **Error! Reference source not found.**, the forest department cleared the forest to inhibit *cacia longifolia's* growth and thus paved the way for native tree species to grow and flourish in the region. Most of the region is seen barren and empty, this illustrates that *Acacia* were cleared from those regions along with shrubs and some *Pinus* species, while keeping only *Eucalyptus* species for growth and conservation. Recently, the forest management to avoid the invasions of the Acacia longifolia and to conserve the other tree species cleared the study area. So it may not be possible to address the issue related to the distribution of the different features in the present time. But it may lead us to indulge in other studies related to change detection and analysis.

Figure 6.1 The current scenario of the study site as in mid of year 2014.

6.5.1 Cost per square km Estimation

The present research can be performed with the high resolution multispectral images such as World-View 1 or World-View 2 images (8 bands in the image), on the basis that they can be used for performing segmentation steps. The segment part of the present technique cannot apply to multispectral images; the limitation is due to a fewer number of bands over the complete electromagnetic spectral ranges and one band in each spectral range chosen to carry out the spectral segmentation.

Table 6.1 General overview of cost per km for different datasets

	Type of Data	Factors	Cost per Square Km
1	Airborne Hyperspectral and Airborne LiDAR data	Cost depend upon the time of flight, distance from airport of sponsors.	Very expensive and data availability is very rare,
2	Satellite borne Hyperspectral (Hyperion or Enmap German Hyperspectral data) and LiDAR data	Limited availability of data for the desired test sites. LiDAR Data acquired upon request	Comparatively less expensive
3	Very high spatial resolution multispectral data and LiDAR data	Available for most sites	Cheaper than above two data types
4	High spatial resolution multispectral image, and hyperspectral image	Available for most sites	Cheaper than all above

The cost per square km depend upon the type of data used for the new study area, it also depends upon the user's needs and their requirement for high resolution images such as 2 m, 1 m, or less. It will also depend upon the selected field site for which data will be used such as airborne data or satellite based images. The satellite data will provide a cheaper cost when compared to the airborne data, a Hyperion image will be of limited use due to low spatial resolution (30 m spatial resolution of Hyperion, 7.75 m swath width, spectral bandwidth 10 nm). AVIRIS data with 10 m spatial resolution may prove relevant for use with fusion technique.

Therefore, the cost per square km depends upon many factors, which should be considered before the selection of data [data types, study regions for field sampling, software requirements such as ENVI, Arc GIS or free ware software for data processing (geometric, atmospheric correction, mapping, and classifications)]. It may vary depending upon the use of airborne or Hyperion images. The approximate cost per square km estimation is based on the price of the images being considered for the study site, expenses to the field trip, software cost, processing instruments such as GPS, Computers facility (the EUFAR Project acquired and provided the datasets for test site, Portugal).

6.5.2 Adaptation to Different Conditions and Use of Open Source Software

Homogenous standalone test sites are studied by the present methods, these techniques can be applied in the other forests such as tropical forest. This also depends upon the types of the tree species or their structure. When the types and structure differ in the different complex sites, the segment part may be considered in respect to chlorophyll content, cellular structures and water content. It can be adapted to different species depending upon their leaf structures and the colour combination of all tree species present in the field site (for leaf structure and colour please refer to the text in segment part). There is potential for the adaptation of hyperion images in certain cases where it will be dealt with higher spatial resolution than AISA eagle images in the open tropical or Mediterranean region.

Thus, the applicability of the approaches used in the study can be applied in different forest regions (tropical or temperate forest), though the denser canopy must also be addressed, as well as the possibility of including data containing temporal resolution. This study can prove to be beneficial in other research fields and hilly terrains. The inclusion of other parameters with HSI, such as Intensity may provide a similar or even better result. Intensity value may provide some more valuable information regarding tree species and ground features, the use of different fusion methods for integrating the LiDAR and hyperspectral properties. It may be challenging to use different techniques to combine hyperspectral and LiDAR data. In the future, one can include other classifier techniques to see the robustness and applicability of the techniques presented in the study. We can try to use class separability with the fusion image, as this also provides a similar spectrum for all features with different patterns. This may further include techniques like transformed divergence (TD) and Jeffries Matusita distance (JM) techniques for the feature identification in the fusion image. Further, I would recommend the use of first derivatives and second derivatives of the spectral profile for differentiating and the identification of tree species and surrounding features, as it would provide more separation capabilities than spectral profile alone. Moreover, differences between the first and second derivative may be beneficial to assess species variation at different ranges.

Identification of tree species and mapping different tree species is a major concern of RS communities using space borne satellite or airborne images, which continues to be the subject of major research all around the world. Despite the fact that there is a difference in the spectral reflectance recording of handheld radio-spectrometer and airborne hyperspectral images, due to the BRDF effect, reflectance from the airborne AISA provides useful information in the identification of species related to their pigments, intercellular spaces and water content of different species in the study site. Therefore, as discussed in Chapter 3 and 4, different conditions of tree species (such as leaf pigments, cellular structures, water content or stress) and homogenous conditions for the field measurements (type of species, structure of leaf, sky condition) should be taken into account. Spectral reflectance of tree species (either at leaf level using radio-spectrometer or at canopy level using hyperspectral image) and classification results may show a discrepancy if any of the listed factors differ in the context of the classification. In the context of species identification and classification using the spectral segmented PC and fusion data, it may provide a better platform to the above issue in simple, open, tall stand communities.

RS communities can use the methods and can break free from expensive software by utilising different open source software. Open source software can be an alternative for the expensive commercial software. The open source tools such as LAS tools, Fusion software, Canupo software and Spectral Python will be helpful for processing the data, but airborne hyperspectral data is processed by the *apl* Software suite that is specific for the processing of the airborne hyperspectral data. It is somewhat limited to the *apl* software suite for various corrections, and ENVI FLAASH module for atmospheric corrections. The lesson for the design of the new hyperspectral sensor may involve decreasing the atmospheric effects such as BRDF, Haze, and aerosol effect. The noisy bands present in the electromagnetic region such as 1349-1462 nm and 1790-1999.0 nm may be taken extra care for either improving the windows for collection of surface reflectance or dropped it from the sensor. The exact nature of the design can be seen after the experimental setup with such suggestions. For the development of HSI sensors, one needs to know the spectral ranges, as well as purposes and the use of hyperspectral data. Most of the noises in the hyperspectral data are found in the spectral range such as 1191.55-1197.85 nm, 1349.3-1462 nm and 1790.8-1999.0 nm (based on the information from Airborne Eagle and Hawk data- refer to Figure 4.10). These regions are severely affected due to atmospheric oxygen and water absorption. In most cases, these bands were either removed or dropped to achieve the desired results. All bands are not useful for each study and depends upon the type of research such as spectral characteristics (visible range), structural behaviour (NIR range), water stress, tree surface temperature, and carbon content (thermal range). Thus, the present study is beneficial to the RS forest communities in terms of classification results specifically to open and sparse vegetation conditions.

The main part of the work has been the use of spectral PC segmentation and PC image fusion of airborne hyperspectral and LIDAR data in Mediterranean forest associated with the classification of different tree species and associated ground features in an open, tall, simple community. Finally, different classification maps were generated with accuracy results derived from segmentation and fusion techniques using both hyperspectral and LiDAR data. The fused hyperspectral and LiDAR image has generated overall accuracy ($\leq$ 3% than segmented pc image) hence it is concluded that the CHM does not contribute in enhancing the classification results when compared to the segmented PC technique. Perhaps one can think of other parameters from the LiDAR data such as intensity or texture that may assist in enhancing the information and provide a better platform for classification. Therefore, the selection of the spectral ranges such as blue, green, red, NIR, and SWIR from the high spatial resolution hyperspectral image can provide precise information on different tree species and associated ground features for enhanced mapping. These can provide knowledge in the open, tall stand with accurate and precise results, however not be suitable or capable in the Amazon rain forest or complex forest stands. It can be conferred from the study that the AISA and LiDAR are capable of identifying, discriminating and classifying different tree species and ground features with appropriate classifier. It is obvious from the study that the classification algorithm with segmented PC image and PC fusion image helped to improve classification accuracy either in overall accuracy or κappa coefficient. Thus, airborne HSI and LiDAR data, together are potential remote sensors for identification of different tree species and ground features, because the integration of two data at single platform offers distinguishing capabilities of different feature, and can provide better and improved classification results than individual images. The aim of the study is to employ the synergistic use of hyperspectral and LiDAR dataset and uses hyperspectral image. The two different approaches (segmented PC technique and PC fusion) were employed to achieve the objectives resulting in new images, segmented PC image and PC fusion image. It proved to be an important finding for identification and classification of different tree species and ground features in Mediterranean forest.

Appendix-1

Script for removing the noises from the LiDAR las file

(a) Script to remove noises from the Las file (lidar data) using software pt_cloud filter.exe provided by NERC-ARSF in command prompt

-pt_cloud_filter.exe [Input file] [classification number to remove] > [filtered output name]

for example:

-pt_cloud_filter.exe LDR-EUFAR_201109809.txt 7 > filtered_strip9.txt

Appendix-2

Script for the smoothening of spectral profile

Savitzky-Golay filter- Script for removing noises from spectral profile of different features.

```
% Load data
load input.txt
%plot(1:400, input (1:400))
output =sgolayfilt(input,2,21);
% Apply 3rd-order filter
%plot(1:250, output (1:250))
 %axis([0 980 0 2000]),
title( 'S-Golayfilter')
wave = output1(:,1);   % to separate the first column
data = output(:,2);  % to separate the 2nd column
data2 =output(:,3);
plot (wave,data,'k', wave,data2,'g')
%plot (wave,data2,'g', ':')
title( 'title')
```

The original script can be found on matlab site:

```
{
load mtlb                          % Load data
smtlb = sgolayfilt(mtlb,2,51);   % Apply 2nd-order filter
subplot (2,1,1)
plot([1:2000],mtlb(350:2600));
title('      ');
subplot (2,1,2) % if want to plot other wise not necessary-
plot([1:2000],smtlb(1:2000)); axis([0 2000 -4 4]);
title('       '); grid;}
```

Note: in syntax - smtlb = sgolayfilt(mtlb,2,51);}, Third number must be odd number like 51, 53, 99. It can be used according to user need and applications. The initial odd numbers such as 1, 3, 5 when used removes some of the noises, when 111, 121, 131 are used it makes the line much flatter, so this number is checked by putting numbers in a sequence so that to find the best smoothening curve.

References

ABIBULLAEV, B. & AN, J. 2012. Classification of frontal cortex haemodynamic responses during cognitive tasks using wavelet transforms and machine learning algorithms *Medical Engineering and Physics,* 34**,** 1394-1410.

ADLER-GOLDEN, S. M., BERNSTEIN, L. S., LEVINE, R. Y., BERK, A., RICHTSMEIER, S. C., ACHARYA, P. K., ANDERSSON, G. P., FELDE, G., GARDNER, J., HOKE, M., JEONG, L. S., PUKALL, B., RATKOWSKI, A. & BURKE, H. H. 1999. Atmospheric Correction for Short-wave Spectral Imagery Based on MODTRAN4. *In:* DESCOUR, M. R. & SHEN, S. S. (eds.) *SPIE's International Symposium on Optical Science, Engineering, and Instrumentation.* Denver, CO: International Society for Optics and Photonics.

ALEXANDRIAN, D., ESNAULT, F. & CALABRI, G. 1999. Forest fires in the Mediterranean area. *Unasylva -197 Mediterranean Forests,* 50**,** 30-42.

ALLARD, G., BERRAHMOUNI, N., BESACIER, C., BOGLIO, D., BRIENS, M., BRIZAY, A., CAMIA, A., COLLETTI, L., CONIGLIARO, M. & D'ANNUNZIO, R. 2013. State of Mediterranean forests 2013. *In:* CHRISTOPHE, B., CENCIARELLI, R., GIRAUD, J.-P., GARAVAGLIA, V. & SARRE, A. D. (eds.). Rome, Italy: FAO.

ALONSO, M. C., MALPICA, J. A. & MARTINEZ DE AGIREE, A. 2011. Consequences of the Hughes phenomenon on some classification Techniques. *ASPRS 2011 Annual Conference* Milwaukee, Wisconsin

ALONZO, M., BOOKHAGEN, B. & ROBERTS, D. A. 2014. Urban tree species mapping using hyperspectral and lidar data fusion. *Remote Sensing of Environment,* 148**,** 70-83.

AMÉRICO, M. S. & MENDES, C. 2005. Portugal: country situations *In:* LIEUTIER, F. & GHAIOULE, D. (eds.) *Entomological research in Mediterranean forest ecosystems.* France: Editions Quae.

ANDERSON, G. P., FELDE, G. W., HOKE, M. L., RATKOWSKI, A. J., COOLEY, T. W., CHETWYND JR, J. H., GARDNER, J., ADLER-GOLDEN, S. M., MATTHEW, M. W. & BERK, A. 2002. MODTRAN4-based atmospheric correction algorithm: FLAASH (Fast Line-of-sight Atmospheric Analysis of Spectral Hypercubes). *Algorithms and Technologies for Multispectral, Hyperspectral, and Ultraspectral Imagery VIII AeroSense 2002.* Orlando, FL: International Society for Optics and Photonics.

ANDERSON, J. E., DUCEY, M. J., FAST, A., MARTIN, M. E., LEPINE, L., SMITH, M. L., LEE, T. D., DUBAYAH, R. O., HOFTON, M. A., HYDE, P., PETERSON, B. E. & BLAIR, J. B. 2011. Use of waveform lidar and hyperspectral sensors to assess selected spatial and structural patterns associated with recent and repeat disturbance and the abundance of sugar maple (Acer saccharum Marsh.) in a temperate mixed hardwood and conifer forest. *Journal of Applied Remote Sensing,* 5**,** 053504-053504.

ANDERSON, J. E., PLOURDE, L. C., MARTIN, M. E., BRASWELL, B. H., SMITH, M. L., DUBAYAH, R. O., HOFTON, M. A. & BLAIR, J. B. 2008. Integrating waveform lidar with hyperspectral imagery for inventory of a northern temperate forest. *Remote Sensing of Environment,* 112**,** 1856-1870.

ANGER, C. D., BABEY, S. K. & ADAMSON, R. J. 1990. New approach to imaging spectroscopy. *Imaging Spectroscopy of the Terrestrial Environment.* International Society for Optics and Photonics.

ARSF 2012. Airborne Processing Library Getting started with APL - Command line. Natural Environment Research Council.

ARSL. 2014. *What is Lidar ?* [Online]. Arizona: The Atmospheric Remote Sensing Laboratory, Electrical and Computer Engineering, University of Arizona. Available: http://www2.engr.arizona.edu/~arsl/lidar.html [Accessed April 20 2014].

ASD 2002. FieldSpec Pro User's Guide. Boulder, CO USA: Analytical Spectral Devices, Inc.

ASD INC 2008. ViewSpec Pro™ User Manual. *600555 Rev. A.* Boulder, CO USA: ASD Inc.

ASNER, G. P., KNAPP, D. E., KENNEDY-BOWDOIN, T., JONES, M. O., MARTIN, R. E., BOARDMAN, J. & HUGHES, R. F. 2008. Invasive species detection in Hawaiian rainforests using airborne imaging spectroscopy and LiDAR. *Remote Sensing of Environment,* 112**,** 1942-1955.

ASPRS 2005. LAS Specification Version 1.1. ASPRS

BAATUUWIE, N. & VAN LEEUWEN, L. 2011. Evaluation of three classifiers in mapping forest stand types using medium resolution imagery: a case study in the Offinso Forest District, Ghana. *African Journal of Environmental Science and Technology,* 5**,** 25-36.

BALTSAVIAS, E. P. 1999. Airborne laser scanning: basic relations and formulas. *Isprs Journal of Photogrammetry and Remote Sensing,* 54**,** 199-214.

BALZTER, H., LUCKMAN, A., SKINNER, L. & DAWSON, T. 2007. Observations of forest stand top height and mean height from interferometric SAR and LiDAR over a conifer plantation at Thetford Forest, UK. *International Journal of Remote Sensing,* 28**,** 1173-1197.

BANSKOTA, A., WYNNE, R. H., JOHNSON, P. & EMESSIENE, B. 2009. Synergistic use of very high frequency radar and discrete-LiDAR return for estimating biomass in temperate hardwood and mixed forests. *In: Proceedings of: SILVILASER 2009-The 9th international conference on lidar applications for assessing forest ecosystems* College Station Texas USA.

BARBEITO, I., PARDOS, M., CALAMA, R. & CAÑELLAS, I. 2008. Effect of stand structure on Stone pine (Pinus pinea L.) regeneration dynamics. *Forestry,* 81**,** 617-629.

BARBERO, M., BONIN, G., LOISEL, R. & QUÉZEL, P. 1990. Changes and disturbances of forest ecosystems caused by human activities in the western part of the Mediterranean basin. *Vegetatio,* 87**,** 151-173.

BELLMAN, R. 1961. *Adaptive Control Processes: A Guided Tour,* Princeton, Princeton University Press.

BENEDIKTSSON, J. A., SWAIN, P. H. & ERSOY, O. K. 1990. Neural network approaches versus statistical-methods in classification of multisource remote-sensing data. *IEEE Transactions on Geoscience and Remote Sensing,* 28**,** 540−552.

BERGEN, K., GOETZ, S., DUBAYAH, R., HENEBRY, G., HUNSAKER, C., IMHOFF, M., NELSON, R., PARKER, G. & RADELOFF, V. 2009. Remote sensing of vegetation 3-D structure for biodiversity and habitat: Review and implications for lidar and radar spaceborne missions. *Journal of Geophysical Research: Biogeosciences (2005–2012),* 114.

BERNSTEIN, L. S., ADLER-GOLDEN, S. M., SUNDBERG, R. L., LEVINE, R. Y., PERKINS, T. C., BERK, A., RATKOWSKI, A. J., FELDE, G. & HOKE, M. L. 2005. Validation of the QUick Atmospheric Correction (QUAC) algorithm for VNIR-SWIR multi-and hyperspectral imagery. *Defense and Security.* International Society for Optics and Photonics.

BERTOLDI, W., GURNELL, A. M. & DRAKE, N. A. 2011. The topographic signature of vegetation development along a braided river: Results of a combined analysis of airborne lidar, color air photographs, and ground measurements. *Water Resources Research,* 47**,** 1-13.

BINELLI, E. K., GHOLZ, H. L. & DURYEA, M. L. 2000. Plant succession and disturbances in the urban forest ecosystem. *In:* DURYEA, M. L., KAMPF BINELLI, E. & KORHNAK, L. V. (eds.) *SW-140, "Restoring the Urban Forest Ecosystem", a CD-ROM.* University of Florida, USA: the School of Forest Resources and Conservation, Florida Cooperative Extension Service, Institute of Food and Agricultural Sciences.

BLACKBURN, G. A. 2007. Hyperspectral remote sensing of plant pigments. *Journal of Experimental Botany,* 58**,** 855-867.

BLONDEL, J. & ARONSON, J. 1995. Biodiversity and ecosystem function in the Mediterranean basin: human and non-human determinants. *In:* DAVIS, G. W. & RICHARDSON, D. M. (eds.) *Mediterranean-type ecosystems.* Berlin: Springer Verlag.

BOARDMAN, J. 1992. SIPS User’s Guide Spectral Image Processing System. Version 1.2 ed. Boulder, CO, USA.

BOARDMAN, J. W. 1995. Analysis, understanding and visualization of hyperspectral data as convex sets in n-space. *Imaging Spectrometry,* 2480**,** 14-22.

BOARDMAN, J. W., BICHL, L. L., CLARK, R. N., KRUSE, F. A., MAZER, A. S., TORSON, J. & STAENZ, K. 2006. Development and Implementation of Software Systems for Imaging Spectroscopy. *2006 Ieee International Geoscience and Remote Sensing Symposium, Vols 1-8***,** 1969-1973.

BOARDMAN, J. W. & KRUSE, F. A. 1994. Automated Spectral Analysis - a Geological Example Using Aviris Data, North Grapevine Mountains, Nevada. *Proceedings of the Tenth Thematic Conference on Geologic Remote Sensing - Exploration, Environment, and Engineering, Vol I***,** I407-I418.

BOLAND, J., AGER, T., EDWARDS, E., FREY, E., JONES, P., JUNGQUIET, R., LAREAU, A., LEBARRON, J., KING, C. & KOMAZAKI, K. 2004. Cameras and sensing systems. *In:* MCGLONE, J. C. (ed.) *Manual of Photogrammetry.* Bethesda: ASPRS.

BOLLE, H.-J. 2003. *Mediterranean climate: variability and trends,* Berlin, Springer Verlag.

BORENGASSER, M., HUNGATE, W. S. & WATKINS, R. 2010. *Hyperspectral remote sensing: principles and applications,* Boca Raton, FL, CRC Press, Taylor and Francis group.

BOSCHETTI, M., BOSCHETTI, L., OLIVERI, S., CASATI, L. & CANOVA, I. 2007. Tree species mapping with Airborne hyper-spectral MIVIS data: the Ticino Park study case. *International Journal of Remote Sensing,* 28**,** 1251-1261.

BOWLES, J. H., MANESS, S. J., CHEN, W., DAVIS, C. O., DONATO, T. F., GILLIS, D. B., KORWAN, D., LAMELA, G., MONTES, M. J., RHEA, W. J. & SNYDER, W. A. 2005. Hyperspectral imaging of an inter-coastal waterway. *In:* EHLERS, M. & MICHEL, U. (eds.) *Remote Sensing for Environmental Monitoring, GIS Applications, and Geology V.* Bruges, Belgium: International Society for Optics and Photonics.

BRANDTBERG, T., WARNER, T. A., LANDENBERGER, R. E. & MCGRAW, J. B. 2003. Detection and analysis of individual leaf-off tree crowns in small footprint, high sampling density lidar data from the eastern deciduous forest in North America. *Remote Sensing of Environment,* 85**,** 290-303.

BRUCE, L. M., KOGER, C. H. & LI, J. 2002. Dimensionality reduction of hyperspectral data using discrete wavelet transform feature extraction. *IEEE Transactions on Geoscience and Remote Sensing,* 40**,** 2331-2338.

BRUNZELL, H. & ERIKSSON, J. 2000. Feature reduction for classification of multidimensional data. *Pattern Recognition,* 33**,** 1741-1748.

BUDDENBAUM, H., SCHLERF, M. & HILL, J. 2005. Classification of coniferous tree species and age classes using hyperspectral data and geostatistical methods. *International Journal of Remote Sensing,* 26**,** 5453-5465.

CALKINS, H. A. & YULE, J. G. B. 1927. *The Abney level handbook,* Washington, United States Forest Service Government Printing Office.

CAMPBELL, J. B. 2002. *Introduction to remote sensing,* London, CRC Press, Taylor and Francis.

CARLETTA, J. 1996. Assessing agreement on classification tasks: the kappa statistic. *Computational linguistics,* 22**,** 249-254.

CARLSON, K. M., ASNER, G. P., HUGHES, R. F., OSTERTAG, R. & MARTIN, R. E. 2007. Hyperspectral remote sensing of canopy biodiversity in Hawaiian lowland rainforests. *Ecosystems,* 10**,** 536-549.

CARTER, R. W. G. 1988. *Coastal environments: an introduction to the physical, ecological and cultural systems of coastlines,* UK, Academic Press.

CASTRO-ESAU, K., SÁNCHEZ-AZOFEIFA, G. & CAELLI, T. 2004. Discrimination of lianas and trees with leaf-level hyperspectral data. *Remote Sensing of Environment,* 90**,** 353-372.

CETIN, H., PAFFORD, J. T. & MUELLER, T. G. 2005. Precision agriculture using hyperspectral remote sensing and GIS. *RAST 2005: Proceedings of the 2nd International Conference on Recent Advances in Space Technologies***,** 70-77.

CHAN, Y. C., CHEN, Y. G., SHIH, T. Y. & HUANG, C. 2007. Characterizing the Hsincheng active fault in northern Taiwan using airborne LiDAR data: Detailed geomorphic features and their structural implications. *Journal of Asian Earth Sciences,* 31**,** 303-316.

CHANG, C. I., DU, Q., SUN, T. L. & ALTHOUSE, M. L. G. 1999. A joint band prioritization and band-decorrelation approach to band selection for hyperspectral image classification. *IEEE Transactions on Geoscience and Remote Sensing,* 37**,** 2631-2641.

CHASMER, L., HOPKINSON, C. & TREITZ, P. 2006. Investigating laser pulse penetration through a conifer canopy by integrating airborne and terrestrial lidar. *Canadian Journal of Remote Sensing,* 32**,** 116-125.

CHATURVEDI, R. K., GOPALAKRISHNAN, R., JAYARAMAN, M., BALA, G., JOSHI, N., SUKUMAR, R. & RAVINDRANATH, N. 2011. Impact of climate change on Indian forests: a dynamic vegetation modeling approach. *Mitigation and adaptation strategies for global change,* 16**,** 119-142.

CHAVEZ, P. S. & KWARTENG, A. Y. 1989. Extracting Spectral Contrast in Landsat Thematic Mapper Image Data Using Selective Principal Component Analysis. *Photogrammetric Engineering and Remote Sensing,* 55**,** 339-348.

CHEN, Z., CURRAN, P. J. & HANSOM, J. D. 1992. Derivative reflectance spectroscopy to estimate suspended sediment concentration. *Remote Sensing of Environment* 40**,** 67-77.

CHERIYADAT, A. & BRUCE, L. M. 2003. Why principal component analysis is not an appropriate feature extraction method for hyperspectral data. *Geoscience and Remote Sensing Symposium, 2003. IGARSS'03. Proceedings.* IEEE International.

CHO, M. A., DEBBA, P., MATHIEU, R., NAIDOO, L., VAN AARDT, J. & ASNER, G. P. 2010. Improving discrimination of savanna tree species through a multiple-endmember spectral angle mapper approach: Canopy-level analysis. *Geoscience and Remote Sensing, IEEE Transactions on,* 48**,** 4133-4142.

CHO, M. A., SKIDMORE, A. K. & SOBHAN, I. 2009. Mapping beech (Fagus sylvatica) forest structure with airborne hyperspectral imagery. *International Journal of Applied Earth Observation and Geoinformation,* 11**,** 201-211.

CHO, M. A., SOBHAN, I., SKIDMORE, A. K. & DE LEEUW, J. 2008. Discriminating species using hyperspectral indices at leaf and canopy scales. *The International Archives of the Photogrammetry, Remote Sensing and Spatial Information Sciences,* XXXVII**,** 369-376.

CHUST, G., GRANDE, M., GALPARSORO, I., URIARTE, A. & BORJA, A. 2010. Capabilities of the bathymetric Hawk Eye LiDAR for coastal habitat mapping: A case study within a Basque estuary. *Estuarine Coastal and Shelf Science,* 89**,** 200-213.

CHYTRÝ, M., PYŠEK, P., WILD, J., PINO, J., MASKELL, L. C. & VILÀ, M. 2009. European map of alien plant invasions based on the quantitative assessment across habitats. *Diversity and Distributions,* 15**,** 98-107.

CLARK, M. 2011. Identification of Canopy Species in tropical Forests using Hyperspectral data. *In:* THENKABAIL, P. S. L., J.G. AND HUETE, A. (ed.) *Hyperspectral Remote Sensing of Vegetation.* Boca Raton, FL: CRC Press, Taylor and Francis Group.

CLARK, M. L., ROBERTS, D. A. & CLARK, D. B. 2005. Hyperspectral discrimination of tropical rain forest tree species at leaf to crown scales. *Remote Sensing of Environment,* 96**,** 375-398.

CLARK, M. L., ROBERTS, D. A., EWEL, J. J. & CLARK, D. B. 2011. Estimation of tropical rain forest aboveground biomass with small-footprint lidar and hyperspectral sensors. *Remote Sensing of Environment,* 115**,** 2931-2942.

CLARK, R. N. 1999. Spectroscopy of Rocks and Minerals, and Principles of Spectroscopy. *In:* RENCZ, A. N. (ed.) *Manual of Remote Sensing.* New York: John Wiley and Sons.

COCHRANE, M. A. 2000. Using vegetation reflectance variability for species level classification of hyperspectral data. *International Journal of Remote Sensing,* 21**,** 2075-2087.

COLEMAN, T., GUDAPATI, L. & DERRINGTON, J. 1990. Monitoring forest plantations using Landsat Thematic Mapper data. *Remote Sensing of Environment,* 33**,** 211-221.

CONGALTON, R. G. 1991. A review of assessing the accuracy of classifications of remotely sensed data. *Remote Sensing of Environment,* 37**,** 35-46.

CONGALTON, R. G. & GREEN, K. 2008. *Assessing the accuracy of remotely sensed data: principles and practices,* Boca Raton, FL, CRC press, Taylor and Francis Group.

CONGALTON, R. G., ODERWALD, R. G. & MEAD, R. A. 1983. Assessing Landsat classification accuracy using discrete multivariate analysis statistical techniques. *Photogrammetric Engineering and Remote Sensing,* 42**,** 1671-1678.

COOLEY, T., ANDERSON, G., FELDE, G., HOKE, M., RATKOWSKI, A., CHETWYND, J., GARDNER, J., ADLER-GOLDEN, S., MATTHEW, M., BERK, A., BERNSTEIN, L., ACHARYA, P., MILLER, D. & LEWIS, P. 2002. FLAASH, a MODTRAN4-based atmospheric correction algorithm, its application and validation. *Geoscience and Remote Sensing Symposium, 2002. IGARSS '02.* IEEE International

COPLEY, V. R. & MOORE, J. M. 1993. Debris provenance mapping in braided drainage using remote sensing. *Geological Society,* Special Publications**,** 405-412.

CORP, L. A., CHENG, Y. B., MIDDLETON, E. M., PARKER, G. G., HUEMMRICH, K. F. & CAMPBELL, P. K. E. 2009. Hyperspectral-LIDAR system and data product integration for terrestrial applications. *Imaging Spectrometry XIV.* San Diego, CA.

COSTA, J. C., LOUSA, M., CAPELO, J., SANTO, M. D. E., SEVILLANO, J. I. & ARSENIO, P. 2000. The Coastal vegetation of the Portuguese divisory sector: Dunes cliffs and Low-scrub Communities. *Finisterra, XXXV,* 69**,** 69-93.

COWLING, R. M., RUNDEL, P. W., LAMONT, B. B., KALIN ARROYO, M. & ARIANOUTSOU, M. 1996. Plant diversity in Mediterranean-climate regions. *Trends in Ecology and Evolution,* 11**,** 362-366.

CROITORU, L. 2007. How much are Mediterranean forests worth? *Forest Policy and Economics,* 9**,** 536-545.

CRONK, Q. & FULLER, J. 1995. *Plant invader,* Chapman and Hall, London.

D'ANTONIO, C. & MEYERSON, L. A. 2002. Exotic plant species as problems and solutions in ecological restoration: a synthesis. *Restoration Ecology,* 10**,** 703-713.

DALPONTE, M., BRUZZONE, L. & GIANELLE, D. 2008. Fusion of hyperspectral and LIDAR remote sensing data for classification of complex forest areas. *IEEE Transactions on Geoscience and Remote Sensing,* 46**,** 1416-1427.

DALPONTE, M., BRUZZONE, L. & GIANELLE, D. 2009a. Fusion of hyperspectral and LIDAR remote sensing data for the estimation of tree stem diameters. *Geoscience and Remote Sensing Symposium, IGARSS 2009.* IEEE International.

DALPONTE, M., BRUZZONE, L., VESCOVO, L. & GIANELLE, D. 2009b. The role of spectral resolution and classifier complexity in the analysis of hyperspectral images of forest areas. *Remote Sensing of Environment,* 113**,** 2345-2355.

DALPONTE, M., ORKA, H. O., ENE, L. T., GOBAKKEN, T. & NAESSET, E. 2014. Tree crown delineation and tree species classification in boreal forests using hyperspectral and ALS data. *Remote Sensing of Environment,* 140**,** 306-317.

DATA BASIN 2014. Global ecofloristic zones mapped by the United Nations Food and Agricultural Organization. *In:* RUESCH, A. & GIBBS, H. K. (eds.) 2000 ed.: Data Basin (databasin.org). Service of Conservation Biology Institute.

DAVIS, G. W. & RICHARDSON, D. M. 1995. *Mediterranean-type ecosystems: the function of biodiversity,* Berlin, Springer-Verlag.

DAVIS, J. C. 1986. *Statistical and data analysis in geology,* NewYork, USA, John Wiley and Sons.

DAVIS, O. 2012. Processing and Working with LiDAR Data in ArcGIS:A Practical Guide for Archaeologists. Plas Crug, Aberystwyth, Cymru/Wales, SY23 1NJ: The Royal Commission on the Ancient and Historical Monuments of Wales.

DEBES, C., MERENTITIS, A., HEREMANS, R., HAHN, J., FRANGIADAKIS, N., VAN KASTEREN, T., LIAO, W., BELLENS, R., PIZURICA, A., GAUTAMA, S., PHILIPS, W., PRASAD, S., DU, Q. & PACIFICI, F. 2014. Hyperspectral and LiDAR data fusion: Outcome of the 2013 GRSS Data Fusion Contest. *Selected Topics in Applied Earth Observations and Remote Sensing, IEEE Journal of,* 7**,** 2405-2418.

DEES, M., STRAUB, C., LANGAR, P. & KOCH, B. O., 10, 53-78. 2006. Remote sensing based concepts utilising SPOT 5 and LIDAR for forest habitat mapping and monitoring under the EU Habitat Directive. *In:* LAMB, A., HILL, R., WILSON, D., BLOCK, M., IVIITS, E., DEES, M., HEMPHIL, S. & KOCH, B. (eds.) *ONP 10 Test & Benchmarks report.*

DEMETRIADES-SHAH, T. H., STEVEN, M. D. & CLARK, J. A. 1990. High resolution derivative spectra in remote sensing. *Remote Sensing of Environment,* 33**,** 55-64.

DENNISON, P. E. & ROBERTS, D. A. 2003. The effects of vegetation phenology on endmember selection and species mapping in southern California chaparral. *Remote Sensing of Environment,* 87**,** 295-309.

DEVLIN, R. & BAKER, A. 1971. *Photosynthesis,* New York: Van Nostrand Reinhold.

DIBLEY, G., TURNER, B. & SKIDMORE, A. 1997. Determination of eucalyptus forest landscape characteristics from high-resolution hyperspectral data. *Proceedings of the 4th Joint Conference of the Institute of Foresters of Australia and the New Zealand Institute of Forestry. Canberra, ACT, Australia.* Canberra, ACT, Australia.

DISNEY, M. I., LEWIS, P. E., BOUVET, M., PRIETO-BLANCO, A. & HANCOCK, S. 2009. Quantifying surface reflectivity for spaceborne lidar via two independent methods. *Geoscience and Remote Sensing, IEEE Transactions on,* 47**,** 3262-3271.

DIXON, R. K., BROWN, S., HOUGHTON, R. A., SOLOMON, A. M., TREXLER, M. C. & WISNIEWSKI, J. 1994. Carbon pools and flux of global forest ecosystems. *Science,* 263**,** 185-190.

DONG, J., ZHUANG, D. F., HUANG, Y. H. & FU, J. Y. 2009. Advances in Multi-Sensor Data Fusion: Algorithms and Applications. *Sensors,* 9**,** 7771-7784.

DU, Q. & CHANG, C. I. 2003. Segmented PCA-based compression for hyperspectral image analysis. *Chemical and Biological Standoff Detection,* 5268**,** 274-281.

DU, Q., RAKSUNTORN, N., CAI, S. & MOORHEAD, R. J. 2008. Color display for hyperspectral imagery. *Geoscience and Remote Sensing, IEEE Transactions on,* 46**,** 1858-1866.

DUBAYAH, R., KNOX, R., HOFTON, M., BLAIR, J. B. & DRAKE, J. 2000. Land surface characterization using lidar remote sensing. *Spatial information for land use management***,** 25-38.

DUBAYAH, R. O. & DRAKE, J. B. 2000. Lidar remote sensing for forestry. *Journal of Forestry,* 98**,** 44-46.

EISMANN, M. T. 2012. *Hyperspectral remote sensing,* International Society for Optics and Photonics.

ELACHI, C. & VAN ZYL, J. 2006. *Introduction to the physics and techniques of remote sensing,* New Jersey, John Wiley & Sons.

ELAKSHER, A. F. 2008. Fusion of hyperspectral images and lidar-based dems for coastal mapping. *Optics and Lasers in Engineering,* 46**,** 493-498.

ELHADI, A., MUTANGA, O. & RUGEGE, D. 2009. Multispectral and hyperspectral remote sensing for identification and mapping of wetland vegetation: a review. *Wetlands Ecology and Management,* 18**,** 281-296.

ERDODY, T. L. & MOSKAL, L. M. 2010. Fusion of LiDAR and imagery for estimating forest canopy fuels. *Remote Sensing of Environment,* 114**,** 725-737.

ERICKSON, M. 1914. The Use of the Abney Hand Level. *Forestry Quarterly,* XXII**,** 370-375.

ESRI WHITE PAPER 2011. Lidar Analysis in ArcGIS® 10 for Forestry Applications New York Street, Redlands, CA, USA ESRI.

FADY-WELTERLEN, B. 2005. Is there really more biodiversity in Mediterranean forest ecosystems? *Taxon***,** 905-910.

FANNING, D. W. 2004. *What do BSQ, BIL, and BIP mean, really?* [Online]. Available: http://idlcoyote.com/ip_tips/where3.html [Accessed March, 18 2014].

FAO 2000. Global Eco floristic zones mapped by the United Nations Food and Agricultural Organization. *Credits: FAO, 2000. Adapted by Ruesch, Aaron, Holly K. Gibbs 2008*.

FAO 2001. Global Forest Resources Assessment 2000. *FAO Forestry Paper 140.* Rome, Italy: Food and Agriculture Organization of the United Nations.

FAO 2003. State of the World's Forests. Rome, Italy: Food and Agriculture Organization of the United Nations.

FAO 2010. Global forest resources assessment 2010. Main report. *FAO Forestry Paper 163.* Rome, Italy: Food and Agriculture Organization of the United Nations.

FAOSTAT, F. 2012. *Statistical database* [Online]. Rome, Italy: Food and Agriculture Organization of the United Nations. Available: http://faostat.fao.org/site/377/DesktopDefault.aspx?PageID=377#ancor.

FAUVEL, M., BENEDIKTSSON, J. A., CHANUSSOT, J. & SVEINSSON, J. R. 2008. Spectral and spatial classification of hyperspectral data using SVMs and morphological profiles. *Geoscience and Remote Sensing, IEEE Transactions on,* 46**,** 3804-3814.

FELDE, G. W., ANDERSON, G. P., COOLEY, T. W., MATTHEW, M. W., ADLER-GOLDEN, M. A. & BERK, A. 2003. Analysis of Hyperion data with the FLAASH Atmospheric Correction Algorithm. *Geoscience and Remote Sensing Symposium, Proceedings IGARSS '03.* IEEE

FLOOD, M. 2001. Laser altimetry: From science to commercial lidar mapping. *Photogrammetric Engineering and Remote Sensing,* 67**,** 1209-1217.

FLOOD, M. & GUTELIUS, B. 1997. Commercial implications of topographic terrain mapping using scanning airborne laser radar. *Photogrammetric Engineering and Remote Sensing,* 63**,** 327-332.

FORRESTER, D. I., THEIVEYANATHAN, S., COLLOPY, J. J. & MARCAR, N. E. 2010. Enhanced water use efficiency in a mixed Eucalyptus globulus and Acacia mearnsii plantation. *Forest Ecology and Management,* 259**,** 1761-1770.

FRANK, M., PAN, Z., RABER, B. & LENART, C. 2010. Vegetation management of utility corridors using high-resolution hyperspectral imaging and LIDAR. *Hyperspectral Image and Signal Processing: Evolution in Remote Sensing (WHISPERS), 2010 2nd Workshop on.* Reykjavik, Iceland: IEEE.

FRANKLIN, S. E. 1994. Discrimination of subalpine forest species and canopy density using digital CASI, SPOT PLA, and Landsat TM data. *Photogrammetric Engineering and Remote Sensing,* 60**,** 1233-1241.

FUKUNAGA, K. & HAYES, R. R. 1989. Effects of Sample Size in Classifier Design. *IEEE Transactions on Pattern Analysis and Machine Intelligence,* 11**,** 873-885.

GALIL, B. S. 2000. A sea under siege–alien species in the Mediterranean. *Biological Invasions,* 2**,** 177-186.

GAMBA, P. & CHANUSSOT, J. 2008. Guest editorial: Foreword to the special issue on data fusion. *IEEE Transactions on Geoscience and Remote Sensing,* 46**,** 1283-1288.

GAO, B.-C., HEIDEBRECHT, K. & GOETZ, A. 1996. Atmosphere Removal Program (ATREM) Version 2.0 Users Guide. *Center for the Study of Earth from Space/CIRES, University of Colorado, Boulder, Colorado,* 26**,** 19.

GAO, B.-C., MONTES, M. J., DAVIS, C. O. & GOETZ, A. F. 2009. Atmospheric correction algorithms for hyperspectral remote sensing data of land and ocean. *Remote Sensing of Environment,* 113**,** S17-S24.

GARCÍA, M., RIAÑO, D., CHUVIECO, E., SALAS, J. & DANSON, F. M. 2011. Multispectral and LiDAR data fusion for fuel type mapping using Support Vector Machine and decision rules. *Remote Sensing of Environment,* 115**,** 1369-1379.

GARMIN 2008. Oregon Series owner's manual. Taiwan: Garmin Ltd.

GASSÓ, N., SOL, D., PINO, J., DANA, E. D., LLORET, F., SANZ-ELORZA, M., SOBRINO, E. & VILÀ, M. 2009. Exploring species attributes and site characteristics to assess plant invasions in Spain. *Diversity and Distributions,* 15**,** 50-58.

GHIYAMAT, A., SHAFRI, H. Z. M., AMOUZAD MAHDIRAJI, G., SHARIFF, A. R. M. & MANSOR, S. 2013. Hyperspectral discrimination of tree species with different classifications using single-and multiple-endmember. *International Journal of Applied Earth Observation and Geoinformation,* 23**,** 177-191.

GHOSH, A., FASSNACHT, F. E., JOSHI, P. K. & KOCH, B. 2014. A framework for mapping tree species combining hyperspectral and LiDAR data: Role of selected classifiers and sensor across three spatial scales. *International Journal of Applied Earth Observation and Geoinformation,* 26**,** 49-63.

GILDEMEISTER, H. 2004. *What is a mediterranean climate?* [Online]. Gardening in mediterranean climates worldwide Mediterranean Garden Society. Available: http://www.mediterraneangardensociety.org/climate.html [Accessed 20 2014].

GILMORE, M. S., WILSON, E. H., BARRETT, N., CIVCO, D. L., PRISLOE, S., HURD, J. D. & CHADWICK, C. 2008. Integrating multi-temporal spectral and structural information to map wetland vegetation in a lower Connecticut River tidal marsh. *Remote Sensing of Environment,* 112**,** 4048-4060.

GOETZ, A. F. 2009. Three decades of hyperspectral remote sensing of the Earth: A personal view. *Remote Sensing of Environment,* 113, Supplement 1**,** S5-S16.

GOMES, J. F. P. 2006. Forest Fires in Portugal: How it happened and why it happened. *International Journal of Environmental Studies,* 63**,** 109-119.

GONG, P., PU, R. & R., M. J. 1992. Correlating leaf area index of ponderosa pine with hyperspectral CASI data. *Canadian Journal of Remote Sensing,* 18**,** 275-282.

GONG, P., PU, R. & YU, B. 1997. Conifer species recognition: an exploratory analysis of in situ hyperspectral data. *Remote Sensing of Environment,* 62**,** 189-200.

GOODENOUGH, D. G., BHOGAL, A., CHEN, H. & DYK, A. 2001. Comparison of methods for estimation of Kyoto Protocol products of forests from multitemporal LANDSAT. *Geoscience and Remote Sensing Symposium, IGARSS 2001.* Sydney, NSW: IEEE.

GOODENOUGH, D. G., CHEN, H., DYK, A., HAN, T. & Y., L. J. 2005. Multisensor Data fusion for aboveground carbon estimation. *Proceedings of XXVIIIth General Assembly of the International Union of Radio Science.* New Delhi, India: URSI.

GOODENOUGH, D. G., CHEN, H., DYK, A., HOBART, G. & RICHARDSON, A. 2008. Data fusion study between polarimetric SAR, hyperspectral and lidar data for forest information. *Geoscience and Remote Sensing Symposium, 2008. IGARSS 2008.* 1 ed.: IEEE International.

GOODWIN, N., TURNER, R. & MERTON, R. 2005. Classifying Eucalyptus forests with high spatial and spectral resolution imagery: an investigation of individual species and vegetation communities. *Australian Journal of Botany,* 53**,** 337-345.

GOVENDER, M., CHETTY, K. & BULCOCK, H. 2007. A review of hyperspectral remote sensing and its application in vegetation and water resource studies. *Water SA,* 33**,** 145-152.

GOWARD, S. N., ARVIDSON, T., WILLIAMS, D. L., IRISH, R. & IRONS, J. R. 2009. Moderate spatial resolution optical sensors. *In:* WARNER, T. A., NELLIS, M. D. & FOODY, G. M. (eds.) *The SAGE Handbook of Remote Sensing.* London, UK: SAGE Publications Ltd.

GRAHAM, L. 2012. The LAS 1.4 specification. *Photogrammetric Engineering and Remote Sensing,* 78**,** 93-102.

GREBBY, S., CUNNINGHAM, D., NADEN, J. & TANSEY, K. 2012. Application of airborne LiDAR data and airborne multispectral imagery to structural mapping of the upper section of the Troodos ophiolite, Cyprus. *International Journal of Earth Sciences,* 101**,** 1645-1660.

GRITTI, E., SMITH, B. & SYKES, M. 2006. Vulnerability of Mediterranean Basin ecosystems to climate change and invasion by exotic plant species. *Journal of biogeography,* 33**,** 145-157.

GUANTER, L., ESTELLES, V. & MORENO, J. 2007. Spectral calibration and atmospheric correction of ultra-fine spectral and spatial resolution remote sensing data: Application to CASI-1500 data. *Remote Sensing of Environment,* 109**,** 54-65.

GUPTA, R., VIJAYAN, D. & PRASAD, T. 2001. New hyperspectral vegetation characterization parameters. *Advances in Space Research,* 28**,** 201-206.

GUTIERRES, F., GIL, A., REIS, E., LOB, A., NETO, C., CALADO, H. & COSTA, J. C. 2011. Acacia saligna (Labill.) H. Wendl in the Sesimbra County: invaded habitats and potential distribution modeling. *Journal of Coastal Research***,** 403-407.

HALL, D. L. & MCMULLEN, S. A. 2004. *Mathematical techniques in multisensor data fusion,* Norwood, MA, Artech House.

HALL, R. K., WATKINS, R. L., HEGGEM, D. T., JONES, K. B., KAUFMANN, P. R., MOORE, S. B. & GREGORY, S. J. 2009. Quantifying structural physical habitat attributes using LIDAR and hyperspectral imagery. *Environmental monitoring and assessment,* 159**,** 63-83.

HANSON, H. & LINDH, G. 1993. Coastal erosion: an escalating environmental threat. *Ambio***,** 188-195.

HARVEY, N. R. & PORTER, R. B. 2005. Spectral morphology for feature extraction from multi- and hyper-spectral imagery. *Proceedings of SPIE Algorithms and Technologies for Multispectral, Hyperspectral, and Ultraspectral Imagery XI, 100.* Orlando, Florida, USA International Society for Optics and Photonics.

HE, K. S., ROCCHINI, D., NETELER, M. & NAGENDRA, H. 2011. Benefits of hyperspectral remote sensing for tracking plant invasions. *Diversity and Distributions,* 17**,** 381-392.

HELD, A., TICEHURST, C., LYMBURNER, L. & WILLIAMS, N. 2003. High resolution mapping of tropical mangrove ecosystems using hyperspectral and radar remote sensing. *International Journal of Remote Sensing,* 24**,** 2739-2759.

HESE, S., LUCHT, W., SCHMULLIUS, C., BARNSLEY, M., DUBAYAH, R., KNORR, D., NEUMANN, K., RIEDEL, T. & SCHRÖTER, K. 2005. Global biomass mapping for an improved understanding of the CO2 balance—the Earth observation mission Carbon-3D. *Remote Sensing of Environment*, 94**,** 94-104.

HILL, R., WILSON, A., GEORGE, M. & HINSLEY, S. 2010. Mapping tree species in temperate deciduous woodland using time-series multi-spectral data. *Applied vegetation science,* 13**,** 86-99.

HILL, R. A. & THOMSON, A. G. 2005. Mapping woodland species composition and structure using airborne spectral and LiDAR data. *International Journal of Remote Sensing,* 26**,** 3763-3779.

HOBBS, R. J., RICHARDSON, D. & DAVIS, G. 1995. Mediterranean-type ecosystems: opportunities and constraints for studying the function of biodiversity. *In:*

RICHARDSON, D. M. & DAVIS, G. W. (eds.) *Mediterranean-Type Ecosystems.* New York: Springer-Verlag.

HODGSON, M. E. & BRESNAHAN, P. 2004. Accuracy of Airborne Lidar-Derived Elevation. *Photogrammetric Engineering & Remote Sensing,* 70**,** 331-339.

HODGSON, M. E., JENSEN, J., RABER, G., TULLIS, J., DAVIS, B. A., THOMPSON, G. & SCHUCKMAN, K. 2005. An evaluation of lidar-derived elevation and terrain slope in leaf-off conditions. *Photogrammetric Engineering & Remote Sensing,* 71**,** 817-823.

HOPKINSON, C., CHASMER, L., YOUNG-POW, C. & TREITZ, P. 2004. Assessing forest metrics with a ground-based scanning lidar. *Canadian Journal of Forest Research,* 34**,** 573-583.

HUG, C., KRZYSTEK, P. & FUCHS, W. 2004. Advanced lidar data processing with LasTools. *XXth ISPRS Congress.*

HUGHES, R. F. 1968. On the mean accuracy of statistical pattern recognizers. *IEEE Trans. Information Theory,* IT-14**,** 55-63.

HUNTER, E. L. & POWER, C. H. 2002. An assessment of two classification methods for mapping Thames Estuary intertidal habitats using CASI data. *International Journal of Remote Sensing,* 23**,** 2989–3008.

HYYPPÄ, J., HYYPPÄ, H., LITKEY, P., YU, X., HAGGRÉN, H., RÖNNHOLM, P., PYYSALO, U., PITKÄNEN, J. & MALTAMO, M. 2004. Algorithms and methods of airborne laser-scanning for forest measurements. *International Archives of Photogrammetry, Remote Sensing and Spatial Information Sciences,* 36**,** 82-89.

HYYPPÄ, J., WAGNER, W., HOLLAUS, M. & HYYPPÄ, H. 2009. Airborne laser scanning. *The SAGE Handbook of Remote Sensing. SAGE***,** 199-211.

ICN 2006. Plano Sectorial da Rede Natura 2000. Instituto da Conservacã o de Natureza (ICN), Lisbon.

IPCC 2007. Climate Change 2007. Impacts, Adaptation and Vulnerability. *In:* PARRY, K. L., CANZIANI, O. F., PALUTIKOF, J. P., VAN DER LINDEN, P. J. & HANSON, C. E. (eds.) *Contribution of Working Group II to the Fourth Assessment Report of the Intergovernmental Panel on Climate Change.* Cambridge, UK: Cambridge University Press.

IRONS, J. R., RANSON, K., WILLIAMS, D. L., IRISH, R. R. & HUEGEL, F. G. 1991. An off-nadir-pointing imaging spectroradiometer for terrestrial ecosystem studies. *Geoscience and Remote Sensing, IEEE Transactions on,* 29**,** 66-74.

ISENBURG, M. & SCHEWCHUCK, J. 2007. *LAStools: converting, viewing, and compressing LIDAR data in LAS format* [Online]. Available: www.cs.unc.edu/~isenburg/lastools/ [Accessed April 12, 2013.

ISIK, K., YALTIRIK, E. & AKESEN, A. 1997. The interrelationship of forests, biological diversity and the maintenance of natural resources. *Unasylva-190-191 Eleventh World Forestry Congress,* 48**,** 19-29.

JACQUEMOUD, S. & BARET, F. 1990. PROSPECT: A model of leaf optical properties spectra. *Remote sensing of environment,* 34**,** 75-91.

JENSEN, J. R. 2000. *Remote sensing of the environment an earth resource perspective,* New Jersey, Prentice Hall.

JIA, X. & RICHARDS, J. A. 1999. Segmented principal components transformation for efficient hyperspectral remote-sensing image display and classification. *Geoscience and Remote Sensing, IEEE Transactions on,* 37**,** 538-542.

JONES, T. G., COOPS, N. C. & SHARMA, T. 2010. Assessing the utility of airborne hyperspectral and LiDAR data for species distribution mapping in the coastal Pacific Northwest, Canada. *Remote Sensing of Environment,* 114**,** 2841-2852.

JUSOFF, K. 2009. Land Use and Cover Mapping with Airborne Hyperspectral Imager in Setiu, Malaysia. *Journal of Agricultural Science,* 1**,** 120-131.

KAASALAINEN, S., SUOMALAINEN, J., HAKALA, T., CHEN, Y., RÄIKKÖNEN, E., PUTTONEN, E. & KAARTINEN, H. 2010. Active hyperspectral LIDAR methods for object classification. *Hyperspectral Image and Signal Processing: Evolution in Remote Sensing (WHISPERS), 2010 2nd Workshop on.* Reykjavik, Iceland: IEEE.

KAEWPIJIT, S., MOIGNE, J. L. & T. EL-GHAZAWI, T. 2003. Automatic reduction of hyperspectral imagery using wavelet spectral analysis. *IEEE Transactions on Geoscience and Remote Sensing,* 41**,** 863-871.

KARATHANASSI, V., KOLOKOUSIS, P. & IOANNIDOU, S. 2007. A comparison study on fusion methods using evaluation indicators. *International Journal of Remote Sensing,* 28**,** 2309-2341.

KE, Y. H., QUACKENBUSH, L. J. & IM, J. 2010. Synergistic use of QuickBird multispectral imagery and LIDAR data for object-based forest species classification. *Remote Sensing of Environment,* 114**,** 1141-1154.

KEMPENEERS, P., DERONDE, B., PROVOOST, S. & HOUTHUYS, R. 2009. Synergy of Airborne Digital Camera and Lidar Data to Map Coastal Dune Vegetation. *Journal of Coastal Research,* 25**,** 73-82.

KEUFFEL, W. L. 1942. Clinometer. *US Patent 2285285*.

KIM, M., PARK, J. Y. & TUELL, G. 2010. A constrained optimization technique for estimating environmental parameters from CZMIL hyperspectral and lidar data. *In:* SHEN, S. S. & PAUL E. LEWIS, P. E. (eds.) *SPIE defense, security, and sensing.* Orlando, Florida International Society for Optics and Photonics.

KIRBY, R. P. 1995. Remote-Sensing and Image Interpretation, 3rd Edition - Lillesand,Tm, Kiefer,Rw. *International Journal of Geographical Information Systems,* 9**,** 345-348.

KOCH, B. 2010. Status and future of laser scanning, synthetic aperture radar and hyperspectral remote sensing data for forest biomass assessment. *Isprs Journal of Photogrammetry and Remote Sensing,* 65**,** 581-590.

KOETZ, B., MORSDORF, F., VAN DER LINDEN, S., CURT, T. & ALLGÖWER, B. 2008. Multi-source land cover classification for forest fire management based on imaging spectrometry and LiDAR data. *Forest Ecology and Management,* 256**,** 263-271.

KOUKOULAS, S. & BLACKBURN, G. A. 2005. Mapping individual tree location, height and species in broadleaved deciduous forest using airborne LIDAR and multi spectral remotely sensed data. *International Journal of Remote Sensing,* 26**,** 431-455.

KOULAS, C. E. 2009. Extracting wildfire characteristics using hyperspectral, LiDAR and thermal IR remote sensing systems. *SPIE Defense, Security, and Sensing.* Orlando, Florida, USA: International Society for Optics and Photonics.

KRAMER, K., LEINONEN, I. & LOUSTAU, D. 2000. The importance of phenology for the evaluation of impact of climate change on growth of boreal, temperate and Mediterranean forests ecosystems: an overview. *International Journal of Biometeorology,* 44**,** 67-75.

KRAUS, K. & PFEIFER, N. 1998. Determination of terrain models in wooded areas with airborne laser scanner data. *Isprs Journal of Photogrammetry and Remote Sensing,* 53**,** 193-203.

KRUSE, F. 2004. Comparison of ATREM, ACORN, and FLAASH atmospheric corrections using low-altitude AVIRIS data of Boulder, CO. *13th JPL Airborne Geoscience Workshop.* Pasadena, CA: Jet Propulsion Laboratory.

KRUSE, F. A., LEFKOFF, A. B., BOARDMAN, J. W., HEIDEBRECHT, K. B., SHAPIRO, A. T., BARLOON, P. J. & GOETZ, A. F. H. 1993. The Spectral Image-Processing System (Sips) - Interactive Visualization and Analysis of Imaging Spectrometer Data. *Remote Sensing of Environment,* 44**,** 145-163.

LACH, S. R., KEREKES, J. P. & FAN, X. 2009. Fusion of multiple image types for the creation of radiometrically-accurate synthetic scenes. *Journal of Applied Remote Sensing,* 3**,** 033501-033501.

LANDGREBE, D. A. 1999a. Information extraction principles and methods for multispectral and hyperspectral image data. *Information processing for remote sensing,* 82**,** 3-38.

LANDGREBE, D. A. 1999b. Some fundamentals and methods for hyperspectral image data analysis. *In:* GERALD E. COHN & JOHN C. OWICKI (eds.) *Systems and Technologies for Clinical Diagnostics and Drug Discovery II.* San Jose, CA: International Society for Optics and Photonics.

LANEVE, G., CASTRONUOVO, M. M. & CADAU, E. G. 2006. Continuous Monitoring of Forest Fires in the Mediterranean Area Using MSG. *Geoscience and Remote Sensing, IEEE Transactions on,* 44**,** 2761-2768.

LANGE, H. & SOLBERG, S. 2008. Leaf area index estimation using lidar and forest reflectance modelling of airborne hyperspectral data. *Geoscience and Remote Sensing Symposium, IGARSS 2008.* Boston, MA: IEEE International.

LAU, K. K., BICO, J., TEO, K. B., CHHOWALLA, M., AMARATUNGA, G. A., MILNE, W. I., MCKINLEY, G. H. & GLEASON, K. K. 2003. Superhydrophobic carbon nanotube forests. *Nano Letters,* 3**,** 1701-1705.

LAUER, D. T., MORAIN, S. A. & SALOMONSON, V. V. 1997. The Landsat program: Its origins, evolution, and impacts. *Photogrammetric Engineering and Remote Sensing,* 63**,** 831-838.

LE CUSSAN, J. 1991. Report on the intertidal and adjacent vegetation of the Daintree, Endeavour and Russell/Mulgrave Rivers. Brisbane, Australia: Queensland National Parks and Wildlife Service.

LEE, K.-S., COHEN, W. B., KENNEDY, R. E., MAIERSPERGER, T. K. & GOWER, S. T. 2004. Hyperspectral versus multispectral data for estimating leaf area index in four different biomes. *Remote Sensing of Environment,* 91**,** 508-520.

LEFSKY, M. A., COHEN, W. B., ACKER, S. A., PARKER, G. G., SPIES, T. A. & HARDING, D. 1999. Lidar remote sensing of the canopy structure and biophysical properties of Douglas-fir western hemlock forests. *Remote Sensing of Environment,* 70**,** 339-361.

LEFSKY, M. A., COHEN, W. B., ACKER, S. A., SPIES, T. A., PARKER, G. G. & HARDING, D. 1998. Lidar remote sensing of forest canopy structure and related biophysical parameters at H.J. Andrews Experimental forest, Oregon, USA. *Igarss '98 - 1998 International Geoscience and Remote Sensing Symposium, Proceedings Vols 1-5***,** 1252-1254.

LEFSKY, M. A., COHEN, W. B., PARKER, G. G. & HARDING, D. J. 2002. Lidar Remote Sensing for Ecosystem Studies Lidar, an emerging remote sensing technology that directly measures the three-dimensional distribution of plant canopies, can accurately estimate vegetation structural attributes and should be of particular interest to forest, landscape, and global ecologists. *BioScience,* 52**,** 19-30.

LEFSKY, M. A., HARDING, D. J., KELLER, M., COHEN, W. B., CARABAJAL, C. C., ESPIRITO-SANTO, F. D., HUNTER, M. O. & DE OLIVEIRA, R. 2005. Estimates of forest canopy height and aboveground biomass using ICESat. *Geophysical Research Letters,* 32.

LEWIS, P. & HANCOCK, S. 2007. LiDAR for vegetation applications. *UCL, Gower St, London, UK.*

LI, Y., DEMETRIADES-SHAH, T. H., KANEMASU, J. K., SHULTIS, E. T. & KIRKHAM, M. B. 1993. Use of second derivatives of canopy reflectance for monitoring prairie vegetation over different soil backgrounds. *Remote Sensing of Environment,* 44**,** 81-87.

LIEUTIER, F. & GHAIOULE, D. 2005. *Entomological research in Mediterranean forest ecosystems,* France, Editions Quae.

LILLESAND, T. M., KIEFER, R. W. & CHIPMAN, J. W. 2004. *Remote Sensing and Image Interpretation,* New York, John Wiley & Sons.

LIM, K., TREITZ, P., WULDER, M., ST-ONGE, B. & FLOOD, M. 2003. LiDAR remote sensing of forest structure. *Progress in Physical Geography,* 27**,** 88-106.

LIU, L., PANG, Y., FAN, W., LI, Z. & LI, M. 2011. Fusion of airborne hyperspectral and LiDAR data for tree species classification in the temperate forest of northeast China. *Geoinformatics, 2011 19th International Conference on.* Shanghai China: IEEE.

LU, D., CHEN, Q., WANG, G., MORAN, E., BATISTELLA, M., ZHANG, M., LAURIN, G. V. & SAAH, D. 2012. Aboveground forest biomass estimation with Landsat and lidar data and uncertainty analysis of the estimates *International Journal of Forestry Research***,** 1-16.

LUCAS, R. M., LEE, A. C. & BUNTING, P. J. 2008. Retrieving forest biomass through integration of CASI and LiDAR data. *International Journal of Remote Sensing,* 29**,** 1553-1577.

LUO, J., YING, K. & BAI, J. 2005a. Savitzky–Golay smoothing and differentiation filter for even number data. *Signal Processing,* 85**,** 1429-1434.

LUO, J., YING, K., HE, P. & BAI, J. 2005b. Properties of Savitzky–Golay digital differentiators. *Digital Signal Processing,* 15**,** 122-136.

M'HIRIT, O. 1999. Mediterranean forests: Ecological space and economic and community wealth. *Unasylva -197 Mediterranean Forests,* 50**,** 3-15.

MA, R. 2005. DEM generation and building detection from lidar data. *Photogrammetric Engineering & Remote Sensing,* 71**,** 847-854.

MA, W., GONG, C., HU, Y., MENG, P. & XU, F. 2013. The Hughes phenomenon in hyperspectral classification based on the ground spectrum of grasslands in the region around Qinghai Lake. *In:* LIFU, Z. & YANG, J. (eds.) *ISPDI 2013-Fifth International Symposium on Photoelectronic Detection and Imaging.* Beijing, China: International Society for Optics and Photonics.

MA, W. & ZHANG, L. 2011. Bands Selection to Invert Remote Sensing Model for Retrieving the Leaf Biochemical Components. *Journal of Geomatics Science and Technology,* 28**,** 209-212.

MAKISARA, K., MEINANDER, M., RANTASUO, M., OKKONEN, J., AIKIO, M. & SIPOLA, K. 1993. Airborne imaging spectrometer for applications (AISA). *Geoscience and Remote Sensing Symposium, IGARSS'93. Better Understanding of Earth Environment., International.* Tokyo, Japan: IEEE.

MALLET, Y., COOMANS, D. & DE VEL, O. 1996. Recent Developments in Discriminant Analysis on High Dimensional Spectral Data. *Journal of Chemometrics and Intelligent Laboratory Systems,* 11**,** 157-173.

MALLET, Y., COOMANS, D., KAUTSKY, J. & DE VEL, O. 1997. Classification using adaptive wavelets for feature extraction. *Pattern Analysis and Machine Intelligence, IEEE Transactions on,* 19**,** 1058-1066.

MALTAMO, M., MALINEN, J., PACKALN, P., SUVANTO, A. & KANGAS, J. 2006. Nonparametric estimation of stem volume using airborne laser scanning, aerial photography, and stand-register data. *Canadian Journal of Forest Research-Revue Canadienne De Recherche Forestiere,* 36**,** 426-436.

MANOLAKIS, D., MARDEN, D. & SHAW, G. A. 2003. Hyperspectral image processing for automatic target detection applications. *Lincoln Laboratory Journal,* 14**,** 79-116.

MARCHANTE, H., MARCHANTE, E. & FREITAS, H. 2003. Invasion of the Portuguese dune ecosystems by the exotic species Acacia longifolia (Andrews) Willd.: effects at the community level. *Plant Invasions: Ecological Threats and Management Solutions. Leiden, The Netherlands: Backhuys***,** 75-85.

MCCOY, R. M. 2005. Field spectroscopy. *Field methods in remote sensing.* New York: Guilford Press.

MARTIN, M. E., NEWMAN, S. D., ABER, J. D. & CONGALTON, R. G. 1998. Determining forest species composition using high spectral resolution remote sensing data. *Remote Sensing of Environment,* 65**,** 249-254.

MATHWORKS. 1994. *Savitzky-Golay filtering* [Online]. United Kingdom: MathWorks, Inc. Available: http://uk.mathworks.com/help/signal/ref/sgolayfilt.html#zmw57dd0e103588.

MATTHEW, M. W., ADLER-GOLDEN, S. M., BERK, A., FELDE, G., ANDERSON, G. P., GORODETZKY, D., PASWATERS, S. & SHIPPERT, M. 2002. Atmospheric correction of spectral imagery: evaluation of the FLAASH algorithm with AVIRIS data. *Applied Imagery Pattern Recognition Workshop, 2002. Proceedings. 31st.* IEEE.

MAUNE, D. F. 2001. Digital elevation model technologies and applications: the DEM users manual. 5th ed. Bethesda: ASPRS Publications.

MAUSEL, P. W., KRAMER, H. J. & LEE, J. K. 1990. Optimum band selection for supervised classification of multispectral data. *Photogrammetric Engineering and Remote Sensing,* 56**,** 55-60.

MCGLONE, J. C. 2004. Manual of photogrammetry. 5th ed. Bethesda: ASPRS.

MENG, X. L., WANG, L. & CURRIT, N. 2009. Morphology-based Building Detection from Airborne Lidar Data. *Photogrammetric Engineering and Remote Sensing,* 75**,** 437-442.

MERLO, M. & ROJAS, B. E. 2000. Public goods and externalities linked to Mediterranean forests: economic nature and policy. *Land Use Policy,* 17**,** 197-208.

MIAO, X., GONG, P., PU, R., CARRUTHERS, R. I. & HEATON, J. S. 2007. Applying Class-based feature extraction approaches for supervised classification of hyperspectral imagery. *Canadian Journal of Remote Sensing,* 33**,** 162-175.

MILLER, C. J. 2001. Fusion of high resolution LIDAR elevation data with hyperspectral data to characterize tree canopies. *Proc. SPIE 4381, Algorithms for Multispectral, Hyperspectral, and Ultraspectral Imagery VII.* Orlando, FL: International Society for Optics and Photonics.

MILLER, C. J. 2002. Performance assessment of ACORN atmospheric correction algorithm. *AeroSense 2002.* International Society for Optics and Photonics.

MILLER, S. B. 2004. Photogrammetric products. *In:* MCGLONE, J. C. (ed.) *ASPRS Manual of Photogrammetry.* Bethesda: ASPRS.

MILLETTE, T. L., ARGOW, B. A., MARCANO, E., HAYWARD, C., HOPKINSON, C. S. & VALENTINE, V. 2010. Salt Marsh Geomorphological Analyses via Integration of Multitemporal Multispectral Remote Sensing with LIDAR and GIS. *Journal of Coastal Research,* 26**,** 809-816.

MÖCKEL, T., DALMAYNE, J., PRENTICE, H. C., EKLUNDH, L., PURSCHKE, O., SCHMIDTLEIN, S. & HALL, K. 2014. Classification of grassland successional stages using airborne hyperspectral imagery. *Remote Sensing,* 6**,** 7732-7761.

MOGHADDAM, M., DUNGAN, J. L. & ACKER, S. 2002. Forest variable estimation from fusion of SAR and multispectral optical data. *IEEE Transactions on Geoscience and Remote Sensing,* 40**,** 2176-2187.

MOJARADI, B., ABRISHAMI-MOGHADDAM, H., ZOEJ, M. J. V. & DUIN, R. P. W. 2009. Dimensionality Reduction of Hyperspectral Data via Spectral Feature Extraction. *IEEE Transactions on Geoscience and Remote Sensing,* 47**,** 2091-2105.

MOONEY, H. A. & HOBBS, R. J. 2000. *Invasive species in a changing world,* USA, Island Press.

MUNDF, J. T., STREUTKER, D. R. & GLENN, N. F. 2006. Mapping sagebrush distribution using fusion of hyperspectral and lidar classifications. *Photogrammetric Engineering and Remote Sensing,* 72**,** 47-54.

MUTKE, S., SIEVÄNEN, R., NIKINMAA, E., PERTTUNEN, J. & GIL, L. 2005. Crown architecture of grafted Stone pine (Pinus pinea L.): shoot growth and bud differentiation. *Trees,* 19**,** 15-25.

MYERS, N., MITTERMEIER, R. A., MITTERMEIER, C. G., DA FONSECA, G. A. & KENT, J. 2000. Biodiversity hotspots for conservation priorities. *Nature,* 403**,** 853-858.

MYNENI, R. B., HALL, F. G., SELLERS, P. J. & MARSHAK, A. L. 1995. The Interpretation of Spectral Vegetation Indexes. *IEEE Transactions on Geoscience and Remote Sensing,* 33**,** 481-486.

NÆSSET, E. 1997a. Determination of mean tree height of forest stands using airborne laser scanner data. *ISPRS Journal of Photogrammetry and Remote Sensing,* 52**,** 49-56.

NÆSSET, E. 1997b. Estimating timber volume of forest stands using airborne laser scanner data. *Remote Sensing of Environment,* 61**,** 246-253.

NÆSSET, E. 2002. Predicting forest stand characteristics with airborne scanning laser using a practical two-stage procedure and field data. *Remote Sensing of Environment,* 80**,** 88-99.

NÆSSET, E., BOLLANDSAS, O. M., GOBAKKEN, T., GREGOIRE, T. G. & STAHL, G. 2013a. Model-assisted estimation of change in forest biomass over an 11 year period in a sample survey supported by airborne LiDAR: A case study with post-stratification to provide "activity data". *Remote Sensing of Environment,* 128**,** 299-314.

NÆSSET, E., GOBAKKEN, T., BOLLANDSAS, O. M., GREGOIRE, T. G., NELSON, R. & STAHL, G. 2013b. Comparison of precision of biomass estimates in regional field sample surveys and airborne LiDAR-assisted surveys in Hedmark County, Norway. *Remote Sensing of Environment,* 130**,** 108-120.

NAGENDRA, H. & ROCCHINI, D. 2008. High resolution satellite imagery for tropical biodiversity studies: the devil is in the detail. *Biodiversity and Conservation,* 17**,** 3431-3442.

NAVEH, Z. 1974. Effects of fire in the Mediterranean region. *Fire and ecosystems,* 321**,** 364.

NEIGH, C. S. R., NELSON, R. F., RANSON, K. J., MARGOLIS, H. A., MONTESANO, P. M., SUN, G. Q., KHARUK, V., NAESSET, E., WULDER, M. A. & ANDERSEN, H. E. 2013. Taking stock of circumboreal forest carbon with ground measurements, airborne and spaceborne LiDAR. *Remote Sensing of Environment,* 137**,** 274-287.

NEVILLE, R. A., ROWLANDS, N., MAROIS, R. & POWELL, I. 1995. SFSI: Canada's first airborne SWIR imaging spectrometer. *Canadian Journal of Remote Sensing,* 21**,** 328-336.

NIEMANN, K. O. 1995. Remote sensing of forest stand age using airborne spectrometer data. *Photogrammetric Engineering and Remote Sensing,* 61**,** 1119-1127.

NIEMANN, K. O., FRASER, G., GOODENOUGH, D. & LOOS, R. 2005. Integration of LiDAR-based metrics with AVIRIS hyperspectral data: An exploration of the effects of canopy structure on canopy reflectance. *26th Canadian Symposium on Remote Sensing* Wolfville, Nova Scotia, Canada: IEEE.

NIEMANN, K. O., FRAZER, G., LOOS, R., VISINTINI, F. & STEPHEN, R. 2007. Integration of first and last return LiDAR with hyperspectral data to characterize forested environments. *Geoscience and Remote Sensing Symposium, IGARSS 2007.* IEEE International.

NISHII, R., KUSANOBU, S. & NAKAOKA, N. 1997. Hughes phenomenon in the spatial resolution enhancement of low resolution images and derivation of selection rule for high resolution images. *Geoscience and Remote Sensing, 1997. IGARSS '97. Remote Sensing - A Scientific Vision for Sustainable Development., 1997 IEEE International.*

NOAA 2012. Tutorial: Working with Lidar in ArcGIS 10 NOAA Coastal Services Center.

NOAA. 2014. *What is LIDAR?* [Online]. United States Department of Commerce. Available: http://oceanservice.noaa.gov/facts/lidar.html [Accessed 03 July 2014 2014].

NOAA COASTAL SERVICES CENTER. 2012. *Lidar 101: An Introduction to Lidar Technology, Data, and Applications* [Online]. Charleston, SC. Available: http://coast.noaa.gov/digitalcoast/_/pdf/lidar101.pdf [Accessed July 21 2013].

O'HARA, S. 1994. *Characteristics of mediterranean climates* [Online]. The Mediterranean Garden Society Available: http://gimcw.org/climate/characteristics.cfm [Accessed 20 2014].

OLIVEIRA, G., CORREIA, O., MARTINS-LOUÇÃO, M. & CATARINO, F. 1994. Phenological and growth patterns of the Mediterranean oak Quercus suber L. *Trees,* 9**,** 41-46.

OLSON, D. M. & DINERSTEIN, E. 1998. The Global 200: a representation approach to conserving the Earth's most biologically valuable ecoregions. *Conservation Biology,* 12**,** 502-515.

OLSON, D. M., DINERSTEIN, E., WIKRAMANAYAKE, E. D., BURGESS, N. D., POWELL, G. V. N., UNDERWOOD, E. C., D'AMICO, J. A., ITOUA, I., STRAND, H. E., MORRISON, J. C., LOUCKS, C. J., ALLNUTT, T. F., RICKETTS, T. H., KURA, Y., LAMOREUX, J. F., WETTENGEL, W. W., HEDAO, P. & KASSEM, K. R. 2001. Terrestrial ecoregions of the world: a new map of life on Earth. *Bioscience,* 51**,** 933-938.

ONOJEGHUO, A. O. & BLACKBURN, G. A. 2011. Optimising the use of hyperspectral and LiDAR data for mapping reedbed habitats. *Remote Sensing of Environment,* 115**,** 2025-2034.

ORFANIDIS, S. J. 1996. *Introduction to signal processing,* Englewood Cliffs, NJ, Prentice-Hall, Inc.

ØRKA, H., NÆSSET, E. & BOLLANDSÅS, O. 2007. Utilizing airborne laser intensity for tree species classification. *International Archives of the Photogrammetry, Remote Sensing and Spatial Information Sciences,* 36**,** 300-304.

ORTENBERG, F. 2011. Hyperspectral sensor characteristics: airborne, Space borne, hand-held and truck-mounted; integration of hyperspectral data with LiDAR. *In:* THENKABAIL, P. S., LYON, J. G. & HUETE, A. (eds.) *Hyperspectral Remote Sensing of Vegetation.* Boca Raton, FL: CRC press, Taylor and Francis group.

PAAP, A., ASKRABA, S., ALAMEH, K. & ROWE, J. 2008. Photonic-based spectral reflectance sensor for ground-based plant detection and weed discrimination. *Opt Express,* 16**,** 1051-5.

PACKHAM, J., HARDING, D., HILTON, G. & STUTTARD, R. 2004. *Functional ecology of woodlands and forests,* Dordrecht, Netherlands, Kluwer academic publishers.

PAGLIANI, M. 2001. *The unveiled wealth of the Mediterranean forests* [Online]. Rome, Italy: World Wide Fund for Nature. Available: assets.panda.org/downloads/brochure_english.pdf [Accessed August 19 2014].

PAL, M. & FOODY, G. M. 2010. Feature selection for classification of hyperspectral data by SVM. *Geoscience and Remote Sensing, IEEE Transactions on,* 48**,** 2297-2307.

PALAHI, M., MAVSAR, R., GRACIA, C. & BIROT, Y. 2008. Mediterranean forests under focus. *International Forestry Review,* 10**,** 676-688.

PALMASON, J. A., BENEDIKTSSON, J. A. & ARNASON, K. 2003. Morphological transformations and feature extraction for urban data with high spectral and spatial resolution. *Geoscience and Remote Sensing Symposium, 2003. IGARSS'03. Proceedings.* Toulouse, France: IEEE International.

PANDEY, P. C., TATE, N. & BALZTER, H. 2014. Mapping Tree Species in Coastal Portugal using Statistically Segmented Principal Component Analysis and Other Methods. *Sensors Journal, IEEE,* 14**,** 4434-4441.

PANG, Y., TAN, B., SOLBERG, S. & LI, Z. 2009. Forest LAI estimation comparison using LiDAR and hyperspectral data in boreal and temperate forests. *In:* GAO, W. & JACKSON, T. J. (eds.) *SPIE Optical Engineering+ Applications.* International Society for Optics and Photonics.

PATENAUDE, G., MILNE, R., VAN OIJEN, M., ROWLAND, C. S. & HILL, R. A. 2008. Integrating remote sensing datasets into ecological modelling: A Bayesian approach. *International Journal of Remote Sensing,* 29**,** 1295-1315.

PE'ERI, S., MORRISON, J. R., SHORT, F., MATHIESON, A., BROOK, A. & TROWBRIDGE, P. 2008. Microalgae and eelgrass mapping in Great Bay Estuary using AISA hyperspectral imagery. New Hampshire: US. Environmental Protection Agency

PEARLMAN, J. S., BARRY, P. S., SEGAL, C. C., SHEPANSKI, J., BEISO, D. & CARMAN, S. L. 2003. Hyperion, a space-based imaging spectrometer. *Ieee Transactions on Geoscience and Remote Sensing,* 41**,** 1160-1173.

PEDERGNANA, M., MARPU, P. R., DALLA MURA, M., BENEDIKTSSON, J. A. & BRUZZONE, L. 2011. Fusion of hyperspectral and lidar data using morphological attribute profiles. *In:* BRUZZONE, L. (ed.) *Image and Signal Processing for Remote Sensing XVII.* Prague, Czech Republic: International Society for Optics and Photonics

PEÑA, M. A., CRUZ, P. & ROIG, M. 2013. The effect of spectral and spatial degradation of hyperspectral imagery for the Sclerophyll tree species classification. *International Journal of Remote Sensing,* 34**,** 7113-7130.

PESARESI, M. & BENEDIKTSSON, J. A. 2001. A new approach for the morphological segmentation of high resolution satellite imagery. *IEEE Transactions on Geoscience and Remote Sensing,* 39**,** 309–320.

PETROPOULOS, G. P., ARVANITIS, K. & SIGRIMIS, N. 2012. Hyperion hyperspectral imagery analysis combined with machine learning classifiers for land use/cover mapping. *Expert Systems with Applications,* 39**,** 3800-3809.

PLAZA, A., MARTÍNEZ, P., PÉREZ, R. & PLAZA, J. 2002. Spatial/spectral endmemebr extraction by multidimensional morphological operations. *Transactions on Geoscience and Remote Sensing,* 40**,** 2025-2041.

PLAZA, A., MARTÍNEZ, P., PLAZA, J. & PÉREZ, R. 2005. Dimensionality reduction and classification of hyperspectral image data using sequences of extended morphological transformations. *Geoscience and Remote Sensing, IEEE Transactions on,* 43**,** 466-479.

PLOURDE, L. C., OLLINGER, S. V., SMITH, M. L. & MARTIN, M. E. 2007. Estimating species abundance in a northern temperate forest using spectral mixture analysis. *Photogrammetric Engineering and Remote Sensing,* 73**,** 829-840.

POHL, C. & VAN GENDEREN, J. L. 1998. Multisensor image fusion in remote sensing: concepts, methods and applications. *International Journal of Remote Sensing,* 19**,** 823-854.

POPESCU, S. C., WYNNE, R. H. & NELSON, R. F. 2003. Measuring individual tree crown diameter with lidar and assessing its influence on estimating forest volume and biomass. *Canadian Journal of Remote Sensing,* 29**,** 564-577.

PORTER, W. M. & ENMARK, H. T. 1987. A system overview of the airborne visible/infrared imaging spectrometer (AVIRIS). *In:* GREGG, V. (ed.) *Proceedings, Society of Photo-Optical Instrumentation Engineers (SPIE) Imaging Spectroscopy II.* San Diego, CA: International Society for Optics and Photonics.

PRESS, W. H., TEUKOLSKY, S. A., VETTERLING, W. T. & FLANNERY, B. P. 1996. *Numerical recipes in C,* Cambridge, UK, Cambridge University Press.

PRICE, J. C. 1994. How Unique Are Spectral Signatures. *Remote Sensing of Environment,* 49**,** 181-186.

PU, R. 2009. Broadleaf species recognition with in situ hyperspectral data. *International Journal of Remote Sensing,* 30**,** 2759-2779.

PU, R. & GONG, P. 2000. *Hyperspectral Remote Sensing and its Applications,* Beijing, China, Higher Education Press.

PUTTONEN, E., SUOMALAINEN, J., HAKALA, T., RÄIKKÖNEN, E., KAARTINEN, H., KAASALAINEN, S. & LITKEY, P. 2010. Tree species classification from fused active hyperspectral reflectance and LIDAR measurements. *Forest Ecology and Management,* 260**,** 1843-1852.

QU, Z., GOETZ, A. F. & HEIDEBRECHT, K. B. 2001. High-accuracy atmosphere correction for hyperspectral data (HATCH). *Proceedings of the Ninth JPL Airborne Earth Sceince Workshop.*

QU, Z., KINDEL, B. C. & GOETZ, A. F. 2003. The high accuracy atmospheric correction for hyperspectral data (HATCH) model. *Geoscience and Remote Sensing, IEEE Transactions on,* 41**,** 1223-1231.

RABER, G. T., JENSEN, J. R., SCHILL, S. R. & SCHUCKMAN, K. 2002. Creation of digital terrain models using an adaptive lidar vegetation point removal process. *Photogrammetric Engineering and Remote Sensing,* 68**,** 1307-1314.

RANSON, K. J., IRONS, J. R. & WILLIAMS, D. L. 1994. Multispectral bidirectional reflectance of northern forest canopies with the Advanced Solid-State Array Spectroradiometer (ASAS). *Remote Sensing of Environment,* 47**,** 276-289.

RASCHER, K. G., GROßE-STOLTENBERG, A., MÁGUAS, C., MEIRA-NETO, J. A. A. & WERNER, C. 2011a. Acacia longifolia invasion impacts vegetation structure and regeneration dynamics in open dunes and pine forests. *Biological Invasions,* 13**,** 1099-1113.

RASCHER, K. G., GROßE-STOLTENBERG, A., MÁGUAS, C. & WERNER, C. 2011b. Understory invasion by Acacia longifolia alters the water balance and carbon gain of a Mediterranean pine forest. *Ecosystems,* 14**,** 904-919.

READ, J. M. & TORRADO, M. 2009. Remote Sensing. *In:* ROB, K. & NIGEL, T. (eds.) *International Encyclopedia of Human Geography.* Oxford: Elsevier.

REES, G. & REES, W. G. 2012. *Physical principles of remote sensing,* Cambridge, UK, Cambridge University Press.

RESEARCH SYSTEMS INC 1999. ENVI users guide and tutorials.

RESEARCH SYSTEMS INC 2009. Atmospheric Correction Module: QUAC and FLAASH user's guide. *In:* TUTORIALS., E. U. G. A. (ed.).

RICHARDS, J. A. & JIA, X. 1999. *Remote Sensing Digital Image Analysis-An introduction,* Berlin, Germany, Springer-Verlag.

RICHTER, R. 1997. Correction of atmospheric and topographic effects for high spatial resolution satellite imagery. *International Journal of Remote Sensing,* 18**,** 1099-1111.

RICHTER, R. 1998. Correction of satellite imagery over mountainous terrain. *Applied Optics* 37**,** 4004-4015.

RICHTER, R. 2004. ATCOR: Atmospheric and Topographic Correction. *DLR-German Aerospace Center. Remote Sensing Data Center*.

RICHTER, R. & SCHLÄPFER, D. 2002. Geo-atmospheric processing of airborne imaging spectrometry data. Part 2: atmospheric/topographic correction. *International Journal of Remote Sensing,* 23**,** 2631-2649.

RODRÍGUEZ-ECHEVERRÍA, S., CRISÓSTOMO, J. A., NABAIS, C. & FREITAS, H. 2009. Belowground mutualists and the invasive ability of Acacia longifolia in coastal dunes of Portugal. *Biological Invasions,* 11**,** 651-661.

ROSENQVIST, A., SHIMADA, M., CHAPMAN, B., FREEMAN, A., DE GRANDI, G., SAATCHI, S. & RAUSTE, Y. 2000. The global rain forest mapping project-a review. *International Journal of Remote Sensing,* 21**,** 1375-1387.

ROSSO, P. H., USTIN, S. L. & HASTINGS, A. 2005. Mapping marshland vegetation of San Francisco Bay, California, using hyperspectral data. *International Journal of Remote Sensing,* 26**,** 5169-5191.

ROTTENSTEINER, F., TRINDER, J., CLODE, S. & KUBIK, K. 2007. Building detection by fusion of airborne laser scanner data and multi-spectral images: Performance evaluation and sensitivity analysis. *Isprs Journal of Photogrammetry and Remote Sensing,* 62**,** 135-149.

SALEHI, B., ZOEJ, M. J. V. & VARSHOSAZ, M. 2008. Projection Pursuit and Lowpass Filtering for Preprocessing of Hypespectral Images. *World Applied Sciences Journal,* 3**,** 785-796.

SARHAN, A. M. 2013. Wavelet-based Feature Extraction for DNA Microarray Classification. *Artificial Intelligence Review,* 39**,** 237-249.

SARRAZIN, D., VAN AARDT, J., ASNER, G. P., MCGLINCHY, J., MESSINGER, D. W. & WU, J. 2010. Fusing waveform LIDAR and hyperspectral data for species-level structural assessment in savanna ecosystems. *In:* TURNER, M. D. & KAMERMAN, G. W. (eds.) *SPIE Defense, Security, and Sensing.* International Society for Optics and Photonics.

SCARASCIA-MUGNOZZA, G. & MATTEUCCI, G. 2012. Mediterranean forest research: challenges and opportunities in a changing environment. *Energia, Ambiente e Innovazione,* N.1 /2012.**,** 58-65.

SCARASCIA-MUGNOZZA, G., OSWALD, H., PIUSSI, P. & RADOGLOU, K. 2000. Forests of the Mediterranean region: gaps in knowledge and research needs. *Forest Ecology and Management,* 132**,** 97-109.

SCHMIDT, K. A., HADLEY, B. C. & WIJEKOON, N. 2011. Vertical Accuracy and Use of Topographic LiDAR Data in Coastal Marshes. *Journal of Coastal Research,* 27**,** 116-132.

SCHOTT, J. R. 2007. *Remote sensing,* Oxford, UK, Oxford University Press.

SCOTT, D. W. 1992. The curse of dimensionality and dimension reduction. *Multivariate Density Estimation: Theory, Practice, and Visualization.* New York: Wiley.

SHAFRI, H. Z. M., SUHAILI, A. & MANSOR, S. 2007. The Performance of Maximum Likelihood, Spectral Angle Mapper, Neural Network and Decision Tree Classifiers in Hyperspectral Image Analysis. *Journal of Computer Science,* 3**,** 419-423.

SHAHSHAHANI, B. M. & LANDGREBE, D. A. 1994. The effect of unlabeled samples in reducing the small sample size problem and mitigating the Hughes phenomenon. *Geoscience and Remote Sensing, IEEE Transactions on,* 32**,** 1087-1095.

SHAPIRO, J. & GOOD, S. 2010. Rural Mapping Techniques Using Low to No Technology.

SHEN, S. S. 1990. Summary of types of data fusion methods utilized in workshop papers. *Proceedings of the Workshop on Multisource Data Integration in Remote Sensing.* Greenbelt, MD: NASA Conference Publication 3099.

SHIPPERT, P. 2004. Why use hyperspectral imagery? *Photogrammetric engineering and remote sensing,* 70**,** 377-396.

SKIDMORE, A. K. 2002. Accuracy assessment of spatial information. *In:* STEIN, A., VAN DER MEER, F. & GORTE, B. (eds.) *Spatial statistics for remote sensing.* Netherlands: Springer.

SMITH, K., STEVEN, M. & COLLS, J. 2004. Use of hyperspectral derivative ratios in the red-edge region to identify plant stress responses to gas leaks. *Remote Sensing of Environment,* 92**,** 207-217.

SOHN, G. & DOWMAN, I. 2007. Data fusion of high-resolution satellite imagery and LiDAR data for automatic building extraction. *Isprs Journal of Photogrammetry and Remote Sensing,* 62**,** 43-63.

SONG, C. & WOODCOCK, C. E. 2002. The spatial manifestation of forest succession in optical imagery: the potential of multiresolution imagery. *Remote Sensing of Environment,* 82**,** 271-284.

SONG, C., WOODCOCK, C. E. & LI, X. 2002. The spectral/temporal manifestation of forest succession in optical imagery: The potential of multitemporal imagery. *Remote Sensing of Environment,* 82**,** 285-302.

SPANO, D., SNYDER, R. & CESARACCIO, C. 2013. Mediterranean Phenology. *In:* SCHWARTZ, M. D. (ed.) *Phenology: An Integrative Environmental Science.* Springer Netherlands.

SPECHT, R. L. (ed.) 1988. *Mediterranean-type ecosystems,* Netherlands: Springer Verlag.

SPECIM 2012. AISA Hawk hyperspectral sensor datasheet. Oulu, Finland: Spectral Imaging Limited.

SPECIM 2013. AISA Eagle hyperspectral sensor datasheet. Oulu, Finland: Spectral Imaging Limited.

STANLEY, W. F. R. 1901. *Surveying and levelling instruments,* E. & FN Spon.

STEHMAN, S., FOODY, G., WARNER, T. & NELLIS, M. 2009. *The SAGE handbook of remote sensing,* New York, Sage Publications.

STERN, A., YITZHAK, A., FARBER, V., OIKNINE, Y. & RIVENSON, Y. 2013. Hyperspectral Compressive Imaging. *12th Workshop on Information Optics (WIO), 2013* Tenerife, Spain: The Institute of Electrical and Electronics Engineers.

STORY, M. & CONGALTON, R. G. 1986. Accuracy assessment-A user's perspective. *Photogrammetric Engineering and Remote Sensing,* 52**,** 397-399.

STRAUB, C., DEES, M., WEINACKER, H. & KOCH, B. 2009. Using Airborne Laser Scanner Data and CIR Orthophotos to Estimate the Stem Volume of Forest Stands. *Photogrammetrie Fernerkundung Geoinformation***,** 277-287.

STREUTKER, D. R. & GLENN, N. F. 2006. LiDAR measurement of sagebrush steppe vegetation heights. *Remote Sensing of Environment,* 102**,** 135-145.

SUGUMARAN, R. & VOSS, M. 2007. Object-oriented classification of LIDAR-fused hyperspectral imagery for tree species identification in an Urban environment. *Urban Remote Sensing Joint Event, 2007.* Paris, France: IEEE.

SUN, G., RANSON, K. J., GUO, Z., ZHANG, Z., MONTESANO, P. & KIMES, D. 2011. Forest biomass mapping from lidar and radar synergies. *Remote Sensing of Environment,* 115**,** 2906-2916.

SUNDSETH, K. 2009. Natura 2000 in the Mediterranean Region, European Commission. Luxembourg, Belgium: Publications Office of the European Union

SWATANTRAN, A., DUBAYAH, R., ROBERTS, D., HOFTON, M. & BLAIR, J. B. 2011. Mapping biomass and stress in the Sierra Nevada using lidar and hyperspectral data fusion. *Remote Sensing of Environment,* 115**,** 2917-2930.

SWIFT, D. J. 1968. Coastal erosion and transgressive stratigraphy. *The Journal of Geology***,** 444-456.

TATE, N. J., BRUNSDON, C., CHARLTON, M., FOTHERINGHAM, A. S. & JARVIS, C. S. 2005. Smoothing/filtering LiDAR digital surface models. Experiments with loess regression and discrete wavelets. *Journal of Geographical Systems,* 7**,** 273-290.

THENKABAIL, P. S. 2012. Hyperspectral Remote Sensing of Vegetation: Knowledge Gain and Knowledge Gap After 40 years of Research. *Landsat Science Team Meeting.* Sioux Falls, SD, USA: USGS EROS Data Center.

THENKABAIL, P. S. & HUETE, A. R. 2012. Hyperspectral Remote Sensing of Vegetation: Knowledge Gain and Knowledge Gap after 40 years of research. *AGU Fall Meeting Abstracts.* San Francisco: American Geophysical Union.

THENKABAIL, P. S., LYON, J. G. & HUETE, A. 2011. Advances in Hyperspectral remote sensing of vegetation and agricultural croplands. *In:* THENKABAIL, P. S., LYON, J. G. & HUETE, A. (eds.) *Hyperspectral Remote Sensing of Vegetation.* Boca Raton, FL: CRC Press, Taylor and Francis Group.

THIRGOOD, J. 1981. *Man and the Mediterranean forest,* Canada, Academic Press.

THOMAS, V., FINCH, D. A., MCCAUGHEY, J. H., NOLAND, T., RICH, L. & TREITZ, P. 2006. Spatial modelling of the fraction of photosynthetically active radiation absorbed by a boreal mixedwood forest using a lidar-hyperspectral approach. *Agricultural and Forest Meteorology,* 140**,** 287-307.

THOMAS, V., MCCAUGHEY, J. H., TREITZ, P., FINCH, D. A., NOLAND, T. & RICH, L. 2009. Spatial modelling of photosynthesis for a boreal mixedwood forest by integrating micrometeorological, lidar and hyperspectral remote sensing data. *Agricultural and Forest Meteorology,* 149**,** 639-654.

THOMAS, V., NOLAND, T., TREITZ, P. & MCCAUGHEY, J. H. 2011. Leaf area and clumping indices for a boreal mixed-wood forest: Lidar, hyperspectral, and Landsat models. *International Journal of Remote Sensing,* 32**,** 8271-8297.

THOMAS, V., TREITZ, P., MCCAUGHEY, J. H., NOLAND, T. & RICH, L. 2008. Canopy chlorophyll concentration estimation using hyperspectral and lidar data for a boreal mixedwood forest in northern Ontario, Canada. *International Journal of Remote Sensing,* 29**,** 1029-1052.

THUILLER, W., RICHARDSON, D. M., PYŠEK, P., MIDGLEY, G. F., HUGHES, G. O. & ROUGET, M. 2005. Niche-based modelling as a tool for predicting the risk of alien plant invasions at a global scale. *Global Change Biology,* 11**,** 2234-2250.

TICKLE, P. K., WITTE, C., LEE, A., LUCAS, R. M., JONES, K. & AUSTIN, J. 2001. Use of airborne scanning lidar and large scale photography within a strategic forest inventory and monitoring framework. *Igarss 2001: Scanning the Present and Resolving the Future, Vols 1-7, Proceedings***,** 1000-1003.

TONOLLI, S., DALPONTE, M., NETELER, M., RODEGHIERO, M., VESCOVO, L. & GIANELLE, D. 2011. Fusion of airborne LiDAR and satellite multispectral data for the estimation of timber volume in the Southern Alps. *Remote Sensing of Environment,* 115**,** 2486-2498.

TREITZ, P. M. & HOWARTH, P. J. 1999. Hyperspectral remote sensing for estimating biophysical parameters of forest ecosystems. *Progress in Physical Geography,* 23**,** 359-390.

TREUHAFT, R. N., ASNER, G. P. & LAW, B. E. 2003. Structure-based forest biomass from fusion of radar and hyperspectral observations. *Geophysical Research Letters,* 30**,** 25(1-4).

TREUHAFT, R. N., CHAPMAN, B. D., DOS SANTOS, J., GONÇALVES, F. G., DUTRA, L. V., GRAÇA, P. & DRAKE, J. B. 2009. Vegetation profiles in tropical forests from multibaseline interferometric synthetic aperture radar, field, and lidar measurements. *Journal of Geophysical Research: Atmospheres (1984–2012),* 114.

TREUHAFT, R. N., LAW, B. E. & ASNER, G. P. 2004. Forest attributes from radar interferometric structure and its fusion with optical remote sensing. *BioScience,* 54**,** 561-571.

TSAGARIS, V., ANASTASSOPOULOS, V. & LAMPROPOULOS, G. A. 2005. Fusion of hyperspectral data using segmented PCT for color representation and classification. *Geoscience and Remote Sensing, IEEE Transactions on,* 43**,** 2365-2375.

TSAI, F., LIN, E. K. & YOSHINO, K. 2007. Spectrally segmented principal component analysis of hyperspectral imagery for mapping invasive plant species. *International Journal of Remote Sensing,* 28**,** 1023-1039.

TSUI, O. W., COOPS, N. C., WULDER, M. A. & MARSHALL, P. L. 2013. Integrating airborne LiDAR and space-borne radar via multivariate kriging to estimate above-ground biomass. *Remote Sensing of Environment,* 139**,** 340-352.

TUCKER, C. J. & GARRATT, M. W. 1977. Leaf optical system modeled as a stochastic process. *Applied Optics,* 16**,** 635-642.

TUELLER, P. T. 1989. Remote-Sensing Technology for Rangeland Management Applications. *Journal of Range Management,* 42**,** 442-453.

TYO, J. S., KONSOLAKIS, A., DIERSEN, D. I. & OLSEN, R. C. 2003. Principal-components-based display strategy for spectral imagery. *Geoscience and Remote Sensing, IEEE Transactions on,* 41**,** 708-718.

USTIN, S. & XIAO, Q. 2001. Mapping successional boreal forests in interior central Alaska. *International Journal of Remote Sensing,* 22**,** 1779-1797.

USTIN, S. L. & GAMON, J. A. 2010. Remote sensing of plant functional types. *New Phytologist,* 186**,** 795-816.

USTIN, S. L., ROBERTS, D. A., GAMON, J. A., ASNER, G. P. & GREEN, R. O. 2004. Using image spectroscopy to study ecosystem processes and properties. *Bioscience,* 54**,** 523-534.

VAN AARDT, J. & WYNNE, R. 2007. Examining pine spectral separability using hyperspectral data from an airborne sensor: An extension of field-based results. *International Journal of Remote Sensing,* 28**,** 431-436.

VAN DER PUTTEN, W. & PETERS, B. 1995. Possibilities for management of coastal foredunes with deteriorated stands ofAmmophila arenaria (marram grass). *Journal of Coastal Conservation,* 1**,** 29-39.

VAN LEEUWEN, M. & NIEUWENHUIS, M. 2010. Retrieval of forest structural parameters using LiDAR remote sensing. *European Journal of Forest Research,* 129**,** 749-770.

VANE, G., GREEN, R. O., CHRIEN, T. G., ENMARK, H. T., HANSEN, E. G. & PORTER, W. M. 1993. The airborne visible/infrared imaging spectrometer (AVIRIS). *Remote Sensing of Environment,* 44**,** 127-143.

VARGA, T. A. & ASNER, G. P. 2008. Hyperspectral and LiDAR remote sensing of fire fuels in Hawaii volcanoes National Park. *Ecological Applications,* 18**,** 613-623.

VÉLEZ, R. 1982. Forest fires in the Mediterranean region. *In:* VAN NAO, T. (ed.) *Forest Fire Prevention and Control.* Netherlands: Springer Verlag.

VÉLEZ, R. 2002. Causes of forest fires in the Mediterranean Basin. *Risk management and sustainable forestry. EFI Proceedings.*

VIERA, A. J. & GARRETT, J. M. 2005. Understanding interobserver agreement: the kappa statistic. *Fam Med,* 37**,** 360-363.

VOHLAND, M., STOFFELS, J., HAU, C. & SCHULER, G. 2007. Remote sensing techniques for forest parameter assessment: multispectral classification and linear spectral mixture analysis. *Silva Fennica,* 41**,** 441.

WANG, K., FRANKLIN, S. E., GUO, X. & CATTET, M. 2010. Remote sensing of ecology, biodiversity and conservation: A review from the perspective of remote sensing specialists. *Sensors,* 10**,** 9647-9667.

WARNER, T. A., FOODY, G. M. & NELLIS, M. D. 2009. *The SAGE handbook of remote sensing,* New York, Sage Publications.

WEHR, A. & LOHR, U. 1999. Airborne laser scanning—an introduction and overview. *ISPRS Journal of Photogrammetry and Remote Sensing,* 54**,** 68-82.

WELCH, R. & EHLERS, M. 1987. Merging Multiresolution Spot Hrv and Landsat Tm Data. *Photogrammetric Engineering and Remote Sensing,* 53**,** 301-303.

WESSMAN, C. A., ABER, J. D., PETERSON, D. L. & MELILLO, J. M. 1988. Remote sensing of canopy chemistry and nitrogen cycling in temperate forest ecosystems.

WINNETT, S. M. 1998. Potential effects of climate change on U.S. forests: a review. *Climate Research,* 11**,** 39-49.

WISEGEEK. 2014. *What Is an Abney Level?* [Online]. Available: http://www.wisegeek.com/what-is-an-abney-level.htm 2014].

XIAO, Q., USTIN, S. L. & MCPHERSON, E. G. 2004. Using AVIRIS data and multiple-masking techniques to map urban forest tree species. *International Journal of Remote Sensing,* 25**,** 5637-5654.

XU, B. & GONG, P. 2007. Land-use/land-cover classification with multispectral and hyperspectral EO-1 data. *Photogrammetric Engineering and Remote Sensing,* 73**,** 955.

YANG, C. H., EVERITT, J. H., FLETCHER, R. S., JENSEN, R. R. & MAUSEL, P. W. 2009. Evaluating AISA plus Hyperspectral Imagery for Mapping Black Mangrove along the South Texas Gulf Coast. *Photogrammetric Engineering and Remote Sensing,* 75**,** 425-435.

YOKOYA, N., NAKAZAWA, S., MATSUKI, T. & IWASAKI, A. 2014. Fusion of Hyperspectral and LiDAR Data for Landscape Visual Quality Assessment. *Selected Topics in Applied Earth Observations and Remote Sensing, IEEE Journal of,* 7**,** 2419-2425.

YUAN, L., ZHANG, J., SHI, Y., NIE, C., WEI, L. & WANG, J. 2014. Damage Mapping of Powdery Mildew in Winter Wheat with High-Resolution Satellite Image. *Remote Sensing,* 6**,** 3611-3623.

YUNFEI, B., GUOPING, L., CHUNXIANG, C., XIAOWEN, L., HAO, Z., QISHENG, H., LINYAN, B. & C., C. 2008. Classification of LIDAR point cloud and generation of DTM from LIDAR height and intensity data in forested area. *In:* JUN, C., JIE, J. & WOLFGANG, F. (eds.) *XXIst ISPRS Congress Technical Commission III* Beijing China: The International Archives of the Photogrammetry, Remote Sensing and Spatial Information Sciences.

ZARCO-TEJADA, P. J., MILLER, J. R., MOHAMMED, G. H., NOLAND, T. L. & SAMPSON, P. H. 2001. Estimation of chlorophyll fluorescence under natural illumination from hyperspectral data. *International Journal of Applied Earth Observation and Geoinformation,* 3**,** 321-327.

ZHANG, J., RIVARD, B., SÁNCHEZ-AZOFEIFA, A. & CASTRO-ESAU, K. 2006. Intra-and inter-class spectral variability of tropical tree species at La Selva, Costa Rica: Implications for species identification using HYDICE imagery. *Remote Sensing of Environment,* 105**,** 129-141.

ZHANG, Y., XIE, P. & LI, H. 2007. Data Fusion And Integration For Multi-Resolution Online 3d Environmental Monitoring. *In:* JIE JIANG, R. Z. (ed.) *ISPRS Workshop on Updating Geo-spatial Databases with Imagery & The 5th ISPRS Workshop on Dynamic and Multi-dimensional GIS Urumchi, China.*

ZHENG, L. & WANG, J. 1992. Analysis and Study on Hyperspectral Technology and Feature Extraction of Hyperspectral Data. *Environment and Remote Sensing,* 17**,** 49-57.

ZIMBLE, D. A., EVANS, D. L., CARLSON, G. C., PARKER, R. C., GRADO, S. C. & GERARD, P. D. 2003. Characterizing vertical forest structure using small-footprint airborne LiDAR. *Remote Sensing of Environment,* 87**,** 171-182.